

UNIVERSITY OF MINES AND TECHNOLOGY

TARKWA

FACULTY OF ENGINEERING

DEPARTMENT OF ELECTRICAL AND ELECTRONIC ENGINEERING

A THESIS REPORT ENTITLED

NUMERICAL APPROACH FOR PREDICTING CORROSION RATE OF  
BURIED EARTH ELECTRODES USING BACKFILL MATERIALS

BY

SHIPHRAH OHENE ADU

SUBMITTED IN FULFILMENT OF THE REQUIREMENT FOR THE  
AWARD OF THE DEGREE OF DOCTOR OF PHILOSOPHY IN  
ELECTRICAL AND ELECTRONIC ENGINEERING

THESIS SUPERVISORS

.....

ASSOC PROF S. NUNOO

.....

ASSOC PROF J. R. DANKWAH

TARKWA, GHANA

FEBRUARY 2022

## DECLARATION

I declare that this thesis is my own work. It is being submitted for the degree of Doctor of Philosophy in Electrical and Electronic Engineering in the University of Mines and Technology (UMaT), Tarkwa. It has not been submitted for any degree or examination in any other University.

.....

(Signature of Candidate)

.....day of February, 2022

## ABSTRACT

The issue of corrosion has been an inevitable canker that keeps affecting all facets of human lives; from industry, utilities, transport, production, to manufacturing fields. Issues of corrosion in sectors like oil, water, gas, etc. have been tackled, leaving behind electricity. The generation, transmission and distribution systems have well-installed backfilled earthing systems for protection against all abnormalities such as fire, shocks and electrocution which are very fatal, but much attention has not been given to the protection at the consumers' end. There are faulty, improperly installed, corroded or absence of earthing systems at the consumers' end. Some backfill materials have been applied to some rods to reduce earth resistance and minimise corrosion of these earthing systems. It also seeks to tackle the usage of numerical approach for reducing corrosion of buried earth electrodes using two artificial intelligence techniques. Five copper-coated cast-iron rods were utilised for this investigation; one (reference) was buried without backfill material whereas the other four were buried with tyre ash, palm kernel cake, charred coconut husk and coconut coir as backfill materials for twenty-two months. A visual inspection along with measurement of thickness, analyses by X-Ray Fluorescence Spectroscopy (XRF), and Scanning Electron Microscopy coupled with backscattered Energy Dispersive Spectroscopy (SEM-EDS) were conducted to determine the extent of corrosion. Six parameters, namely, resistance, rainfall, temperature, backfill materials, time (weeks), and corrosion rates were used to compare the results from the use of Mamdani Fuzzy Logic and Artificial Neural Network (ANN) techniques. The results obtained showed a colour change of all the rods from reddish-brown to grey, suggesting that corrosion might have taken place. This was confirmed by the increase in thickness for all the buried rods as against the unburied rod. The XRF analysis recorded an increase in the percentage values of the iron content for all buried rods with charred coconut husk recording the highest value of 99.42% and 88.58% as least for the unburied rod. SEM-EDS results showed a percentage of oxygen in all the buried rods' analyses. The rod buried in tyre ash backfill recorded 29.73% for the highest oxygen value with no oxygen value for the reference. These were proof of corrosion activity for the two analyses. Lastly, the ANN had a lower Mean Square Error (MSE) of 0.0865 compared to that of the Mamdani Fuzzy Logic Model 0.3583, showing that ANN performed better than the Mamdani Fuzzy Logic Model when both techniques were used to predict the corrosion rates of the rods. Out of the four backfill materials used, charred coconut husk gave the best results in terms of reduced resistance values and lower rate of corrosion value.

## **DEDICATION**

*I dedicate this work to my first love*

## ACKNOWLEDGEMENTS

First and foremost, a very sincere gratitude to Almighty God for all He has done to bring me this far. The completion of this thesis would not have been possible without the expertise of my Supervisors, Associate Professor Solomon Nunoo and Associate Professor James R. Dankwah. Their continuous motivation, encouragement, patience, guidance and immense knowledge led to the success of this PhD work. Dean of School of Postgraduate Studies, Professor Grace Ofori-Sarpong and the entire School. I am very grateful to you.

A special gratitude to Dr Joseph C. Attachie, Head of the Department Electrical and Electronic Engineering and all lecturers of this same department and the entire University for their support.

I would like to thank my colleagues, demonstrators, postgraduate assistants, the SQUAD, National Service Personnel, the leaders and entire members of The Church of Pentecost Kumasi, Tarkwa and Tema.

In addition, a thank you to Ing Godwin Amenuvor, the Manager of Electricity Company of Ghana, Tarkwa, and the entire workers of ECG for their tremendous help with my work.

Last, but not the least, the Aboagye Dacosta, Gaisie, Luguje, Forson and the entire Burah Families have been my backbone from day one and I say God bless you all.

Anthony Amponsah, Frederick Ahenkorah Abagyinah, Richmond Kwesi Amoah, Kobina Painstil, Jacob Atewin Abaare, Nana Kobina Amoako Amoah, Michael Asamoah, Isaac Bugase, Mr Erwin Normanyo, Dr Louis Brew, Dr Yao Ziggah, Dr Clement Arthur, Dr Ishmael Quaicoe, Professor William Buah, Linda Osae Bentuma, Isaac Adeti, Janet Angoh, Emefa Priscilla Amenyah Kove, George Owusu and Yolanda Buadee, I say thank you.

Finally, Alma Gemela, I am glad you came into my life when you did.

# TABLE OF CONTENTS

<b>Content</b>	<b>Page</b>
<b>DECLARATION</b>	<b>i</b>
<b>ABSTRACT</b>	<b>ii</b>
<b>DEDICATION</b>	<b>iii</b>
<b>ACKNOWLEDGEMENTS</b>	<b>iv</b>
<b>TABLE OF CONTENTS</b>	<b>v</b>
<b>LIST OF FIGURES</b>	<b>x</b>
<b>LIST OF TABLES</b>	<b>xiv</b>
<b>LIST OF ABBREVIATIONS</b>	<b>xvi</b>
<b>LIST OF SYMBOLS</b>	<b>xix</b>
<b>INTERNATIONAL SYSTEM OF UNITS (SI UNITS)</b>	<b>xxi</b>
<b>CHAPTER 1            GENERAL INTRODUCTION</b>	<b>1</b>
1.1    Background to the Research	1
1.2    Problem Definition	2
1.3    Research Questions	3
1.4    Research Objectives	4
1.5    Scope of the Research	4
1.6    Research Methods Used	4
1.7    Facilities Used for the Research	5
1.8    Significance of the Research	5
1.9    Limitations of the Research	5
1.10   Applications of the Research	6
1.11   Definition of Terms and Key Concepts	6
1.12   Organisation of the Thesis	6
<b>CHAPTER 2            LITERATURE REVIEW</b>	<b>8</b>
2.1    Introduction	8
2.2    Earthing	8
2.2.1    Need for Earthing	9
2.2.2    Components of an Earthing System	9

2.2.3	Types of Earth Electrodes	10
2.2.4	Ground Measurement Principles	14
2.2.5	Testing an Earthing System	18
2.3	Factors that Influence the Performance of Ground Electrode	20
2.4	The Nature of Soil	20
2.4.1	Makeup of Soil	21
2.4.2	Types of Soil	21
2.4.3	Soil pH	22
2.5	Soil Resistivity	22
2.5.1	Measuring Soil Resistivity	23
2.5.2	Ways of Measuring Soil Resistivity	24
2.6	Corrosion	27
2.6.1	Corrosion Phenomenon	27
2.6.2	Types of Corrosion	30
2.6.3	Causes of Corrosion	36
2.6.4	Factors That Affect Rate of Corrosion	36
2.6.5	Corrosion Detection Devices	38
2.6.6	Corrosion Monitoring Techniques	40
2.6.7	Analytical Techniques for Corrosion Phenomenon	42
2.6.8	Effects of Corrosion	47
2.6.9	Prevention of Corrosion	48
2.6.10	Expressions and Measures of Corrosion	50
2.7	Backfill Materials	51
2.7.1	The Nature of Ground Electrode Enhancing Materials	54
2.7.2	The Purposes of the Backfill Materials	55
2.7.3	Disadvantages of the Backfill Materials	56
2.7.4	Backfill Materials from Local Plants and Materials	56
2.8	Artificial Intelligence	58
2.9	Fuzzy Logic System (FLS)	58
2.9.1	Characteristics of Fuzzy Logic	58
2.9.2	Types of Fuzzy Inference Systems	62
2.10	Neural Network System	65
2.10.1	Types of Neural Network	67

2.10.2	Advantages of Neural Network and Disadvantages of Neural Network	70
2.10.3	Applications of Neural Network	71
2.11	Review of Related Works on this Research	71
2.11.1	Review of Related Works on the Backfill Materials for Reducing Corrosion of Earth Electrodes	71
2.11.2	Review of Related Works on XRF, XRD, and SEM-EDS	73
2.11.3	Review of Related Works on Fuzzy Logic System	75
2.11.4	Review of Related Works on Neural Network System	77
2.12	Summary	79
 <b>CHAPTER 3 METHODS USED</b>		 <b>80</b>
3.1	Introduction	80
3.2	The Study Area	80
3.3	Electrode Selection	81
3.4	Materials and Instruments Used	82
3.4.1	Backfill Materials/Experimental Samples	83
3.5	Measurements Methods	87
3.5.1	Fall-of-Potential Method of Measuring Resistance Measurement Methods	87
3.6	Laboratory Experiments	92
3.6.1	Determination of pH of Samples in Water	92
3.6.2	Determination of Organic Carbon	92
3.6.3	Extraction of Exchangeable Bases	92
3.6.4	Particle Size Distribution	93
3.6.5	Soil Texture	93
3.6.6	Determination of Moisture Content of Soil	94
3.7	Sample Preparation	94
3.8	Corrosion Rate Equation	97
3.8.1	Uniform Corrosion Kinetics	101
3.9	Laboratory Analysis of Buried Rods	103
3.9.1	XRF Analysis	103



3.9.2	SEM-EDS Analysis	104
3.10	Summary	105
	<b>CHAPTER 4 COMPUTER SIMULATIONS</b>	<b>106</b>
4.1	Introduction	106
4.2	Fuzzy Logic System Design	106
4.2.1	Fuzzification of Parameters	108
4.2.2	Inference	112
4.3	Neural Network System Design	113
4.4	Summary	119
	<b>CHAPTER 5 RESULTS AND DISCUSSIONS</b>	<b>120</b>
5.1	Introduction	120
5.2	Soil and Backfill Materials Laboratory Results	120
5.2.1	Physio-Chemical Properties	120
5.2.2	Heavy Metals Content	121
5.3	Field Study Analyses	122
5.4	Laboratory Analyses	124
5.4.1	Visual Inspection	124
5.4.2	Change in Thickness	125
5.4.3	Corrosion Rate Calculation	126
5.4.4	XRF and SEM-EDS Results	128
5.4.5	SEM-EDS Results	129
5.5	Computer Simulation Results	143
5.5.1	Fuzzy Logic System	143
5.5.2	Neural Network System	150
5.6	Summary of Findings	153
5.7	Research Contribution to Knowledge	154
	<b>CHAPTER 6 CONCLUSION AND RECOMMENDATIONS</b>	<b>156</b>
6.2	Conclusion	156
6.3	Recommendations	157
6.4	Future Research Directions	157

<b>REFERENCES</b>	<b>158</b>
<b>APPENDICES</b>	<b>179</b>
APPENDIX A: FIELD RAW DATA OF RESISTANCE READINGS FOR THE YEAR 2018	179
APPENDIX B: FIELD RAW DATA OF RESISTANCE READINGS FOR THE YEAR 2019	181
APPENDIX C: FUZZY LOGIC MATLAB SCRIPT	183
APPENDIX D: ARTIFICIAL NEURAL NETWORK MATLAB SCRIPT	188
APPENDIX E: LIST OF PUBLICATIONS	192
INDEX	193

## LIST OF FIGURES

<b>Fig.</b>	<b>Title</b>	<b>Page</b>
2.1	Components of Earthing System	10
2.2	A Plate for Earthing System	12
2.3	An Example of a Pipe for Earthing System	13
2.4	Copper Rod Electrode Earthing System	13
2.5	Strip Earthing	14
2.6	Wire Earthing	14
2.7	Components to the Resistance	15
2.8	Wenner's Arrangement	25
2.9	Schlumberger Array	26
2.10	Drive Rod (3 pin) Method	27
2.11	A Schematic Representation of Corrosion Mechanism	28
2.12	Classification of Corrosion	30
2.13	A Column Structure of a Conventional SEM	46
2.14	A Permanent Backfill Material Being Installed	52
2.15	A Germinated Coconut	57
2.16	An Oil Palm Tree	57
2.17	Vehicle Tyre Ash	57
2.18	Fuzzy Expert System	59
2.19	Forms of Membership Functions	60
2.20	Design of the Mamdani Fuzzy System	64
2.21	Design of the Sugeno Fuzzy System	65
2.22	The Parts of a Biological Neuron	66
2.23	Parts of the Artificial Neuron	66
2.24	Typical Single-layer Feedforward Network	67
2.25	Structure of Recurrent Network	68
2.26	Structure of A Multi-layered Feedforward Network	68
3.1	Soil Sample	81
3.2	The Design Concept	82
3.3	Coconut Husk being taken from the Refuse Dump	84
3.4	Dried Pieces of Coconut Husk Ready for Milling	84

3.5	Coconut Coir Ready to be backfilled	85
3.6	Sample of the Charred Coconut Husk	86
3.7	Sample of Pounded Charred Coconut Husk	86
3.8	Powdered Palm Kernel being mixed with Water	87
3.9	A Dug Hole for the Rod	87
3.10	A-Rod Hammered in the Dug Hole	88
3.11	An Example of Megger	88
3.12	The Probe and Leads Used	89
3.13	Megger Showing Resistance Value	90
3.14	Backfill Material Being Weighed	90
3.15	Application of Backfill Material	91
3.16	Use of Probe for Resistance Readings	91
3.17	A Soil Textural Triangle Used to Determine Soil Texture	93
3.18	Rod Being Dug Out	94
3.19	Samples of Rods after Removal from the Soil	95
3.20	Rods Being Washed	96
3.21	The Four (4) Rods that were Removed	96
3.22	The Measurement of the Thickness of the Rods	97
3.23	Rod Samples Ready for SEM-EDS Analysis	97
3.24	Process of XRF	104
4.1	Flow Chart of the Fuzzy Logic System	107
4.2	Mamdani-based Fuzzy Logic System GUI	108
4.3	Mamdani-based Triangular Member Function	109
4.4	Mamdani-based Fuzzy Logic Input and Output Variables	110
4.5	The 5 Mamdani-based Membership Functions of the Input Variables of the Fuzzy Sets	111
4.6	Output Membership Functions of Mamdani-based Fuzzy Logic System	112
4.7	Mamdani-based Fuzzy Logic System Rule Formulation	113
4.8	Structure of the Relationship Between the Input and Output Variables	114
4.9	Flow Chart for the Neural Network System	115
4.10	Structure of the Neural Network System	116
4.11	The Structure of the Training Network	117
4.12	The Neural Network Training	118
5.1	Graph of Resistance Before and After Backfilling	122

5.2	Resistance Values for the Year 2018	123
5.3	Resistance Values for the Year 2019	123
5.4	Freshly Buried Rod	124
5.5	A Rod Buried with Tyre Ash	124
5.6	Rods Removed from the Soil	125
5.7	SEM-EDS Analysis of Palm Kernel Cake Buried Rod Region 1	131
5.8	SEM-EDS Analysis of Palm Kernel Cake Buried Rod Region 2	132
5.9	SEM-EDS Analysis of Palm Kernel Cake Buried Rod Region 3	132
5.10	SEM-EDS Analysis of Palm Kernel Cake Buried Rod Region 4	133
5.11	SEM-EDS Analysis of Tyre Ash Rod Region 1	134
5.12	SEM-EDS Analysis of Tyre Ash Rod Region 2	135
5.13	SEM-EDS Analysis of Charred Coconut Husk Region 1	136
5.14	SEM-EDS Analysis of Charred Coconut Husk Region 2	137
5.15	SEM-EDS Analysis of Charred Coconut Husk Region 3	137
5.16	SEM-EDS Analysis of Charred Coconut Husk Region 4	138
5.17	SEM-EDS Analysis of Coconut Coir Region 1	139
5.18	SEM-EDS Analysis of Coconut Coir Region 2	140
5.19	SEM-EDS Analysis of Coconut Coir Region 3	141
5.20	SEM-EDS Analysis of Reference Region 1	142
5.21	SEM-EDS Analysis of Reference Region 2	142
5.22	Rule Viewer for Some Membership Functions	144
5.23	Three-dimensional Plot of Corrosion Rate Against Resistance and Rainfall	144
5.24	Three-dimensional Plot of Corrosion Rate Against Resistance and Time (Weeks)	145
5.25	Graph of Relationship Between Corrosion Rate and Resistance	146
5.26	Three-dimensional Plot of Corrosion Rate Against Temperature and Rainfall	146
5.27	Three-dimensional Plot of Corrosion Rate Against Resistance and Temperature	147
5.28	Three-dimensional Plot of Corrosion Rate Against Resistance and Rainfall	148

5.29	Relationship Between Corrosion Rate and Rainfall	148
5.30	Graph of Predicted and Calculated Corrosion Rates	149
5.31	Results from Network Training	150
5.32	Neural Network Performance at Epoch 478	150
5.33	Neural Network Performance for Regression	151
5.34	Error Histogram	152
5.35	Graph of Predicted and Calculated Corrosion Rates	152

## LIST OF TABLES

<b>Table</b>	<b>Title</b>	<b>Page</b>
2.1	Types of Metals for Earth Electrodes	11
2.2	A Summary of Ground Testing Methods Chart	18
2.3	Types of Soil	21
2.4	Differences between Dry and Wet Corrosion	31
2.5	Types of Corrosion and Examples	33
2.6	Summary of Types of Corrosion and Examples	33
2.7	Detection Methods and their Uses	39
2.8	A Summary of the Chemical Composition, Resistivity Values and Electrical Conductivity of Electrically Conductive Backfills	52
2.9	A Summary of Some Chemical Properties of Backfill Materials	54
2.10	Backfill Materials, Properties, and Uses	56
2.11	Differences between Mamdani and Sugeno Fuzzy Inference System	63
2.12	Backfill Materials for Reducing Corrosion of Earth Electrodes	71
2.13	Related Works on XRF, XRD, and SEM-EDS	73
2.14	Related Works on Fuzzy Logic System	75
2.15	Related Works on Neural Network System	77
4.1	Backfill Materials of Five Membership Functions	110
4.2	Ranges for the input Variables /Parameters	110
4.3	Membership Function Descriptor and Corresponding Corrosion Rate Ranges	111
5.1	Selected Physio-Chemical Properties of Backfill and Soil Samples	120
5.2	Selected Heavy Metals	121
5.3	The Results of the Weight and Thickness of Rods	125
5.4	Some Parameters for Computing Corrosion Rate	127
5.5	Computation of Corrosion Rates Values	127
5.6	XRF Results after Burying for 22 months	128
5.7	SEM-EDS Analysis of Palm Kernel Cake Buried Rod Region 1	131
5.8	SEM-EDS Analysis of Palm Kernel Cake Buried Rod Region 2	132
5.9	SEM-EDS Analysis of Palm Kernel Cake Buried Rod 3 Region	133
5.10	SEM-EDS Analysis of Palm Kernel Cake Buried Rod 4	133

5.11	SEM-EDS Analysis of Tyre Ash Rod Region 1	134
5.12	SEM-EDS Analysis of Tyre Ash Rod Region 2	135
5.13	SEM-EDS Analysis of Charred Coconut Husk Region 1	136
5.14	SEM-EDS Analysis of Charred Coconut Husk Region 2	137
5.15	SEM-EDS Analysis of Charred Coconut Husk Region 3	138
5.16	SEM-EDS Analysis of Charred Coconut Husk Region 4	139
5.17	SEM-EDS Analysis of Coconut Coir Region 1	140
5.18	SEM-EDS Analysis of Coconut Coir Region 2	140
5.19	SEM-EDS Analysis of Coconut Coir Region 3	141
5.20	SEM-EDS Analysis of Reference Region 1	142
5.21	SEM-EDS Analysis of Reference Region 2	143
5.22	The Computed Errors for Fuzzy Logic System	149
5.23	The Computed Errors for Neural Network	153



## LIST OF ABBREVIATIONS

<b>Abbreviation</b>	<b>Meaning</b>
3-D	Three-dimensional
AAS	Atomic Absorption Spectroscopy
AC	Alternating Current
AI	Artificial Intelligence
AIT	Artificial Intelligence Techniques
ANN	Artificial Neural Network
BP	Back Propagation
BNN	Biological Neural Network
CHA	Coconut Husk Ash
CC	Coconut Coir
CCH	Charred Coconut Husk
CFL	Corrosion Failure Likelihood
CNN	Convolutional Neural Networks
CR	Corrosion Rate
CUI	Corrosion Under Insulation
DC	Direct Current
ECDA	External Corrosion Direct Assessment
ECG	Electricity Company of Ghana
EMAT	Electromagnetic Acoustic Transducer
FES	Fuzzy Expert System
FFNN	Feed-Forward Neural Network
FLS	Fuzzy Logic System
FOSM	First-Order and Second-Moment
GBDT	Gradient Boosting Decision Tree
GEM	Ground Enhancing Material
GI	Galvanised Iron
GIM	Grounding Improvement Material
GRNN	Generalised Regression Neural Network
GRRA	Ground Resistance Reduction Agent
IEEE	Institute of Electrical and Electronics Engineers

LPR	Linear Polarisation Resistance
LRM	Low Resistance Material
MEX	MATLAB Executable
MF	Membership Function
MIMO	Multiple Input Multiple Output
MISO	Multiple Input Single Output
MLR	Multiple Linear Regression
MPIXE	Micro-Particle Induced X-ray Emission
MSE	Mean Square Error
NACE	National Association of Corrosion Engineers
NDIR	Non-Dispersive Infrared
NEC	National Electrical Code
NFPA	National Fire Protection Association
NN	Neural Network
OM	Optical Microscopy
PID	Proportional-integral-derivative
PKC	Palm Kernel Cake
PVC	Polyvinyl Chloride
RBI	Risk Based Inspection
RBNN	Radial-Basis Neural Network
RF	Random Forest
RR	Ridge Regression
RMS	Root Mean Square
RSME	Root Mean Square Error
SCC	Stress-Corrosion Cracking
SEM-EDS	Scanning Electron Microscopy/ Energy Dispersive Spectrometry
SVR	Support Vector Regression
SWG	Standard Wire Gauge
TA	Tyre Ash
TAN	Total Acid Number <sup>3</sup>
TEM	Transmission Electron Microscopy
TOC	Total Organic Carbon
TRIMF	Triangular Membership Function

UMaT

University of Mines and Technology

USA

United States of America

XRD

X-ray Diffraction

XRF

X-ray Fluorescence

## LIST OF SYMBOLS

Absolute temperature	$T$
Actual output of the j-neuron	$y_j(n)$
Anodic current density	$I_{corr}$
Applied current density	$i_{app}$
Average error function	$G_{av}$
Average of set of numbers	mean
Atomic Weight	$W$
Charge transfer coefficient	$\alpha_{a, M}, \alpha_{C, Ox}$
Corrosion current density	$i_{corr}$
Corrosion rate	$B$
Corrosion Rate	CR
Cross-sectional area	$A$
Current density	$J$
Desirable output	$d_j(n)$
Density	$\rho$
Density of dissolved-deposited materials	$\rho_j$
Diameter of electrode	$d$
Dissolved or deposited substances	$j$
Distance between electrodes	$d$
Duration of experiment	$\Delta t$
Electric charge	$q$
Earth resistance	$R_g$
Equivalent Weight	EW
Faraday constant	$F$
Gas constant	$R$
Gravimetric water content	$O_g$
Immersion time	$h$
Length of electrode	$L$
Local current	$I_{loc,m}$
Mass	$m$
Mass lost	$\Delta m$
Measured output	$o_i$

Metal valence	$Z$
Molar mass	$M_j$
Molecular weight of the metal	$M/W_0$
Number of moles of metal	$N$
Number of neurons	$N_n$
Number of patterns of trained/test	$n$
Optimal number of neurons	$N_n$
Partial current	$I$
pi	$\pi$
Polarisation	$E-E_{corr}$
Predicted output	$y_i$
Rate of weight loss	$dw/dt$
Reaction rate of dissolved-deposited substances	$R_{d,j,m}$
Set of neurons	$c$
Set of numbers	$x$
Soil Resistivity	$\rho$
Standard deviation	$\sigma$
Total area of sample	$S$
Total charge	$Q$
Volume	$V$
Volumetric water content	$O_v$
Weight loss	$W/\Delta W$
Weight between k-neuron and v-neuron	$W_{kv}^{(1)}$

## INTERNATIONAL SYSTEM OF UNITS (SI UNITS)

<b>Quantity</b>	<b>Unit</b>	<b>Symbol</b>
Electric current	ampere	A
Electric voltage	volt	V
Electric resistance	ohm	$\Omega$
Frequency	hertz	Hz
Length	meter	m
Amount of Substance	mole	mol
Temperature	degree Celsius	$^{\circ}\text{C}$
Time	second	s

# CHAPTER 1

## GENERAL INTRODUCTION

### 1.1 Background to the Research

The rate at which electrical gadgets, such as electric irons, microwave ovens, fridges, television sets, rice cookers, etc. used in our homes get damaged is very alarming. The question that keeps lingering around is, what could be the cause? Poor considerations and design failure, frequent electrical surges, sags, and dips in power and circuit overloads have often led to many electrical shock accidents (Barbrauskas, 2010; Hamudal *et al.*, 2011). The list goes on and on but finally ends on faulty earth electrodes or the absence of the same. The primary purpose of an ideal and effective earthing system is to minimise the danger of electrocution, fire due to earth leakage current through an undesired path and to ensure that current through current-carrying conductor does not rise above that of the earth than its designed insulation (Ghavamian *et al.*, 2015).

However, soil resistivity, soil stability, and environment are factors that influence the performance of an earthing system. According to National Electrical Code (NEC), for effective earthing, the ground resistance must be less than 25  $\Omega$  whereas the National Fire Protection Association (NFPA) and Institute of Electrical and Electronics Engineers (IEEE) recommend less than 5  $\Omega$ . Electrode deep-driving, use of multiple rods, and the construction of Ufer grounds some commonly utilized ways for minimising earth resistance (El-Tous and Alkhawaldeh, 2014). However, if it is not achieved, the soil must be treated using organic or inorganic materials, termed backfill materials (Siow *et al.*, 2013). Additionally, backfill materials help in prolonging the lifespan of an earthing rod.

Dead sea water was used by El -Tous and Alkhawaldeh (2014) on galvanised steel to reduce resistance values. Further reductions were recorded when coal and iron fillings were added to the dead sea water. Nyuykponge *et al.* (2015) introduced Dry yard waste streams, charcoal (residues from forests or crop production), and livestock feed (manures) were used to treat the soil instead of chemicals in a 1 m depth volume of the earthing part. The strategy resulted in a long-term reduction in earth resistance, avoiding the high expense of these components as well as their secondary effects. Akoto (2014) used tyre ash as a conductive material but concluded that it corroded after a year. Eduful *et al.* (2009) compared the effects of palm kernel cake, powdered cocoa shells and wood ash and on a 0.3 m length of an

electrode with a conclusion that tyre ash recorded the least resistance values. Other materials such as coconut ash, bentonite, granite powder, coke breeze, sodium chloride, etc. have been used as backfill materials (Chandima *et al.*, 2010) with positive results.

## 1.2 Problem Definition

Earthing is of great importance to transmission and distribution systems. Tarkwa, known for its high levels of rainfalls, raises a lot of concerns about its earthing systems. Corrosion of buried electrodes as an environmental factor battles with the effectiveness of these systems. A corroded electrode loses its value and usefulness since resistances and impedances reach their highest peaks.

A recent estimate of the global direct cost of corrosion (that is, for prevention, repair, and replacement) exceeds \$1.8 trillion, or 3 to 4% of industrialised countries' GDP (Anon., 2018). Given this, many studies have been conducted to either prevent, remove or reduce corrosion effects on ground electrodes using organic and inorganic backfill materials. Although the backfill materials will help achieve low and acceptable ground resistance, they are known to cause corrosion of the earthing rods too (Zhang *et al.*, 2020).

Corrosion comes in different forms and its identification and prediction are very vital in controlling and preventing it. The need to predict the rate of corrosion or know how long it would take for a buried rod to corrode in the soil led Zhang *et al.* (2020) and Huang *et al.* (2019) to use parameters such as soil resistivity, pH, water, salt and gas content to predict corrosion of a grounding device. The two researchers based their methodology on two (2) Artificial Intelligence (AI) techniques, namely; Back Propagation Neural Network (BPNN) and Fuzzy Logic System (FLS). The results from Huang *et al.* (2019) were not satisfactory due to inadequate data for the analysis and poor choice of prediction model. Zhang *et al.* (2018) was able to obtain the corrosion matrix but not for prediction due to its inconsistencies.

Tong *et al.* (2018) and Zhang *et al.* (2020) researched using finite element methods to simulate with and without direct current the The vertical grounding electrode's corrosion rates at various burial altitudes were measured. They also assessed the influence of electrode potential, pH value, anode iron dissolution and corrosion on the grounding electrode, respectively on the corrosion rates. Hameed *et al.* (2016) used the boundary element technique to model corrosion problems for a cathodic protection system with an average percentage error of 1.27. Using the damp and cylinder probes Linear Polarisation Resistance



(LPR) measurements, Vilda (2009) electrochemically determined the corrosion rate of the *in-situ* soil environments and concluded that the development of a linear model to predict corrosion rate from pH and soil resistivity was not possible with the data that was derived.

There have been many laboratory studies on determining the corrosion rates of buried earth rods alone (Loboda and Marciniak, 2006) and (Vilda, 2009). Others used the application of mathematical models to determine corrosion rates with some soil parameters (Tong *et al.*, 2018, and Hameed *et al.*, 2016). However, Zhang *et al.* (2018) determined corrosion rates using both results of laboratory tests and a mathematical model. The use of the laboratory analysis gave tangible evidence (change in thickness or weight) to show corrosion has taken place and to buttress it, the mathematical model made it possible to predict corrosion rates of different items using the parameters that were provided. The only disadvantage is that the data sample was mostly taken from other works or websites whose authenticity might be questionable.

In this research work, the rods were buried with backfill materials for two years, X-ray Fluorescence (XRF) and Scanning Electron Microscopy with Energy Dispersive X-ray Spectroscopy (SEM-EDS) techniques were utilised for surface analysis of the rods. Furthermore, two Artificial Intelligence (AI) techniques; Fuzzy Logic System (FLS) and Neural Network (NN) predicted the corrosion rates of the rods using five parameters to bridge the gap between field study and modelling.

This research used a numerical approach for corrosion to define the rate of buried electrodes. The rods were buried using coconut coir, palm kernel cake, tyre ash, and charred coconut husk as backfill materials.

### **1.3 Research Questions**

The research questions are stated as follows:

- a. What causes corrosion of buried earth electrodes?
- b. Can backfill materials be used to reduce the corrosion phenomenon of buried earth electrodes?
- c. What are the parameters that need to be considered to determine corrosion rate?
- d. What laboratory tests need to be done to know the parameters of the soil sample, backfill materials and predict corrosion rate?

- e. What are the considerations for developing mathematical models for corrosion rates?

The research study offers this hypothesis: Local backfill materials can be used to reduce corrosion of earth electrodes.

The purpose of this research is to reduce corrosion of buried earth electrodes.

#### **1.4 Research Objectives**

The main objective is to use a numerical approach to predict the rate of corrosion and also to use locally acquired backfill materials to improve earth resistance and prevent corrosion of some buried rods. To achieve this general objective, the specific objectives of this research study are to:

- a. Perform a field study to determine the resistance and corrosion rate of rods;
- b. Determine the best backfill material derived from local sources that reduces earth resistance and mitigates corrosion of earth electrodes;
- c. Test corrosion behaviour of buried earthing electrodes through laboratory experiments; and
- d. Use Fuzzy Logic System and Artificial Neural Network to model and simulate the rate of corrosion against soil parameters and parameters of the backfill materials.

#### **1.5 Scope of the Research**

This research is limited to the use of local backfill materials to reduce corrosion of buried copper-coated cast iron electrodes, use of numerical methods to model and simulate laboratory tests on soil samples, backfill materials, and corrosion rate.

#### **1.6 Research Methods Used**

The methods employed in this research include the following:

- a. Review of related literature;
- b. Collection and preparation of backfill materials (palm kernel cake, tyre ash, coconut coir and charred coconut husk) readily available in Ghana;
- c. Use of Fall-of-Potential Method of measuring soil resistance;
- d. Physio-chemical analyses of the soil and backfill materials samples from the study site using AA240FS Atomic Adsorption Spectrometer;

- e. Determination of corrosion rates of buried rods using Corrosion Rate Equation;
- f. Use of Non-electrochemical Quantitative Method of Estimating the Corrosion; and
- g. Use of a Mamdani Fuzzy Logic Model (FLM) and Artificial Neural Network (ANN) to predict corrosion rate of buried earth rods using field study parameters such as rainfall, temperature, backfill materials and time.

### **1.7 Facilities Used for the Research**

The following facilities were used for the research:

- a. Library, Laboratory, Computer, and Internet Facilities at UMaT;
- b. Digital camera;
- c. Resistivity meter (MEGER DET5 / 4R);
- d. Resistance meters for the ground (Digital earth resistance meter KYORITSU MODEL4105A); and
- e. Backfill materials (coconut coir, charred coconut husk, palm kernel cake, and tyre ash).

### **1.8 Significance of the Research**

The significance of this research include:

- a. To explore the use of local backfill materials in enhancing earthing systems; and
- b. To develop reliable techniques, instruments, and models to predict the corrosivity of buried earth rods using soil parameters and backfill materials parameters.

### **1.9 Limitations of the Research**

- a. The utilisation of only copper-coated cast iron type of earth electrodes; and
- b. Field Study is restricted to a piece of land adjacent UMaT campus.

### **1.10 Applications of the Research**

The outcome of this research work will find applications in generation, transformation, and distribution stations. Electrical technicians and consumers of electrical power would need this thesis.

### **1.11 Definitions of Terms and Key Concepts**

*Electrode:* Any constructed earth ground electrode should have a resistance of less than 25 ohms, according to IEEE standards. This target figure will change depending on the circumstances. Commercial codes and US Government tactical and long-haul communications system standards both use figures of ten or fewer. Lower values, in the 1 to 5 range, are only useful for dc and 50/60 Hertz electrical safety.

*Earth leakage:* The current that ordinarily runs in the earth conductor of a protectively earthed piece of equipment is known as earth leakage current. The mains are frequently linked to a transformer with an earthed screen in medical electrical equipment.

*Backfill material:* An organic (waste) material that lowers ground system resistance and its resistivity.

*Soil resistivity:* The degree of the resistance offered by the soil in the flow of electricity.

*Soil conductivity:* An indirect measurement that correlates very well with different soil physical and chemical properties.

*Soil stability:* Refers to a soil's engineering properties, particularly its resistance to failure when disturbed.

*Corrosion:* Corrosion is a chemical or electrochemical reaction that occurs between a material, usually a metal, and its surroundings, causing the material and its properties to decay.

*Numerical approach:* A numerical method is a tool used in mathematics to solve numerical issues.

### **1.12 Organisation of the Thesis**

The remainder of the thesis is organized in the following manner.

Chapter 2 was devoted to the literature review, which consisted of a review of theory, a look at some comparable studies, and a statement of the gap in the literature that this research sought to address. Keynote words in the research topic such as earthing, corrosion,

numerical approach and backfill materials were discussed. Earthing, the types, the types of earth rods, factors influencing earthing systems, the ways of measuring soil resistivity came up. Corrosion, its phenomenon, types, causes, detective, predictive and preventive methods were also stated. The various backfill materials, their properties and some related works all come under this chapter.

Chapter 3 dealt with methods used consisting of the materials, methods, and the methods of data analysis used. The preparation of the study area and the backfill materials, how the rods were buried, and the measurement of resistance was done. Laboratory experiments to determine the pH, organic carbon, exchangeable bases, particle size etc of the backfill materials and soil was developed. The chapter ended with the various corrosion rate equations and laboratory analysis of these rods.

Chapter 4 took care of the types of data to be collected, reviewed data collection procedures, methods of data analysis to be employed, representation and interpretation. The FLS and ANN techniques were utilised here for modelling.

Chapter 5 deliberated on the 1st laboratory results on soil and backfill materials. Graphs showing resistance values of the rods were discussed. The results of the three (3) corrosion rate analyses namely: visual inspection, change of thickness, and use of XRF and SEM-EDS were also elaborated with tables, pictures, and graphs.

Chapter 6 gave the findings summary, conclusions, and recommendations.

## CHAPTER 2

### LITERATURE REVIEW

#### 2.1 Introduction

For a buried electrode to achieve a corrosion-free life span of twenty to thirty years, the precise assessment of Conditions on the site, environmental considerations, soil resistivity levels, conductor kinds, and components must all be properly examined (Ghavamian *et al.*, 2015). Correct site evaluations, design, and construction should help to minimise premature corrosion of earthing and lightning protection wires, connectors, and components, extending the lifetime of these safety systems. (Manas, 2016).

In this chapter, under earthing, its types, the types of rods, different methods of measuring resistance were discussed. The types, the phenomenon, causes, effects, preventive measures, prediction, and measurement of corrosion were elaborated. Backfill materials, their characteristics, and some related works were discussed exclusively.

#### 2.2 Earthing

The phrase "earthing" refers to the connection of a conduit or device's frame to the earth's general mass. It is often used interchangeably with grounding (Eduful and Cole, 2009). At the consumer end, It entails connecting a component of the electrical system to the earth, such as the metallic coating of metals, the earth termination of socket cables, and non-current stay wires (Eduful and Cole, 2009). It is the connection of a power supply system's neutral point to the earth in order to avoid or minimise risk during the discharge of electrical energy. The developed system must be able to manage currents in all frequency windows to qualify as an overall earthing system.

For the safe and proper operation of any electric system, earthing is critical in the generation, transmission, and distribution of electric power. Electrical safety is important. Earthing is a method for dumping unwelcome electric charge into the ground or returning it to the generator via earth mass. Charge transfer could be caused by low-frequency earth faults, transients, or high-frequency noise (e.g., lightning or switching impulses)) (Gomes *et al.*, 2013).

### 2.2.1 Need for Earthing

The primary purpose of earthing is to minimize or minimise the extent of electrocution and fire caused by current leakage to the earth through an unintentional channel, as well as to guarantee that a current-carrying conductor's potential does not exceed its designed insulation (Salam *et al.*, 2015).

Once the metallic component of an electrical device, that is, parts that may conduct or enable the channel of electric current, comes into touch with a live wire, Static charge increases on the metal as it becomes charged, possibly due to installation or cable insulation failure. A significant shock occurs when a person comes into contact with such a charged metal (Feldman, 2019). To avoid this, power supply systems and portions of appliances must be earthed, allowing the charge to be transferred straight to the earth. The most basic requirements of earthing are to (Yu, 2018):

- a. Safeguard human lives as well as electrical gadgets and appliances against leakage current;
- b. maintain a steady voltage in the healthy phase in the event of a malfunction on any phase;
- c. protect electric systems and structures from lightning strikes;
- d. function as a return conductor in electric traction and communication systems; and
- e. eliminate the possibility of a fire in electrical installation systems.

### 2.2.2 Components of an Earthing System

The earth continuity conductor, earthing lead, and earth electrode make up a full electrical earthing system. Figure 2.1 shows the components of an earthing system (Mohan, 2016).

*Earthing leads or earthing joint:* The conductor wire connecting the ground continuity conductor to the earth electrode or earth plate is known as the earthing junction or earthing lead. The earth continuous conductor and the earth electrode meet at a connecting point (Mohan, 2016). The earthing lead, which is linked to the earth rod (which is underground) through the earth's connection point, is the last component of the earthing system. Copper wire can be utilised as an earthing lead in most cases. An earthing lead is made up of two copper wires that link the device's metallic body to the earth electrode or earth plate, which

increases the safety factor of installations. The maximum size for an earthing lead is 3 SWG, with a minimum size of 8 SWG (Jithin, 2016).

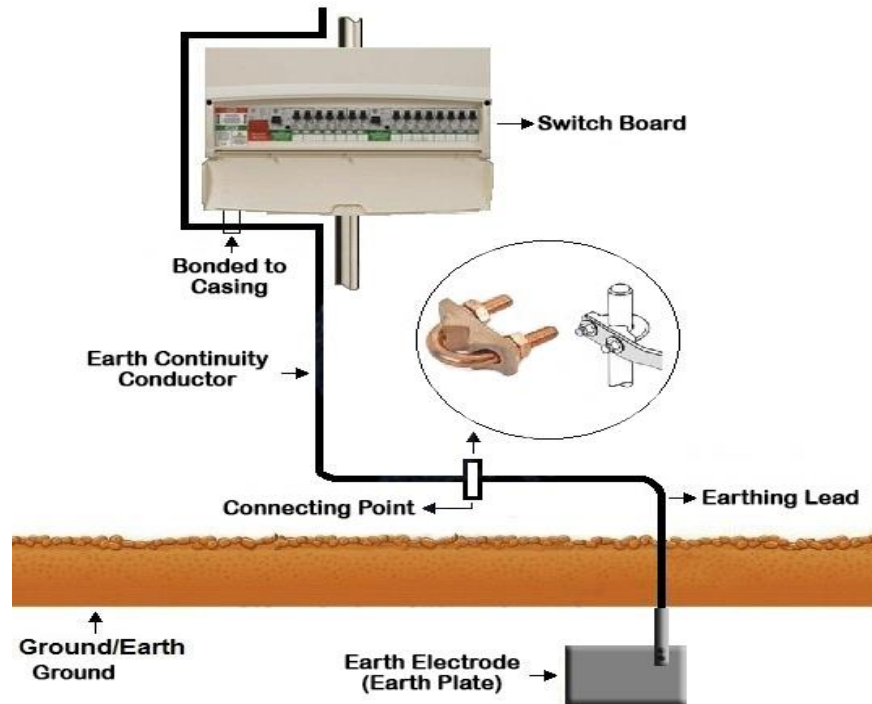


**Figure 2.1 Components of Earthing System**

*Earthing electrode or earth plate:* The final portion of the electrical earthing system, according to Sundaravaradan and Reddy (2018), is a metallic rod or plate submerged in the earth (underground). As an earth electrode, a metallic plate, pipe, or rod with a small resistance be able to be utilised to safely transmit the fault current to the ground (earth).

### 2.2.3 Types of Earth Electrodes

The moisture level below the ground level must be penetrated by earth electrodes. They must also be made of a metal (or a mix of metals) that will not degrade excessively over the projected service life. Copper is the most often utilised material for earth electrodes due to its excellent conductivity and corrosion resistance. Steel, stainless steel, aluminum, and lead are all hot-galvanized are also popular materials (Csanyi, 2018). A comparison of different metals used for earth electrodes is shown in Table 2.1.



**Table 2.1 Types of Metals for Earth Electrodes**

SN	Name of Metal	Composition (%)	Characteristics
1.	Stainless Steel	Carbon – 1.2 Steel – 88.30 Chromium – 10.5	Resistivity: $1.45 \times 10^{-6} \Omega\text{m}$ Colour: blue, black, gold, green Reactivity: not reactive Lustre: metallic Malleability: yes Melting Point: 1510 °C Conductivity: 1,37 S/m
2.	Copper		Resistivity: $1.68 \times 10^{-8} \Omega\text{m}$ Colour: reddish-brown Reactivity: reactive Lustre: metallic Malleability: yes Melting Point: 1,085 °C Conductivity: 58,7 S/m
3.	Galvanised Iron	Carbon – 0.25 Iron – 98.4 Phosphorus – 0.05 Manganese – 1.3	Resistivity: $5.5 \times 10^{-6} \Omega\text{m}$ Colour: Bright silver, dull grey Reactivity: reactive Lustre: light bluish grey Malleability: yes Melting Point: 650°C Conductivity:
4.	Aluminium		Resistivity: $2.82 \times 10^{-6} \Omega\text{m}$ Colour: silver Reactivity: reactive Lustre: dull Malleability: yes Melting Point: 660.3 °C Conductivity: 36,9 S/m
5.	Lead		Resistivity: $2.2 \times 10^{-7} \Omega\text{m}$ Colour: bluish-white, dull grey Reactivity: reactive Lustre: dull Malleability: yes Melting Point: 327.5 °C Conductivity: 4,7 S/m

**(Source: Arnoux, 2012)**

Rods, plates, strips, solid section wire, and mats can all be used as earth electrodes. Earthing can be done in many ways following subsections that give a list of the many earthing methods used (in-house wiring or factory and other connected electrical equipment and machines).

### *Plate earthing*

A plate earthing system consists of a plate comprised of either copper or steel with dimensions of 0.6 m by 0.6 m by 0.00318 mm or Galvanised iron (GI) of dimensions 0.6 m by 0.6 m by 0.00635 m is buried vertically in the dirt (earth pit), with a minimum of 3 m from the ground level (Iyer, 2018). Its advantages include its availability, suitability, and easiness of installing. Figure 2.2 is an example of a plate.

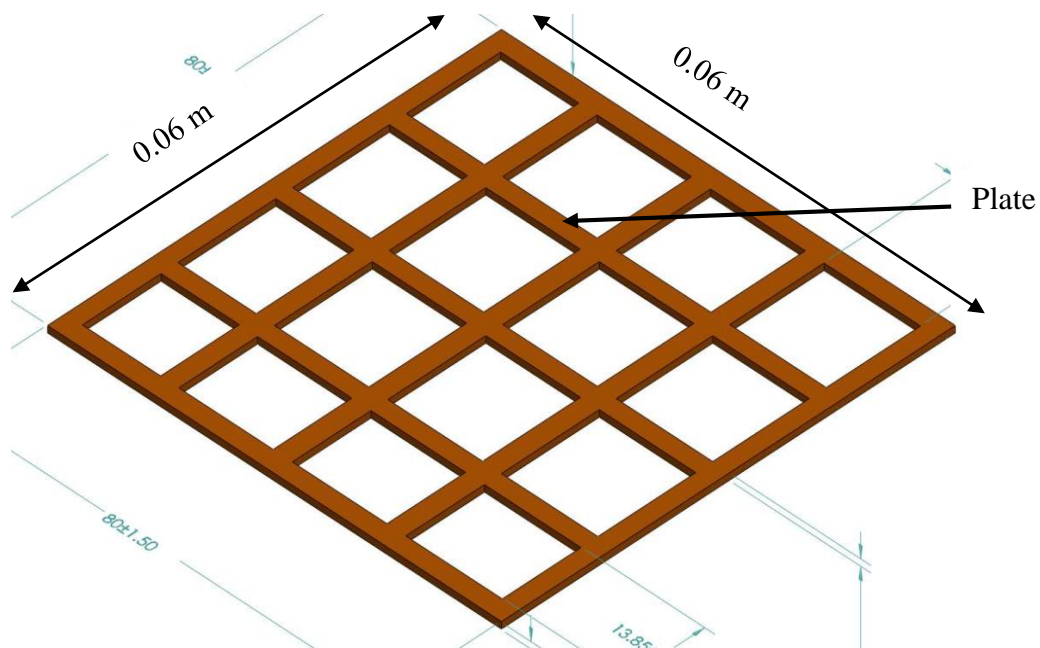


**Figure 2.2 A Plate for Earthing System**

### *Pipe earthing*

The moisture level below the ground level must be penetrated by earth electrodes. They must also be made of a metal (or a mix of metals) that will not corrode excessively over the projected service life. The most abundant metal is copper and is often used material for earth electrodes due to its excellent conductivity and corrosion resistance. Steel, stainless steel, aluminum, lead and hot-galvanized are also popular materials (Csanyi, 2018). A comparison of different metals used for earth electrodes is shown in Table 2.1.

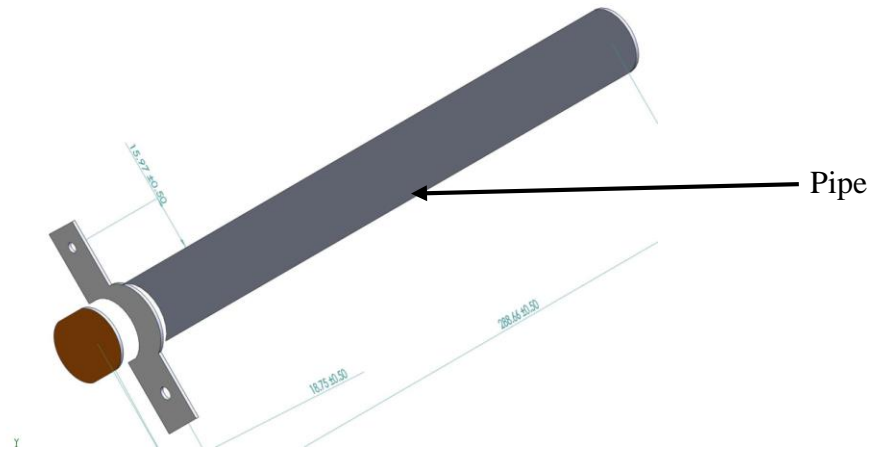


**Figure 2.3 An Example of a Pipe for Earthing System**

*Rod earthing*

Lamay (2017) agreed with (Iyer, 2018) that is the same method as pipe earthing. In rod earthing, a copper rod of 0.0125 m diameter or 0.016 m diameter of galvanised steel or hollow section 0.025 m of GI pipe of length higher 2.5 m are manually or with the aid of a pneumatic hammer sunk upright in the earth (Lamay, 2017; Iyer, 2018). Shankland (2017) answered that these rods are employed in situations when returning an earth wire to the source would be impracticable or cost-prohibitive since the earth resistance is reduced to a desired value by the length of buried electrodes in the soil.. Figure 2.4 is Copper Rod Electrode Earthing System.

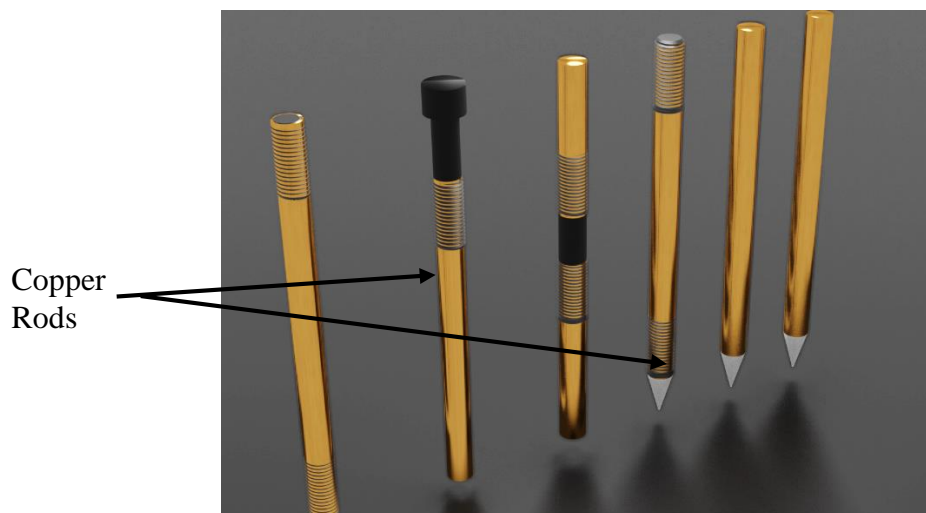


**Figure 2.4 Copper Rod Electrode Earthing System**

### *Earthing through the waterman*

Zai *et al.* (2018) This type of earthing, in which waterman pipes, usually made of GI, are employed for earthing reasons, was considered. To ensure correct earthing connection, examine the resistance of GI pipes and apply earthing clamps to diminish the resistance. However, if a conductor is utilised as an earth wire, the wire's end strands must be cleaned to ensure that they are straight and parallel so that the waterman pipe may be connected snugly.

### *Strip or wire earthing*

Strip electrodes having a minimum cross-section of 0.025 m by 0.001 6 m are buried in parallel trenches with a lowest depth of 0.5 m in this practice of earthing (Kuppan, 2017). Figures 2.5 and 2.6 depict strip and wire earthing, respectively.

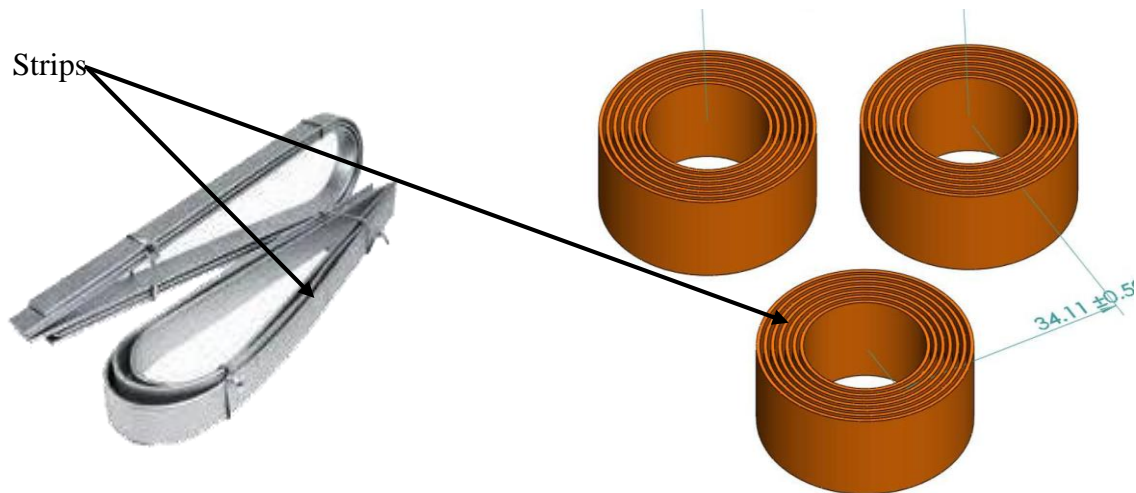


**Figure 2.5 Strip Earthing**

**Figure 2.6 Wire Earthing**

When using round conductors, the cross-sectional area of the GI or steel shall not be less than 0.006 m<sup>2</sup>. The length of the conductor buried in the ground should be at least 15 m to provide adequate earth resistance (Iyer, 2018).

#### 2.2.4 Ground Measurement Principles

An earth electrode system's purpose is to offer low resistance to external currents that could harm, damage, or disturb equipment. When the currents are appropriately carried to ground via the electrode, they will dissipate safely. As seen in Figure 2.7, the resistance is made up of three components.

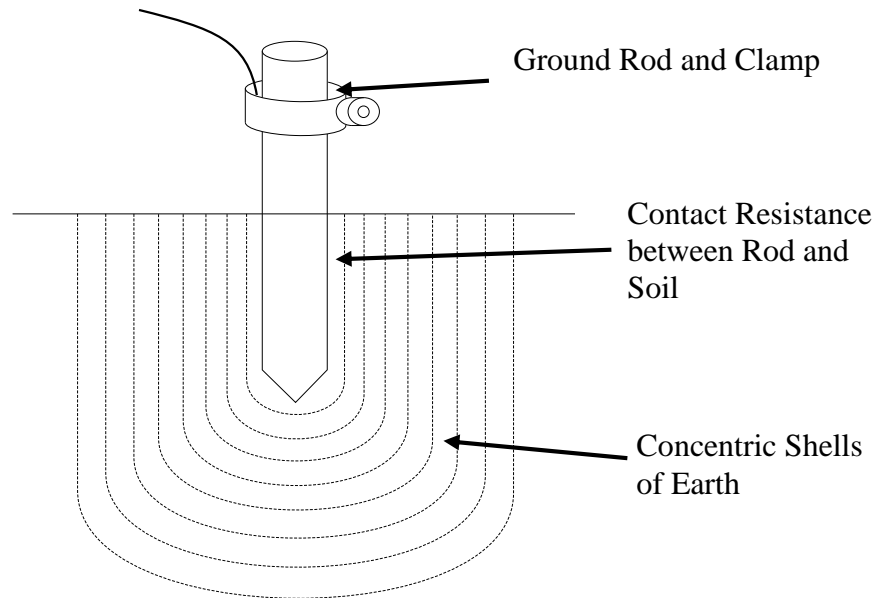


**Figure 2.7 Components to the Resistance**

*The electrode materials' resistance, as well as their connections,*

Earth connections are typically made via rods, pipes, metal masses, constructions, and other methods. The electrode materials' resistance is intentionally low, so their contribution to the total resistance is insignificant (Sundaravaradan and Reddy, 2018).

*Contact resistance between the electrode and the soil surrounding it*

According to Trifunovic and Kostic (2014), if the electrode materials are clean, unpainted, and tightly packed, the contact resistance sandwiched between the electrode and the soil must be low. Unlike other soils, it is less resistant to water, even oxidized steel ground rods have low contact resistance. Rusted ground rods, on the other hand, may gradually rust away, reducing their efficiency significantly.

*Resistance of the surrounding earth*

The surrounding earth's resistance will, on average, be the highest of the three constituents. A buried earth electrode system radiates current in all directions and diminishes over time due to the soil's resistance to current flow, as measured by its resistivity. A uniformly resistive electrode driven into the earth radiates current in all directions (Yadav, 2017). When one imagines the electrode as being encircled by equal-thickness earth shells, a visual realisation occurs. The earth shell that is closest to the electrode. receives the greatest

resistance due to its small surface area. The next earth shell experiences the opposite, that is, a large surface area and less resistance (Arnoux, 2012).

Arnoux (2012) stated that there will come a point where additional earth shells will not appreciably increase the resistance of the earth adjoining the rod. The efficiency of the ground electrode is determined by the critical volume of soil, which is effectively assessed to make this determination in this situation. When compared to other types of electrical measurement, ground testing is unique in that it is a volumetric measurement that cannot be observed as a "point" attribute (Prithwiraj *et al.*, 2013). The surrounding earth's resistance is usually the biggest of the three components that make up the resistance of a ground construction.

#### *Calculation of earth resistance of an electrode*

There is some resistance between the earth electrode and "real Earth" once dirt exhibits resistance to the flow of electrical current and is no longer a "perfect" conductor. The Earth Resistance of an electrode is the resistance between the earth electrode and "actual Earth," and it is determined by soil resistivity, electrode type and size, and burying depth (Baljlit *et al.*, 2020).

According to Csanyi (2016), the earth resistance of an electrode configuration may be estimated for different types and sizes of earth electrodes if the soil resistivity is known or measured using the 4-point Method. The formulae for estimating earth resistance of all types and configurations of electrodes can be found in equations. Rods driven vertically into the ground and rod electrodes in parallel are the most popular designs.

*Rods driven vertically into the ground:* Bico and Bizjak (2019) mentioned the Earth Resistance ( $R_g$ ) of a single spike driven vertically into the soil can be computed as follows:

$$R_g = \frac{\rho}{2\pi L} \left[ \ln \left( \frac{8L}{d} \right) - 1 \right] \quad (2.1)$$

where,  $\rho$  = Soil Resistivity in ohmmeter;

$L$  = Buried Length of the Electrode in m; and

$d$  = Diameter of the Electrode in m.

If a single earth electrode cannot provide the appropriate earth resistance, the overall resistance is decreased by connecting many electrodes in parallel, sometimes known as "arrays of rod electrodes."

The cumulative resistance of parallel electrodes, according to Gerrit (2014), is a complex combination of various elements, including the number and arrangement of electrodes, their distance apart, their diameters, and soil resistivity. The influence of the horizontal wires connecting the rods in the array has no bearing on this. To get the most out of the extra rods, rods in parallel should be spaced at least twice their length apart, according to the rule of thumb.

The cumulative resistance of parallel electrodes, according to Gerrit (2014), is a complex combination of various elements, including the number and arrangement of electrodes, their distance apart, their diameters, and soil resistivity. The influence of the horizontal wires connecting the rods in the array has no bearing on this. The rule of thumb states that rods in parallel should be spaced at least twice their length apart in order to get the most out of the extra rods.

#### *Improvement of earth resistance*

There are several ways of improving the resistance of the earth once it is detected that the earth electrode resistance is not low enough (Naxakis *et al.*, 2018).

*Lengthen the earth electrode in the earth:* Longer rods are especially useful when low-resistance soils are too deep below the surface to reach with standard length rods. The degree of benefit from the longer rods is determined on the deepness of the low resistance soils. When the rod has been driven to a low-resistance level, the resistance readings usually show a fast reduction (Nyuykponge *et al.*, 2015).

*Use multiple rods:* Nyuykponge *et al.* (2015) also recommended that adding more ground rods is one of the greatest ways to lower ground resistance. For example, the combined resistance of two correctly spread out and connected in parallel rods should be 60% of one rod's resistance, and the combined resistance of three rods should be 40% of one rod's resistance.

*Treat the soil:* When you can't drill deeper ground rods due to hard underlying rock, chemical treatment of the soil is a useful approach to improve earth electrode resistance. The addition of a ground enhancement compound will improve grounding efficacy in

practically all soil situations. Some are permanent and don't require any upkeep (Naxakis et al., 2018). They can be used in areas with low conductivity, such as rocky ground, mountaintops, and sandy soil, where ground rods cannot be driven or standard grounding is impractical due to space constraints. (Naxakis *et al.*, 2018).

### 2.2.5 Testing an Earthing System

Once the earthing system to be installed is done, there is the need to measure and approve the earth resistance between the electrode and the “true Earth” (Gerrit, 2014). Different methods have been utilised to achieve this aim. Table 2.2 A Summary of Ground Testing Methods Chart.

**Table 2.2 A Summary of Ground Testing Methods Chart**

<b>SN</b>	<b>Method</b>	<b>Best Applications</b>	<b>Advantages</b>	<b>Limitations</b>
1.	Fall of Potential	Small electrode systems (1 or 2 rods/plates), complex systems if full resistance curve is plotted	Extremely reliable conforms to IEEE 81, the operator has complete control of test set-up	On medium and large systems, extensive distances (and long test leads) to the test probes are required, which is time-consuming and labor-intensive. If the electrical center is unknown, it is ineffective.
2.	Simplified Fall of Potential	Systems with small and medium electrodes	Easier to carry out than full Fall of Potential, much faster	Because fewer measurements are taken, it is less precise than full Fall of Potential. It also assumes optimal conditions, which is unhelpful if the electrical center is unknown.



**Table 2.2 Cont'd**

SN	Method	Best Applications	Advantages	Limitations
3.	61.8% Rule	Small and medium electrode systems	Simplest to carry out, requires the least amount of math, and requires the fewest number of test probe moves.	The soil must be homogeneous, which is less precise, and vulnerable to non-homogeneous soil, which is less precise and necessitates math.
4.	Slope	Large ground systems like substations	Long distances to testing probes are not required, nor is knowledge of the electrical center. Knowledge of electrical centre not necessary	Numerous calculations and drawings of curves
5.	Intersecting Curves	Large ground systems like substations	Long distances between testing probes aren't required, and the procedure is straightforward.	Potential resistance overlap issues, non-metallic (high resistance) return
6.	Dead Earth (Two (2) Point)	Not recommended	Long distances are not required for test probe location.	Many computations are required since resistance areas should not overlap.
7.	Star Delta	Ground systems in dense metropolitan areas and/or rocky terrain with problematic probe location.	It is not necessary to know anything about the electrical center.	Long distances between test probes are still required, as are some calculations.

**Table 2.2 Cont'd**

SN	Method	Best Applications	Advantages	Limitations
8.	Four (4) Potential	Medium to large ground systems	Quick and simple, with bonding and overall connection resistance included.	Only works in instances where there are numerous grounds running in parallel, is subject to noise, has no basis in standards, and has no built-in evidence.
9.	Clamp-On	A simple ground system with a pre-existing return path that passes through several grounds		

(Source: Gerrit, 2014)

### 2.3 Factors that Influence the Performance of Ground Electrode

Some factors influence the performance of the ground electrode. These include materials used in making the ground electrode, depth of ground electrode, the nature of the soil which compasses the moisture content, resistivity, temperature, and corrosion (Stott and John, 2010).

### 2.4 The Nature of Soil

Stott and John (2010) defined soil as the top layer of the land surface of the earth consisting of a mixture of organic remains and rock particles. The rock particles may be the most important aspect since they break down through weathering from the soil over thousands of years. LaCroix *et al.* (2020) also described the soil as a mixture of minerals, air, water, and organic matter. Arriba *et al.* (2018) observed that soil may be a broad topic, which covers the distribution of the mineral particles, water content, aeration, in other words, redox potential (a measure of the degree of soil air), pH, resistivity, ions content and presence of bacteria. Pole and Sharma (2013) emphasised that the conductivity of soil rest on on some factors such as nature of soil, salt composition, temperature, pressure and packing closeness, moisture content, and grain size and distribution. Of the aforementioned factors, moisture

content and temperature are quite pertinent due to their variations with the seasons, and hence, can affect resistance values of electrodes.

#### 2.4.1 Makeup of Soil

LaCroix *et al.* (2020) classified soils to the size range of the particulate elements, otherwise known as the texture, the structure, the colour, and the horizons. Soil texture is grouped into three systems by size; sand, silt, and clay. Clay particles are the tiniest and that of sand is the largest. The clumps come in forms such as balls, blocks, plates, and columns with spaces in between for air, water, and movement of organisms. Colour speaks volumes of the soil's mineral content and behaviour. Orange-brown to yellow-brown are colours for soils rich in iron and dark brown or black is for those with high organic matter (Gillaspy, 2019).

#### 2.4.2 Types of Soil

The four main forms of soil namely; sandy, silt, clay, and loamy all are defined according to their constituents. The relative percentages of sand, clay, and silt define the texture of the soil. Table 2.3 shows the types of soil.

**Table 2.3 Types of Soil (Source: Gillaspy, 2019)**

SN	Type of Soil	Formation	Characteristics
1.	Sand	The breakdown of rocks such as quartz, limestone, and granite	Particle size: 0.07 mm to 2 mm Texture: coarse
2.	Silt	Silt is formed when water and ice erode (or wear away) rock.	Particle size: 0.005 to 0.07 mm Texture: loose and smooth
3.	Clay	Contact of minerals form where rocks with water, air, or steam	Particle size: 0.005 mm Texture: fine
4.	Loamy	Combination of clay, loam, and silt with organic matter	Particle size: 0.002 to 0.05 mm Texture: coarse

### 2.4.3 Soil pH

The term "soil response" refers to the pH of the soil. It is a extent of the soil's acidity or alkalinity. Soil pH can range from 2.5 to 10, indicating a wide range of acidity. A pH of 5 or less can cause rapid corrosion and impulsive pitting of metallic items, whereas a neutral pH of around 7 is preferred to reduce the risk of damage. Rainfall can also change the soil's intrinsic pH level (Arbabi, 2018). Extremely high alkalinity diminishes soil resistivity and surges soil corrosivity, according to experimental findings, whereas mild alkalinity resists corrosion for longer. In addition, soils with a pH of 5 (acidic) or lower might cause rapid corrosion (Oyubu, 2015).

## 2.5 Soil Resistivity

Soil resistivity is a feature of soil that determines how conductive it is to effective earth currents (Siow *et al.*, 2012). Because current conductivity is equal to resistivity's reciprocal, this parameter should have as low a value as feasible. It can also be defined as a measurement of the capacity of the ground to carry an electrical current, which is crucial for building an earthing system. The system establishes a secure link between an electrical circuit and the ground, allowing electrical faults to be dissipated, lightning strikes to be grounded, and electrical equipment to function properly (Murad, 2012).

Because soil resistivity is a unique key characteristics that defines earthing impedance, it has an impact on the design of an earthing system. Soil resistivity determines how high or low an earthing electrode's resistance and impedance are, as well as the depth to which an earthing electrode is installed and the sort of configuration of an earthing electrode (Gomes *et al.*, 2013). To obtain the most cost-effective grounding installation, locate the location with the lowest soil resistance.

One primary variable impacting resistance to the earth of an electrode system is the term "earth resistivity," which is expressed in ohmmeter or ohm-centimetre. To assess the electrode earth resistance, the definite value of earth resistivity does not need to be measured. The kind of soil, salt concentration, moisture content, and temperature all affect soil resistivity (Naxakis *et al.*, 2018). Earth electrodes are unsuccessful with icy and very dry soils because they are good insulators with high resistance. The goal of resistivity testing is to collect a set of measurements that may be inferred to provide an equivalent model of the earth's electrical performance as viewed by the earthing system in question. (Akwukwaegbu and Okwe, 2017),

There are numerous factors which characterise soil resistivity, (Kouchaki, 2017) namely

- a. Moisture content;
- b. Temperature;
- c. Environmental factor;
- d. Type of earth;
- e. Stratification: soil layers of various sorts (loam backfill on a clay foundation);
- f. Moisture content; when moisture content rises, resistivity drops rapidly; however, after a rate of around 20%, the rate of reduction is substantially slower. It is uncommon to find soil with a composition of more than 40%;
- g. Temperature; extreme soil temperature and drought, or temperatures below freezing point increase soil resistivity. Above the freezing point, the effect on earth resistivity is virtually negligible;
- h. Chemical position and concentration of dissolved salt;
- i. Presence of metal and concrete pipes, tanks, bulky slabs, cable ducts, rail tracks, metal pipes;
- j. Topography; rough topography has a similar influence on resistivity measurements as weathering and moisture-induced local surface resistivity change;
- k. Seasonal variation circumstances that alter the distribution of moisture content in the soil alter the soil resistivity in the same way.; and
- l. Current magnitude; The thermal characteristics and moisture content of the soil determine whether a certain current size and duration will cause significant drying and so elevate soil resistivity..

### 2.5.1 Measuring Soil Resistivity

When discussing the electrical resistivity of soil, these main principles are used: When voltage is practical across the two ends of a wire, resistance is the property of the conductor to oppose electric current passage. The unit of measurement is the ohm ( $\Omega$ ), and the commonly used symbol is R. The renowned linear equation from ohm's law defines resistance as the fraction of the applied voltage (V) to the resulting current flow (I):

$$V = I \times R \quad (2.2)$$

where, V = Potential difference across the conductors (volts);

I = current flowing through the conductors in (amperes); and

R = resistance of the conductors in (ohms).

Low resistance conductors are good conductors, while high resistance conductors are lousy conductors. Insulators are extremely poor conductors. The resistance of a conductor is determined by the material's atomic structure or resistivity (measured in ohm-m or -m). The most frequent symbol for resistivity is " $\rho$ ". (Greek symbol Rho) (Oyubu, 2015). All grounding designs start with good soil models, which are created using precise soil resistivity testing. The resistance (R) of a conductor can be derived from the resistivity and vice versa as:

$$R = \rho \times L \times A \quad (2.3)$$

where,  $\rho$  = resistivity ( $\Omega$ -m) of the material;

L= length of the conductor;

A= cross-sectional area ( $m^2$ ); and

R= resistance of the material.

Resistivity ( $\rho$ ) is the resistance between the opposite faces of a cubic material having a side size of 1 m, as determined by equations (2.2) and (2.3).

#### *Basic formulae for measuring the electrical resistivity of the soil*

Electrical resistivity is calculated using four fundamental formulas. Current, current density, Ohm's law, and resistivity are the four concepts. The charge in coulombs over a time period in seconds determines current, with current denoted by "I" coulombs denoted by "q" and time denoted by "t" (Murad, 2012).

The amount of current flowing through a given region is mentioned to as current density. The current density is denoted by the letter "J" whereas the area is denoted by the letter "A".

The Ohms law is the equation (2.2) that describes the relationship between voltage, resistance, and current.

#### 2.5.2 Ways of Measuring Soil Resistivity

In choosing the test type of soil resistivity measuring technique, consider factors such as the maximum probe depth, the length of cables required, the effectiveness of the measuring technique, cost (decided by the duration and number of the survey crew), and ease of data interpretation (Arriba *et al.*, 2018). Wenner, the Driven Rod Method, and the Schlumberger Array Method are some of the existing approaches. If a current source of adequate power is

utilised, the Schlumberger array is considered more precise and cost-effective than the Wenner or Driven Rod approaches (Wenner *et al.*, 2010).

#### Wenner 4 pin method

A four-terminal instrument is used to measure earth resistivity. In a straight line, four tiny electrodes are driven down to the same depth and spaced equally apart (Figure 2.9). As depicted, four independent lead wires link the electrodes to the instrument's four terminals. As a result, this test is known as the four-terminal approach. The Wenner method, invented by Dr Frank Wenner of the US Bureau of Standards in 1915, is used in the following measuring procedure (Wenner *et al.*, 2010). Per the Wenner 4pin method, the average soil resistivity is given as:

The following is the formula:

$$r = 2\pi d R \quad (2.4)$$

where,  $r$  = the average soil resistivity to depth  $A$  in ohm-cm;

$\pi = 3.1416$ ;

$d$  = the distance between the electrodes in cm; and

$R$  = the measured resistance value in ohms from the test instrument.

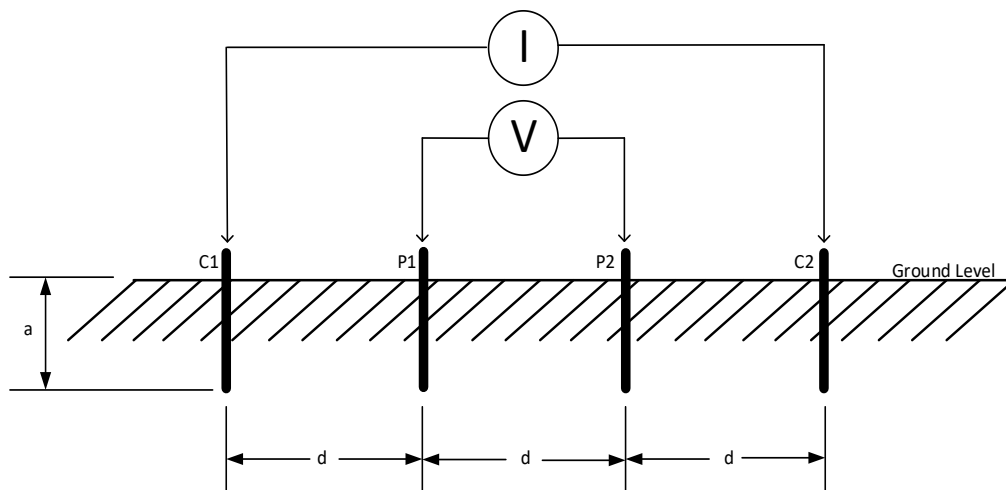


**Figure 2.8 Wenner's Arrangement**

*The schlumberger method:* is based on the same notion of measuring. The only variation is in the electrode placement; the distance between the two outside stakes is  $2d$ , whereas the distance between the two inner stakes is " $d$ ." When it comes to the labor necessary to do the operation, Wenner *et al.* (2010) noted that this soil resistivity testing method is more cost-

effective than the Wenner 4 Probe Test. For each shift of the inner electrode, the outside It is possible to move the electrode four or five times.

This method saves a lot of time in the field, especially when you need to take numerous soil resistivity measurements for a terrain profile. The extra time saved is due to the fact that just the two outer electrodes must be moved, whereas the Wenner approach requires all four electrodes to be moved at the same time. Despite the fact that the Schlumberger approach saves time, the Wenner method is more frequently known and employed. The Schlumberger Array is depicted in Figure 2.9.

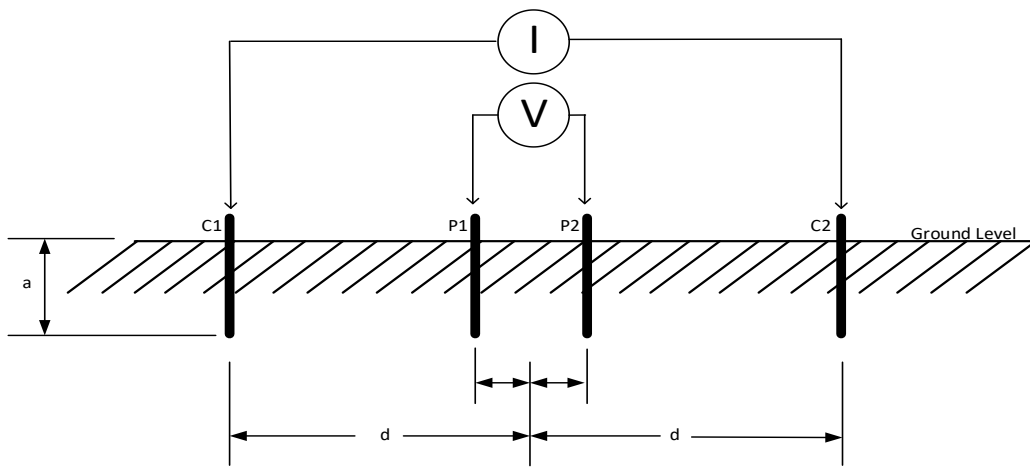


**Figure 2.9 Schlumberger Array (Hasan, 2017)**

*The driven rod method:* This method saves a lot of time in the field, especially when you need to take numerous soil resistivity measurements for a terrain profile. The extra time saved is due to the fact that just the two outer electrodes must be moved, whereas the Wenner approach requires all four electrodes to be moved at the same time. Despite the fact that the Schlumberger approach saves time, the Wenner method is more frequently known and employed. The Schlumberger Array is depicted in Figure 2.9. (2.5).

$$\rho = \frac{2\pi l R}{8l \ln \frac{d}{a}} \quad (2.5)$$

where,  $l$  = length of the driven rod in contact with the earth; and

$d$  = driven rod diameter.

Figure 2.10 shows the Drive Rod (3 Pins) Method (Wenner *et al.*, 2010).



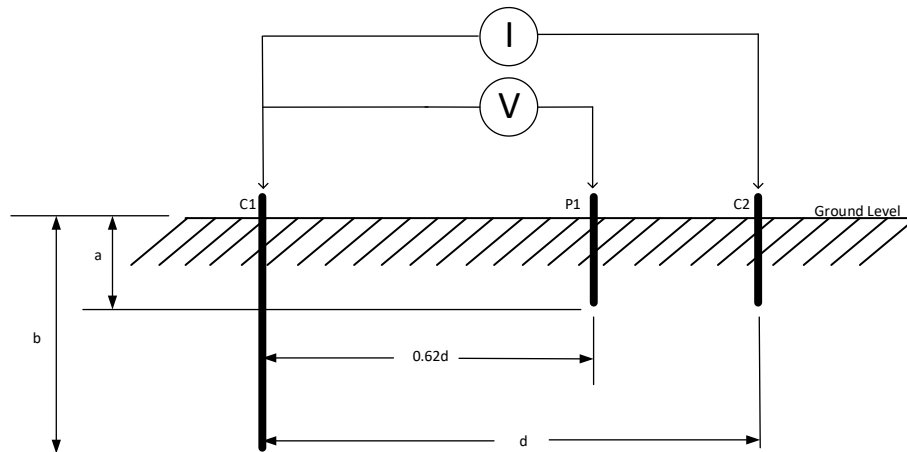


**Figure 2.10 Drive Rod (3 Pins) Method**

## 2.6 Corrosion

Corrosion occurs when a metal deteriorates as a effect of chemical reactions between the material and its surroundings (Bell, 2017). It converts a polished metal into a chemically further stable (natural) state, such as oxide, hydroxide or sulphide. It is the continuing disintegration of materials (metals) as a result of chemical and/or electrochemical interactions with their surroundings. Corrosion would be discussed in terms of its sources, effects, and preventative actions.

Corrosion is traditionally characterised into eight types based on the morphology of the outbreak and the type of environment to which the material is visible.

### 2.6.1 Corrosion Phenomenon

Corrosion phenomena have been grouped into two concerning this research. The general or surface corrosion has been described followed by underground corrosion, also termed as corrosion in soil.

#### *Surface corrosion*

Although the concept of corrosion has been generalised, there is the need to elaborate on corrosion that takes place in the soil and surface too. Corrosion of steel can be well-thought-out as an electrochemical process that takes place in stages. Groysman (2010) pointed that for corrosion to occur, four elements, an anode, a cathode, an electrolyte, and a conductor need to be present. These elements were defined as follows: the anode is a positively charged electrode and an example is a metal. The cathode is a negatively charged electrode and an example is oxygen. An electrolyte is a continuous conductive liquid path and water

was its example. Lastly, a conductor, which is a material to carry electrons from the anode to the cathode.

The initial attack that leads to corrosion starts in anodic spots on the metal's surface, where ferrous ions dissolve. Electrons are freed by the anode and move through the metallic structure to nearby cathodic sites on the surface, where they react with oxygen and water to create hydroxyl ions. The newly created chemical combines with ferrous ions from the anode to form ferrous hydroxide, which is then reacted in the air to form hydrated ferric oxide, also identified as red rust. Equations (2.6) to (2.8) can be used to show the reactions outlined above (2.10).

However, polarisation effects in the form of the formation of corrosion products on the surface lead the corrosion progression to be suppressed after a period of time. New reactive anodic sites are frequently produced, allowing for more corrosion (Bensaada *et al.*, 2013). In this situation, the loss of metal is consistent across the surface over time, and this is referred to as 'general corrosion' (Rothwell, 2014). The rusting phenomenon is depicted in Figure 2.11.

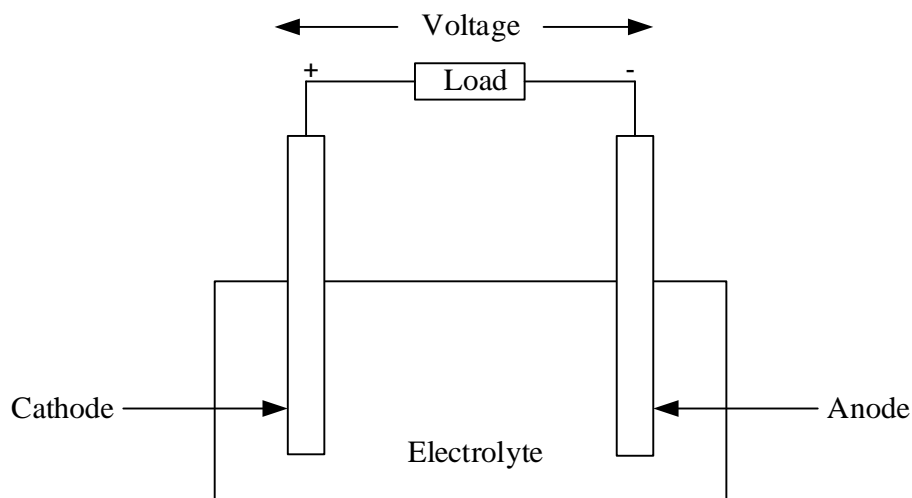
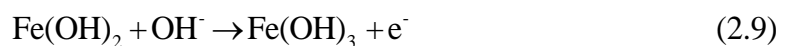


**Figure 2.11 A Schematic Representation of Corrosion Mechanism**





### *Corrosion in the soil*

Metals in contact with soil bring about corrosion of all kinds depending on the type of metal and soil. Soil corrosion refers to the corrosion of ingredients of different compositions, soil properties, and soil corrosion factors, mainly, soil chemical properties, physical properties, and electrochemical properties (Wang *et al.*, 2014). Like surface corrosion, anode, cathode, and electrolyte play a major role for corrosion to take place in the soil. Here, the soil acts as the anode, electrolyte, and cathode at the same time. However, the anodic part becomes the most conductive part, the cathode being the less conductive part. The metal serves as the required contact for the formation of a corrosion cell. The current has to go through a complete cycle. This means that it travels through the ground to its anodic area before returning to its cathodic area. Once that is accomplished, it flows through the metal to its cathodic area then back to the anodic end of the metal to complete the circuit. Corrosion occurs at the anodic location, where the metal's current has been discharged into the ground. Arriba *et al.* (2018) defined oxidation as the gain of oxygen and reduction as the loss of oxygen. Oxidation occurs at the anodic area, hence, corrosion whilst the opposite (reduction) occurs at the cathodic side forming protection around the metal (Arriba *et al.*, 2018).

### *Conditions contributing to underground copper corrosion*

Noble metals are corrosion resistant regardless of the conditions in which they are found at any one moment. Copper, on the other hand, can be corroded by certain subterranean circumstances. Atypically aggressive soils, localised and long-line-type concentration cells caused by differences in soil composition, stray Direct Currents (DC) flowing in the ground, faulty design and workmanship, specific conditions produced by Alternating Currents (AC), thermogalvanic effects, and galvanic action linking dissimilar materials are examples (Myers and Cohen, 1987).

These are the characteristic of soils that are termed aggressive, hence, can induce corrosion (Wasim *et al.*, 2018):

- a. soil full of sulphates or chlorides or both together with poor drainage, high water; holding capacity and heavy annual rainfall of more than 76 cm;
- b. soil with a very low resistivity value less than 500 ohm-cm;

- c. soil containing huge quantities of organic matter (organic acids) and inorganic acids;
- d. combination of soils such as clay, sand, gravel, loam, and chalk; and
- e. soil containing a large number of ammonia compounds.

### 2.6.2 Types of Corrosion

There are several types of corrosion. The immediate category to be reviewed is to know whether corrosion is predictable, unpredictable but expected, and unpredictable. Corrosion is said to be predictable when the material for example a pipe or a vessel, is used at a given temperature and pressure, hence, expecting a particular type of corrosion to take place (Agyenim-Boateng, 2014). Instances like these permit preparations, such as monitoring, prediction, and maintenance mechanisms.

Agyenim-Boateng (2014) pinned that there are cases where these objects have been insulated but certain conditions lead to the degradation of the insulation. It is quite expensive to replace the insulation although prediction measures bring out the areas affected by corrosion. The corrosion caused here is called corrosion under corrosion and termed unpredictable but expected. The introduction of sand and other foreign materials into these objects leads to fast-acting corrosion. In the nutshell, it is worth noting that corrosion can take place at areas least expected, so, all measures need to be put in place in cases where they take place (Ward, 2015). Corrosion may also be classified into dry and wet corrosion (Paritosh, 2016) as shown in Figure 2.12.

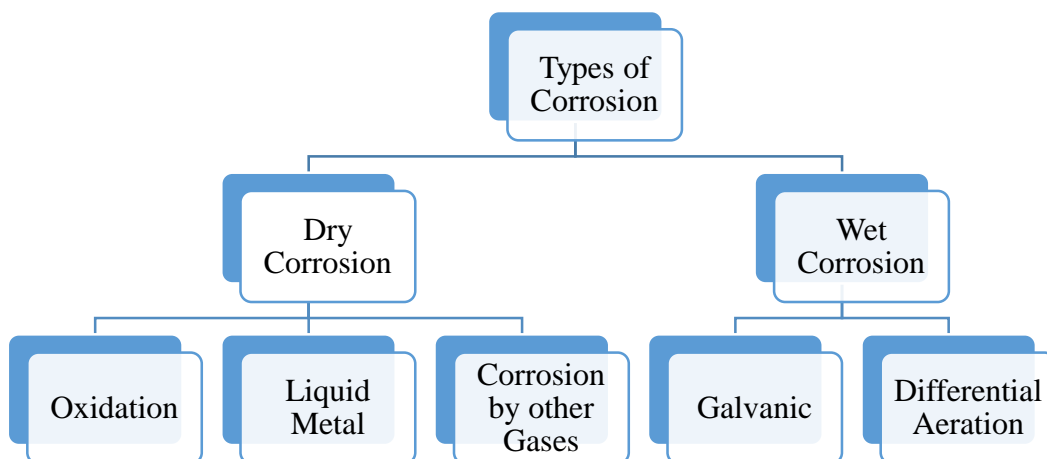


**Figure 2.12 Classification of Corrosion**

Dry corrosion, or chemical corrosion, is formed as a result of the direct chemical outbreak of metal surfaces by atmospheric gases, such as oxygen, halogens, nitrogen, and hydrogen

sulphide. The forms of dry corrosion are oxidation corrosion, which involves the direct attack at small or high temperature on metal surfaces in the nonexistence of moisture. Corrosion by other gases such as hydrogen is caused by its reaction with certain gases and the formation of a protective or non-protective layer on a metallic surface (Palanisamy, 2019).

The last type of dry corrosion, according to Palanisamy (2019), is liquid metal corrosion, which is induced by the high temperatures, the chemical action of flowing liquid metal on a solid metal or alloy. This type of corrosion can be found in nuclear-powered devices. The corrosion reaction involves either a liquid metal suspending a solid metal or a liquid metal penetrating the solid metal from within. The solid metal fails due to these two forms of corrosion.

Zarras and Stenger-Smith (2015) dealt with wet corrosion and observed that it is caused by the movement of electrons from the metal surface anodic area headed for the cathodic area over a conducting solution Galvanic corrosion, also known as bimetallic corrosion, is a type of wet corrosion in which different metals, such as zinc and copper, are electrically linked and exposed to an electrolyte, with the metal higher in the electrochemical series corroding (Paritosh, 2016). Differential aeration corrosion, also known as concentration cell corrosion, is a kind of corrosion in which the electrochemical attack on the metal surface is visible to an electrolyte with variable concentrations or aeration. It happens when one area of a metal is exposed to a different amount of air than the other. This results in a difference in potential between locations with differing levels of aeration. Poorly oxygenated areas have been discovered to be anodic in an experimental setting. Table 2.4 is the differences between dry and wet corrosion.

**Table 2.4 Differences between Dry and Wet Corrosion**

SN	Dry or Chemical	Wet or Electrochemical
1.	Is a gradual condition caused by a direct chemical attack by atmospheric gases such as oxygen, halogen, and nitrogen without the presence of moisture.	It is a fast non-uniform process that occurs due to an electrochemical attack in the presence of moisture

**Table 2.4 Cont'd**

SN	Dry or Chemical	Wet or Electrochemical
2.	It takes place on both homogeneous and heterogeneous surfaces, with corrosion products collecting at the point of corrosion.	It occurs only on heterogeneous metal surfaces at anode, but products accumulate near the cathode
3.	It is caused by the environment's direct chemical attack on the metal.	It is because a huge number of anodic and cathodic zones have formed.
4.	It works on the basis of adsorption	It occurs as a result of an electrochemical reaction.
5.	Its main feature is the creation of a mild scale on the iron surface.	The rusting of iron in a damp environment is one of its features.

(Source: Paritosh, 2016)


Another school of thinking believed corrosion to be divided into internal and exterior categories, but only in the context of pipes (Chen and Zhao, 2017). Dissolved oxygen corrosion, H<sub>2</sub>S corrosion, CO<sub>2</sub> corrosion, multiphase flow erosion-corrosion, and sulphate-reducing bacteria corrosion were the most common types of internal corrosion mentioned (Liu, 2013). The types of external corrosion that were pinned down were soil corrosion, casing corrosion, and erosion-corrosion.

Again, Sully and Taylor (1987) grouped corrosion into general, localised, metallurgical influenced, mechanically assisted, and environmentally induced cracking. A few of the various forms grouped are presented in pictures in Table 2.5 and Table 2.6.






**Table 2.5 Types of Corrosion and Examples**

<b>General Corrosion</b>	<b>Localised Corrosion</b>	<b>Metallurgically Influenced Corrosion</b>	<b>Mechanically Assisted Degradation</b>	<b>Environmentally Induced Cracking</b>
Uniform thinning dominated the corrosive attack. Atmospheric, Galvanic, Stray-current, General biology, Molten salt are some examples. Liquid metal Corrosion with high temperatures.	Metal penetration rates in specific locations are extremely high. Crevice, for instance, is an example. Filiform, Pitting and biologically localised	Alloy chemistry and heat treatment have an impact. Intergranular and Dealloying are two examples.	Corrosion in the presence of a mechanical component. Erosion, Fretting, Cavitation, Water Drop Impingement, and Corrosion Fatigue are some examples.	Corrosion-induced cracking in the presence of stress. Stress – Corrosion Cracking (SCC), Hydrogen Damage, Liquid metal embrittlement, and Solid metal-induced Embrittlement are some examples.

**Table 2.6 Summary of Types of Corrosion and Examples**






<b>SN</b>	<b>Example</b>	<b>Types of Corrosion</b>
1.		<p>Uniform Corrosion</p> <p>It usually happens as a result of direct chemical attacks.</p>

**Table 2.6 Cont'd**

SN	Example	Types of Corrosion
2.		<p><b>Galvanic Corrosion</b></p> <p>When two unlike metals come into touch with each other, an electrochemical reaction ensues.</p>
3.		<p><b>Concentration Cell Corrosion</b></p> <p>When two metal surfaces collide with differing concentrations of the same solution, this phenomenon occurs.</p>
4.		<p><b>Pitting Corrosion</b></p> <p>A brand of localised corrosion that occurs when corrosion products accumulate beneath the surface, resulting in pits.</p>
5.		<p><b>Crevice Corrosion</b></p> <p>When metals come into touch with non-metals, something happens. Corrosion is usually limited to a single localised area on a single metal and is triggered by concentration gradients (owing to ions or oxygen).</p>
		<p><b>Filiform Corrosion</b></p> <p>It happens on painted surfaces as a result of moisture in the form of filaments penetrating coated surfaces.</p>



**Table 2.6 Cont'd**

SN	Example	Types of Corrosion
7.		<p><b>Intergranular Corrosion</b></p> <p>It occurs when a metal or alloy is attacked locally at the edge and near to the grain boundaries. It causes the alloy to dissolve.</p>
8.		<p><b>Stress Corrosion Cracking</b></p> <p>Applied loads, residual stresses, or a combination of both cause it.</p>
9.		<p><b>Corrosion Fatigue</b></p> <p>Owing to the simultaneous united effects of cyclic stress and a specific corrosive media, a peculiar case of stress corrosion occurs. The result is a brittle mechanical fracture.</p>
10.		<p><b>Fretting Corrosion</b></p> <p>Vibrational motions cause fast corrosion at the interface of heavily stressed metal surfaces.</p>
11.		<p><b>Erosion Corrosion</b></p> <p>It happens as a result of a chemical environment combined with high fluid-surface velocities..</p>

(Source: Bell, 2017)

### 2.6.3 Causes of Corrosion

Physical, chemical, electrochemical, and microbiological factors all have the potential to induce corrosion (Palou *et al.*, 2014).

*Physical corrosion:* Impact, tension, or fatigue of the material produce this. Chemical corrosion is induced by gases such as oxygen, sulphur, fluorine, chlorine, or other gases acting directly on the metal under favourable environmental circumstances.

*Electrochemical corrosion:* This is a natural procedure that requires the presence of anodic and cathodic zones, as well as an electrolyte. There must also be electrical connection between the anodic and cathodic zones.

*Microbiological corrosion:* This is the corrosion of a metal as a result of its use of microorganisms such as bacteria and algae, either directly or indirectly. These microorganisms are dropped on the metal, creating a "living" area, where they need nitrogen, oxygen, hydrogen, and/or carbon from the environment to carry out their metabolic processes, producing metabolites that can be deposited on the metal, increasing corrosion. Corrosion can occur in a diversity of media, including natural water, seawater, petroleum products, and oil emulsions (Shreir, 2010).

### 2.6.4 Factors That Affect the Rate of Corrosion

The type of corrosion is influenced by the environment, corrosion protection effect, steel pipe material and manufacturing method, and stress level (Chen and Zhao, 2017). An anode (+), a cathode (-), a metallic conductor and an electrolyte are the four essentials required for corrosion to occur and are together referred to as the corrosion cell (Bell, 2018). The rate of corrosion is affected by changing the electrolyte's potency. Oxygen concentration, temperature, chemical salts, humidity, pollutants, pH of the medium, nature of the metals, ratio of cathodic to anodic regions, and type of the corrosion product are all elements that influence corrosion rates.

*Oxygen:* Corrosion is accelerated by oxygen, just as it is by water. Although corrosion can occur in an oxygen-deficient environment, the pace of corrosion and metal loss is often substantially slower (Sahoo *et al.*, 2017). When an electrolyte is in touch with one region of metal that contains more oxygen than the electrolyte in contact with another area of metal in submerged conditions, the greater oxygen-concentration area is cathodic in comparison

to the remaining surface. The formation of an oxygen concentration cell results in speedy corrosion regions, and type of the corrosion product.

*Temperature:* Because corrosion reactions are electrochemical and often increase with rising temperature, corrosion occurs faster in warmer surroundings than in cooler ones, according to Popov (2015).

*Chemical salts:* Chemical salts accelerate corrosion by increasing the electrolyte's efficiency (conductivity). Sodium chloride, a major component of saltwater, is the most prevalent chemical salt. When sodium chloride is placed on atmospherically exposed surfaces, it behaves as a hygroscopic substance, absorbing moisture from the air and causing corrosion in non-immersed areas (Czichos *et al.*, 2011).

*Humidity:* Humidity and time-of-wetness are important factors in encouraging and speeding up corrosion rates (Schindelholz and Robert, 2012). The time-of-wetness refers to how long an atmospherically exposed substrate has adequate moisture to support the corrosion process. Corrosion is more prone to occur in a wetter climate.

*Pollutants:* Corrosion is promoted by acid rain (a chemical by-product from manufacturing and processing plants) and chlorides, which are usually prevalent in coastal areas (Alcántara *et al.*, 2017). Acid gases, such as carbon dioxide, can dissolve in a moisture coating on a metal surface.

*pH of the medium:* According to Ismail *et al.* (2014), Corrosion occurs more quickly in acidic pH than in neutral and alkaline pH. In the case of iron, a protective covering of iron oxide forms at a relatively high pH, preventing corrosion. At low pH, however, significant corrosion occurs. However, even at high pH, the corrosion rate of metals like aluminum is substantial.

*Nature of the metals:* Metals with greater electrode potentials, such as gold, platinum, and silver, do not corrode easily, according to Sunil (2020). Metals having lower electrode potentials, such as zinc, magnesium, and aluminum, are more susceptible to corrosion. When two metals with a large electrode potential difference come into contact with each other, the bigger the electrode potential difference, the greater the rate of corrosion. The potential difference between iron and copper, for example, is 0.78 V, which is higher than the potential difference between iron and tin (0.3 V). As a result, when iron comes into touch with copper, it corrodes faster than when it comes into contact with tin. As a result, if

possible, the usage of dissimilar metals should be avoided (Prabhakar and Goswami, 2019). For instance, a bolt and nut or a screw and washer should be used together.

*The ratio of cathodic to the anodic region:* The magnitude of the cathodic to anodic area has an impact on the rate of corrosion. The corrosion rate is extremely high if the metal has a tiny anode and a big cathodic area. The corrosion rate increases as the ratio falls. This is because electrons are liberated at the anode and consumed at the cathodic region (Krishnamurthy *et al.*, 2019). The freed electrons are quickly consumed at the cathode if the cathodic area is greater. This accelerates the anodic reaction, resulting in a higher overall rate of corrosion. Corrosion is more quick and severe when two different metals come into contact. Also, if the anodic area is tiny and the cathodic region is vast, examples include a modest anodic area and a big cathodic area are both present.

*Nature of the corrosion product:* If the corrosion product, such as metal oxide, is stable, insoluble, and nonporous, it may operate as a protective coating. If it works as a protective coating, it functions as a barrier between the metal surface and the environment and the corrosion medium, preventing additional corrosion. If the corrosion product, on the other hand, is unstable, porous, and soluble, it accelerates corrosion (Krishnamurthy *et al.*, 2019). Metals like aluminium, chromium, and titanium, for example, are very passive in oxidising situations because their oxides as corrosion products form protective layers on the metal surface, inhibiting further corrosion. When exposed to an oxidising atmosphere, metals such as iron, zinc, and magnesium, for example, do not develop a protective coating and are particularly prone to continual corrosion (Moudgil, 2015).

#### 2.6.5 Corrosion Detection Devices

Identifying or detecting corrosion without excavation or laboratory analysis has been a major drawback in corrosion research. There is no ideal method for detecting corrosion, although, that method should be able to give an accurate, reliable, and useful data about the condition of an object for easy examination and implementation. The most widely used assessment methods are Non-Destructive and External Corrosion Direct Assessment (ECDA) (NACE 0502-2008). ECDA is a field assessment with strategic steps for evaluating the integrity of buried metals. This method is usually utilised to exhibit areas prone to corrosion or already undergoing external corrosion. ECDA includes four steps: pre-assessment, indirect assessment, direct assessment, and post-assessment (Smith and Barret, 2006). Automated ultrasonic mapping systems, digital radiography imaging devices,

infrared imaging, and eddy current mapping systems are all prevalent equipment (Howard *et al.*, 2004). Table 2.7 gives the various corrosion detection methods, their uses, advantages, and disadvantages.

**Table 2.7 Detection Methods and their Uses**

SN	Non-destructive Examination Methods	Description	Uses/Advantages	Disadvantages
1.	Visual Inspection	It is the primary and commonly used method. It requires the use of eyes and hands for a touch and other devices such as borescopes and video camera	Used by pilots for inspection of aircraft before take-off	Time-consuming and requires good vision, proper illumination, and familiarity of the examination area.
2.	Ultrasonic Inspection	Use of high-frequency sound waves of 0.2 MHz for its methodology. It consists of a transducer, receiver, and display device	Measurement of thickness, length, and detection of objects such rods, concrete for cracks or pitting and corrosion	The inability to the detection of localised and internal corrosion.
3.	Radiographic Inspection	Requires the use of recording devices and photostimulable plates for filming. Usually used in the petrochemical industry	Its image gathering devices, the most authentic of all ways, may be enhanced, saved, and retrieved.	The use of dangerous ionising radiation in a form of x-rays, neutrons, or gamma rays. Its high cost and the need for all sides to be inspected for results.

**Table 2.7 Cont'd**

<b>SN</b>	<b>Non-destructive Examination Methods</b>	<b>Description</b>	<b>Uses/Advantages</b>	<b>Disadvantages</b>
4.	Eddy Current Inspection	Finds its use in the aerospace industry	Authentic and less expensive, sorting and measuring coating of materials, aluminium aircraft skins	Works with current so cannot be used for non-conductive materials
5.	Electromagnetic Acoustic Transducer (EMAT)	Induction of ultrasonic waves in metals without a medium. Use of magnetometers and electrometers	Suitable for pipes of high temperatures of 500 °C. Detection of erosion, pitting, and cracks	Need to access the object from all sides
6.	Thermographic Inspection	Use of infrared for inspection	Location of hot spot defects, determination of process liquid levels in towers and columns, portable	Exposure of the electronic components to be scanned can be hazardous.
7.	Ground Penetrating Radar	Operates with 3-dimensional in both hardware and software	Needs just a surface for detection, safer and less expensive than radiography	Costly, time-consuming and requires very intense training

**(Source: Farid, 2012)**

#### 2.6.6 Corrosion Monitoring Techniques

The three main techniques that were used decades ago under conventional methods for monitoring corrosion were visual, microscopic observation, and gravimetric. Because the optical technique cannot measure quantitatively, and the weightless method is tedious and time-consuming, a superior methodology known as an electrochemical technique emerged, which could only make available information on the metal's condition and corrosion rates. Corrosion potential mapping, concrete resistivity measurements, electrochemical noise

(non-perturbative methods), polarisation technique, and impedance measurement (perturbative methods) are all electrochemical approaches (Revie and Uhlig, 2008).

#### *Methods of estimating corrosion in soils*

There are two types of corrosion estimation methods: electrochemical and non-electrochemical. With the electrochemical system of estimation of corrosion, voltage and current are the main parameters considered but, in most cases, impedance and electrochemical noise are not left out (Bullard *et al.*, 2003). Three parameters, i.e., voltage, current, and impedance, are of importance here. Voltage refers to the observed corroding electrode voltage in an electrolyte open circuit, current refers to the changes that occur in the corrosion process and its properties, and impedance refers to the resistance to current flow (Baboian, 2005). Examples of electrochemical methods include conductivity and electrochemical methods.

Unlike the electrochemical method, non-electrochemical data concentrates on the direct assessment of buried rod corrosion using samples in specific terrains or simulated settings in the laboratory or a genuine field investigation. The most common non-electrochemical method is the mass loss and localised corrosion. Mass loss simply involves burying a weighed rod into the ground for a while, then removing it from the ground to measure the weight again to know the difference in weight. The localised corrosion involved the comparison of quantitative and qualitative measurements of the soil characteristics to predict corrosion (Haynes, 1985).

The two methods, electrochemical and non-electrochemical methods, can predict corrosion from their sources through two means, i.e., qualitative and quantitative methods. The qualitative method gives the prediction of future corrosion without the use of numerical values. This method depends solely on the main variables defined by the corrosion prediction process. It is accompanied by disadvantages such as its simplicity using tables and diagrams to summarise results for easy formatting and measurement (Arriba-Rodriguez *et al.*, 2018). Another characteristic of the qualitative method is the use of parameters with soil corrosion. The parameters that have been used so far are soil resistivity, pH, potential, and redox power (Cole and Marney, 2012).

Roberg (2016) summarised the work developed by the American Iron and Steel Institute on an extensive soil evaluation in Europe which resulted in the emergence of other parameters such as water content, groundwater, horizontal and vertical homogeneity, buffering

capacity, and some sulphates. The recent approach in the qualitative method is the use of a model called the Decision Model (Arriba-Rodriguez *et al.*, 2018). This model allows the entering of appropriate points on a graph according to some of the mentioned parameters to reach an intersection that establishes corrosion mitigation recommendations.

The quantitative method, unlike the qualitative, has its main feature being its ability to assess corrosion of buried structures using numerical values. Of all research works on the use of quantitative methods, Romanoff's studies conducted on corrosion of steel in different soil types for the National Bureau of Standards of the United States of America (USA) from 1910 – 1955 remains the most important as a result of the many samples on different soil types, different metal samples and the duration the rods had to stay buried (Ricker, 2010). Some deficiencies came up, which included unrepresentative values for some variables, different depths of burial, and poor statistical design of the experiments. The mass loss method is used to evaluate the corrosion that took place.

It ought be eminent that Stratful in 1961 used resistivity and pH parameters in a model to compare with the weightless method. His work's limitation was that the parameters were quite a few (Wang *et al.*, 2015). Overall, there are two approaches to quantitative methods: those based on field studies or tests, and those based on models through experiments in simulated environments (Allahkaram *et al.*, 2015).

#### 2.6.7 Analytical Techniques for Corrosion Phenomenon

Most aspects of corrosion have been treated except for its laboratory analysis. Although non-destructive methods have been treated, other aspects need to be considered. This area deals with the surface morphology, chemical composition, micro-chemical structure of the corrosion products or samples, and other materials, which are studied employing Scanning Electron Microscopy (SEM), Optical Microscopy (OM), Energy Dispersive Spectrometry (EDS), X-ray Fluorescence (XRF), X-ray Diffraction (XRD) and Micro-Particle Induced X-ray Emission (Olise *et al.*, 2017). Some of these techniques are discussed touching on the history, principles, uses, advantages, and disadvantages.

##### *X-ray fluorescence*

Wirth (2019) described an XRF spectrometer as an x-ray instrument for the sole purpose of non-destructive chemical analysis of materials in the form of rocks, minerals, metals, and sediments. XRF determines the quantitative and qualitative analysis of unknown samples



either after their preparation or not to enable accurate matrix corrections. Its range of detection varies from for heavier elements of 0.5 ppm and 100 ppm for lightest elements. XRF is restricted to giving the chemical composition of the sample eliminating the phases that are present in the sample.

*Principles of XRF:* XRF shares common principles with other instruments that utilise the interaction between electron beams and x-rays with samples. The behaviour of atoms interacting with radiation makes it possible for the analysis of samples with x-ray fluorescence. Materials become excited once they reach their high energy where they are ionised (Weltje and Tjallingii, 2008).

*Uses:* The elemental composition of samples is determined using XRF. Depending on whether energy dispersive or wavelength dispersive techniques are used, XRF can distinguish the presence of elements stretching from sodium or beryllium to uranium by percentage or parts per million. Soil surveys, ceramic and glass manufacture, metallurgy, and environmental studies are among its many uses (analyses of particulate matter on air filters). Finally, XRF can analyse the elements in almost any sample as long as it has a surface on which to redirect the x-ray beams while maintaining mathematical validity (Ikechukwu *et al.*, 2014).

*Strengths:* Oyedotun (2018) commented on the investigations that displaced bulk chemical analyses of major elements such as Silicon, Aluminium, Magnesium, Manganese, Calcium, and Phosphorus and trace elements such as Copper, Zinc, Chromium, Cerium, Cobalt, and Niobium in rock and sediment. It is simple to use, systematic and gives fast sample preparation.

*Limitations:* A major drawback of XRF is its inability to give an accurate measure of the sample as a metal. It cannot differentiate the distinctions amongst isotopes of an element and also ions of the identical element in different valence states (Loubser and Verryin, 2008).

### *X-ray diffraction*

*History:* XRD is older than XRF and was brought to light in 1912. Eckert (2012) showed that for x-ray wavelengths, crystalline solids act as three-dimensional diffraction gratings with plane spacing related to that of a crystal lattice (Shabalin, 2016). It indicates phases, measures, and shows the amount of the metal or minerals and their species in the sample.

*Uses:* The crystalline structure of samples is determined using the diffractive design of an x-ray beam. XRD can reveal the crystalline configuration and specific crystalline phases that form at different temperatures, possibly indicating anthropogenic firing practices, through spectrum identification of the collective intensity and interference of the crystalline structure. It's also utilised to figure out which crystalline phases and polymorphic forms are present in a given sample (Manso *et al.*, 2011).

*Disadvantages:* Shabalin (2016) concluded that;

- a. XRD's capacity to classify stone, metals, ceramics, opaque glasses, and opaque glazes is limited to biological materials.
- b. When it comes to archaeological analysis, XRD has a number of drawbacks. Because the approach is destructive, certain critical or diagnostic samples are instantly ruled out of consideration.
- c. XRD's capabilities with organic materials, which are frequently encountered in archaeological contexts, are likewise limited (Wolf, 2012).

#### *Relationship between XRF and XRD*

Michaud (2017) analysed the relationship between XRF and XRD. XRD and XRF are two analytical techniques that utilise x-ray technology for detection, process control, screening metals and alloys exhibiting differing methods and results. They share similarities such as the use of x-ray source and detector, degree of the response to x-rays interacting with substances. Their difference is that XRF is typically a non-destructive technique whilst XRD entails a powdered sample to diffract an x-ray beam, which in some situations necessitates sample obliteration. Smith (2010) further points out that XRF deals with elemental analysis like iron and calcium, whereas XRD works with compounds like  $\text{Fe}_2\text{O}_3$  and  $\text{CaCO}_3$ . The sample size for both procedures is constrained by the dimensions of the in-house XRF and XRD equipment. Despite this, the handheld XRF enables for the identification of a considerably greater spectrum of samples outside of the lab settings.

#### *Scanning electron microscopy/energy dispersive spectroscopy SEM-EDS*

*Description:* Energy Dispersive X-Ray Spectroscopy (EDXS) with Scanning Electron Microscopy (SEM) (EDS) The non-destructive grouping of high magnification microscopy (SEM) with elemental analysis is known as SEM-EDS (EDS) (Ebnesajjad and Ebnesajjad, 2014). Both methods can be used alone, but they are used to compare chemical compositions

between layers and to identify the constituents that make up a sample region. The SEM provides for a micron-level visual investigation of sample surfaces, whereas the EDS uses x-ray spectroscopy to assess elemental composition (Smith, 2010). While the SEM-EDS technique is non-invasive, the coatings and mountings mentioned can be quite harmful depending on how they are prepared. It appears that any sample smaller than 5 cm × 3 cm can be analysed as long as it is dead, dry, and conductive in some way (Smith, 2010).

*SEM:* This high-powered electron microscope can magnify objects up to 500,000 times (Kamnitsas *et al.*, 2017). SEM Analysis is more powerful than Optical Microscopy not only because to the higher magnification power, but also due to the greater depth of field.

*Principle of SEM:* SEM uses a high-energy concentrated ray of electrons to magnify a specific sample location. The sample is kept under vacuum to ensure that the electron beam remains focussed and does not collide with airborne particles. When an electron beam strikes a sample, secondary electrons are discharged from the sample, which are detected and used to create an image of the surface's topography. The Secondary Electron Detector (SED) and the Backscattered Electron (BSE) Detector are the most often utilised detectors. To form an image, electrons interact with the detector (Ng, 2015). A column structure of a standard SEM is shown in Figure 2.13. (Aharinnejad and Lametschwandtner, 1992). Electron source (gun), electron lenses, sample stage, and detectors are all key components of any SEM.

*Applications:* SEM is used by scientists in the composition and topography of both natural and artificial materials. In biology, it has aided in the study of microscopic organisms such as viruses and bacteria. Geologists use SEM to study crystalline structures. SEM is utilised to investigate the surface structure of products in industries such as microelectronics, semiconductors, medical devices, general manufacturing, insurance, and litigation assistance, and food processing (Mathias, 2015).

*Strength:* The SEM can analyse any organic or inorganic substance under specified conditions, is simple to use, and has a user-friendly interface (Swapp, 2017).

*Limitation:* Samples in a form of coal, organic materials, and samples beyond the size 10 cm are unsuitable for SEM Analysis (Swapp, 2017).

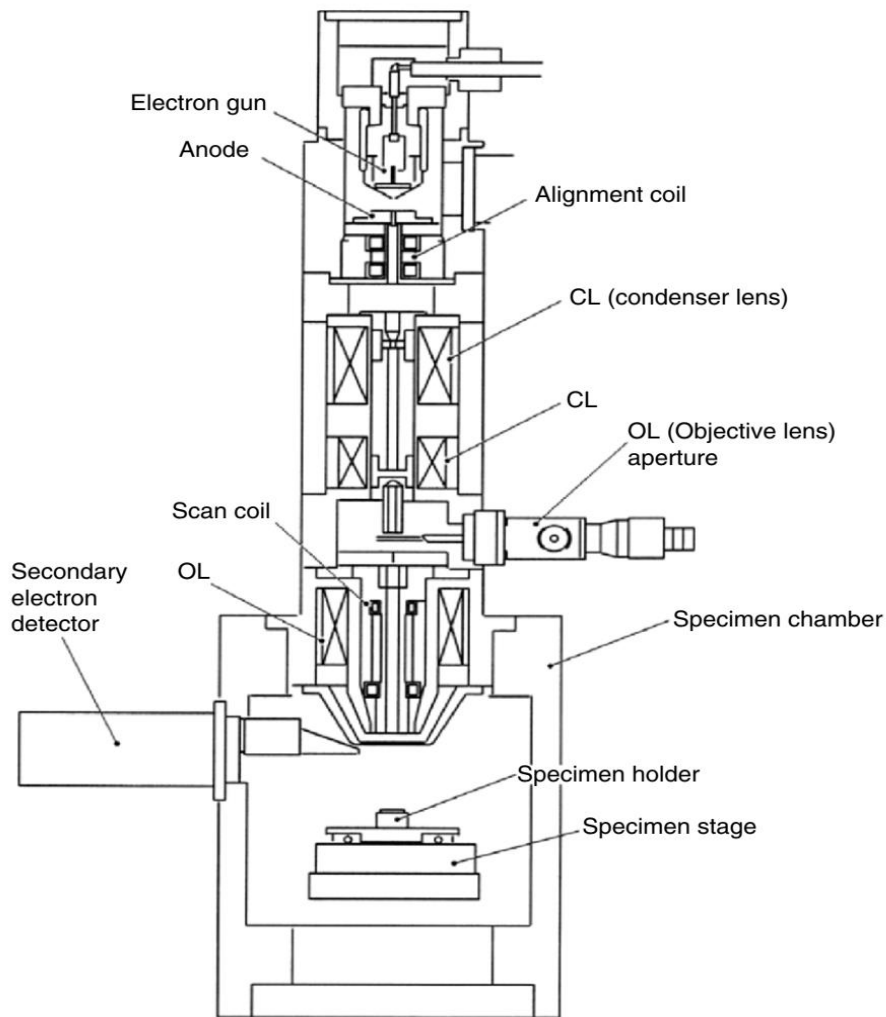


**Figure 2.13 A Column Structure of a Conventional SEM**

*Energy dispersive spectroscopy (EDS)*

The distinct x-rays of individual elements are separated into an energy spectrum using an energy-dispersive (EDS) detector, and the energy spectrum is analysed by means of EDS system software to calculate the abundance of specific elements (Swapp, 2017).

*Principle of EDS:* Using EDS, the sample region analysed with SEM analysis can be further examined to establish the exact elements that make up the sample region (Manso *et al.*, 2011). X-rays are also emitted from the sample's surface, each with a distinct energy signature that is specific to the elements present. The EDS detector detects these x-rays, providing elemental information about the material. EDS gives information on the sample's chemical composition as well as additional information on the features visible in SEM micrographs. SEM-EDS or SEM-EDX analysis is the name for this integrated technology (Ng, 2015).

Zhao *et al.* (2019) revealed that are dependent on the type of material and the information sought, samples involve various processing. Metals, in general, require little more than simple mounting (not necessarily in resin). To prevent electron beam distortion, non-metals must be glazed with a conductive substance (such as gold, graphite, or platinum). Samples are inserted in epoxy resin and refined to a flat surface if back-scattered detector imaging is needed.

Secondary electron pictures reveal the sample's surface texture in great detail. Based on the heterogeneity of the material, back-scattered electron pictures provide visual representations of compositional information (Febrero *et al.*, 2015). Energy dispersive x-ray spectroscopy (EDXRF) is a type of elemental analysis that is attached to the SEM and uses the same sample chamber as XRF.

*Strength:* In just a few seconds, the full elemental spectrum may be obtained, and it can be used in semi-quantitative mode to estimate chemical composition using a peak-height ratio relative to a standard (Swapp, 2017).

*Limitation:* Cases of overlaps among different elements are recorded. Similar to SEM, it cannot detect lighter elements below atomic number 11 (Smith, 2010).

#### 2.6.8 Effects of Corrosion

There are many harmful effects of corrosion (Arriba-Rodriguez *et al.*, 2018) including the following:

- a. Efficiency loss;
- b. Product contamination;
- c. Deterioration of metallic equipment;
- d. Inability to use metallic materials;
- e. Material losses, such as pipe blockages and mechanical damage to underground water pipes;
- f. Collisions caused by the mechanical failure of metal bridges, automobiles, and airplanes etc.;
- g. Pollutants are released as a result of corrosion products escaping; and
- h. Natural resource depletion (metals);

### 2.6.9 Prevention of Corrosion

Corrosion control comes into mind when discussing the prevention of corrosion which is the umbrella. Corrosion control is made up of inspection, monitoring, assessment, and prevention which have been discussed earlier in this chapter except the latter. Some ways of preventing corrosion are as follow:

#### *Cathodic protection*

Hu *et al.* (2014) Cathodic protection works by suppressing the corrosive current that damages a corrosion cell and forcing it to course to the metal structure that are necessitated to be protected. Corrosion and metal disintegration are thus avoided. Cathodic protection can be done in practice by means of one of two approaches, which varies subject to the source of the protective current. A sacrificial-anode system employs active metal anodes, such as zinc or magnesium, that are attached to the structure and offer cathodic protection.

The second technique of cathodic protection is known as impressed current protection (Popov, 2015). A power source is used to force current from inert anodes to the structure to be protected in an impressed-current system. This approach, which is commonly used to safeguard subterranean pipelines and ship hulls, necessitates the electrolyte receiving an alternate source of direct electrical current. The current source's negative terminal is coupled to the metal, while the positive terminal is connected to an auxiliary anode that completes the electrical circuit. Unlike a galvanic (sacrificial) anode system, the auxiliary anode in an impressed current protection system is not sacrificed.

#### *Coatings*

Metallic and non-metallic coatings are the two types of corrosion prevention coatings (organic and inorganic). The goal is the same with either type of coating: to protect the underlying metal from corrosive agents.

*Metallic coatings:* Cottis (2010) agreed to the fact that the idea of casing an active metal with a more noble metal using the noble metal's higher corrosion resistance. Tin-plated steel is one case in point of this application. Alternatively, a more active metal can be used, in which case the coating corrodes the substrate preferentially, or sacrificially. Galvanised steel is an example of this system, in which the sacrificial zinc coating corrodes differently and shields the steel.

*Organic coatings:* Organic coatings' principal purpose in corrosion protection is to insulate metal from corrosive environments. The organic coating can comprise corrosion inhibitors in total to establishing a barrier layer to prevent corrosion. There are numerous organic coating formulations available, as well as a number of application procedures to select from depending on the product situation (Yajima, 2015).

*Inorganic coatings:* Fayomi and Popoola (2019) mentioned that porcelain enamels, chemical-setting silicate cement linings, glass coatings, and linings, and other corrosion-resistant ceramics were some of the inorganic coatings that can be applied to the metal. Inorganic coatings for corrosion applications, like organic coatings, act as barrier coatings. Wear-resistant and heat-resistant ceramic coatings, such as carbides and silicide, are employed in these applications. Paints and other organic coatings shield metals against the metabolizing impacts of ambient gases. Coatings were categorised by the type of polymer used by Cottis (2010). Common organic coatings include alkyd and epoxy ester paints that stimulate cross-link oxidation when air-dried, multiple urethane, both acrylic and epoxy polymer radioactive material, vinyl, acrylic or styrene polymer latex, water-soluble, high-solid, and powder coatings.

### *Inhibitors*

Corrosion inhibitors are constituents that react with the metal's surface or the gases in the atmosphere that cause corrosion, halting the chemical reaction. Inhibitors function by adsorbing to the metal's surface and producing a protective layer. Dispersion techniques can be utilised to apply these substances as a solution or as a protective coating (Emran *et al.*, 2018). Inhibitors capable of slowing down corrosion depends on (Palnisamy, 2019):

- a. Altering the anodic or cathodic polarisation behaviour;
- b. Lessening the diffusion of ions to the metal's surface; and
- c. Increasing the electrical resistance of the metal's surface.

Petroleum refining, oil and gas exploration, chemical production, and water treatment services are all major end-use sectors for corrosion inhibitors (Fayomi and Popoola, 2019). Corrosion inhibitors have the advantage of being able to be implemented in-situ to metals as a remedial step to prevent unforeseen corrosion. Some chemical species (for example, salt) cause corrosion, while others inhibit corrosion. Inhibitors such as chromates, silicates, and organic amines are widespread (Palnisamy, 2019). Inhibition mechanisms can be fairly complicated. The inhibitor is adsorbed on anodic and cathodic sites and chokes the corrosion

current in the case of organic amines. Other inhibitors have a special impact on the anodic or cathodic processes. Others advocate for protective coatings to form on the metal surface. The use of inhibitors is preferred in closed systems, according to Boukerche *et al.* (2019), because the required inhibitor concentration is more easily maintained. The rising usage of cooling towers stimulated the development of new corrosion and biofouling inhibitor/water-treatment packages. Inhibitors can be used as a protective coating or as a primer for a protective coating. When there is a flaw in the coating, the inhibitor leaks out and controls the corrosion.

### *Design*

Many corrosion problems can be eradicated and the time and expenditure of corrosion maintenance and patch-up can be considerably reduced by using rational design principles. Corrosion most commonly occurs in dead spaces or fissures, where the corrosive environment has become more corrosive. These sites can be deleted or minimized throughout the design phase. The components can be constructed to operate at stress levels below the cracking threshold where stress-corrosion cracking is a possibility (Brycki *et al.*, 2017).

#### 2.6.10 Expressions and Measures of Corrosion

The corrosion rate is expressed using four different approaches (Khatak and Baldev, 2010).

##### *Material thickness reduction per unit time*

Thickness decrease per unit time is the most practical and intriguing metric. This measurement is commonly stated in millimeters per year in the metric system (Křivý *et al.*, 2016).

##### *Loss of weight per unit of area and time*

In the past, weight loss per unit area and unit time were frequently utilised, owing to the fact that weight loss was often the directly determined extent in corrosion tests (Heißing and Ersoy, 2011). Before and after exposure to the corrosion medium, the test specimens are weighed. On this basis, the thickness decrease might be calculated as weight loss per unit area/density (Schmitt, 2009).



### *Corrosion current density*

Heißing and Ersoy (2011) emphasised that when dealing with corrosion theory and electrochemical corrosion testing, corrosion current density was defined as a particularly acceptable metric of corrosion rate. The number of metal ions lost from the metal per unit area and unit time is known as the dissolving rate (corrosion rate). The electric current per area unit can be used to express the ion movement.

$$\text{anodic current density } (i_a) = \text{corrosion current density } (i_{\text{corr}}) \quad (2.11)$$

### *Electrical resistance method*

In comparison to the weight loss approach, electrical resistance measurement is a better technique. In this procedure, a coupon of material that is similar to the alloy whose corrosion rate is being studied is exposed to the corrodent and extracted at regular intervals to measure its weight loss, which is directly related to the corrosion rate. It works by increasing the electrical resistance of a corrosion coupon material that has been exposed to the elements. The process stream is exposed to a metallic conductor sensing probe, which is often a thick wire, strip, or tube made of the same material as the equipment under test. This probe's electrical resistance is related to that of a similar reference probe that is insulated from the corrodent. The electrical resistance of the exposed probe grows as it corrodes, and this change is related to the extent of corrosion.

## **2.7 Backfill Materials**

Conductive backfills otherwise known as Grounding Improvement Material (GIM), Ground Enhancing Material (GEM), Low Resistivity Material (LRM), or Ground Resistance Reduction Agent (GRRR), are materials needed to improve the resistance to ground of earthing electrodes in areas of poor conductivity. They reduce soil resistivity through conditioning the soil (Idoniboyeobu *et al.*, 2018). Soil conditioning is the act of evenly adding the right quantity of metallic salts into the soil to achieve the required conductivity. Some backfill materials are considered to be permanent while others are not.

Permanent backfill materials are materials that do not need to be replaced irrespective of how long the rod it is preserving stays in the ground. Examples are local wastes like coco peat and rice straw ashes and refined brands include Matrix, FurseCEM, Loresco, and Duval messien. The commonest brand used in Ghana is the Matrix and its products are active backfill compound ABC, bentonite compound, matconite, and bentonite powder (Anon.,

2019). The other types are known as temporary materials due to their leaching abilities. They include gypsum, coke powder, palm kernel cake, and tyre ash (Akoto, 2014). Figure 2.14 shows an installation of an earth rod with permanent backfill material (Anon., 2020). Table 2.8 is a summary of the chemical composition, resistivity values, and electrical conductivity of electrically conductive backfill materials, and 2.9 is a summary of some chemical properties of electrically conductive backfill materials.



**Figure 2.14 A Permanent Backfill Material Being Installed**

**Table 2.8 A Summary of the Chemical Composition, Resistivity Values, and Electrical Conductivity of Electrically Conductive Backfill Materials**

SN	Conductive Backfill Material	Chemical Composition	Resistivity Values of Backfill Material/ $\Omega\text{m}$	Electrical Conductivity
1.	Bentonite	Na <sub>2</sub> O(Soda), K <sub>2</sub> O (Potash), CaO (Lime), MgO (Magnesia), Feldspar, Biotite, Crystalline quartz, Cristobalite, Kaolinite, Volcanic glass, Organic matter, Gypsum, Pyrite and Montmorillonite	2.5 - 5	High

**Table 2.8 Cont'd**

<b>SN</b>	<b>Conductive Backfill Material</b>	<b>Chemical Composition</b>	<b>Resistivity Values of Backfill Material/<math>\Omega</math>m</b>	<b>Electrical Conductivity</b>
2.	Gypsum	CaSO <sub>4</sub> , 2H <sub>2</sub> O (Hydrated calcium Sulphate), H <sub>2</sub> O(Water), SO <sub>3</sub> , (Sulphur trioxide), CaO (Calcium oxide)	5 - 10	Medium
3.	Marconite	A crystalline form of Carbon, Sulphur, Chlorine	0.001 - 0.19	High
4.	Electrically Conductive Concrete	Steel admixtures-steel fibres, Shaving dust from steel, Carbon Admixtures-Graphite powder, Coke powder, Carbon fibres, Carbon nanofibers	2 - 19	Medium
5.	Tyre ash	Zinc oxide, Silica oxide, Lime, Ferric oxide, Sulphate ions, Titanium oxide, Magnesium oxide, Sodium Oxide, Potassium Oxide, Copper, Barium, Lead, Chromium, Nickel, Strontium, Vanadium	0.2	High
6.	Rice straw ash	Carbon, Hydrogen, Oxygen, Nitrogen, Silica	Not determined	Not determined
7.	Coco peat	Carbon, Potassium, Chlorine	Not determined	Not determined
8.	Palm kernel oil cake	Carbon, Nitrogen, Protein, Calcium, Magnesium, Phosphorus, Potassium, Sodium	5.7	Medium
9.	Coke powder	Carbon, Sulphur, Nitrogen, Crude Protein, Calcium, Magnesium, Phosphorus	5	High

**(Source: Akoto, 2014)**

**Table 2.9 A Summary of Some Chemical Properties of Backfill Materials**

SN	Conductive Backfill Material	pH Value	Corrosive Property	Leaching Ability	Make/Texture/ Colour
1.	Bentonite	10.5	Non-corrosive material	Disperses when added to water	Pale olive brown
2.	Gypsum	6.2 - 6.9	Slightly corrosive	Leaches soluble salts	Transparent Texture like coarse sand
3.	Marconite	7	Non-corrosive	Does not leach	Granular material Dark grey
4.	Electrically conductive concrete	9	Non-corrosive	Does not leach	Dark grey
5.	Tyre ash	5.4 - 6.22	Slightly corrosive	Leaches	Black
6.	Rice straw ashes	5 - 7	Corrosive	Does not leach	Gray
7.	Coco peat	5 - 7	Corrosive	Does not leach	Texture is coarse
8.	Palm kernel oil cake	4.51	Corrosive	Leaches	Texture is smooth Dark brown
9.	Coke powder	4 - 10	Corrosive	Leaches	Black

(Source: Yilmaz *et al.*, 2011; Siow *et al.*, 2013)

### 2.7.1 The Nature of Ground Electrode Enhancing Materials

The nature of ground electrode enhancing materials are characterised (Rotvold, 2011; Jasni *et al.*, 2010; Azmi *et al.*, 2019) by:

- a. Low resistivity, if possible, below 0.2-ohm meter;
- b. Conductivity not dependent on the continuous presence of water;
- c. Being a little alkaline in nature with a pH value greater than 7 but less than 9;
- d. Better hygroscopic properties to absorb moisture;
- e. The capacity to remain above 10% moisture;
- f. Less than 5% water solubility;

- g. Being granular with granules size 0.1 mm to 3 mm;
- h. Being non-toxic, non-reactive, non-explosive, and non-corrosive;
- i. Being thermally stable between – 10 °C to +60 °C ambient temperature;
- j. Not decomposing or leaching out with time;
- k. Not polluting the soil or local water table and meeting environmental and friendly requirements for landfills;
- l. To make a firm connection between electrode and soil, it expands and swells significantly while also eliminating entrapped air.
- m. Diffusing into the soil pores and creating conductive roots thus enlarging the conductive zone of earth pit;
- n. Being permanent and no needing maintenance;
- o. Maintaining constant earth resistance with time in its “set form”;
- p. Not requiring periodic charging treatment or replacement;
- q. Being suitable for any kind of electrode and all kinds of solids of different resistivity;
- r. Not causing burns, irritation to eyes, skin, etc.;
- s. Ground enhancement material shall be packed specifically for ground enhancement; and
- t. Earth enhancement materials shall be supplied in sealed, moisture-proof bags.

### 2.7.2 The Purposes of the Backfill Materials

Backfill materials are used to:

- a. Create perfect contact between grounding electrodes and surrounding soil (Trifunovic and Kostic, 2014);
- b. Reduce the impedance between the grounding electrode and the soil and therefore improving its conductivity (Azmi *et al.*, 2019);
- c. Reduce the cost of the grounding system (Jasni *et al.*, 2010); and
- d. Provide grounding systems with an ultra-low and stable ground resistance value. (Gerrit, 2014).

### 2.7.3 Disadvantages of the Backfill Materials

The many uses of the backfill materials have been exhausted here but there is the need to discuss the few disadvantages of these materials. Azmi *et al.* (2019) reported that some of the backfill materials are of high cost and others are not found in some countries unless they are imported. Most industrial wastes that serve as backfill materials cause a lot of pollution to the environment and may corrode the material it is protecting.

### 2.7.4 Backfill Materials from Local Plants and Materials

The backfill materials used in Ghana are mostly products of the following plants and materials. Their properties (chemical, physical, mechanical) and uses are addressed. Table 2.10 Backfill Materials, Properties and Uses and Figures 2.15 to 2.17 are images of the coconut fruit, oil palm tree and a vehicle tyre.

**Table 2.10 Backfill Materials, Properties, and Uses**

SN	Backfill Materials	Properties	Uses
1	Coconut Plant <i>Cocos nucifera</i>	Thrives well on sandy soil, does not increase in diameter by age, and a good water-absorbent	Provides sweet sap, edible kernel, oil, fibre, foliage, and fuel. Source of building materials from the trunk, coir parts for brushes, mats, ropes, and soil enhancing materials. The juice treats hung-over, diarrhoea, and cancers
2	Oil palm tree <i>Elaies guineensis</i>	Does well in sandy clay and silty clay soils lack the arboreal characteristic of wood, bark, and cambium, possesses bending modulus of elasticity and strength.	Produces palm oil, palm kernel oil, margarine, pastry, and soap. The oil and leaves treat headaches, pains, rheumatism, cardiovascular diseases. The cake from the kernel serves as enhancing material for earthing systems.
3	Tyre ash	Contains heavy metals such as Manganese, Fe, cobalt, Nickle, Copper, It has high calorific power, a low density of 641.48 Kg/m <sup>3</sup> , and a fine particle size between 0.0001 mm to 0.008 mm and back colour.	Its recycled tyre aggregate concrete is used for pavements, residential driveways, structural fills, sidewalk, curbs, and concrete shoulders. Waste tyres are incinerated for the production of heat and electricity and also serve as a backfill material for earthing systems.

(Source: Djokoto, 2013; Adkins *et al.*, 2011; Srivaro *et al.*, 2018; Owoyele and Owolabi, 2014; Amfo-Otu *et al.*, 2014; Senin *et al.*, 2016; Shukla and Singh, 2018)

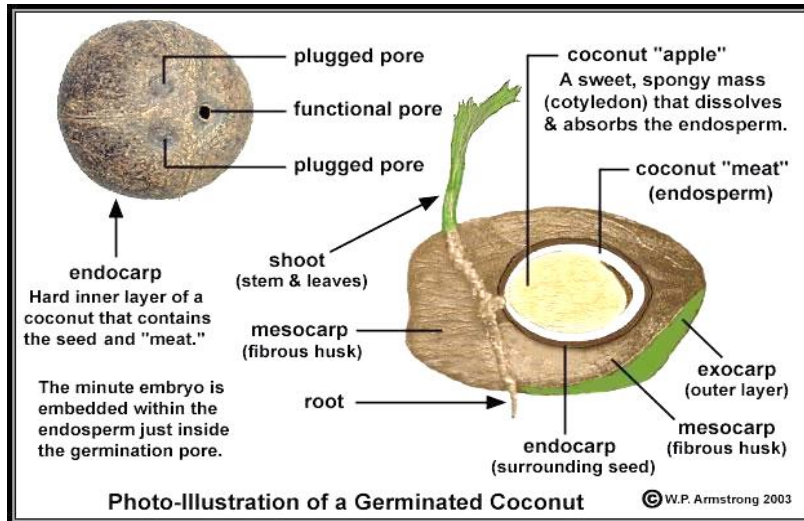


Figure 2.15 A Germinated Coconut

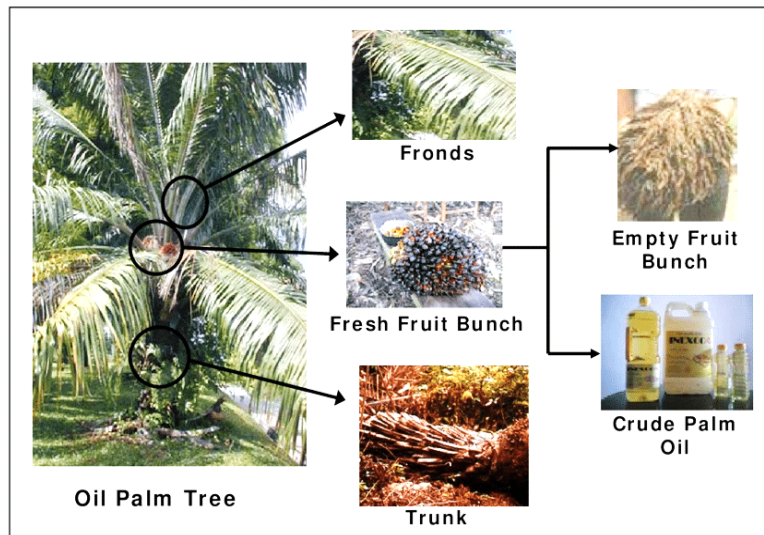


Figure 2.16 is an Oil Palm Tree

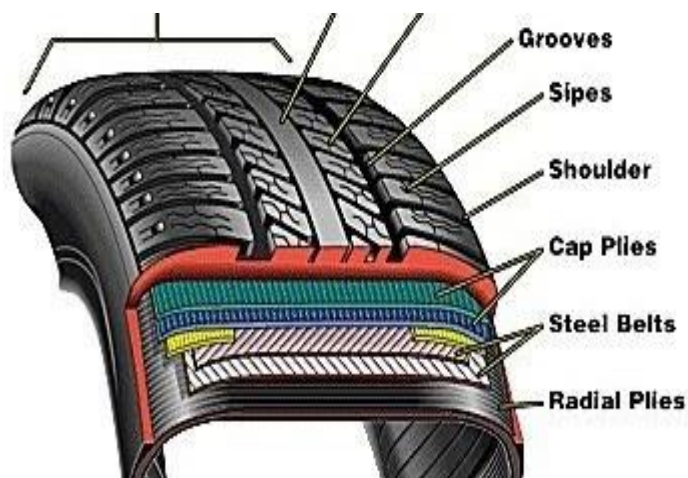


Figure 2.17 Vehicle Tyre Ash

## 2.8 Artificial Intelligence

Artificial Intellectual (AI) is a field of computer science that deals with simulating human intelligence operations in machines, particularly in computer systems that would otherwise require human intelligence. Learning, thinking, problem-solving, language comprehension, and logical reasoning are all tasks that AI can do (Ziyad, 2019). The types of AI are type 1, which is non-sentient machine intelligence, the meaning is designed for a specific purpose, such as facial recognition or only driving. However, type 2 is very broad (based on functionalities) to tackle any problem depending on the training it receives (Ziyad, 2019). By applying the following branches, processes, or approaches, AI can be utilised to solve real-world problems: Neural Networks, Robotics, Expert Systems, Fuzzy Logic, and Natural Language Processing are all examples of machine learning (Lateef, 2020). For the sake of this research Fuzzy Logic and Neural Network Systems are discussed in detail.

## 2.9 Fuzzy Logic System

Zadeh (1965) established fuzzy logic as a powerful modeling tool for dealing with natural language and approximate reasoning. It processes linguistic inputs into output decisions (Kechit, 2020). This study allowed for the incorporation of expert information into the logic of a problem in which a deterministic method is not feasible due to a lack of data, varied measurable data, or inaccuracy in expert knowledge. Zadeh (1973) gave three (3) features of a fuzzy model:

- a. language variables can be used in numerical variables instead of or in addition to them;
- b. basic IF-THEN rule-based relationships between variables; and
- c. an inference method that formulates complex links using approximate reasoning algorithms.

### 2.9.1 Characteristics of Fuzzy Logic

A few elementary principles of fuzzy logic have been established (Zadeh, 1973):

- a. Exact reasoning is thought to be a special case of approximation reasoning.
- b. It is all a stock of degree.
- c. Knowledge is defined as a set of elastic, ambiguous constraints on a set of variables.
- d. The inference is understood as a process of elastic constraint propagation.



- e. It is possible to "fuzzify" any logical system.

Typically, a Fuzzy Logic System (FLS) comprises four (4) major components instead of Boolean logic (Ziyad, 2019) as seen from Figure 2.18.

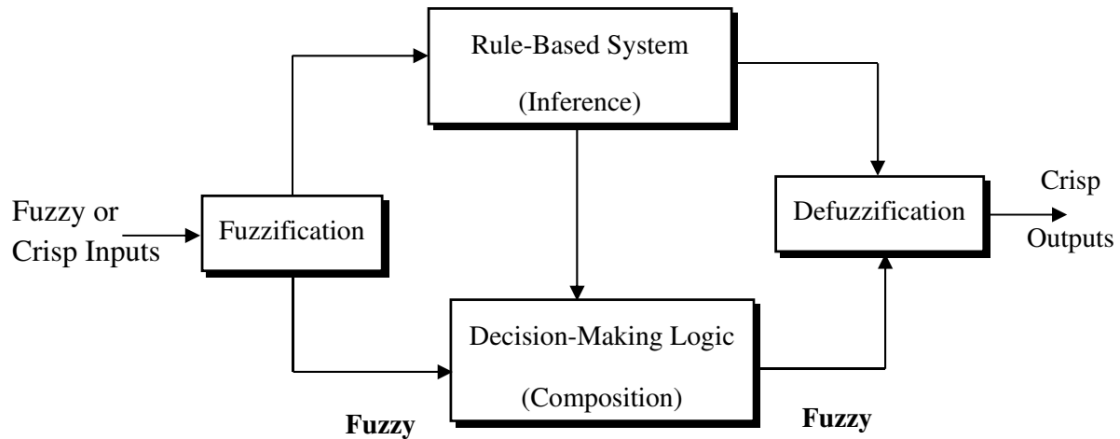


**Figure 2.18 is a Fuzzy Expert System**

*Fuzzifier or fuzzification*

To determine the amount of truth for each fuzzy rule premise, there is the need to apply the membership function interpreted on the fuzzy input variables to their precise values to convert crisp input values to fuzzy sets.

*Fuzzy rule base*

Keeps track of all the hazy "if-then" rules. Also known as a knowledge base. It assigns individual output variable to all of the fuzzy subsets and then combines them to generate a single fuzzy subset for separate output variable.

*Fuzzy inference engine*

Calculates the true value for each fuzzy rule's premise and applies it to the conclusion component of each rule to perform the fuzzy inference operation.

*Defuzzifier*

This function converts fuzzy output sets to crisp output. The fuzzy logic concepts of fuzzy number, fuzzy set, fuzzy relations and implications, fuzzy variables and their principles, and fuzzy rules are used to choose a FES. An FES completes a task defined by a set of fuzzy if/then rules. These rules represent a linguistic if-then statement that administers or restricts

a FES. The various stages of the FLS are extensively studied and addressed in the following subsections.

*Fuzzifier or fuzzification*

In the fuzzification and defuzzification processes of a FLSs, Membership Functions (MFs) are employed to assign non-fuzzy input data to fuzzy linguistic concepts and vice versa. The degree to which a given input belongs to a set is specified by this function. The MFs are the fundamental units of fuzzy set theory; a fuzzy set's fuzziness is determined by its MF (Sadollah, 2018). The choice of MF is largely determined by the size and type of problem, despite the fact that its interval and quantity have a significant impact on the outcomes of a fuzzy logic system. Membership functions come in a variety of shapes and sizes, including triangular, trapezoidal, piecewise linear, gaussian, and singleton. The only need for an MF is that it must vary between 0 and 1. Figure 2.22 is a diagram showing the different forms of membership functions.

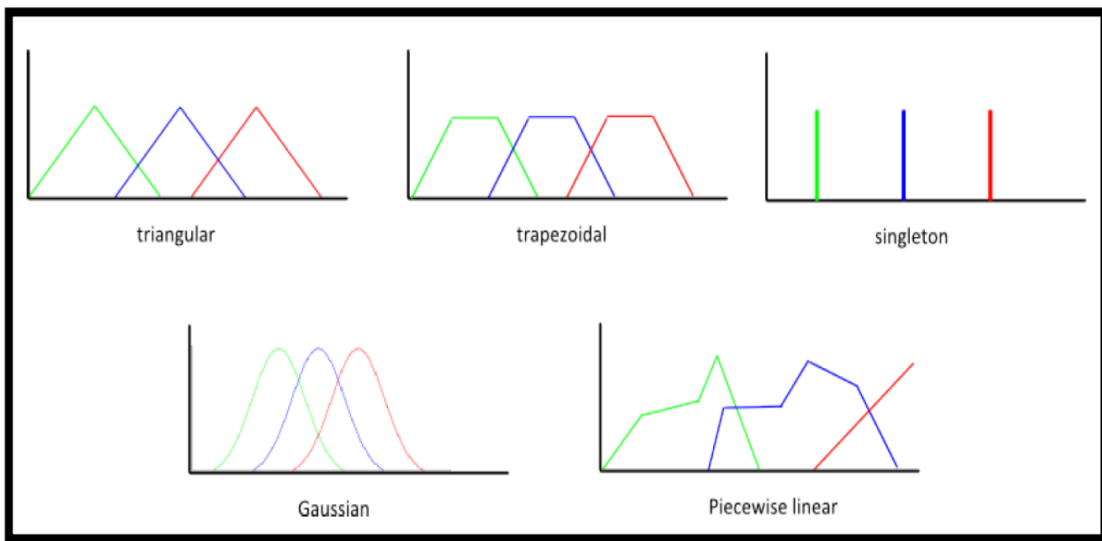


**Figure 2.19 Forms of Membership Functions**

Membership functions define the specific parameters that have been chosen and their intervals. Some common parameters that come up when modelling include temperature, pressure, rainfall, depth, corrosion rate, etc. The temperature may record a membership function such as too-cold, cold, warm, hot, and too hot. One of the complications of the membership functions is deciding on what type of shape to implement since there are different ways to characterise fuzziness. The choice entirely hinges on the problem size and problem type (Sadollah, 2018).

### *Fuzzy rule base and fuzzy inference engine*

A fuzzy decision rule is a set of rules that define a decision-maker's level when confronted with unclear outcomes. Fuzzy sets depend on certain rules. The fuzzy rules are managed in the form of if-then rules. The fuzzy rule is built on the “if...then” rule and links the different input and output fuzzy variables (Godil *et al.*, 2011). The fuzzy sets and membership functions are first defined. Then, for the specific control, the If-Then rules for the membership functions are determined. These input rules have an influence on the output. Because fuzzy rules mirror human reasoning and are founded on human experience, they are akin to common sense principles.

The antecedent and the consequence or conclusion are the two parts of a standard If-Then rule. The antecedent is the 'If' statement, and the consequence is the 'Then' statement. If the (fan) is slow, then increase the speed; if the (temperature) AND (target) are both warm, then lower the air conditioner's setting (Krishna and Biswal, 2015). Each fuzzy rule must meet the rule base's completeness requirement. The knowledge representation method that can represent every entity inside the intended domain is said to be complete (universe of discourse) (Chao and Skibniewski, 1998).

### *Defuzzifier*

Defuzzification is the practice of converting a fuzzy output of a fuzzy inference system into a crisp output. The result from the inference engine is a fuzzy value and, therefore, there is the need to defuzzify to attain a crisp output. Defuzzification is only executed depending on the membership function of the output variable (Hamarsheh, 2018).

In all, the fuzzy logic algorithm is summarised as follows:

- a. Initialisation process:
  - i. Define the linguistic variables – A crisp set of input data is acquired and converted to a fuzzy set using fuzzy linguistic variables, fuzzy linguistic words, and membership functions.
  - ii. An inference is formed built on a set of rules - Construct the fuzzy logic membership functions that express the meaning or values of the input and output terms used in the rules.
  - iii. The fuzzy output is plotted to a crisp output using the membership functions, in the defuzzification step.

- iv. Construct the rule base (Break down the control problem into a series of IF X AND Y, THEN Z rules based on the fuzzy logic rules).
- b. Convert crisp input data to fuzzy values using membership functions (fuzzification).
- c. Convert crisp input data to fuzzy values using membership functions (fuzzification).
- d. Add the outcomes of each rule together (inference).
- e. Convert the output data to values that are not fuzzy. (defuzzification) (Hamarsheh, 2018).

### 2.9.2 Types of Fuzzy Inference Systems

There exist two distinct forms of implication methods, which are the Mamdani and the Sugeno (Detyniecki *et al.*, 2012; Castillo *et al.*, 2008).

#### *Mamdani fuzzy inference systems*

The Fuzzy Interface approach developed by Mamdani is the most commonly used and one of the initial control systems based on fuzzy set theory. It was sent as an effort to operate a steam engine and boiler by synthesising a set of linguistic control rules collected from experienced human operators. The output variable for this inference method is expected to be fuzzy sets (Senouci *et al.*, 2014). Instead of a distributed fuzzy set, a single spike in the output can be used as a membership function, which is both possible and efficient.

Mamdani systems are well-suited to expert system applications where the rules are generated from human expert knowledge, such as medical diagnostics, because their rule bases are more logical and easier to comprehend (Mamdani and Assilian, 1975).

#### *Advantages:*

- a. . It comes naturally. Human intuition may be taught.
- b. More generally acknowledged.
- c. It is more effective to human input.

#### *Sugeno fuzzy inference systems*

Sugeno fuzzy inference, also identified as Takagi-Sugeno-Kang fuzzy inference, is a form of fuzzy inference that utilises singleton output membership functions that are either

constant or linear functions of the input values (Khan *et al.*, 2018). Sugeno defuzzification is more computationally effective than Mamdani defuzzification because it employs a weighted average or weighted sum of a few data points instead of computing the centroid of a two-dimensional area. (Radha Krishna and Biswal, 2015).

The `convertToSugeno` function can be used to transfigure a Mamdani system to a Sugeno system. Sugeno's output membership functions are continuous, and they link to the Mamdani output membership functions' centroids (Sugeno, 1985). Table 2.10 compares and contrasts the Mamdani and Sugeno fuzzy systems. Figures 2.20 and 2.21 show the interface of the two fuzzy systems being discussed.

*Advantages:*

- i. It is quite useful for computations and control.
- ii. It is commonly utilised to improve linear approaches.
- iii. It is used to optimise parameters and works in an adaptive manner.

The disadvantages of both fuzzy inferences have been stated in Table 2.11.

**Table 2.11 Differences between Mamdani and Sugeno Fuzzy Inference System**

SN	Mamdani FLS	Sugeno FLS
1.	Human input is well-suited.	It is ideal for mathematical analysis.
2.	Gives output in a fuzzy set	Gives constant or linear mathematical expression
3.	There is a membership function for the output.	There is no output membership function.
4.	The outcome is crisp because the rules have been defuzzified as a result.	No defuzzification, the crisp result is obtained
5.	Multiple Input Single Output (MISO) and Multiple Input Multiple Output (MIMO) systems	Only MIMO

**Table 2.11 Cont'd**

SN	Mamdani FLS	Sugeno FLS
6.	Consequences of interpretable rules	Interpretability is being lost.
7.	Surface production that is not continuous	Surface of continuous output
8.	System design freedom is limited.	System design is more adaptable.

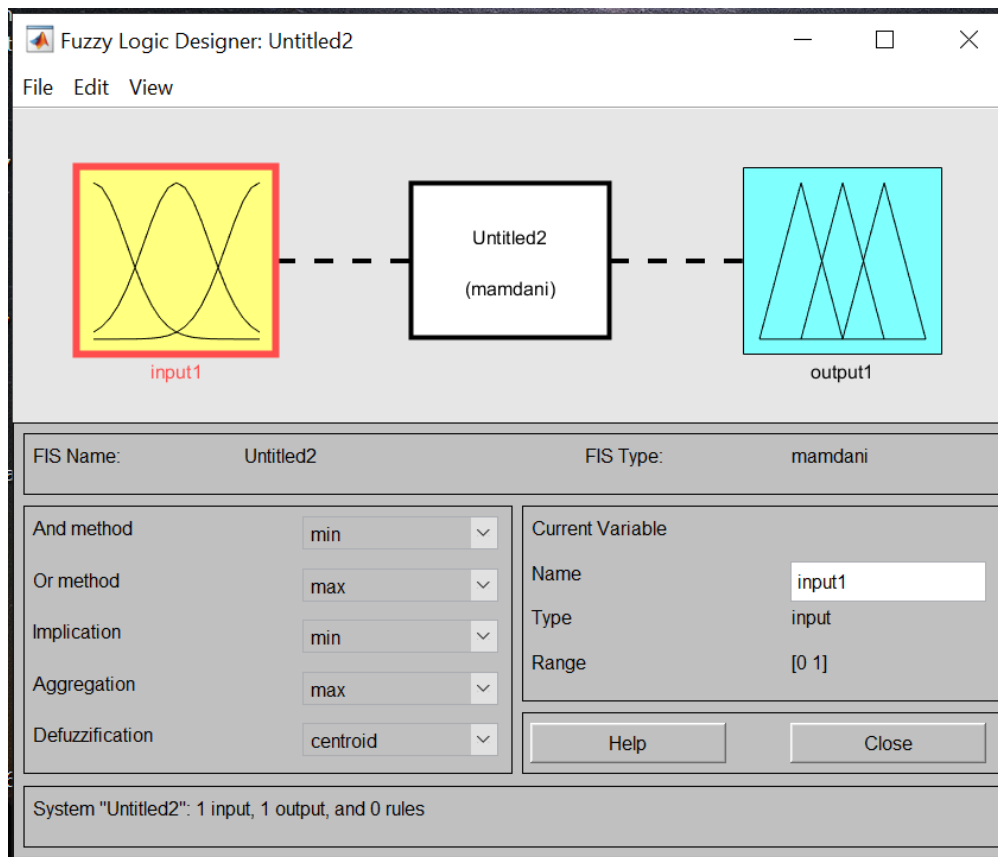


**Figure 2.20 Design of the Mamdani Fuzzy System**

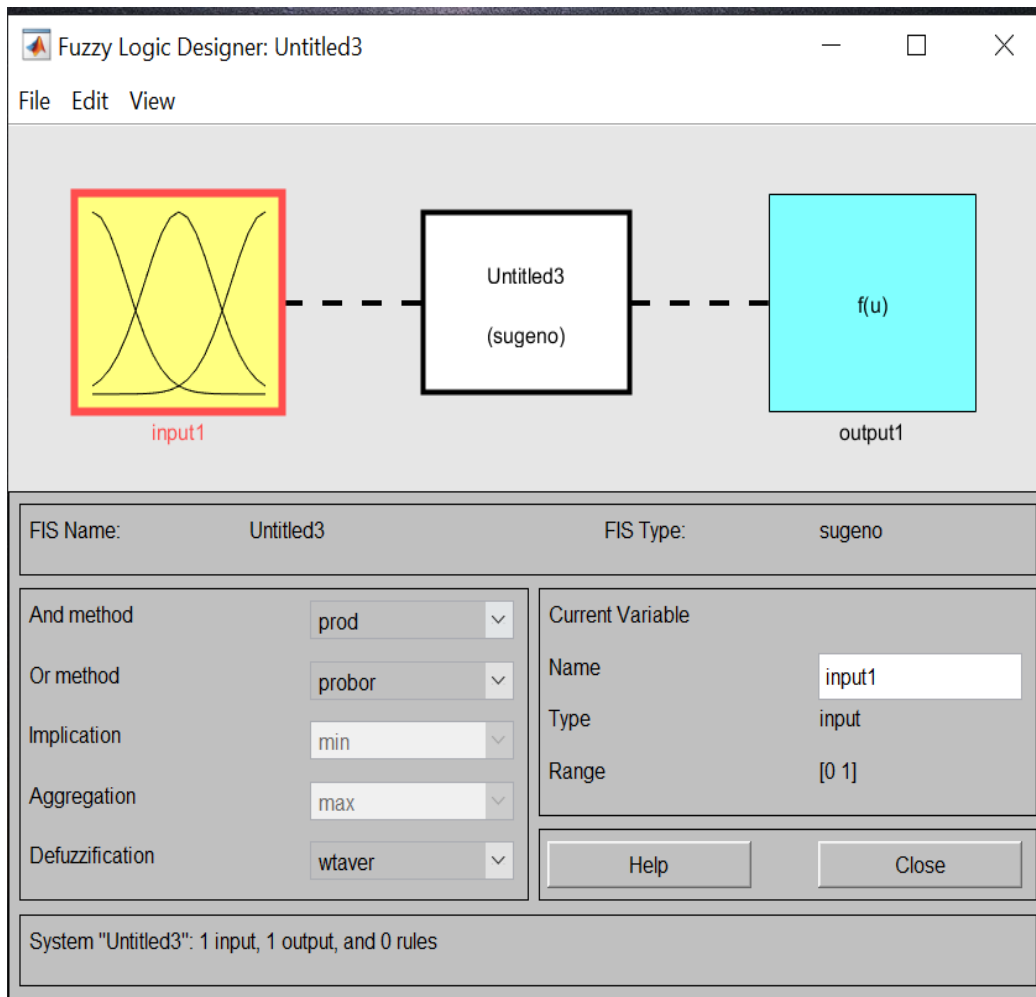


**Figure 2.21 Design of the Sugeno Fuzzy System**

## 2.10 Neural Network System

The neuron is the most powerful part of the brain, which enables the human body to think, understand and make decisions. Scientists observing the functionality of the neuron, have tried to mimic it to make powerful and better robots (Kumar, 2019). Warren McCulloch and Walter Pitts conceived the very first neural Network in 1943 by using electrical circuits to model their idea of a simple neural network. This discovery sparked two major lines of neural network research: biological processes in the brain and neural network applications in AI (Gomez, 2021). The creation of a computational system to mimic the human brain in solving problems was the motive for the neural Network until the focus of NN was directed towards varied tasks such as speech recognition, machine translation, video games, medical diagnosis, etc.

To appreciate an artificial network, the biological neuron needs to be studied. In biological systems, learning entails changes in the synaptic connections that occur between neurons

(Mhatre *et al.*, 2017). Nerve cells, also known as neurons, are the longest and oldest in a human body whose function is to generate action potential and transmission of nerve impulses through the whole extent of the body (Gautam, 2019). The parts of a biological neuron include dendrite, nucleus, axon, hillock, axon, soma myelin, a node of ranvier, and axon terminal as realised in Figure 2.22.

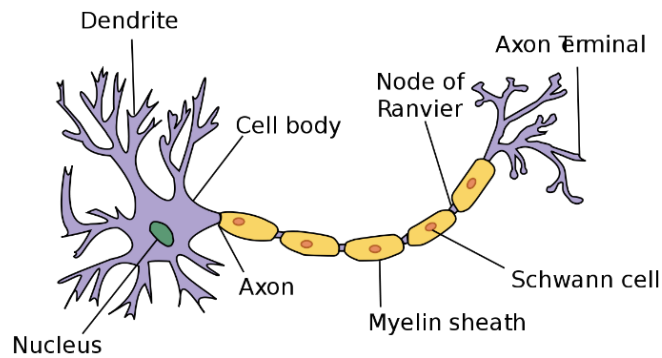


**Figure 2.22 The Parts of a Biological Neuron**

The nerve cell sends a signal by firing spikes from the cell body down through the axon to the terminal buttons, which is the major function of the neuron in the human body that was replicated. The release of neurotransmitters from the nerve cell at the synapse is used to activate a postsynaptic potential in the next nerve cell. The interaction between the nerve cells and their pattern is the main focus of study in cognitive neuroscience (Gautam, 2019; Dilmegani, 2017).

The main focus function can be summarised with Figure 2.23 showing the main parts of the neuron and their functions.

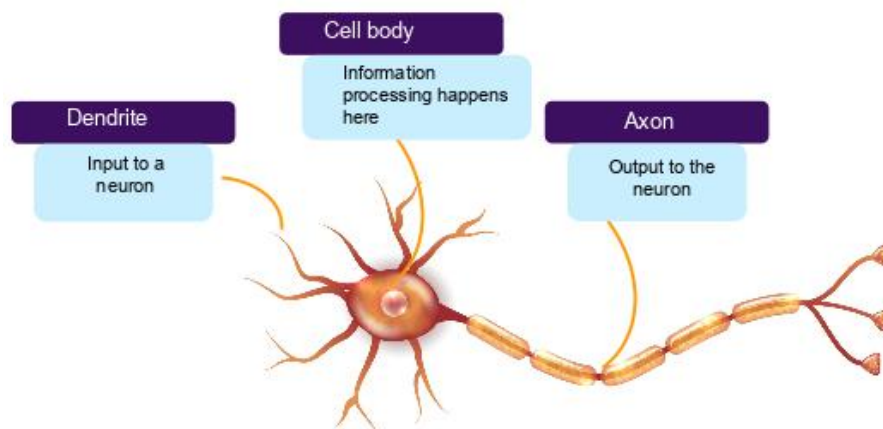


**Figure 2.23 Parts of the Artificial Neuron**



Dendrite receives signals that get connected to it from other neurons. The cell body is in charge of information processing, receiving and processing data from various dendrites. For information flow, the axon sends the output signal to another neuron (Kumar, 2019).

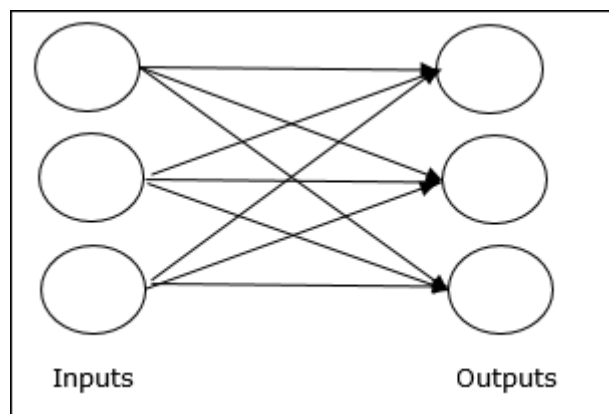
### 2.10.1 Types of Neural Network

There are two categories of neural Networks, namely, Feedforward Neural Network (FFNN) and Radial-Basis Neural Network (RBNN). FFNN can also be grouped into three, viz, single-layer feedforward, recurrent and multi-layered feedforward Networks (Kumar, 2019).

#### *Feed-forward neural network (FFNN)*

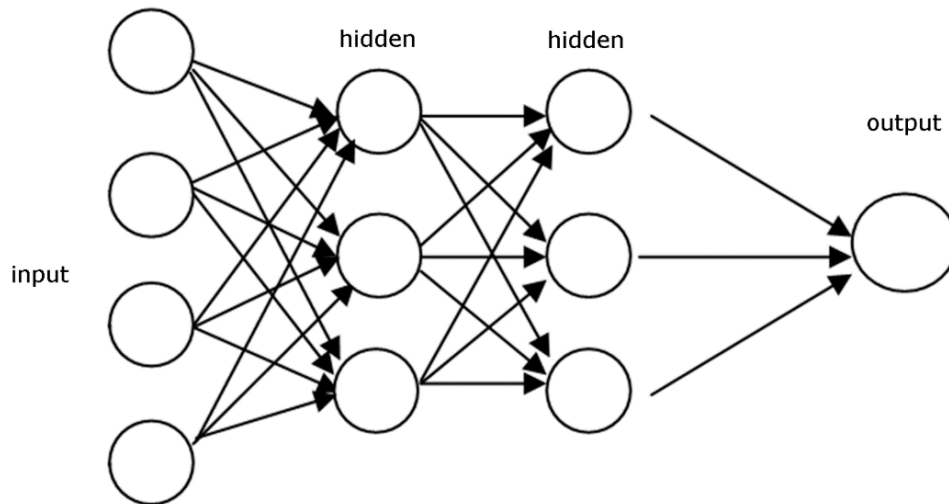
*Single-layer feedforward Networks:* It has an open-chain structure and is made up of a single layer of neurons that transmits to an output layer of neurons from an input source node.

Figure 2.24 is an image of a typical single-layer feedforward Network.



**Figure 2.24 Typical Single-layer Feedforward Network**

*Recurrent networks:* An addition of a feedback loop makes this type differ from that of the single-layer feedforward Networks. It comes with a connection between neurons to form a cyclic pattern whilst introducing a feedback loop which could be a self-feedback loop or not. Self-feedback essentially indicates that a neuron's output is transmitted back into its input, and that its absence results in just forward feedback. The network's internal memory allows it to interpret arbitrary sequences of inputs, making it ideal for tasks like connected handwriting recognition. Figure 2.25 is the structure of the recurrent Network.



**Figure 2.25 Structure of Recurrent Network**

*Multi-layered feedforward networks:* The existence of a hidden layer is what differentiates this type from the former. The hidden layer is introduced to perform the computation (Abbas, 2016). Figure 2.26 shows the structure of a multi-layered feedforward Network.

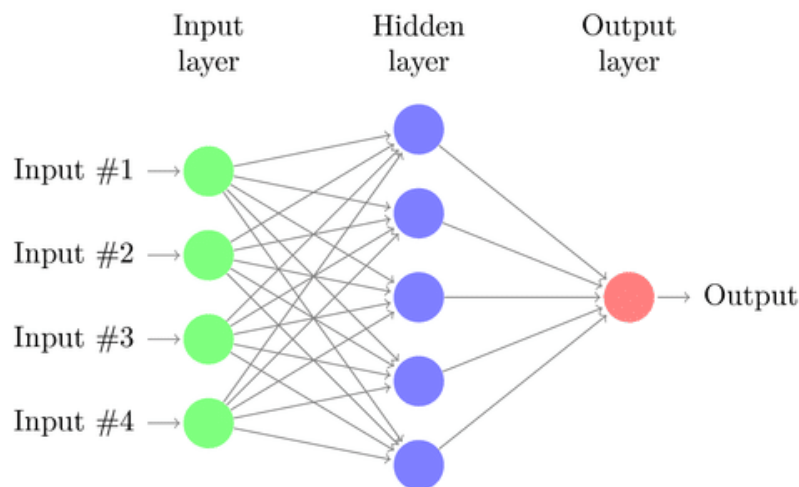


**Figure 2.26 Structure of A Multi-layered Feedforward Network**

The single-layer feedforward, recurrent, and multi-layered feedforward networks all proved that a neural network has input, hidden, and output layers. The entire system starts with an input layer that receives data as input. The weight is then attached to the lines that connect the hidden layers, producing the ANN's core (Bataneh, 2012). Each circle in the hidden layer processes the inputs that feed into the next hidden layer and, eventually, the output layer, by initiating some mathematical calculations that will be detailed later in this chapter.

The ANN is trained with the basic purpose of stochastic training with learning rate and momentum term is to lower the average error function between the estimated and real value by changing the network's parameters (weights). After the random presentation of all the input vectors has been completed, the weights are adjusted to minimise the average error function between the estimated and actual value (Androvitsaneas *et al.*, 2012). For all N patterns, the average error function is given as:

$$G_{av} = \frac{1}{2N} \sum_{n=1}^N \sum_{j \in c} (d_j(n) - y_j(n))^2 \quad (2.13)$$

where “c” is the set of neurons,  $d_j(n)$  the desirable output, and  $y_j(n)$  the actual output of the j-neuron. Until one of the stopping criteria is fulfilled, the weights of the ANN are adjusted. The three (3) stopping criteria include: the weights’ stabilisation criterion, the error function’s minimisation criterion, and the maximum number of epochs’ criterion which are given as:

$$|w_{kv}^{(l)}(ep) - w_{kv}^{(l)}(ep-1)| \leq \text{limit}_1, R_{k,v,l} \quad (2.14)$$

$$|RSME(ep) - RSME(ep-1)| \leq \text{limit}_2 \quad (2.15)$$

$$ep \leq \text{max\_epochs} \quad (2.16)$$

where  $w_{kv}^{(l)}$  is the weight between l-layer’s k-neuron and (l-1) layer’s v-neuron,

$$RSME = \sqrt{\frac{1}{m_2 \cdot q_{out}} \sum_{m=1}^{m_2} \sum_{k=1}^{q_{out}} e_k^2(m)} \quad (2.17)$$

*Advantages and disadvantages of FFNN:* The advantages of FFNN include: performs well in a variety of situations, particularly with data that arrives at varied times; and values; and can also forecast input outside of the system's training limitations. The disadvantages are: the number of neurons can lead to training time and memory issues during training processes; and there are instances of high inaccuracy due to low minima that come from optimisation (Bataneh, 2012).

#### *Radial-basis neural network*

It is a system that is made up of input, output vectors, one hidden layer, and one output layer. Radial basis functions are used as activation functions with its output in a form of a linear

combination of the inputs of the function mentioned and neuron parameters. Exact RBNN, probabilistic RBNN, and Generalised Regression Neural Network are the three varieties of RBNN (GRNN) (Devaraju and Ramakrishnan, 2014).

*Advantages of RBNN (Bataineh, 2012):*

- a. High accuracy within the limits of the training process and best for high-dimensional regression models.
- b. Since this network has a small number of neurons and weights, it is free of computational time and computer memory issues.
- c. The number of hidden neurons is routinely optimised during the training phase, therefore there are no local minima issues.
- d. High fault tolerance potential therefore suitable for debugging and diagnosing a Network on its own.

*Disadvantages of RBNN:*

- a. The determination of the Network parameter (Gaussian width) could give poor results.
- b. Points that are outside of the training grid space are predicted.

## 2.10.2 Advantages and Disadvantages of Neural Networks (Belavkin, 2014; Kumar, 2019)

*Advantages*

- a. Networks are always easy to maintain and give results even when there is incomplete input information.
- b. Applies to any problems in every area on the condition that there is data irrespective of its noisiness or not.
- c. Caters for non-linear dependency models and analytical methods yet to be developed.

*Disadvantages*

- a. Cannot do without any form of data to work with.
- b. They are quite complicated as there are no explanations to support the outcomes of the models.

- c. The various parameters namely; minimal error, learning rate, and hidden nodes play important roles in the final results.

### 2.10.3 Applications of Neural Network

- a. Security (credit card and medicare fraud detection)
- b. Object recognition such as handwriting and voice by converting it into digital characters for machine interpretation.
- c. Pattern classification.
- d. Data compression.
- e. Function approximation
- f. All forms of prediction such as stock exchange, options, currency, bankruptcy, futures, and bond ratings.
- g. Forecasting electrical load and energy consumption.
- h. Optimisation of logistics for transportation Network

## 2.11 Review of Related Works on this Research

2.11.1 Review of Related Works on the Backfill Materials for Reducing Corrosion of Earth Electrodes.

Table 2.12 gives the Backfill Materials for Reducing Corrosion of Earth Electrodes

**Table 2.12 Backfill Materials for Reducing Corrosion of Earth Electrodes**

<b>Author</b>	<b>Objectives</b>	<b>Type of Metal/ Material</b>	<b>Backfill Materials</b>	<b>Remarks</b>
Androvitsaneas <i>et al.</i> (2012)	Investigation into the best backfill materials for earthing systems	-	Natural soil, conductive concrete, bentonite	No mention of corrosion, no laboratory analysis of the rods and backfill materials
Akoto (2014)	Test on use of tyre ash as an earthing enhancement material	-	Tyre ash	Mentioned corrosion without any laboratory analysis. Rod length of 0.5 m

**Table 2.12 Cont'd**

<b>Author</b>	<b>Objectives</b>	<b>Type of Metal/ Material</b>	<b>Backfill Materials</b>	<b>Remarks</b>
Nyuykonge <i>et al.</i> (2015)	Use of biochar for earthing systems to reduce earth resistance	Galvanised copper rod	Biochar	Biochar reduced the earth resistance
Shuhada <i>et al.</i> (2016),	Discussion on the effectiveness of bentonite as grounding enhancement material	Copper rods	Bentonite	Bentonite is good earth enhancing material that depends on factors such as temperature, rainfall, humidity
Idoniboyeobu <i>et al.</i> (2018)	Study of the effects of different soil types on the resistance of backfill materials	Moist loam soil and dry sandy soil	-	Soil structure, chemical constituents are the major factors that affect earthing systems. Moist loam soil recorded the lowest earth resistance value and dry sandy soil recorded the highest earth resistance value
Dārab <i>et al.</i> (2018)	Improvement of the electrical properties of earthing systems	Electrode	Slag, a waste from metallurgy industry	The slag reduced the overall resistance of the grounding system
Kulor <i>et al.</i> (2021)	Investigation into the use of low resistive materials for earthing frameworks	Earth mat	Tyre ash with palm kernel oil cake	When compared to palm kernel oil cake, tyre ash performed better in both dry and wet circumstances.

**Table 2.12 Cont'd**

<b>Author</b>	<b>Objectives</b>	<b>Type of Metal/ Material</b>	<b>Backfill Materials</b>	<b>Remarks</b>
Abdullah <i>et al.</i> (2021)	Investigation into the use of gypsum as a ground enhancement backfill material on earthing systems		Red gypsum and plasterboard gypsum	Both lowered the resistivity, but red gypsum proved to have a shorter life span due to its plastic nature

### 2.11.2 Review of Related Works on XRF, XRD, and SEM-EDS.

Table 2.13 gives the Related Works on XRF, XRD, and SEM-EDS.

**Table 2.13 Related Works on XRF, XRD, and SEM-EDS**

<b>Author</b>	<b>Objectives</b>	<b>Materials</b>	<b>Methods</b>	<b>Results</b>
Loubser and Verryn (2008)	Experimentation of the use of a combination of XRF and XRD		Use of XRF and XRD analysis	XRF determined the bulk chemical composition of the sample and the XRD determined the crystalline phases in the sample
Folorunso <i>et al.</i> (2014)	Investigation of the mineralogical composition, relative proportions of the constituent compounds, the morphology, and the phase identification of samples	Clay samples	XRF, SEM-EDS, XRD, and TEM Analysis	The four (4) (4) techniques showed consistency in the revelation of the different constituents of the clay samples

**Table 2.13 Cont'd**

<b>Author</b>	<b>Objectives</b>	<b>Materials</b>	<b>Methods</b>	<b>Results</b>
West <i>et al.</i> (2014)	Investigation of the elemental, composition of copper-alloyed artifacts	Copper-alloyed artifacts	XRF	Some of the elements that were discovered included copper, tin, zinc, and lead
Veneranda <i>et al.</i> (2016)	Identification of micrometric degradation compounds	Iron matrix	XRF and SEM	These two (2) methods combined gave better results than each achieved separately
Ul-Hamid <i>et al.</i> (2017)	Test for corrosion under atmospheric, underground, and splash zone conditions	Aluminium	The weight-loss method, Visual inspection, SEM, XRD, and XRF	Corrosion activity took place in all conditions due to their corrosive nature after fifteen (15) months of exposure
López <i>et al.</i> (2018)	Investigation into tailings of tin (Sn) mining activities	Tailings of tin (Sn)	$\mu$ -PIXE, XRF, SEM-EDS, and XRD	It was concluded that each technique complimented the other and also served as validation for the results
Robotti <i>et al.</i> (2018)	Examination of corrosion effects on copper-tin alloys	Copper-tin alloys	pXRF	Reliable chemical characterisation of the alloy was obtained.
Katsifas <i>et al.</i> (2019)	Overview of the capabilities of EDXRF spectrometry	Copper artifacts	EDXRF	EDXRF spectrometry maintained the central analytical technique
De Aquino Lima <i>et al.</i> (2021)	Evaluation of the wear of an AISI 316L steel tube	AISI 316L stainless steels	SEM-EDS, XRD, and XRF	The techniques indicated the areas of deterioration



**Table 2.13 Cont'd**

<b>Author</b>	<b>Objectives</b>	<b>Materials</b>	<b>Methods</b>	<b>Results</b>
Alsultani and Mutasher (2021)	Investigation of the external corrosion phenomenon for exporting crude oil pipeline	Oil pipeline	Weight loss, Tafel Extrapolation, and SEM-EDS	Pitting corrosion took place in a very low resistive soil

### 2.11.3 Review of Related Works on Fuzzy Logic System.

Table 2.14 Related Works on Fuzzy Logic System.

**Table 2.14 Related Works on Fuzzy Logic System**

<b>Author</b>	<b>Objectives</b>	<b>Parameters</b>	<b>Methods</b>	<b>Remarks</b>
Abbas (2016)	Prediction of CO <sub>2</sub> corrosion in pipelines	Temperature, pressure, velocity, fluid flow rate, pH, and corrosion rate	Mamdani and Sugeno Fuzzy logic expert systems	Size of data was suitable for only Mamdani, not Sugeno fuzzy system
Khan <i>et al.</i> (2016)	Estimated the Corrosion Under Insulation (CUI) corrosion rate of carbon steel	Operating temperature, type of insulation, type of environment, pipe complexity, insulation condition, and corrosion rate	Fuzzy-based model	The Mean Absolute Deviation (MAD) of 0.104 and the Root Mean Square Error (RSME) of 0.021 were calculated.
Jana <i>et al.</i> (2017)	Corrosion Failure Likelihood (CFL) in oil and gas pipelines estimation	Corrosion cracking, thinning, corrosion thinning, inspection efficacy, and timeframes are all factors to consider.	Fuzzy logic	Fuzzy logic determined the controlling factors and the CFL

**Table 2.14 Cont'd**

<b>Author</b>	<b>Objectives</b>	<b>Parameters</b>	<b>Methods</b>	<b>Remarks</b>
Kim and Choe (2017)	Predicting pipeline failures and a maintenance plan	Pipe diameter, wall thickness, operating pressure, tensile strength, and metal corrosion rates.	Fuzzy logic-based clustering technique	The fuzzy technique was very accurate in the prediction
Han and Du (2017)	Prediction of corrosion rate of a grounding grid	Saltiness, temperature, calcium, sodium, chlorine, and pH	Extension analytic hierarchy process and Fuzzy methods	The relative error was very high with the least value of 20.56%
Okolo (2017)	Diagnosis of all forms of faults in a transformer	Current and rate of change of current with time	Fuzzy logic	A fuzzy logic on transformer fault diagnostic system was designed with two inputs and a single output variable
Biezma <i>et al.</i> (2018)	Pipeline corrosion rate forecasting	Moisture content, redox potential, resistivity, pH, sulphate, and chloride concentration	Fuzzy logic expert system	Used data from other researchers. The parameters were not measured quantitatively from the site
Mohsin <i>et al.</i> (2019)	Prediction of corrosion under the insulation of piping systems	Operating temperature, type of insulation, pipe complexity, type of environment, and insulation condition	Fuzzy logic-based prediction model	Risk-Based Inspection (RBI) tasks in the oil and gas industries were made easier with the fuzzy logic paradigm.
Zhang <i>et al.</i> (2020)	Corrosion Evaluation of Grounding Device	Soil resistivity, pH, moisture, water, and salt content	Fuzzy evaluation method	The fuzzy Method was able to be used to obtain the corrosion matrix but not for prediction due to its inconsistencies.

**Table 2.14 Cont'd**

Author	Objectives	Parameters	Methods	Remarks
Sibiya and Sumbwan yambe (2021)	Prediction of the severities of the maize common rust disease	No parameters were mentioned	Fuzzy logic-based system	A validation accuracy of 95.63% was achieved

#### 2.11.4 Review of Related Works on Neural Network System.

Table 2.15 Related Works on Neural Network System.

**Table 2.15 Related Works on Neural Network System**

Author	Objectives	Parameters	Methods	Remarks
Mabbut <i>et al.</i> (2012)	Monitoring of corrosion using advanced computer application	Temperature, acidity, and exposure time	ANN model	ANN model produced closer results that were favourable.
Jančíková <i>et al.</i> (2013)	Prediction of steel atmospheric corrosion	Relative humidity, temperature, amount of precipitation, pH of rainfall	NN	A relative error of 6% was predicted making the neural Network an ideal model for predicting corrosion.
De Massi <i>et al.</i> (2015)	Improvement in pipelines' predictability of metal loss and corrosion rate	Protective scales, water and electrochemistry, steel composition, flow velocity and localised bacteria attacks	ANN	ANN method was adopted to complement the deterministic approach towards prediction of corrosion rate
Lin <i>et al.</i> (2017)	Prediction of atmospheric corrosion rates of carbon steels	Time of wetness, rain duration time, average temperature, solar radiation, rainfall, average wind velocity with an average wind direction, exposure time	ANN	The prediction made was accurate

**Table 2.15 Cont'd**

<b>Author</b>	<b>Objectives</b>	<b>Parameters</b>	<b>Methods</b>	<b>Remarks</b>
Du <i>et al.</i> (2018)	Classification of degree of corrosion of grounding grid	Corrosion damage and degree of corrosion	CNN	This research filled up the gap in terms of using an imaging approach to identify the degree of corrosion on a grounding grid.
Bastian <i>et al.</i> (2019)	Detection of corrosion in water, oil, and gas pipelines	No parameters were mentioned	CNN	It had a classification accuracy of 98.8%, which was much higher.
Huang <i>et al.</i> (2019)	Prediction of corrosion of grounding grid	Soil resistivity, pH, water content, and gas content	BPNN	The results were not satisfactory due to inadequate data for the analysis and poor choice of the prediction model
Rocabruno-Valdés <i>et al.</i> (2019)	Prediction of corrosion rate of metals in different biodiesel	Temperature and exposure time	NN	A mean square error of $2.15 \times 10^{-4}$ was achieved
Zaranezhad <i>et al.</i> (2019)	Presentation of an accident causation model for oil refinery repair and maintenance.	External, internal, executive, work, behavioural, situational	ANN, Fuzzy systems, and ant Genetic colony algorithms	The neural-GA Network, which was the best algorithm, had the highest prediction accuracy of 95.9% and precision of 96.7%
Adada <i>et al.</i> (2020)	Monitoring corrosion in the classification of guyed structures in transmission lines	pH, moisture content, liquid, plastic limit and passing material	NN	The classification resulted in an 80% correlation

## **2.12 Summary**

This chapter focused on the main topics of the research work. The earthing systems, types, factors that affect it and ways of measuring resistivity were handled. The types of corrosion, causes, effects, inspection, detection, and prediction methods were discussed. The types of backfill materials, their purposes, their properties were mentioned. Two (2) AI techniques namely, fuzzy logic system and neural Network for corrosion prediction were also elaborated. Some related works on the topics; backfill materials, XRF, XRD and SEM-EDS analyses and the two AI techniques mentioned earlier were tabulated.

These related works clearly stated the objectives, methodologies, results, and limitations of the various research works. It was identified that no research work has been conducted considering all the four topics that have been listed. Most of the backfill materials considered were used not more than three per a research, some were also inorganic in nature without any prolong field studies. The laboratory analyses and AI techniques that were reviewed had little to do with earthing systems. The research works were mainly on oil and gas pipelines and concrete work.

This research seeks to utilise the local materials in the environment as backfill materials to bury earth rods to improve earthing systems and prevent corrosion. These rods would be tested in the laboratory by the two analyses for corrosion after which the AI techniques would be used to predict the corrosion rate of the roads and hence identify the best backfill material for effective earthing system and prevent corrosion

## **CHAPTER 3**

### **METHODS USED**

#### **3.1 Introduction**

The only means of determining the effectiveness of a buried rod is through taking measurements of its resistivity or resistance values, depending on the information available to the researcher. Most researchers give little or no knowledge regarding the soil, backfill, or enhancing materials and even the rod being discussed or researched on.

The study area under consideration for this research was surveyed, apportioned measurements, and the soil type (homogeneous or heterogeneous) were considered. Instruments and materials needed for effective data analysis were acquired for readings and studies. The backfill materials were prepared. Soil, backfill materials and the buried rod samples were analysed at the Minerals and Environmental and Safety Engineering Laboratories of University of Mines and Technology. Corrosion rate equation was derived from various formulae from literature.

#### **3.2 The Study Area**

A piece of land located adjacent to the Premises of the Electricity Company of Ghana, and opposite the University of Mines and Technology, Tarkwa was chosen as the study area for reasons of proximity and easy access. An area of 252.81 m<sup>2</sup> was cleared of weeds and debris and five holes were dug for burying of the rods. Each hole had a depth of 1 m and a diameter of 0.38 m. The interval between adjacent holes was 5 m and the holes were dug to form a straight line. Figure 3.1 shows some dug soil from one of the dug holes. The soil had a cream colour mixed with brown and its texture felt in between ones' fingers together with a visual inspection showed it to be clayey. However, soil samples were taken and analysed at the University of Mines and Technology Minerals Laboratory for texture, particle size by weight, water holding capacity, and pH values. Also, organic carbon and some selected trace elements of heavy metals were tested.



**Figure 3.1. Soil Sample**

### **3.3 Electrode Selection**

The electrodes were selected from recommendations from literature and engineers from the Electricity Company of Ghana (ECG), Tarkwa. The rods that are used by ECG ranges in length between 1 m to 2 m. The earth rod used for the study was copper coated cast iron with a length of 1.2 m and a diameter of 0.015 m. 0.1 m of the rod length was driven into one of the dug holes. The hole was then filled with backfill material. Two resistance readings were recorded five minutes apart, one before and the other after the backfilling. The remaining rod length, i.e., 0.1 m, was left in the atmosphere and was used for the resistance measurement. Figure 3.2 shows a sketch of the cross-sectional view of the arrangement of the earth rod and backfill material in the ground.

To ensure that the earth rod had good contact with the backfill material, a 0.9-m long and 0.1-m diameter polyvinyl chloride (PVC) pipe was put in the dug hole to surround the hammered rod. The PVC pipe was then filled with the backfill material and allowed to settle. The space around the PVC pipe was then filled with the dugout soil. The PVC pipe was finally removed. This procedure was repeated for all the backfill materials.

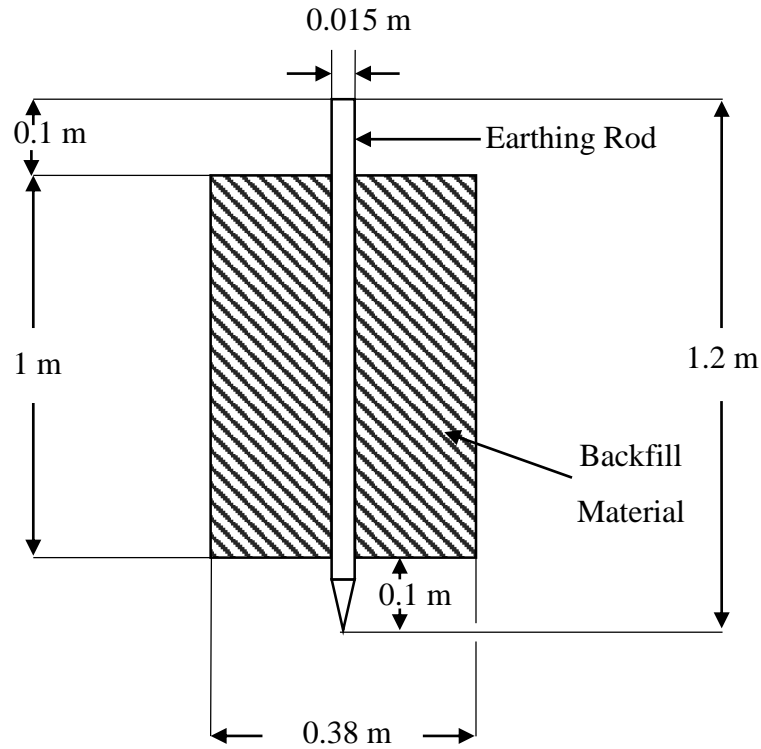


**Figure 3.2 The Design Concept**

### 3.4 Materials and Instruments Used

Four locally acquired materials were obtained to be used for the experiment. These materials were selected because they contained properties that have already been stated in the literature. To perform the field work necessary for determining the resistant values of rods when using the various electrically conductive backfill materials, the following materials and instruments were employed:

- a. Backfill materials (Tyre ash, Palm Kernel Cake, Charred Coconut Husk, and Coconut Coir);
- b. One end threaded 0.013 m in diameter by 1.2 m length copper coated iron earth rod;
- c. A 4-terminal digital earth tester;
- d. Four insulated wire conductors;
- e. 7.5 m long measuring tape;
- f. Hammer;
- g. Gloves;



- h. Scale;
- i. Two PVC pipes of diameter 0.1016 meters;
- j. Machete;
- k. Wooden mortar and pestle;
- l. Beam balance; and
- m. Three pairs of scissors.

#### 3.4.1 Backfill Materials/Experimental Samples

Four different backfill materials were used in this experiment, namely, tyre ash, palm kernel cake, coconut coir, and charred coconut husk. This section provides details of the preparation of the listed materials before usage as backfill materials.

##### *Coconut coir*

Two sacks of coconut husk were collected from a refuse dump close to the Railways Police Station, Tarkwa. A portion of the coconut husk was milled into powder form before being used as backfill material. Figures 3.3, 3.4, and 3.5 depict the stages for the preparation of the coconut coir, i.e., collection of the coconut, cutting the husk into pieces for milling, and the milled coconut husk, respectively. The processes were as follow:

- a. They were dried in the sun for three days on a sand-free veranda within the premises of the University.
- b. A sack of the dried coconut husk was cut into pieces with the aid of a pair of scissors.
- c. The pieces were further dried in an oven in the Mineral Engineering Laboratory of the University at a temperature of 105 °C for six hours daily for an additional four days.
- d. They were finely milled with a milling machine and made ready to be used for backfilling.



Samples  
of  
Coconut  
Husk

**Figure 3.3 Coconut Husk being taken from the Refuse Dump**



Sack

Coconut  
Coir

**Figure 3.4 Dried Pieces of Coconut Husk Ready for Milling**



**Figure 3.5 Coconut Coir Ready to be backfilled**

*Charred coconut husk*

The remaining portion of the coconut husk obtained from the refuse dump was charred and pounded into powder form. Figures 3.6 and 3.7 show the steps for the preparation of charred coconut husk, i.e., the charred coconut husk and pounded charred coconut husk, respectively. Below is the procedure;

- a. A piece of land measuring 1 m × 1 m was cleared of weeds and dug to a depth of 0.3 m.
- b. Fresh logs of wood of length 0.5 m were laid on the ground of the dug hole.
- c. The dried coconut husk was arranged neatly on the logs.
- d. Fresh palm fronds were used to cover the coconut husk leaving a small surface area to set fire to it.
- e. Wet sand of high porosity and different aggregates were used to cover the whole setup until all was covered except the hole for setting the fire.
- f. The fire was set to it and allowed for twenty-four hours before collection.
- g. The now charred coconut husk was pounded in a wooden mortar with a wooden pestle to a powdered form, hence, ready for backfilling.

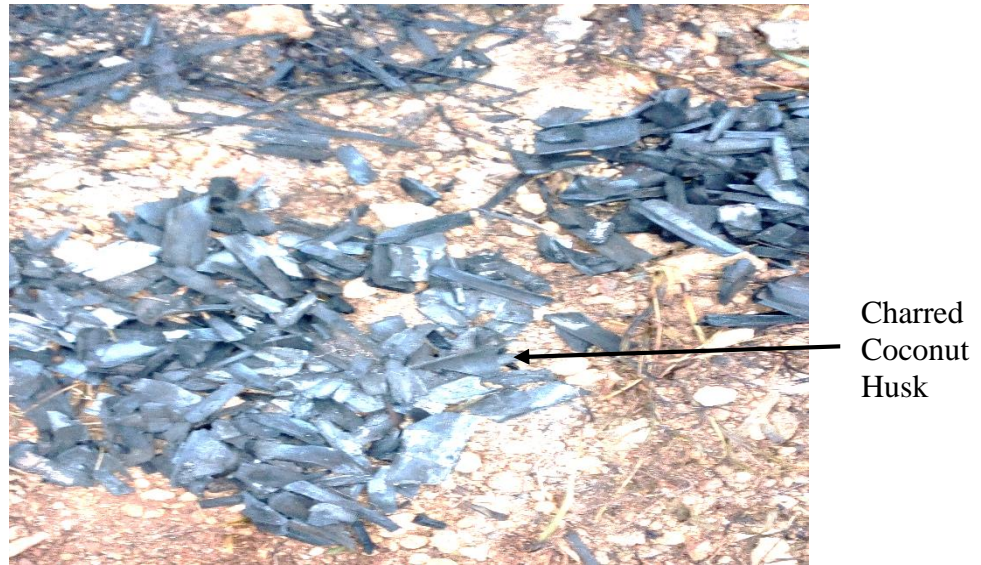


**Figure 3.6 Sample of the Charred Coconut Husk**

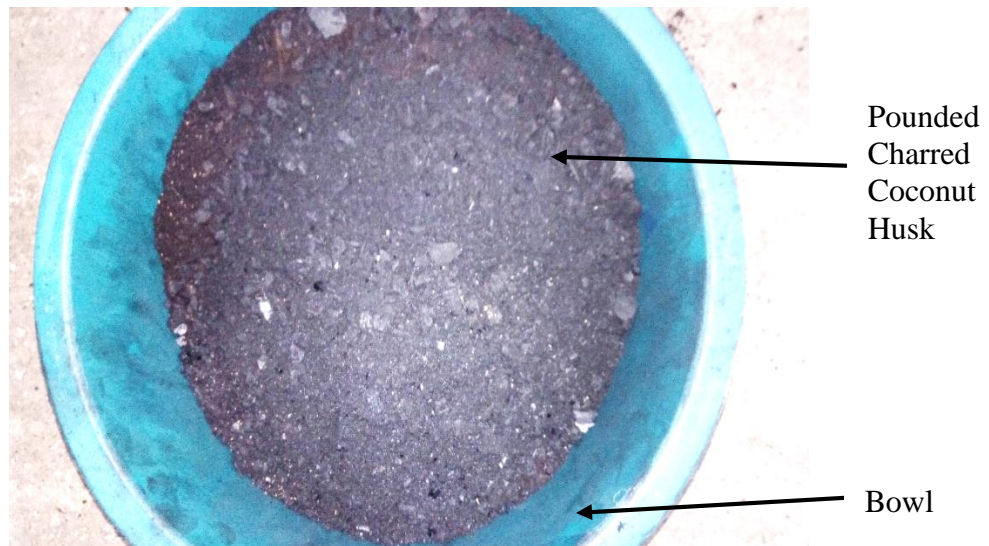


**Figure 3.7 Sample of Pounded Charred Coconut Husk**

#### *Tyre ash*

This was obtained from Ashaiman Tulaaku, around Michelle Camp, in the Greater Accra Region of Ghana, where the vehicle tyres are burnt to singe slaughtered cattle.

#### *Palm kernel cake*

Two cakes of palm kernel were bought at a cost of GHS5.00 (US\$1.00) in December 2019 and pounded into powder using a wooden mortar and pestle. It was mixed with water into a paste before usage. Figure 3.8 shows the powdered palm kernel being mixed with water.



**Figure 3.8 Powdered Palm Kernel being mixed with Water**

### **3.5 Measurement Methods**

#### **3.5.1 Fall-of-Potential Method of Measuring Resistance**

The site was prepared by clearing an area of 300 m<sup>2</sup> of land off weeds adjacent to the premises of the Electricity Company of Ghana, Tarkwa. Five holes of depth 1.2 m and diameter 0.38 m were dug at intervals of 5 m in a straight line from each other forming a rectangle to be precise and pictorial. Figure 3.9 shows a dug hole. 0.3 m of the rod was hammered into the hole as shown in Figure 3.10.



**Figure 3.9 A Dug Hole for the Rod**

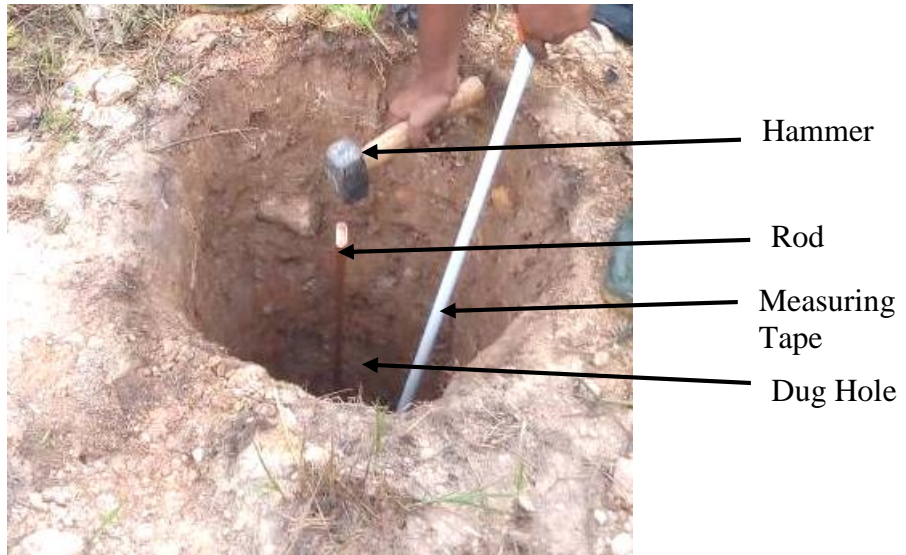


**Figure 3.10 A Rod Hammered in The Dug Hole**

0.1 m length of the rod was hammered into the dug hole leaving 1 m above the soil surface. The 1 m rod was backfilled, and the rest was exposed to the surface of the soil to enable resistance readings to be taken. The instrument that was used for measuring the earth resistance was Megger Det 32 and it comes with three leads; 50 m, 30 m, and 3 m leads, four probes of length 0.03 m, a mallet and a 7.5 m measuring tape. Figure 3.11 is an example of the megger that was used.

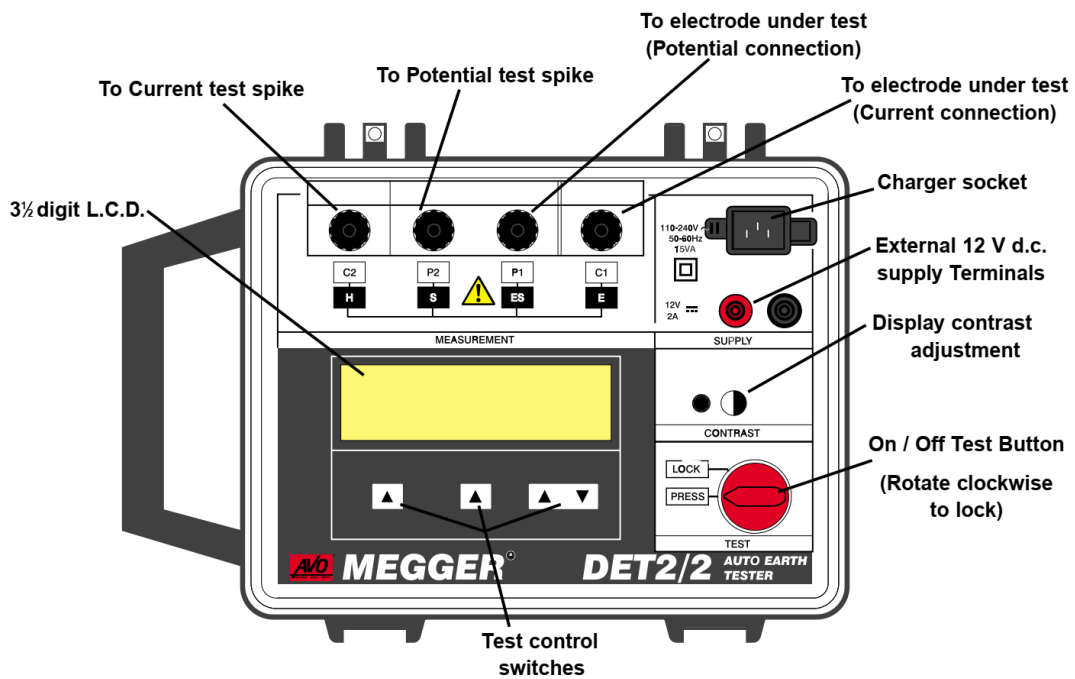


**Figure 3.11 An Example of Megger**

The Fall of Potential Method of testing for the earth resistance was used and the procedure is as follows:

- a. The measuring tape was used to position the probe by hammering it and pegging it with the 50 m lead at a distance of 14 m straight to the dug hole.
- b. A second probe is also hammered and pegged with the 30 m lead 7 m from the hammered probe to the rod as shown in Figure 3.12.
- c. With all the terminals of the leads available at the hammered rod, the 3 m lead is connected to the C1 terminal of the megger, which is already looped to the P1, the 50 m lead to C2 and the 30 m lead to P2.
- d. The hand crank part of the megger was wound until a constant resistance value appeared on the display screen after the selector switch was turned to a range of resistance values as shown in Figure 3.13.
- e. The megger was wound again after five (5) minutes for a second reading and the average of the two values was taken.
- f. The leads were disconnected from the megger for backfilling to be done.

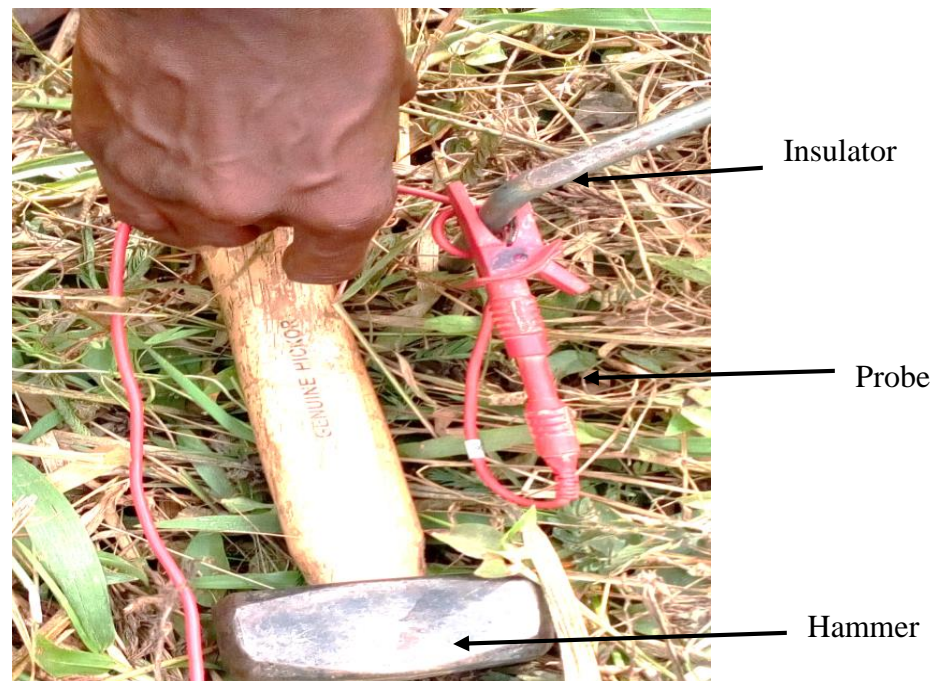


**Figure 3.12 The Probe and Leads Used**



**Figure 3.13 Megger Showing Resistance Value**

The backfill materials were weighed on a beam balance before they were filled into the PVC pipe until it was full as seen in Figure 3.14. The backfill material was allowed to settle for five minutes after which the megger was used this time to take the resistance values after backfilling was done. Figure 3.15 and Figure 3.16 show when the backfill was applied and when the second reading was taken.



**Figure 3.14 Backfill Material being Weighed**



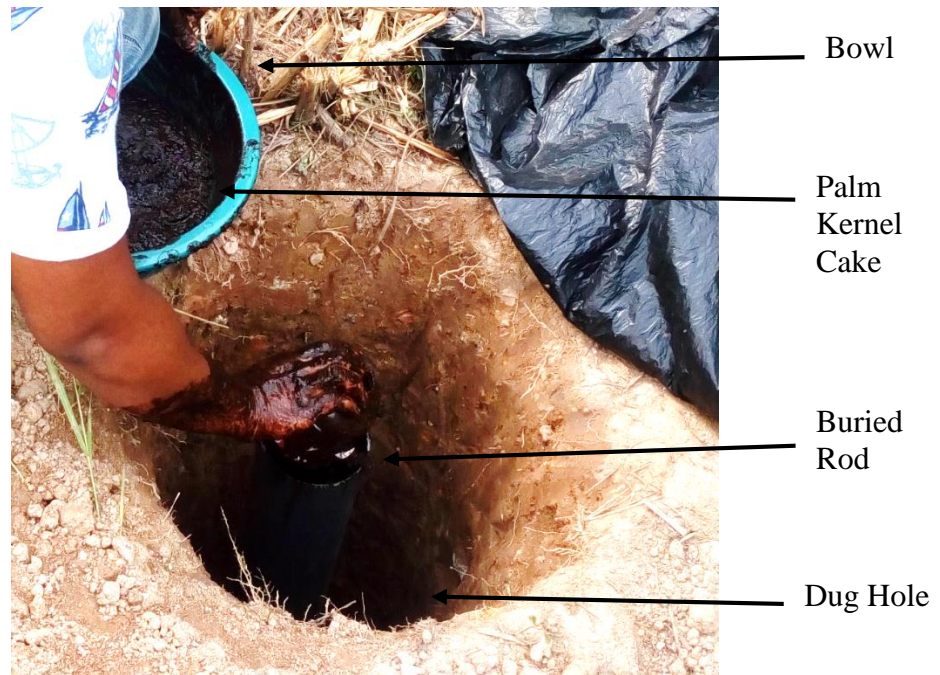


**Figure 3.15 Application of Backfill Material**

The PVC pipe was removed after the two readings were taken and the hole left around the PVC pipe was packed with the soil that was dug out. This procedure was repeated for all the other backfill materials. 0.2 m PVC pipe is cut and put around the buried rods for easy identification and reading. Figure 3.16 shows how the probe was used for the resistance readings.

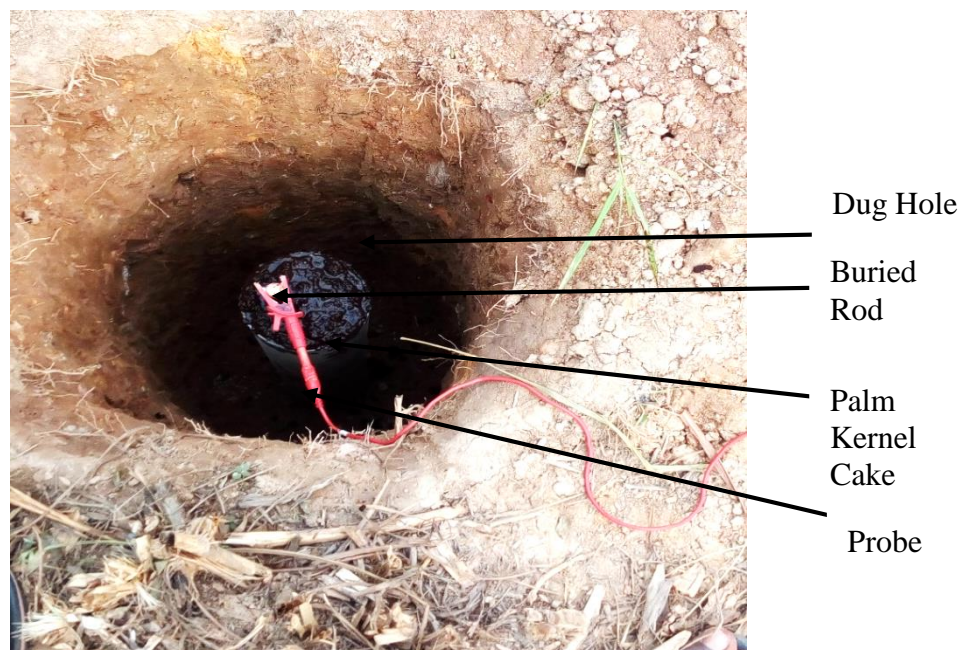


**Figure 3.16 Use of Probe for Resistance Readings**

### 3.6 Laboratory Experiments

The Laboratory Facility at the Minerals Engineering Department of the University of Mines and Technology, Tarkwa was used to perform physio-chemical analysis of the soil sample from the study site and the backfill materials. The pH, organic carbon, exchangeable bases, particle size, soil texture, and soil moisture content were the parameters considered.

#### 3.6.1 Determination of pH of Samples in Water

Ten grams of soil were weighed into a beaker and 10 ml of distilled water was added. This gave a soil-to-solution ratio of 1:1. The mixture was stirred for 30 minutes and left for one hour during which most of the suspended soil had settled from the suspension. The pH meter was calibrated with a standard buffer solution of 4, 7, and 10. The electrode was then immersed into partly settled suspension and the reading recorded.

#### 3.6.2 Determination of Organic Carbon

The Total Organic Carbon (TOC) was determined by treating an aliquot of the dried sample with sufficient phosphoric acid (1:1) to remove inorganic carbon before instrument analysis. Percent TOC was determined in sample dried at 105 °C by using a LECO SC-144DR Carbon Analyser. The prepared sample was combusted at 1350 °C in an oxygen atmosphere using a LECO SC-144DR. Carbon is oxidised to form CO<sub>2</sub>. The gaseous phase flowed through two scrubber tubes. To trap water and chlorine gas, the first scrubber tube was packed with Drierite (CaSO<sub>4</sub>) and copper granules; the second scrubber tube was packed with Anhydron (Mg(ClO<sub>4</sub>)<sub>2</sub>) to remove leftover moisture. The gaseous phase was then passed through an NDIR (Non-Dispersive Infrared) detection cell that was adjusted to respond only to CO<sub>2</sub>. The integrated area under the signal detected is proportional to the amount of CO<sub>2</sub> passing through the NDIR cell. The weight-corrected result is % C. From the results, the percentage of total organic carbon was calculated.

#### 3.6.3 Extraction of Exchangeable Bases

Ten (10) grammes of the samples were weighed into beakers and 25 ml of Nitric Acid (HNO<sub>3</sub>) together with 75 ml of Hydrochloric Acid (HCl), was added to each sample in the beaker. The mixtures were swirled and heated for 30 minutes at 100 °C. The supernatant solutions obtained after heating were filtered through No. 42 Whatman filter paper after which the filtrates were topped up to 100 ml. Both exchangeable base metals and heavy metals were determined using AA240FS Atomic Adsorption Spectrometer. The results

obtained from the Atomic Adsorption Spectrometer were used to calculate the concentration of the metals in the samples.

### 3.6.4 Particle Size Distribution

The soil sample was dehydrated in an oven at 105 °C after which 1 kg of oven-dried soil sample was screened using a set of sieves and a sieve shaker for 20 minutes. The particles remaining on top of each sieve were then weighed and recorded. Also, the particles collected below the last sieve were collected, weighed, and recorded. The results obtained from the screening process were used to calculate the distribution of soil samples according to the particle sizes.

### 3.6.5 Soil Texture

A 250 ml volumetric cylinder was used to measure 100 ml of distilled water in which 50 g of oven-dried soil sample was added. The mixture was shaken for an hour and left to settle overnight. The volume occupied by the different soil fractions was measured and recorded. The percentage of soil fractions were calculated using;

$$\% \text{ Soil Fraction} = \frac{\text{Volume of Soil Fraction}}{\text{Total Volume of Soil}} \times 100 \quad (3.1)$$

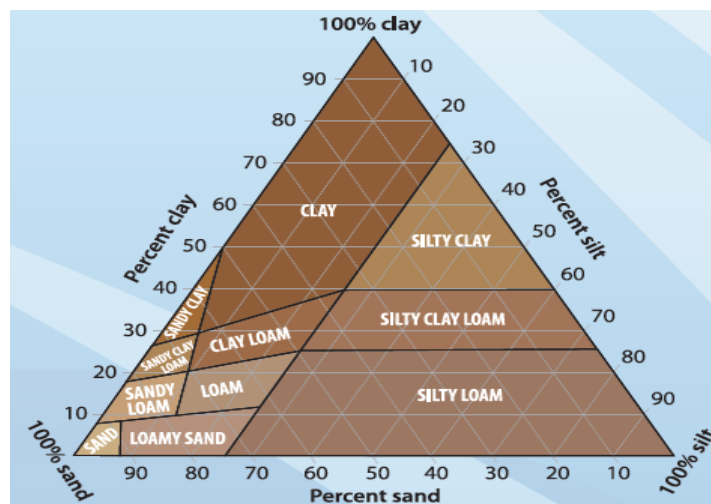


**Figure 3.17 A Soil Textural Triangle Used to Determine Soil Texture Image**

After obtaining a value, Figure 3.17, Hunt and Gilkes (1992) was used to estimate the type of soil.

### 3.6.6 Determination of Moisture Content of Soil

The moisture content of the soil is the water in the soil that can be removed by drying to a constant weight in an oven at 105 °C – 110 °C. Water content is based on oven-dried weight and is usually expressed in units of mass of water per unit mass of soil ( $\text{g g}^{-1}$ ), which is the gravimetric water content ( $O_g$ ) or in the volume of water per unit volume of soil ( $\text{cm}^3 \text{cm}^{-3}$ ), which is the volumetric water content ( $O_v$ ).

The soil sample was uniformly mixed in which 100 g was sampled using a moisture can and dried in the oven overnight at a temperature of 105 °C. After drying, the sample was allowed to cool using a desiccator, and weighed. The moisture content of the soil was calculated using the difference in weight before and after drying.

$$\text{Percentage Moisture} = \frac{\text{Wet Weight} - \text{Dry Weight}}{\text{Wet Weight}} \times 100 \quad (3.2)$$

### 3.7 Sample Preparation

After the five rods had been buried for twenty-two months, they were removed for analysis. They were planted on 6<sup>th</sup> January 2018 and removed on the 19<sup>th</sup> of October, 2019.

The soil surrounding the rod was dug out instead of pulling as this may have caused scratching of the rod surface, scrapping the surface off the corrosion that has taken place. Figures 3.18 and Figure 3.19 show the rod being dug out and the rod after removal from the soil, respectively.



**Figure 3.18 Rod Being Dug Out**

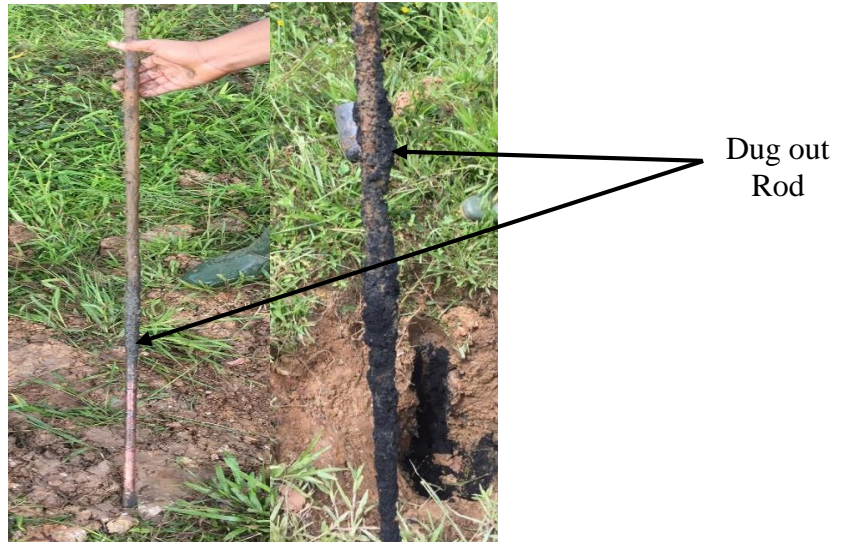


**Figure 3.19 Samples of Rods after Removal from the Soil**

The following measures were put in place to prepare the rods for the laboratory:

- a. Four (4) rods were randomly selected to be uprooted.
- b. The rods were washed with water to clear the soil and backfill materials that were still on the rod as realised in Figure 3.20. Figure 3.21 shows the rods that were removed from the soil.
- c. They were transported to the Geological Engineering Laboratory of UMaT for their thickness and weight to be taken using vernier callipers and beam balance, respectively. Figure 3.22 shows how the thickness was taken and Table 4.1 shows the values for the parameter.
- d. They were cut into 4 unequal parts, except for a portion of height 0.017 m and diameter 0.013 m for SEM-EDS and XRF analysis at the Environmental Engineering Laboratory of UMaT. Figure 3.23 shows the rod samples ready for the SEM-EDS analysis



Dug out  
Rod

**Figure 3.20 Rods Being Washed**



**Figure 3.21 The Four Rods that were Removed**

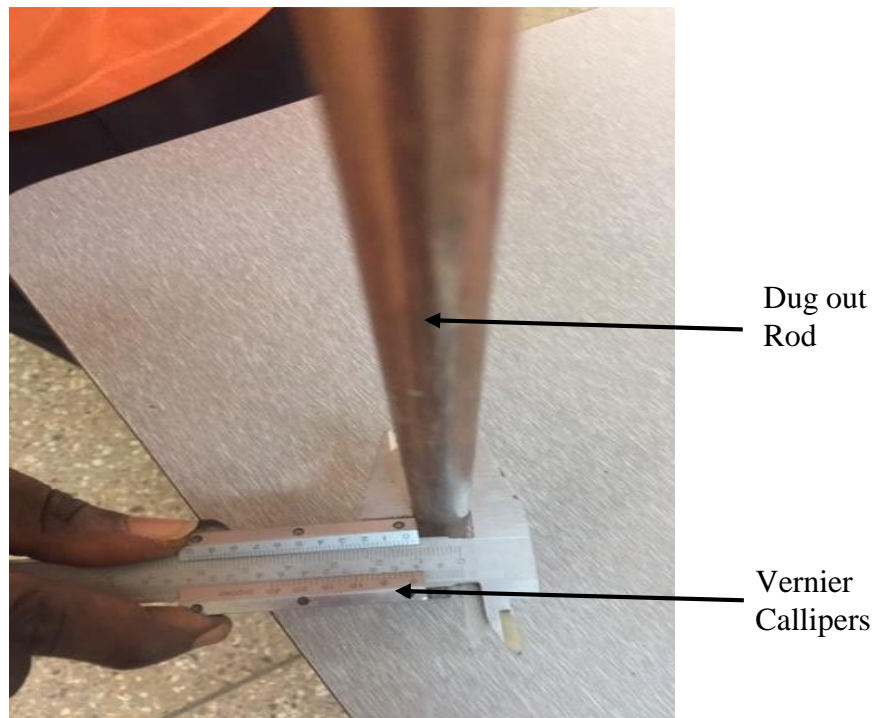


**Figure 3.22 The Measurement of the Thickness of the Rods**

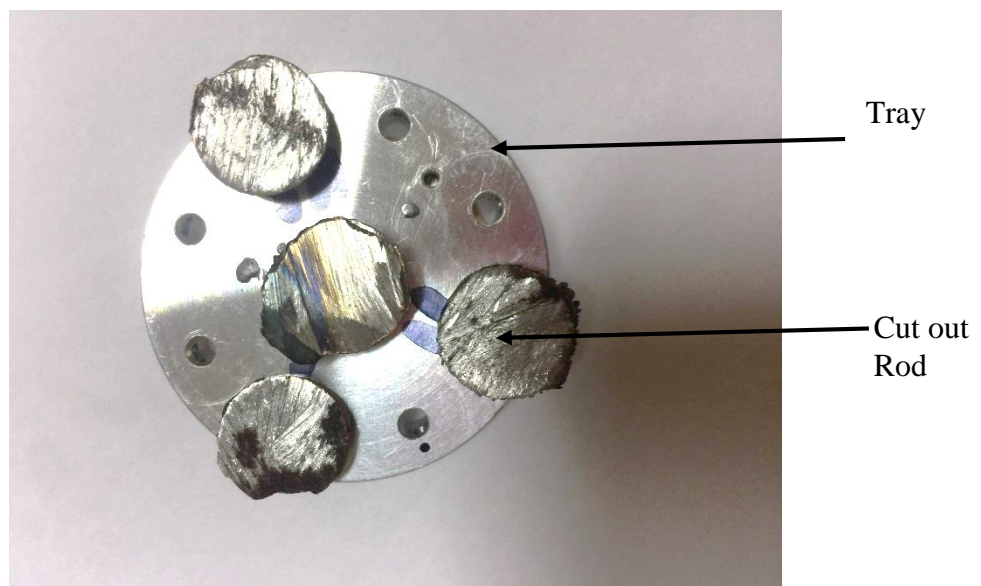


**Figure 3.23 Rod Samples Ready for SEM-EDS Analysis**

### 3.8 Corrosion Rate Equation

Many researchers have come out with different corrosion rate equations based on the parameters under consideration. However, Ahmed *et al.* (2017) formulated the equation for calculating the rate of corrosion that relates to this study. Equation (3.3) is the commonest equation for finding corrosion current density.

$$i_{\text{corr}} = \frac{I}{A} \quad (3.3)$$

where,  $i_{\text{corr}}$  is corrosion current density,  $\mu\text{A}/\text{cm}^2$ ;  $I_{\text{corr}}$  is total anodic current,  $\mu\text{A}$ ; and  $A$  is exposed specimen area,  $\text{cm}^2$

Umoren *et al.* (2012) said the Equivalent Weight (EW) may be understood of as the mass of metal in grams that will be oxidised by the passage of one Faraday (96489 C (amp-sec)) of electric charge. The value of EW is independent on the unit system selected and so may be considered dimensionless. For pure elements, the equivalent weight is given by:

$$\text{EW} = \frac{W}{n} \quad (3.4)$$

where,  $W$  is the atomic weight of the element and  $n$  is the number of electrons required

Faraday's Law can be used to calculate the corrosion rate in terms of penetration rate (CR) (Umoren *et al.*, 2012), given as:

$$\text{CR} = K_1 \frac{i_{\text{corr}}}{\rho} \text{EW} \quad (3.5)$$

where, CR is given in mm/yr,  $i_{\text{corr}}$  in  $\mu\text{A}/\text{cm}^2$ ,  $K_1 = 3.27 \times 10^{-3}$ , mm/  $\mu\text{A cm yr}$ ,  $\rho$  is density in  $\text{g}/\text{cm}^3$  and

$$\text{CR (mm/yr)} = \frac{87.6 W}{\rho A t} \quad (3.6)$$

where, CR is the corrosion rate;  $W$  is the weight loss (mg);  $\rho$  is the density ( $\text{g cm}^{-2}$ );  $A$  is the area ( $\text{cm}^2$ ); and  $T$  is the exposure time (h).

Badea *et al.* (2010) compared the two methods based on polarisation measurements for determining corrosion rates, namely, extrapolation of the Tafel slopes with corrosion potential – Stern method and polarisation resistance – Stern-Geary method:

$$i_{\text{app}} = i_{\text{corr}} \left\{ \exp \left[ \frac{\alpha_{\text{a,M}} z F}{RT} (E - E_{\text{corr}}) \right] - \exp \left[ -\frac{\alpha_{\text{c,Ox}} z F}{RT} (E - E_{\text{corr}}) \right] \right\} \quad (3.7)$$



where,  $i_{app}$  is applied or measured current density,  $i_{corr}$  is the corrosion current density,  $\alpha_{a,M}$ ,  $\alpha_{C,Ox}$  is the charge transfer coefficients for anodic and cathodic reactions, respectively;  $E - E_{corr}$  - polarisation, given by the difference between applied and corrosion potential,  $Z$  is metal valence,  $F$  is Faraday constant,  $R$  is gas constant and  $T$  is the absolute temperature Oloche *et al.* (2009) analysed the correlation between varying corrosion parameters and the corrosion rate of some elements and came out with the equation (3.8):

$$B = \frac{534W}{\rho At} \quad (3.8)$$

where,  $B$  is the corrosion rate (mpy),  $W$  is the weight loss (mg),  $\rho$  is the density ( $g/cm^3$ ),  $A$  is the area ( $in^2$ ), and  $t$  is the immersion time (h) and

$$v_n = \sum_j \sum_m \frac{R_{d,j,m} M_j}{\rho_j} \quad (3.9)$$

Tong *et al.* (2018) used the following parameters for the simulation of some factors that influence a vertical DC grounding electrode with equations 3.8 and 3.9.  $M_j$  is the molar mass of dissolved-deposited materials in  $kg/mol$  and  $\rho_j$  is the density of dissolved-deposited materials in  $kg/m^3$ .  $R_{d,j,m}$  is the reaction rate of dissolved-deposited substances in  $mol/(m^2.s)$  and is expressed as:

$$R_{d,j,m} = \frac{-V_{d,j,m}^{loc,m}}{n_m F} \quad (3.10)$$

Where,  $d$  denotes dissolving or deposition,  $j$  denotes dissolved or deposited substances, including cathodic and anodic reactions,  $V_{d,j,m}$  is the reaction stoichiometric coefficient of dissolved-deposited substances,  $I_{loc,m}$  is the local current produced by the reaction in  $A/m^2$  and  $n_m$  is the number of electrons involved in the reaction and  $F$  is the Faraday constant of the reactive substance in  $C/mol$

The following are more equations that are related to corrosion rates

$$v = \frac{i_{corr} \times \text{Chemical equivalent}}{\rho F} \quad (cm/s) \quad (3.11)$$

where,  $F$  is Faraday constant (Zhengi *et al.*, 2018)

$$v = \frac{8.76 \times 10^4 \times \Delta W}{S \times t \times \rho} \quad (3.12)$$

where,  $v$  is the corrosion rate, mm/a,  $\Delta W$  is the weight loss, g,  $S$  is the total area of the sample,  $\text{cm}^2$  and  $t$  is the immersion time (Wang *et al.*, 2015)

$$v = \frac{1}{\rho \cdot \Delta t} \frac{\Delta m}{S} \quad (3.13)$$

where,  $\rho$  is the material density in  $\text{g/cm}^3$ ,  $\Delta t$  is the duration of the experiment in s and  $\Delta m$  is the mass lost in g (Liengen *et al.*, 2014).

$$\text{Corrosion Rate (mm/yr)} = \frac{K \times W}{A \times T \times D} \quad (3.14)$$

where,  $K$  is a constant =  $8.76 \times 10^4$ ,  $T$  is exposure time in hours,  $D$  = density in  $\text{g/cm}^3$  of material and  $A$  is the area in  $\text{cm}^2$  (Wasim, 2018).

$$\text{CPR} = \frac{KW}{\rho At} \quad (3.15)$$

where,  $t$  is the exposure time,  $W$  is the weight loss, ,  $A$  is the area and  $K$  is the constant

$$v = \frac{8.76 \times 10^4 \times \Delta W}{S \times t \times \rho} \quad (3.16)$$

where,  $v$  is the corrosion rate, mm/a,  $\Delta W$  is the weight loss, g,  $S$  is the total area of the sample,  $\text{cm}^2$ ,  $t$  is the immersion time, h, and  $\rho$  is the density of the sample,  $\text{g/cm}^3$  (Wang *et al.*, 2014).

The change of gravimetric parameters into electrochemical ones is made employing Faraday's law:

$$i_{\text{corr}} = \frac{nF\Delta W}{MTS} \quad (3.17)$$

where,  $I_{\text{corr}}$  is the corrosion current density,  $\text{A/cm}^2$   $n$  is valence,  $F$  is Faraday's constant (96500 coulombs),  $\Delta W$  is weight loss due to corrosion, g,  $M$  is the molecular weight of the metal,  $\text{g/mol}$ ,  $T$  is the immersion time, s,  $S$  is the total area of the sample,  $\text{cm}^2$  (Wang *et al.*, 2014).

### 3.8.1 Uniform Corrosion Kinetics

#### *Faraday's law*

A charge transfer reaction (oxidation or a reduction reaction) at a metal surface generates a partial current, which is proportional to the moles of metals or a reactant oxidised or reduced per second.

$$I = nFN \quad (3.18)$$

where,  $I$  is Partial current due to charge transfer reaction  $A$ ,  $F$  is Faraday's constant ( $96.48 \times 10^3$ ),  $N$  is the number of moles of metal or reactant oxidised or reduced per second ( $\text{mol S}^{-1}$ ),  $n$  is the number of electrons transferred by the charge transfer reaction ( $\text{equiv. mol}^{-1}$ )

For an oxidation reaction, which causes corrosion of metal, Faraday's law becomes:

$$I_{\text{ox}} = nFN_{\text{ox}} = I_{\text{corrosion}} \quad (3.19)$$

Corrosion rates can be expressed in terms of weight loss. Thus:

$$\frac{dw}{dt} N_{\text{ox}} W_0 \quad (3.20)$$

where,  $dw/dt$  is the rate of weight loss (corrosion rate) ( $\text{gs}^{-1}$ ),  $W_0$  is the molecular weight of corroding metal ( $\text{gmol}^{-1}$ ). From equation (3.20),

$$N_{\text{ox}} = \frac{I_{\text{ox}}}{nF} \quad (3.21)$$

Putting the above into equation (3.22)

$$\frac{dw}{dt} = \frac{I_{\text{ox}} W_0}{nF} \quad (3.22)$$

Integrating equation (3.23)

$$W = \frac{W_0}{nF} \int I_{\text{ox}} dt \quad (3.23)$$

$$W = \frac{W_0 Q}{nF} \quad (3.24)$$

where,  $Q$  is the total charge passed in coulombs during the same period,  $W$  is the total weight loss due to corrosion over some "t" seconds

$$\text{Loss of thickness (cm/s)} = \frac{1}{\rho A} \frac{dw}{dt} \quad (3.25)$$

$$= \frac{i_{\text{corr}} W_o}{\rho A n F} \quad (3.26)$$

$$= \frac{i_{\text{corr}} W_o}{\rho n F} \quad (3.27)$$

$$\frac{dx}{dt} = \frac{i_{\text{corr}} M}{\rho n F} \quad (3.28)$$

$$\int dx = \frac{i_{\text{corr}} M}{\rho n F} \int dt \quad (3.29)$$

$$x = \frac{i_{\text{corr}} M t}{\rho n F} \quad (3.30)$$

where, x is corrosion rate, t is time (seconds),  $I_{\text{corr}}$  is corrosion current density ( $\text{Acm}^{-3}$ ), A is the area of corroding metal exposed to the solution, M is the molar mass of metal and n is the charge of metal

The formula for corrosion current density is

$$i_{\text{corr}} = \frac{I}{A} \quad (3.31)$$

$$\rho = \frac{m}{V} \quad (3.32)$$

where, m is mass and V is volume

### 3.9 Laboratory Analysis of Buried Rods

#### 3.9.1 XRF Analysis

### *Sample preparation*

- i. Sample cut across the rod at a thickness of 2 mm.
- ii. The sample was transported to the lab for analysis in an airtight container.

### *Measurement*

- i. The sample was placed on a sample base plate making sure the sample covered the minimum measurement area and covered with an X-ray deflection shield.
- ii. The instrument was configured to alloy steel analyses.
- iii. Analyses began and results produced.

### *X-ray fluorescence process*

- i. A solid sample is irradiated with high-energy X-rays from a controlled X-ray tube.
- ii. An electron from one of the atom's inner orbital shells is expelled when an atom in the sample is attacked by an X-ray of sufficient energy (higher than the atom's K or L shell binding energy).
- iii. The atom regains stability, with an electron from one of the atom's higher energy orbital shells replacing the vacancy left in the inner orbital shell..
- iv. The electron emits a luminous X-ray when it falls to a lower energy state. The particular difference in energy between two quantum states of the electron is equal to the energy of this X-ray. The basis of XRF analysis is the measurement of this energy.. Figure 3.24 is the whole process summarised.

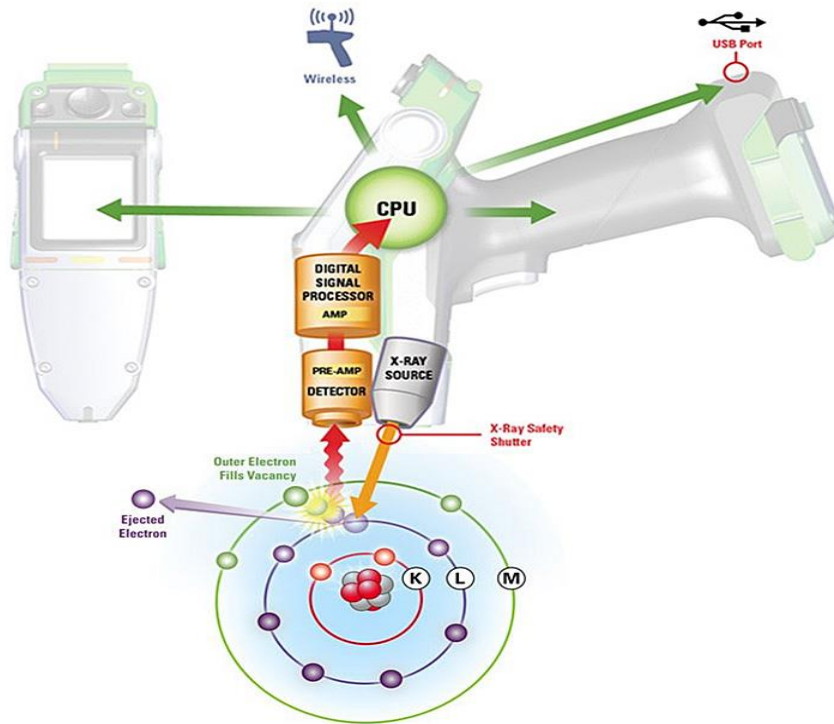


**Figure 3.24 Process of XRF**

### 3.9.2 SEM-EDS Analysis

- i. Scanning electron microscopy (SEM) images were booked using a Zeiss EVO MA 15 SEM.
- ii. The secondary electron (SE) detector allowed visualisation of the samples under high vacuum operation.
- iii. A BRUKER QUATAX EDS system with XFlash Detector 610M was employed as the energy dispersive X-ray detector (EDS).
- iv. SEM micrographs and EDS spectra of the samples were collected using an accelerating voltage of 20 kV, a magnification of x200 with a working distance that ranged between 8 mm to 10 mm.
- v. The obverse and reverse of each coin were analysed with no sample preparation placed in their entirety onto the sample holder.
- vi. Carbon conducting tape was used throughout this study to prevent charging, meaning that the presence of carbon is inevitable on every spectrum collected.
- vii. Oxygen will also be present on every spectrum collected due to outside influences such as contamination from carbon dioxide (CO<sub>2</sub>) or oxygen (O<sub>2</sub>)

in the air. Unless specifically commented on about a corrosion product the existence of C and O in the elemental analysis can be disregarded.

### **3.10 Summary**

This chapter began with the preparation of the field study area, the backfill materials, and how the rods were buried, and readings were taken. The first laboratory analysis of the soil and backfill materials was undertaken. The corrosion rate equation was derived from the different corrosion equations reviewed. The rod samples were removed from the soil and prepared for the second laboratory analysis which involved the use of XRF and SEM-EDS.

## **CHAPTER 4**

### **COMPUTER SIMULATIONS**

#### **4.1 Introduction**

Chapter 4 is the last aspect of the methods that have been treated in chapter 3. It contains stages and methods for corrosion prediction. The traditional means, namely; use of vision, XRF and SEM-EDS are the laboratory analyses that were used to predict corrosion. Two AI techniques were used for the prediction of corrosion of the buried earth rods. These are the Fuzzy Logic System and Neural Network System. Their methods, including design, have been dealt with thoroughly in this chapter.

#### **4.2 Fuzzy Logic System Design**

A fuzzy logic system is a combination of knowledge-based rules and the use of MATLAB. The model was developed using the Mamdani fuzzy inference technique. This system was chosen over the others because the Mamdani system modifies the rules for the input-output parameters without altering the relationship that exists between them. The proposed fuzzy model was based on the field data that was collected over twenty-two (2) months. The five most important factors, namely, backfill materials, temperature, rainfall, resistance, and time (weeks), were used as the input parameters whilst the corrosion rate was designated as the output parameter for the proposed fuzzy logic model. Each of the input and output variables was assigned some member functions depending on the type of parameter. Figure 4.1 is the flow chart of the Fuzzy Logic System and Figure 4.2 is the MATLAB Graphic User Interface (GUI) for Mamdani-based Fuzzy Logic System.



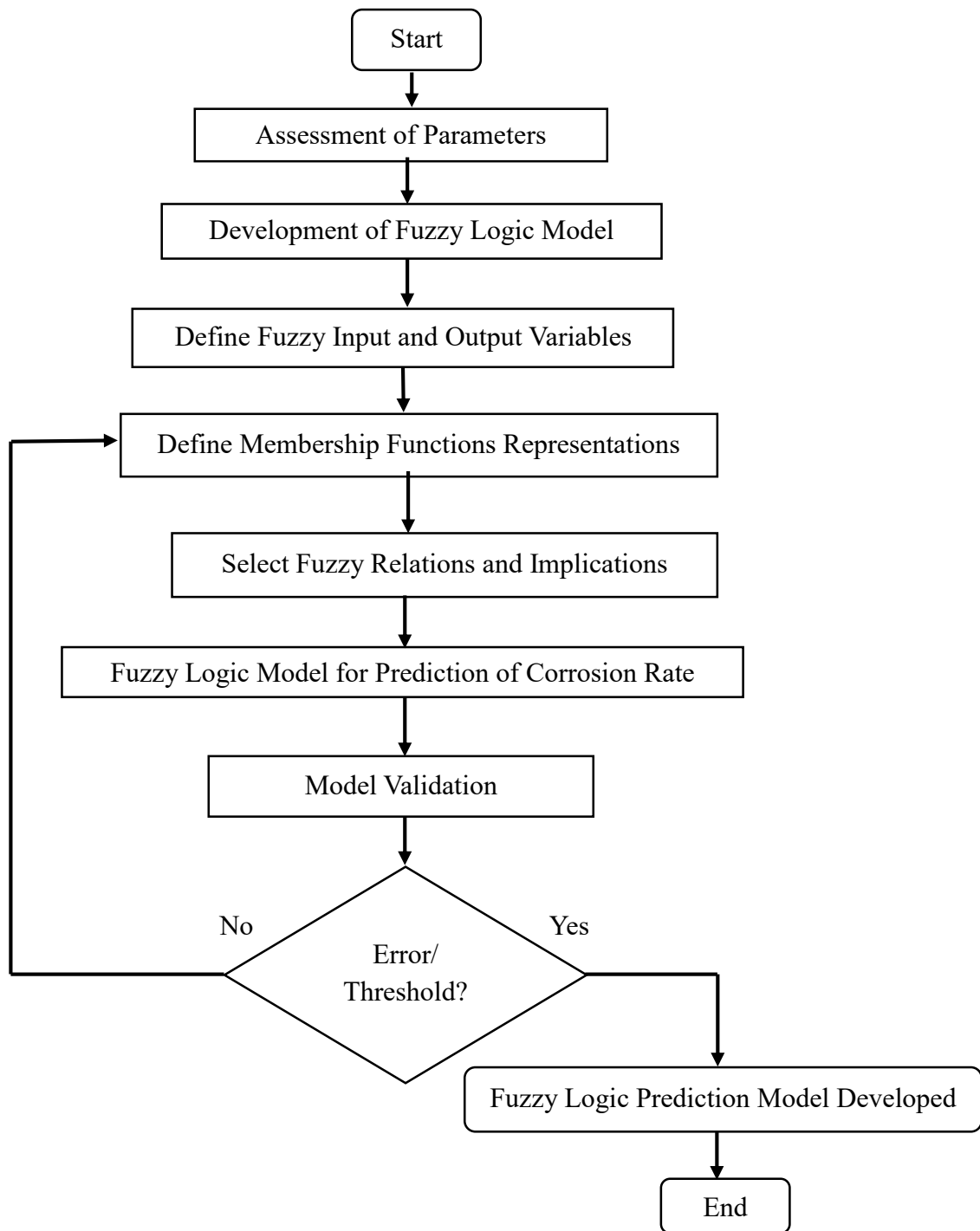


**Figure 4.1 Flow Chart of the Fuzzy Logic System**

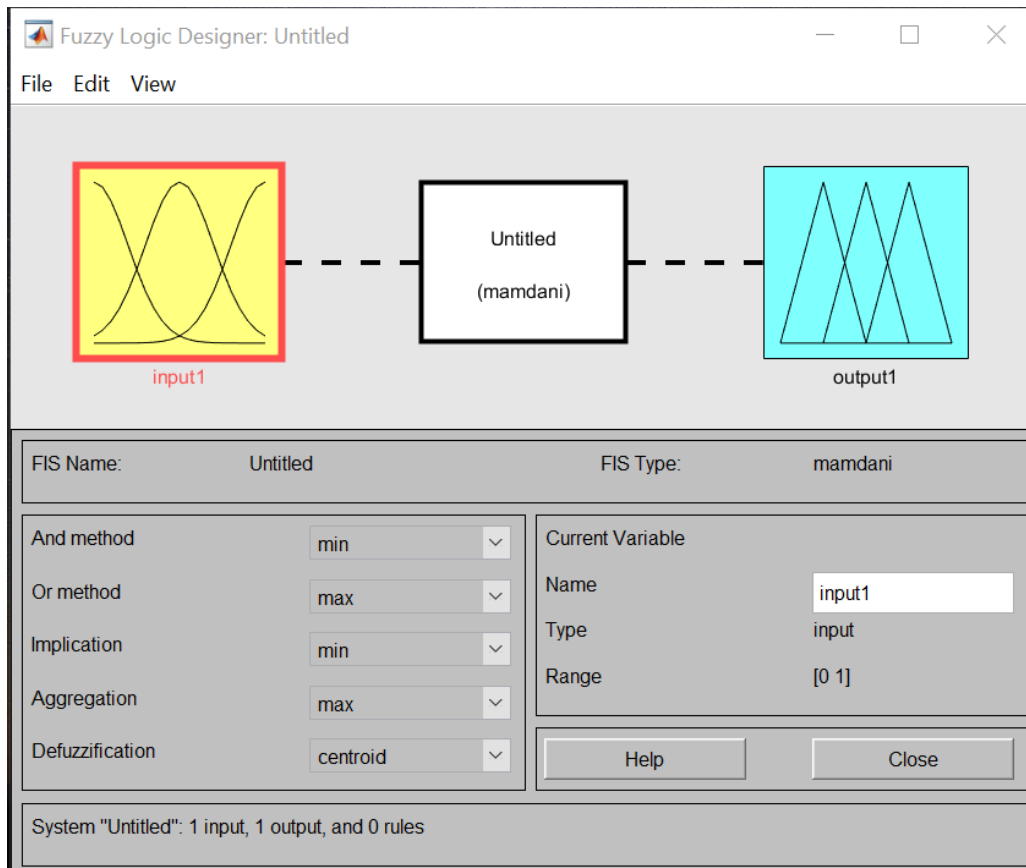


**Figure 4.2 Mamdani-based Fuzzy Logic System GUI**

#### 4.2.1 Fuzzification of Parameters

The fuzzification process of the crisp values of the considered variables was converted into grades of membership sets within the ranges of very low, low, medium, high, and very high. The values were based on the nature of the available data, which also led to the usage of the Triangular Membership Function (TRIMF). TRIMF was used for its simplicity to implement and fastness for computation. Also, the degree of truth that was implemented by the input parameter suited the TRIMF type of membership function. Figure 4.3 is the interface of a typical Mamdani triangular membership function before the variables are inputted.

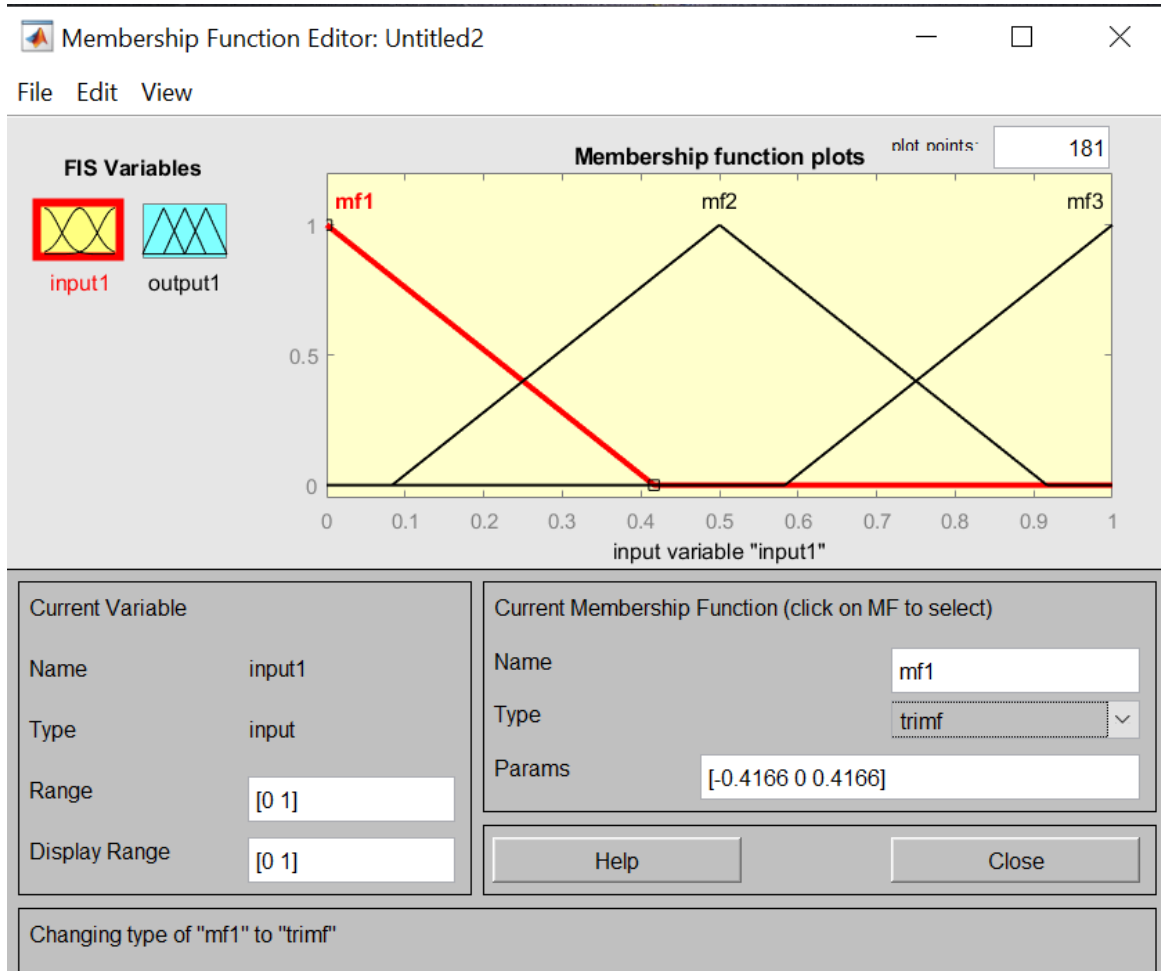


**Figure 4.3 Mamdani-based Triangular Member Function**

The method employed in designing the Mamfis is the GUI of the fuzzy toolbox in MATLAB.

The following steps were used:

- a. The ranges of the input and output variables were defined in Figure 4.4 and Tables 4.1, 4.2, and 4.3.
- b. The MF editor executed the shapes and type of MF that was used which was TRIMF for both input and output variables from Figures 4.4 and 4.5.
- c. Fifty-six rules were formulated using the rule menu editor based on the MFs from Figure 4.6.
- d. The rules were assessed using the rule viewer to see the input and output mappings in Chapter 5 of the results.

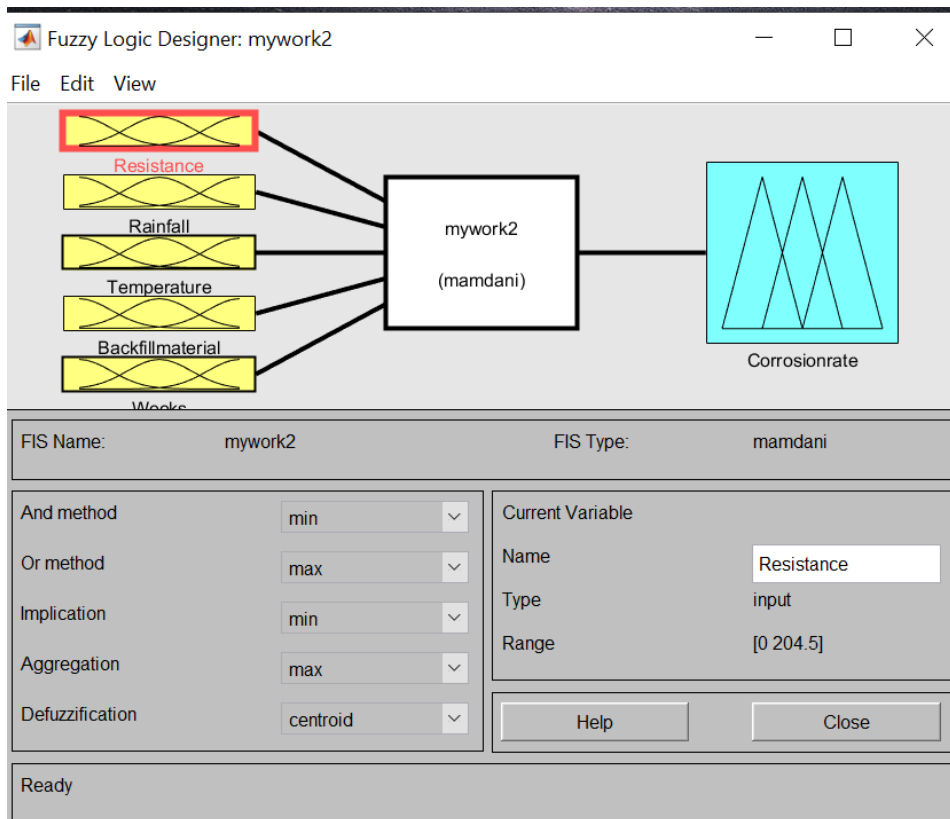


**Figure 4.4 Mamdani-based Fuzzy Logic Input and Output Variables**

**Table 4.1 Backfill Materials of Five Membership Functions**

Parameter: Backfill Material	Symbol	Range/ Membership Function Descriptor
Reference	Ref	0 - 0.2
Palm Kernel Cake	PKC	0.2 - 0.4
Tyre Ash	TA	0.4 - 0.6
Coconut Coir	CC	0.6 - 0.8
Charred Coconut Coir	CCH	0.8 - 1.0

The other input variables, namely, rainfall, resistance, temperature, and weeks were assigned the three membership functions, namely, low, medium, and high.

**Table 4.2 Ranges for the Input Variables /Parameters**

Range/ Parameter	Rainfall	Resistance	Temperature	Weeks
Low	0 - 22.330	0 - 68.16	24.35 - 26.36	1- 34
Medium	22.340 - 44.663	68.17 - 136.33	26.37 - 28.38	35 - 68
High	44.664 - 67.000	136.34 - 204.5	28.39 - 30.41	69 - 104

**Table 4.3 Membership Function of Descriptor and Corrosion Rate Ranges**

Membership Function Descriptor	Corrosion Rate Range ( $\text{Am}^{-2}\text{s}^{-1}$ )
Very Low	0 - 280
Low	281 - 560
Medium	561 - 840
High	841 - 1120
Very High	1121 - 1400

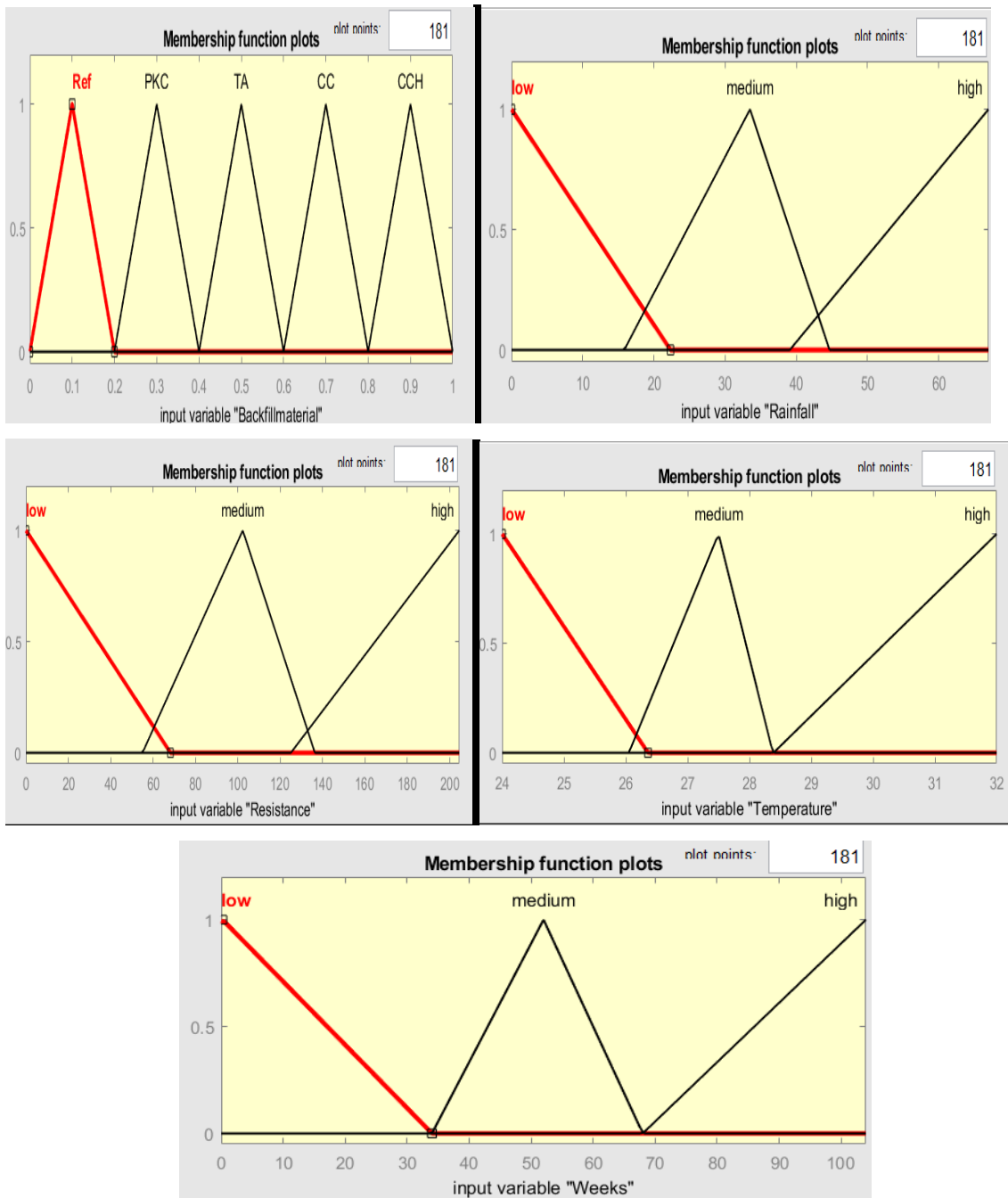


**Figure 4.5 The 5 Mamdani-based Membership Functions of the Input Variables of the Fuzzy Sets**

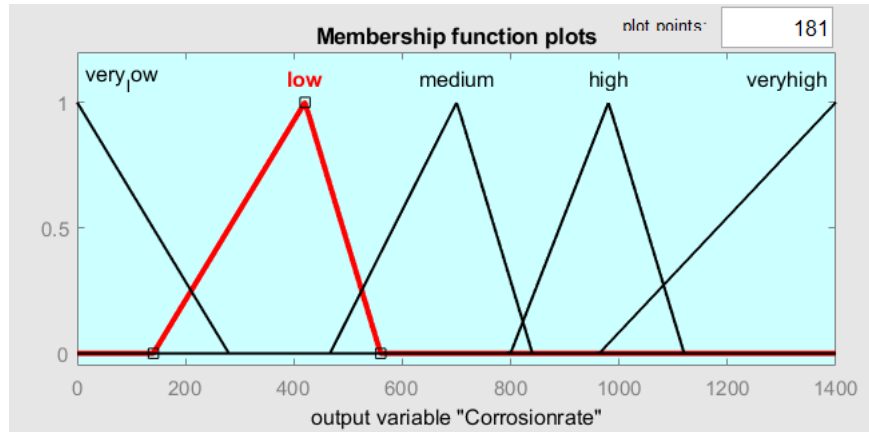


**Figure 4.6 Output Membership Functions of Mamdani-based Fuzzy Logic System**

Once the input and output parameters were ready, several rules must correspond to the member functions of each input parameter. For this model, a total number of thirty-seven rules were generated based on the proposed fuzzy logic model. The membership function that identifies the corrosion rate with the fuzzy sets is shown in Figure 4.6. A triangular membership is also used for this nature of available data.

#### 4.2.2 Inference

The inference introduces the fuzzy logic expert system, that is, it defines the IF-THEN rules which serve as the basis for the creation of the input-output relationships. The Mamdani fuzzy model was used to aggregate the rules. The interface for the Mamdani algorithm for the IF-THEN rules is designed as follows:

IF  $x_1$  is  $A_1$  AND  $x_2$  is  $A_2$  . . . AND  $x_n$  is  $A_n$  THEN  $y$  is  $B$

where,  $X_{1,2n}$  = Inputs,  $A_{1,2n}$  = Value of a certain input (L, M or H),  $y$  = Output,  $B$  = Value of the output (VL, L, M, H, or VH)

The rule for the proposed fuzzy logic expert system that could model the relationship between the considered variables and the corrosion rate was fifty-six (56). The rules were corrected to 56 as indicated in the work. The rules were determined based on expert knowledge and derived from patterns that were realized from the data gathered from field studies.

Figure 4.7 shows some of the rules that were considered.

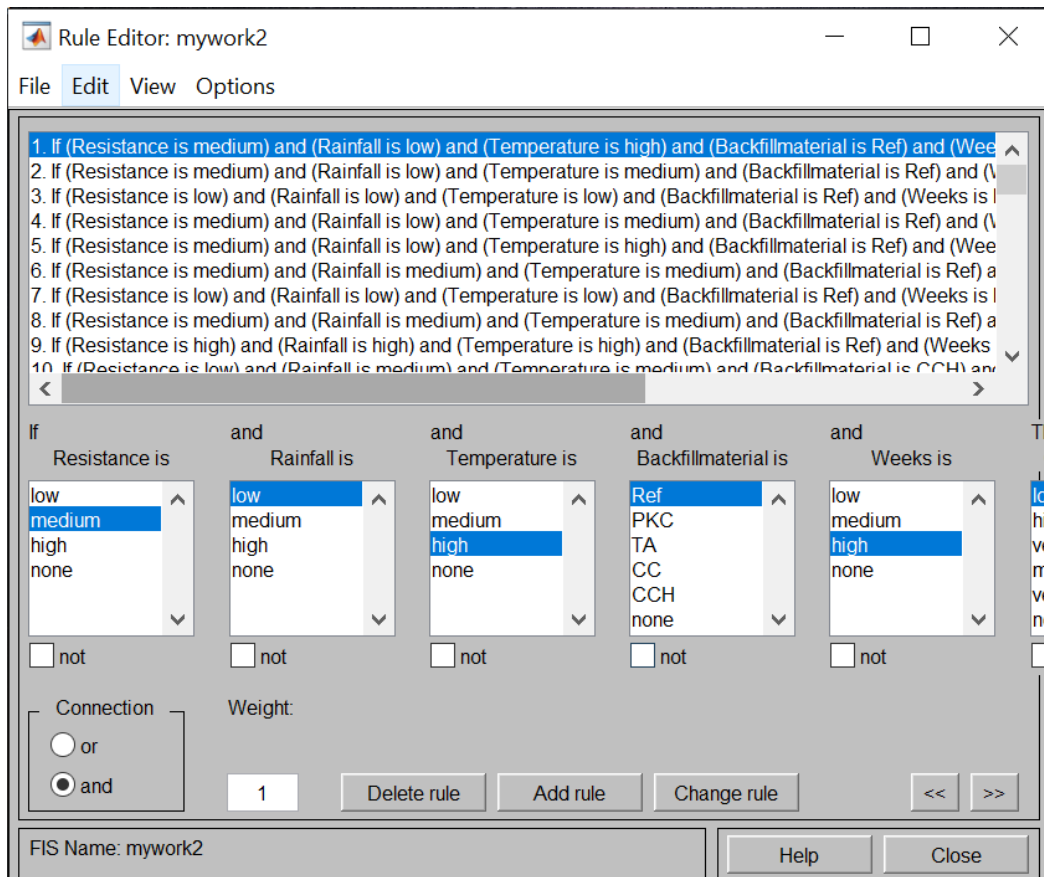


**Figure 4.7 Mamdani-based Fuzzy Logic System Rule Formulation**

### 4.3 Neural Network System Design

In designing and creating the neural network, the data was obtained from the twenty-two months of burial of earth rods adjacent to UMaT. The parameters that were considered in the field study were resistance measurements ( $\Omega$ ) for five buried earth electrodes, average rainfall (mm), temperature during the day on which the grounding resistance is estimated, and time (weeks) that the resistance values were measured. A typical ANN is made up of three layers, the input, the hidden, and the output layer. The input layer encompasses five parameters, namely, resistance measurements ( $\Omega$ ) for buried earth electrodes, average rainfall height (mm), and temperature ( $^{\circ}\text{C}$ ) during the day on which the grounding resistance is estimated and time (weeks) that the resistance values were measured, and the backfill materials that were used as protection against corrosion of the buried earth electrodes and to improve resistance. The hidden layer comprises ten layers too and that of the output layer is made up of only one variable, which is the corrosion rate. Figure 4.8 is the structure of input and output data and Figure 4.9 shows the flow chart for the neural Network.

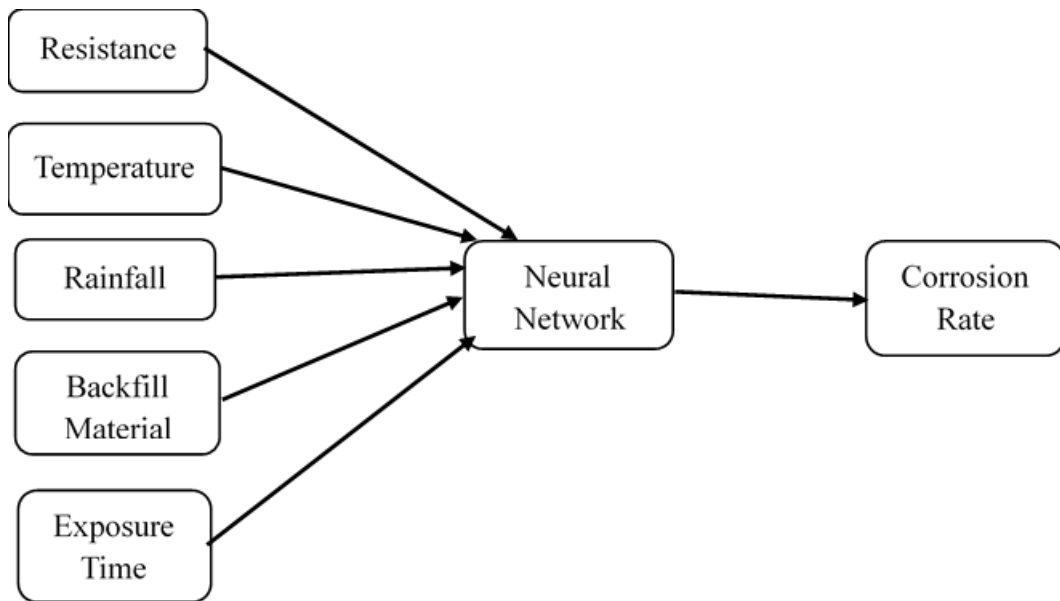


**Figure 4.8 Structure of the Relationship Between the Input and Output Variables**

As one of the prerequisites for the training, the variables needed to be normalised within the range of -2 and + 2. This normalisation was done using the standard deviation formula in Equation (4.1).

$$\sigma = \sqrt{\frac{\sum (x - \text{mean})^2}{n}} \quad (4.1)$$

where, x is a set of numbers, mean is the average of the set of numbers, n is the size of the set and  $\sigma$  is the standard deviation.



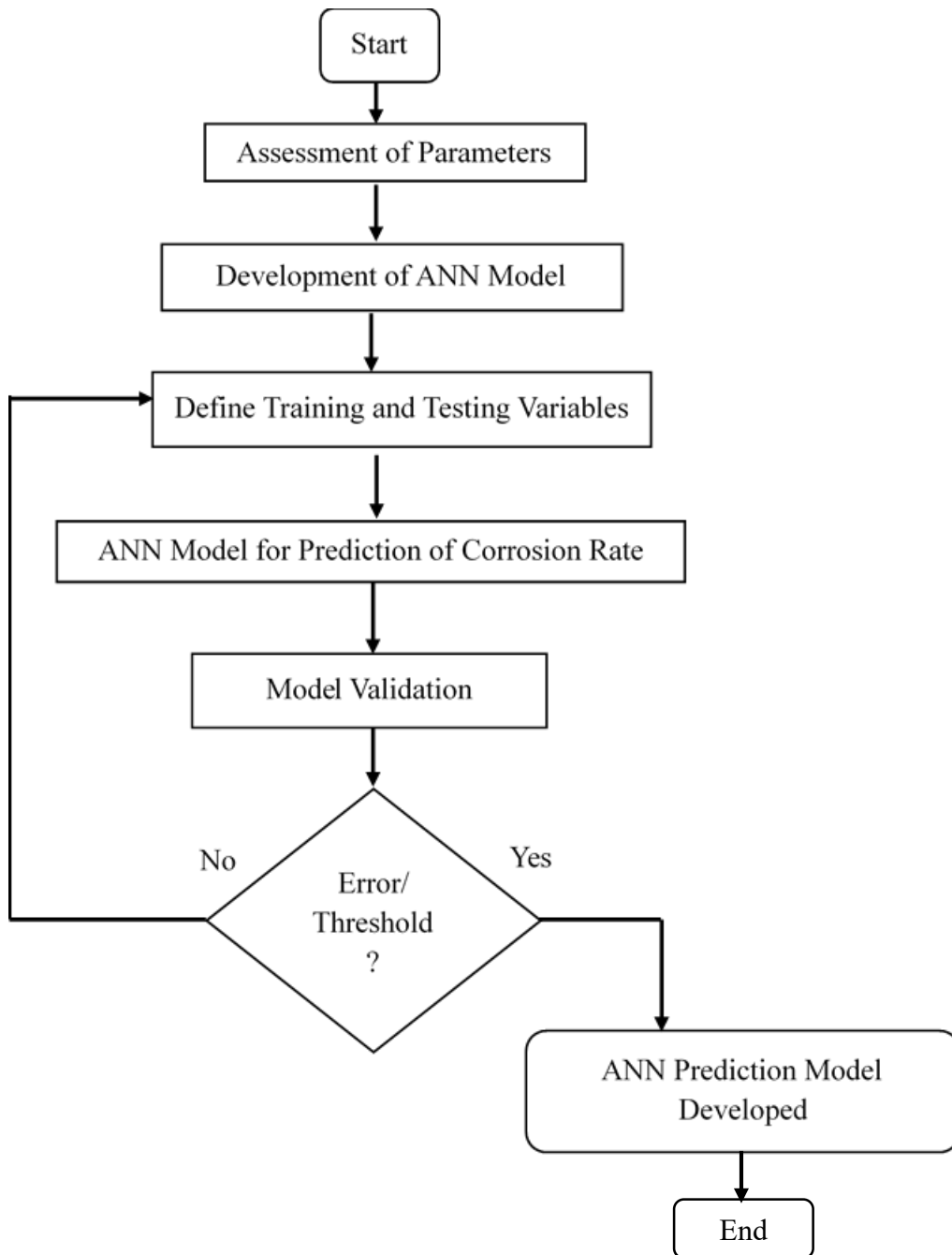


**Figure 4.9 Flow Chart for the Neural Network System**

Most user programs aim at creating algorithms to alter the input base into the output data, however, the neural network adopted to handle this research does not need any algorithm except the simplest called Bayesian Regularisation. The input data would be transformed into the output data by learning (through a training set). Learning is accomplished by adjusting the synaptic weights between neurons. The neural network learns by comparing the actual and expected outputs and adjusting the synaptic weights so that the discrepancy

between the expected and actual outputs diminishes. Figure 4.10 shows the structure of the neural Network system.

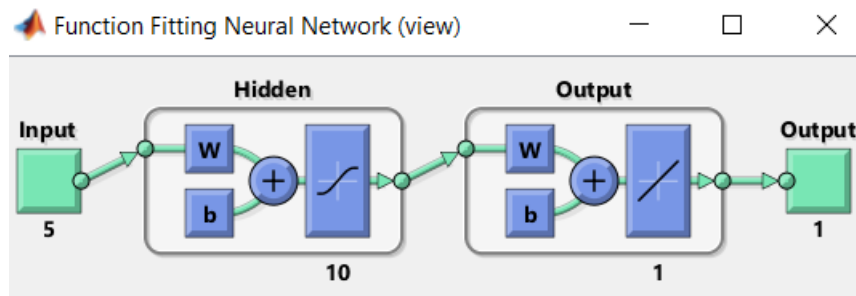


**Figure 4.10 Structure of the Neural Network System**

The size of the input and output data vectors determines the number of neurons in the input and output layers, respectively, whereas the number of neurons in the hidden layer (or layers) must be determined.

The data from the field study was made up of vectors of input-output data, which is mostly shared into three sets namely:

- a. The training set (70), which is used until the relationship between the inputs and the outputs are learned.
- b. The evaluation set (15), which is used for the selection of the ANN parameters (i.e., number of the neurons in the hidden layer, the type and the parameters of the activation functions, learning rate, momentum term).
- c. The test set (15 cases), which verifies the generalisation ability of the ANN by using an independent data set. The figure is the display of the neural fitting. Figure 4.11 shows the error method, the samples that represented the training, validation, and testing.

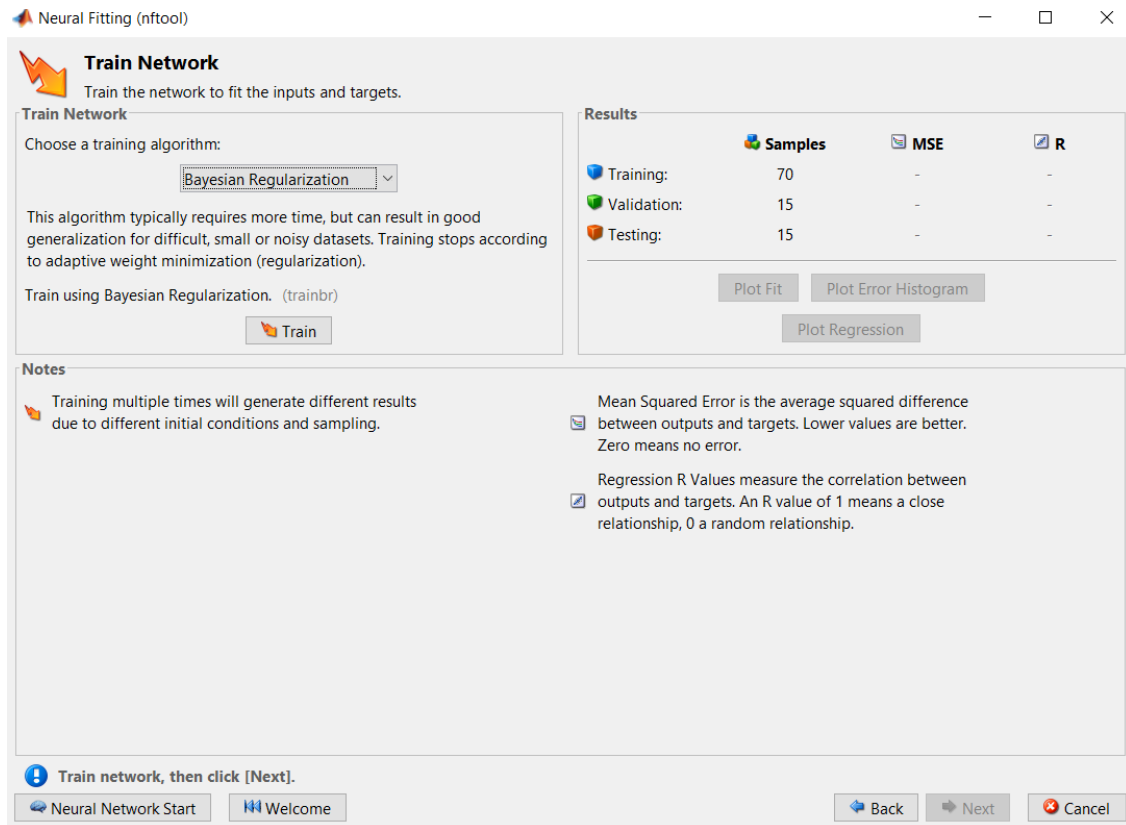


**Figure 4.11 The Structure of the Training Network**

To minimise the average error function between the estimated and the actual value, adjusting the free parameters (weights) of the Network is the sole purpose of the training process.

The number of neurons  $N_n$  that should be used is determined. Fixed values of the parameters were given with a varying number of neurons. The maximum number of epochs was set to 1000. The optimal  $N_n$  is selected as the one with the smallest average error function  $G_{av}$  for the evaluation set. Figure 4.12 shows the iteration process indicating the type of data division, training as Bayesian regularisation, performance as mean square error, and calculation as MATLAB for the algorithms. The epochs represented the number of iterations that were inputted into the training.

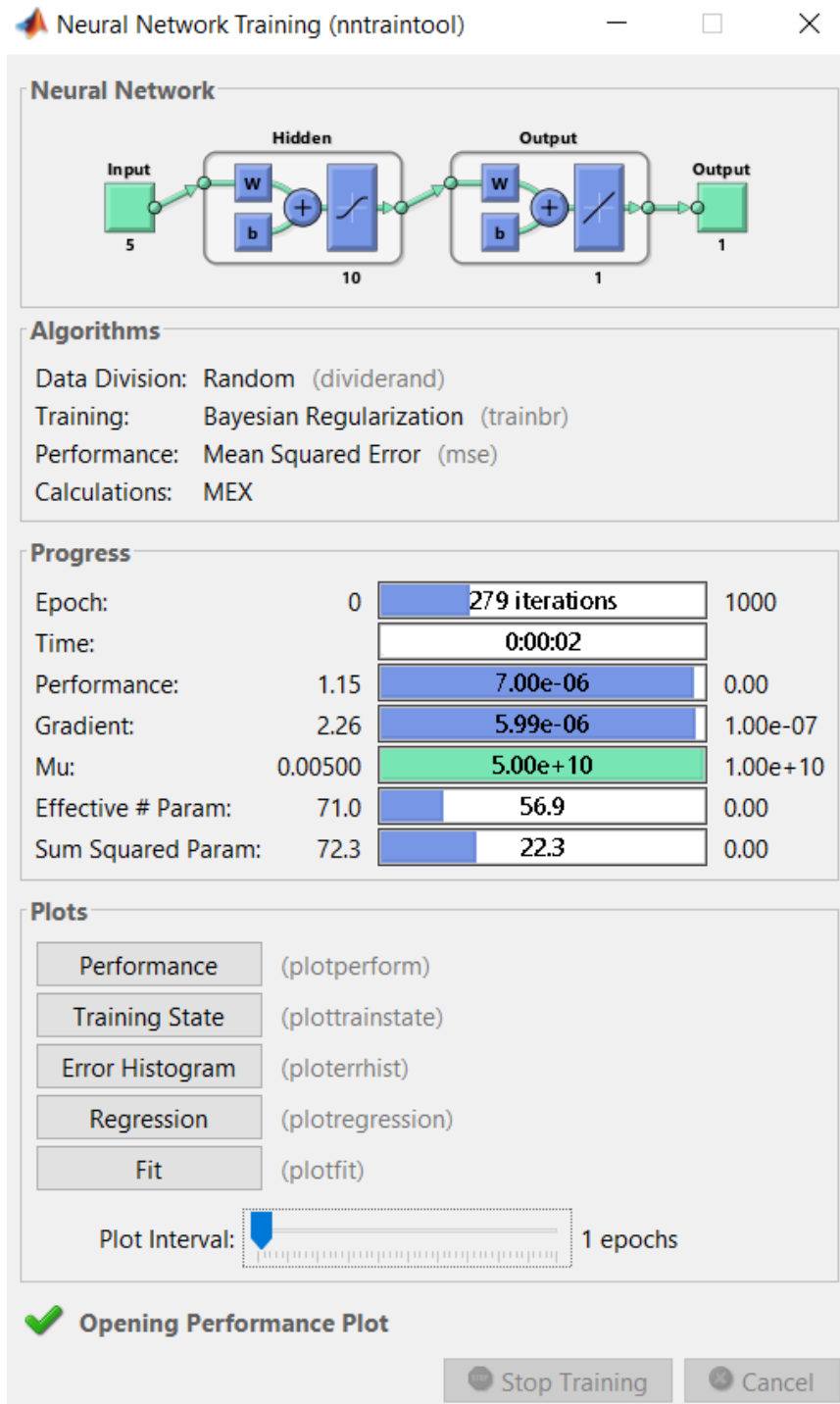


**Figure 4.12 The Neural Network Training**

The inaccuracy rate between the predicted and actual output represented a prediction error. The error, in this case, was represented by the relation for Root Mean Squared Error (RMSE) calculation using Equation (4.1).

$$\text{RMS} = \sqrt{\frac{\sum_{i=0}^{i=n-1} (y_i - o_i)}{n-1}} \quad (4.1)$$

where, n - number of patterns of a training or test set,  $y_i$  - predicted outputs,  $o_i$  - measured outputs.

Another means of evaluating the relationship between the predicted and the calculated values were through the calculation of errors. For the sake of this research, two (2) different error relations were adopted, that is, the error and the relative error. The following were the relations:

$$\text{Error} = \text{Calculated Corrosion Rate} - \text{Predicted Corrosion Rate} \quad (4.2)$$

$$\text{Relative Error} = \frac{\text{Calculated Corrosion Rate} - \text{Predicted Corrosion Rate}}{\text{Calculated Corrosion Rate}} \quad (4.3)$$

#### 4.4 Summary

The chapter presented the Fuzzy Logic System and Neural Network as the two (2) AI techniques that were used for the prediction of the corrosion rates of the rods that were buried with backfill materials. The Mamdani Fuzzy Inference System using the MATLAB Toolbox was preferred for the prediction. A flow chart showed the various stages of the system to when the model was developed. The same was done for the Neural Network system where the Bayesian algorithm feedforward propagation was used for the training.

## CHAPTER 5

### RESULTS AND DISCUSSIONS

#### 5.1 Introduction

This research considered four different ways of predicting the effects of backfill materials on buried earth rods. The two main parameters that came up were the effects of resistance values and corrosion on these materials. Four different approaches were used to determine these parameters, including visual inspection, change in thickness, laboratory analyses (AAS, XRF, and SEM-EDS), and AI techniques (fuzzy logic system and neural network). The soil and backfill materials were also analysed. This chapter presents the results derived from these methods.

#### 5.2 Soil and Backfill Materials Laboratory Results

##### 5.2.1 Physio-Chemical Properties

The soil sample and the backfill materials were analysed for their texture, moisture content, pH, Organic Carbon Content (OC), and Available Phosphorus (Avail. P). The texture of the soil identified the soil type to be clay loamy with sand having the highest soil fraction as seen from Table 5.1. The pH values ranged from 5 - 10, that is from acidity to basicity. Charred coconut husk recorded the highest organic carbon value of 67.73% and 37.74% for palm kernel cake as the least value.

**Table 5.1 Selected Physio-Chemical Properties of Backfill and Soil Samples**

Sample ID	Soil Fraction			Texture	Moisture	pH	OC	Avail. P
	<i>Sand</i>	<i>Silt</i>	<i>Clay</i>		%	<i>1:1</i>	%	<i>mg/kg</i>
Soil Sample	41.38	20.69	34.48	Clay Loamy	13.65	7.82	0.25	1.272
Palm Kennel Cake	-	-	-	-	-	5.36	37.74	71.55
Tyre Ash	-	-	-	-	-	6.06	45.16	10.4

**Table 5.1 Cont'd**

Sample ID	Soil Fraction			Texture	Moisture	pH	OC	Avail. P
	<i>Sand</i>	<i>Silt</i>	<i>Clay</i>		%	<i>1:1</i>	%	<i>mg/kg</i>
Charred Coconut Husk	-	-	-	-	-	9.8	67.73	7.025
Coconut Coir	-	-	-	-	-	6.06	42.00	2.532

### 5.2.2 Heavy Metals Content

In the soil, heavy metals play a significant function, and they are the metallic elements that have a relatively high density matched to water. Examples are lead, mercury, cadmium, chromium, iron, copper, zinc, aluminium, beryllium, cobalt, manganese, and arsenic. Calcium, iron, magnesium, potassium, and sodium were the metals that were analysed. Heavy metals are non-degradable natural components of the earth's crust so there is the need to know their concentrations in the soil and their effects. Their level of concentration in the soil and backfill materials can either increase corrosion activity and vice versa. Their analysis shows that they were environmentally friendly and aid in the preservation of the rods from corrosion activity. Table 5.2 provides the amount of metal content in the soil sample and backfill materials.

**Table 5.2 Selected Heavy Metals**

Sample ID	Calcium	Iron	Magnesium	Potassium	Sodium
	<b>mg/kg</b>				
Soil Sample	13.25	135.70	1.53	2.63	0.977
Palm Kernel Cake	47.04	6.44	46.99	54.63	5.47
Tyre Ash	124.50	296.30	21.98	142.70	53.40
Charred Coconut Husk	13.84	7.21	13.02	123.80	44.06
Coconut Coir	11.66	12.23	5.78	47.07	15.99

The charring that was done to the coconut husk increased its porosity and pore volume, which enabled it to retain water to improve the resistance of the rod. The presence of the oil

that was retained in the palm kernel cake served as a lubricant that protects the rod against corrosion. Tyre ash contained sulphides, which destroyed the protection of the rod from corrosion thereby increasing conductivity, which indirectly decreased the resistance. Coconut coir improved corrosion due to its high moisture absorption.

### 5.3 Field Study Analyses

The resistance values were taken weekly for twenty-two months. Figure 5.1 is a graph of resistance in ohms of rods after and before backfilling.

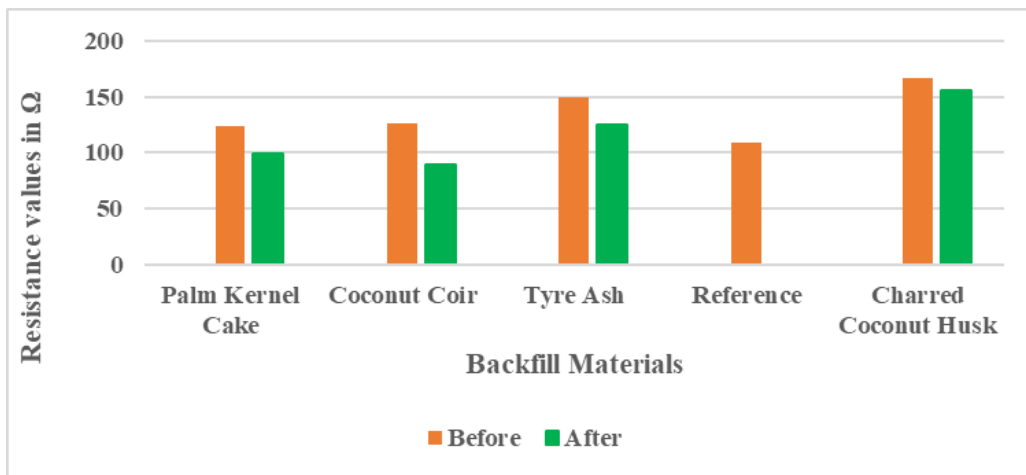


**Figure 5.1 Graph of Resistance Before and After Backfilling**

The effects of the backfill materials varied from each other, as can be seen in Figure 5.1, due to the different compositions and properties of the materials. It can be seen that all the rods that were backfilled recorded resistance values that were less than before the materials were applied. All the same, the reference recorded a resistance value that was less than that of tyre ash and charred coconut husk. This can be related to the composition and properties of the backfill materials as stated in Section 5.2.

Figure 5.2 (Appendix A raw data) is a graph of the resistance values that were recorded for 2018. It was observed that the resistance values increased in the arid season and vice versa in the rainy season. It shows that from 6<sup>th</sup> January to 14<sup>th</sup> April, tyre ash performed very well, followed by charred coconut husk and palm kernel cake. The values reduced drastically from 30<sup>th</sup> May through to the end of August with an average value of 60 Ω. This period was characterised by heavy rains, which led to favourable resistance readings. Tyre ash and charred coconut husk had the least resistance values from September to December. Lastly, the reference rod recorded the highest values ranging from 130 Ω to 210 Ω.



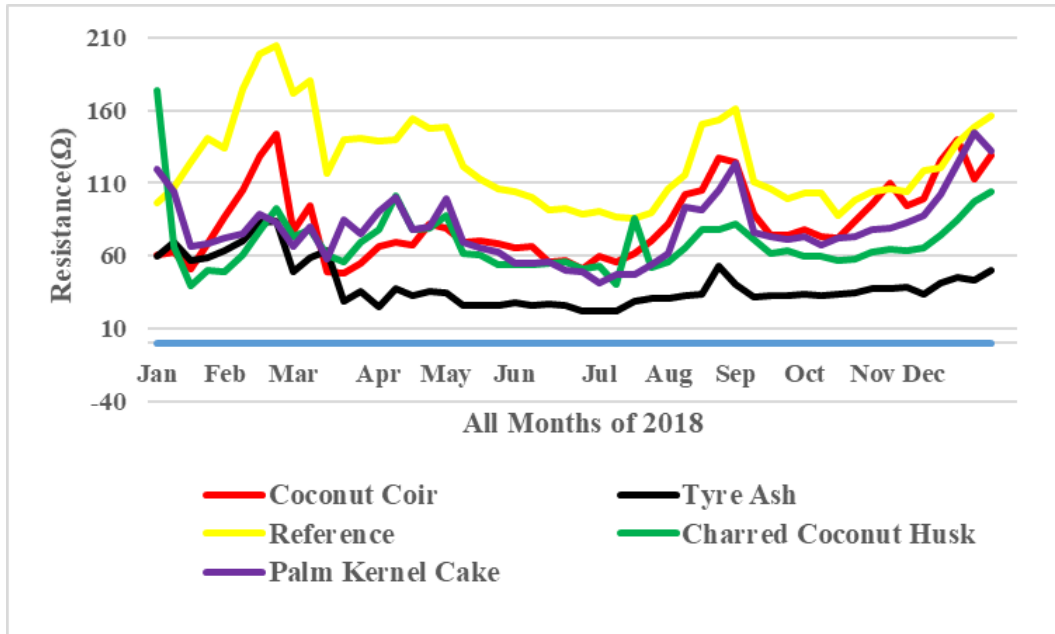


**Figure 5.2 Resistance Values for the Year 2018**

The same went for the year 2019 (Appendix B), however, because the backfill materials had been underground for a year, some of the metals were leached preventing the backfill materials from performing their purpose of protecting the rod from corrosion. Tyre ash performed very well as shown in Figure 5.3. The reference rod also performed very well in the rainy season and even the dry season. The resistance values for all the rods decreased in the wet season and increased in the dry season.

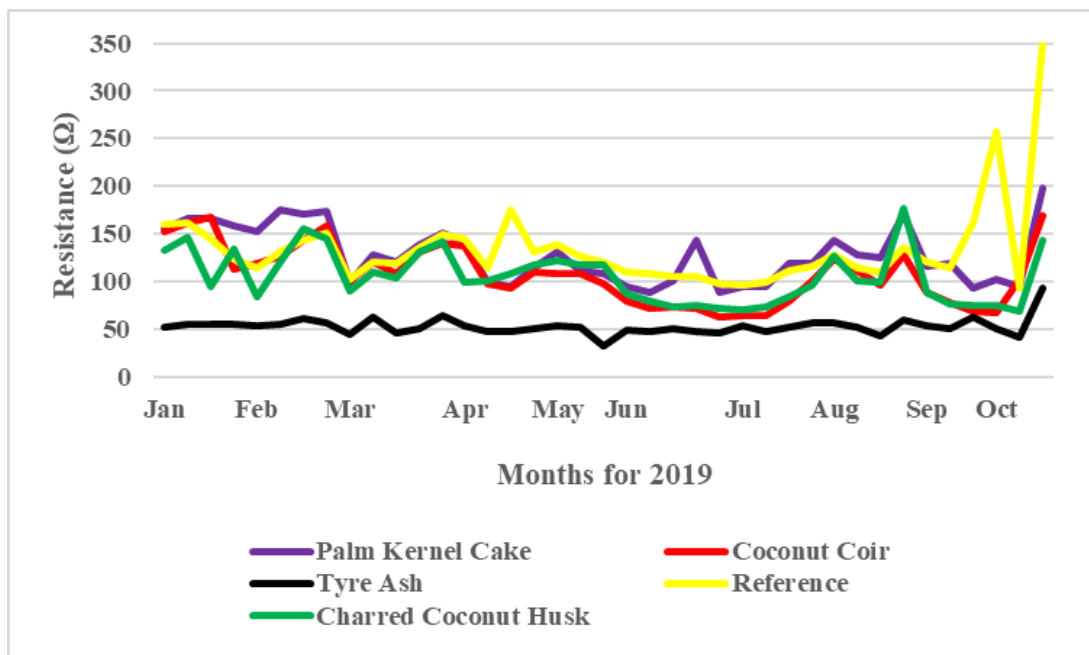


**Figure 5.3 Resistance Values for the Year 2019**

## 5.4 Laboratory Analyses

The corrosion rate was analysed under this section included the following methods: visual inspection, change in thickness, corrosion rate equation, XRF and SEM-EDS analyses.

### 5.4.1 Visual Inspection

Visual inspection has been the oldest traditional method that has been used severally to depict corrosion rates. Figures 5.4 and 5.5, show some rod samples that were analysed visually. Figure 5.4 shows a rod that was buried after a week with its reddish-brown colour still intact. Figure 5.5 shows a rod that was buried after two years with tyre ash backfill material. The edge that was exposed to the atmosphere changed colour from reddish-brown to grey and green beneath. This is evidence that corrosion took place.

The rods that were removed from the soil were washed and laid on the floor to be compared to the reference rod that was not buried. Figure 5.6 is a picture of the rods. All the rods that were removed from the soil differed from that of the unburied. Some of the backfill materials mixed with the soil and attached themselves to the rod increasing the thickness of the rod whereas others only had a colour change.



**Figure 5.4 Freshly Buried Rod**



**Figure 5.5 A rod Buried with Tyre Ash**



**Figure 5.6 Rods Removed from the Soil**

#### 5.4.2 Change in Thickness

One of the pieces of evidence that corrosion has taken place is a change in thickness, mass or weight of the material that has corroded. For this research, there was an increase in thickness which can be seen visually in Figure 5.6 whilst Table 5.3 shows the outcomes of the weight and the thickness of the rods when measured. Tyre ash had the major increase in thickness and automatically the highest weight value too. This is as a result of its inability to leach thereby surrounding the rod and allowing corrosion to occur rapidly. Apart from the unburied reference, whose thickness did not change, the rest recorded an increase in thickness as evidence that corrosion took place. There was no major increase in thickness for the rest of the rods that were backfilled as compared to that of the tyre ash because all the backfill materials leached into the soil. Table 5.3 is The Results of the Weight and Thickness of Rods.

**Table 5.3 is The Results of the Weight and Thickness of Rods**

SN	Backfill Material	Weight (kg)	Thickness (m)				Average Thickness (m)
			0.200	0.300	0.500	0.800	
1	Reference (not buried)	1.200	1.200	1.200	1.200	1.200	1.200
2	Tyre Ash	1.600	1.300	1.900	1.900	1.300	1.600
3	Palm Kernel Cake	1.300	1.300	1.300	1.300	1.300	1.300
4	Reference (buried)	1.441	1.250	1.290	1.300	1.300	1.285
5	Coconut Coir	1.449	1.250	1.250	1.300	1.300	1.275
6	Charred Coconut Husk	1.437	1.250	1.250	1.250	1.250	1.250

### 5.4.3 Corrosion Rate Calculation

The corrosion rate equation was computed from a pile of equations to predict the corrosion rate depending on the parameters that could be measured or calculated. Equation (5.1) was simplified to predict the corrosion rate of the rods. Table 5.4 gives some parameters that aided in the computation.

$$x = \frac{i_{\text{corr}} M t}{\rho n F} \quad (5.1)$$

where,  $x$  is corrosion rate,  $t$  is time (seconds),  $I_{\text{corr}}$  is corrosion current density ( $\text{Am}^{-3}$ ),  $A$  is the area of corroding metal exposed to the solution,  $M$  is the molar mass of metal and  $n$  is the charge of metal

$$i_{\text{corr}} = \frac{I}{A} \quad (5.2)$$

$$\rho = \frac{m}{V} \quad (5.3)$$

where,  $I$  is current. From the field study, the rod had a height of 1.2 m and radius of 0.0065 m.

Therefore, the area of the rod =  $2\pi r h + 2\pi r^2$

$$\begin{aligned} &= \frac{2 \times 22 \times 0.0065 \times 1.2}{7} + \frac{2 \times 22 \times 0.0065^2}{7} \\ &= 0.04929 \text{ m}^2 \end{aligned}$$

and the volume of the rod =  $\pi r^2 h$

$$\begin{aligned} &= \frac{2 \times 0.0065^2 \times 1.2}{7} \\ &= 0.00001 \text{ m}^3 \end{aligned}$$

Table 5.4 gives parameters for computing the corrosion rate of the rod using Microsoft Excel.

**Table 5.4 Some Parameters for Computing Corrosion Rate**

Parameter	Symbol	Value	Unit
Voltage	V	12	V
Area of the Rod	A	0.04926	m <sup>2</sup>
Volume of the Rod	v	0.00001	m <sup>3</sup>
Molar Mass	M	55.845	g/mol
Faraday Constant	F	96500	C/mol
Charge (Fe <sup>+3</sup> )	Q	3	C
Time	t	57024000	s

Table 5.5 gives the mass, thickness, resistance, current and current density values of the rods after burial. It was computed that tyre ash recorded the highest corrosion rate value of 25.20 Am<sup>-2</sup>s<sup>-1</sup> with charred coconut recording the least value of 14.65 Am<sup>-2</sup>s<sup>-1</sup>. Although tyre ash recorded the lowest values of resistance from Figures 5.2 and 5.3, its limitations are the highest corrosion rate value recorded. Simply put, tyre ash can give the lowest resistance value to improve the earthing system, but would not be able to protect the rod from corrosion activity. Charred coconut husk, on the other hand, performed better as compared to the reference and had the lowest corrosion rate value.

**Table 5.5 Computation of Corrosion Rates Values**

Backfill Materials	Mass (kg)	Thickness (m)	Resistance (Ω)	Current (I)	Density (kgm <sup>-3</sup> )	Current Density (A/m <sup>2</sup> )	X (Am <sup>-2</sup> s <sup>-1</sup> )
Reference (buried)	1.277	0.0120	95.00	0.126	801.822	2.564	16.68
Tyre Ash	1.442	0.0157	42.40	0.283	905.779	5.745	25.20
Palm Kernel Cake	1.451	0.0129	94.90	0.126	911.118	2.567	21.50
Coconut Coir	1.449	0.1275	125.30	0.160	910.18	3.24	21.87
Charred Coconut Husk	1.437	0.1250	138.80	0.086	902.64	1.76	14.65

#### 5.4.4 XRF and SEM-EDS Results

The XRF and SEM-EDS analyses were compared to the reference (the unburied rod) to analyse the composition of all of them. The results of the XRF analysis are given in Table 5.6.

**Table 5.6 XRF Results after Burying Rods for 22 months**

Backfill Materials	Elements/Concentrations %									
	Fe	Cr	Ni	Mn	Cu	Zn	Mo	Co	Ti	V
Reference (unburied)	88.581	5.19	0.0	1.233	0.378	0.146	0.099	-	0.036	0
Reference (buried)	99.443			0.470	0.100					
Palm Kernel Cake	99.235	0.12 <sub>9</sub>	0.0	0.494	0.140	0.0	0.0	-	0.0	0
Tyre Ash	99.135	0.08 <sub>9</sub>	0.033	0.449	0.189	0.0	0.0	-	0.102	0
Coconut Coir	99.400	0.08	-	0.45	0.07	-	-	-	-	-
Charred Coconut Husk	99.422	-	0.01	0.51	0.04	0.01	0.01	-	-	-

XRF is known to be a very sensitive technique that analyses to a depth of ~2 mm and, therefore, serves as the starting point to categorise the surface composition and the additional elements introduced from the soil. The results obtained from the experimental work seen in in Table 5.6.

The objective of the analysis was to examine the effects of corrosion on the various rod samples. The results showed consistency in the revelation of the quantities of different elements. The calculation algorithm assumed that the summation of the concentrations of the elements detected should be 100%, exempting the non-detectable light elements, especially oxygen.

Therefore, the expected corrosion products from the rod samples analyses was hydrated iron oxide ( $\text{Fe}_2\text{O}_3 \cdot y\text{H}_2\text{O}$ ) along with minor amounts of oxides from those elements present as alloying additions. The results showed that all the rods had some five (5) metals in common, namely, iron, chromium, manganese, nickel, bismuth and arsenic and copper. The presence of molybdenum, zinc, cobalt and vanadium depicted the influence of the burial environment

on the surface of the rod samples and the other elements were mostly identified as alloying additions.

The five (5) rods that were buried displayed higher values in iron content but lesser values in the rest of the metals. The concentrations of iron in all five (5) samples exceeded 80%, and hence, was the dominating element in the x-ray spectra. Iron recorded 88.581% in the reference sample and increased to 99.235% in the palm kernel cake sample and 99.135% in the tyre ash sample. The next metal with a higher value was chromium recording 5.189% for the reference sample and reduced to 0.129% and 0.089% for palm kernel cake and tyre ash samples, respectively. Iron recorded the highest value of 99.443% for the buried reference rod, 99.40% for coconut coir and 99.422% for charred coconut husk.

This is as a result of the interaction of the rods with the soil and the backfill materials to the extent that some of the metals dissolved and disappeared totally from the rod into the soil indicating the values 0.0 from the table. This was attributable to the formation of soluble corrosion products of the alloying species. Once the metals dissolved, the quantity of iron increased. Iron did not dissolve because it either formed an oxide or hydroxide material which is a solid material.

The reference rod (unburied) recorded quite a low value of iron at 88.581% as compared to that of the buried rods. Contrarily, the other elements recorded the highest values for the rest of the elements namely: chromium, manganese, copper, zinc, molybdenum, and titanium in that order. The rods contained these elemental values because there was no interaction with any external environment then. It can be concluded that the longer the rods stayed in the soil, the higher the iron values increased and the lower the other elemental values too. So, in simple terms, the value of iron is indirectly proportional to the other elements that were also recorded.

#### 5.4.5 SEM-EDS Results

Morphological, qualitative, and quantitative analyses of the rod samples were carried out using a Zeiss EVO MA 15 SEM. The results from the SEM-EDS analysis provided information on the metal phases, giving visual data and enabling more holistic mineralisation information. This analysis focused on a scanned area of the sample instead of a unified analysis showed by XRF. The SEM-EDS provided three different results for analysis. The SEM scanned an area for analysis at a specific time and the EDS showed the

results in a spectrum or graphical way with the quantity of metal in percentages of mass and atom.

For this laboratory analysis, the SEM images showed three different colours: light, grey and dark areas. The light area depicted areas of the rod where corrosion did not take place. The grey showed a slightly corroded area and the dark area showed severe corrosion. One characteristic of the three areas mentioned was that the darker areas were rich in metal content, and they reduced when nearing the grey and light areas. From all the samples that were analysed here, it should be noted that the weight (mass) and atomic percentages have been used to reveal the presence of some elements or metals and their consistency aiming at describing the interaction between the rod and the environment, which gave rise to different elements as a result of the level of corrosion that took place. At the end of the analysis, the metal detected was cast iron and the type of corrosion that took place was pitting corrosion.

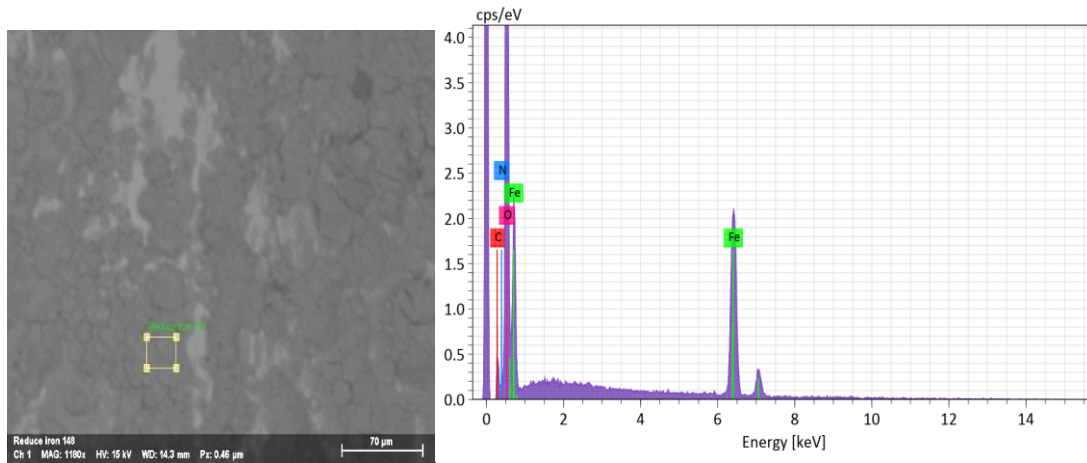
Four different backfill materials that were buried with five rods were analysed. The rods were buried with palm kernel cake, tyre ash, coconut coir and charred coconut husk backfill materials for twenty-two months. The reference rod was buried without any backfill material. Each material captured at least four scanned areas for analysis. The yellow triangle in Figure 5.7 and the rest in all the figures that followed were the scanned areas that were analysed attached, their spectrum or mineral peaks and metal composition. The elements that were present in all the scanned areas included carbon, oxygen and iron. In most of these areas, iron recorded the highest percentage values, followed by oxygen and then carbon. The presence of oxygen was not surprising since it has always been a major element in the corrosion process. One important aspect of iron corrosion is that when iron corrodes, it forms rust, that is, iron oxide and water with “x” as the number of molecules of water ( $\text{Fe}_2\text{O}_3 \cdot x\text{H}_2\text{O}$ ). An SEM analysis would indicate elements such as iron, oxygen and partly carbon as an alloying element. The presence of oxygen anywhere was evidence that corrosion has taken place and its absence indicated otherwise.

Figure 5.7 shows an SEM image with a yellow rectangle indicating the scanned area. The EDS spectra collected showed the presence of the elements found in Table 5.9. There were two batches of analysis just like that of the XRF.



*Palm kernel cake*

The palm kernel cake had four different areas that were captured for analysis for the first surface, From Figure 5.7, the surface was made up of iron, oxygen, carbon and nitrogen in descending order of percentage composition of the least as major elements. The 62.62% of oxygen was present as part of the initial oxide layer on the surfaces as well as from the atmospheric contamination.



**Figure. 5.7 SEM-EDS Analysis of Palm Kernel Cake Buried Rod at Region 1**

**Table 5.7 SEM-EDS Analysis of Palm Kernel Cake Buried Rod at Region 1**

Element	Mass %	Atom %
Carbon	5.72	12.00
Nitrogen	0.60	1.07
Oxygen	39.79	62.63
Iron	53.89	24.30
<b>Total</b>	<b>100.00</b>	<b>100.00</b>

Table 5.7 shows iron (53.89%), followed by oxygen (39.79%) and carbon (5.72%) having high amounts. This region represents a corroded region evidenced by the presence of a large amount of oxygen and the grey colour as shown in Figure 5.7.

For the second surface analysis, the selected sample Figure 5.8 was made up of iron and oxygen as the major elements followed by carbon. This area consisted more of grey colour indicating that corrosion had taken place. There was a small portion of dark spot representing severe corrosion has taken place. The square area captured is made up of a lighter area, hence, the recorded metals with a small percentage of oxygen indicating

corrosion took place but not severe. Table 5.8 shows 86.57% of iron, 8.14% of oxygen and 5.30% of carbon.

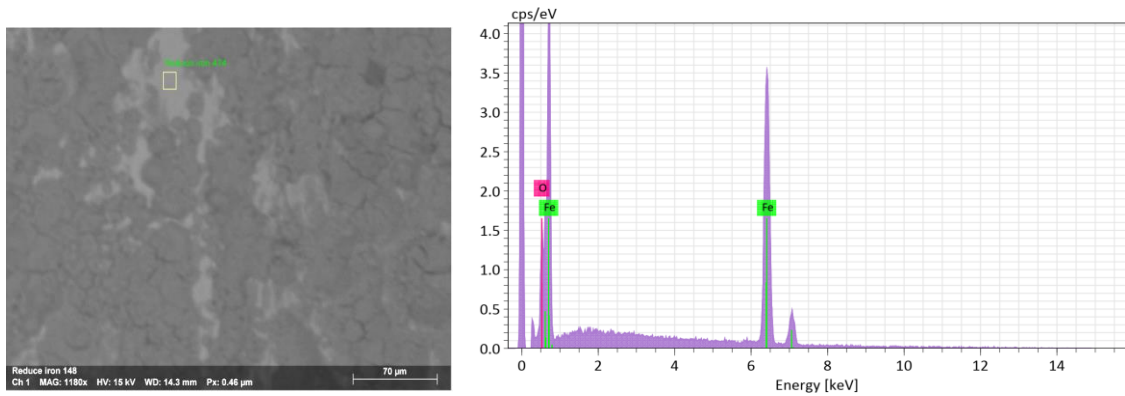


**Figure 5.8 SEM-EDS Analysis of Palm Kernel Cake Buried Rod at Region 2**

**Table 5.8 SEM-EDS Analysis of Palm Kernel Cake Buried Rod at Region 2**

Element	Mass %	Atom %
Carbon	5.30	17.64
Oxygen	8.14	20.34
Iron	86.57	62.01
<b>Total</b>	<b>100.00</b>	<b>100.00</b>

Figure 5.9 shows the third image recorded. The metals that were found included carbon, oxygen, sodium, silicon and iron. The presence of silicon and sodium is a result of the mineral content of the soil. The iron of value (37.99%) and carbon (6.37%) are the elemental compositions of the rod and the oxygen (39.22%) as a result of corrosion that took place as seen in Table 5.9. The captured square was a dark area with few light areas and larger grey areas.

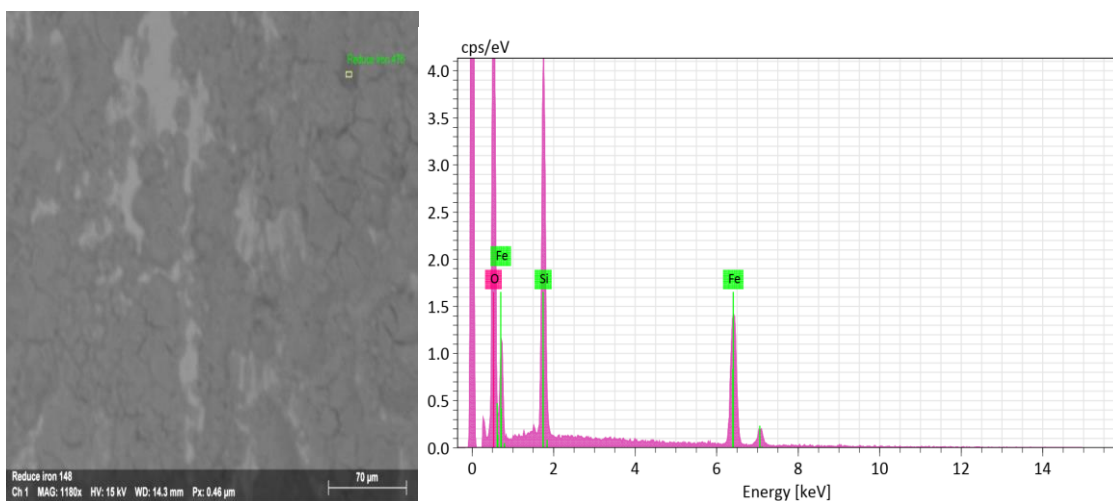


**Figure 5.9 SEM-EDS Analysis of Palm Kernel Cake Buried Rod at Region 3**

**Table 5.9 SEM-EDS Analysis of Palm Kernel Cake Buried Rod at Region 3**

Element	Mass %	Atom %
Carbon	6.37	12.48
Oxygen	39.22	57.71
Sodium	0.15	0.15
Silicon	16.28	13.65
Iron	37.99	16.02
<b>Total</b>	<b>100.00</b>	<b>100.00</b>

Lastly, for the fourth analysis, Table 5.10 shows that 33.36% of oxygen was present and the value was as a result of the area that was captured (grey). Some few areas were seen to be light, and the majority of the parts were grey. It was only some few spots that were seen to be very dark. It is the grey area that was captured here, hence, the metals that came up included iron with the highest percentage (59.11%) followed by oxygen (33.36%), carbon (7.29%) and lastly rhodium (0.24%).

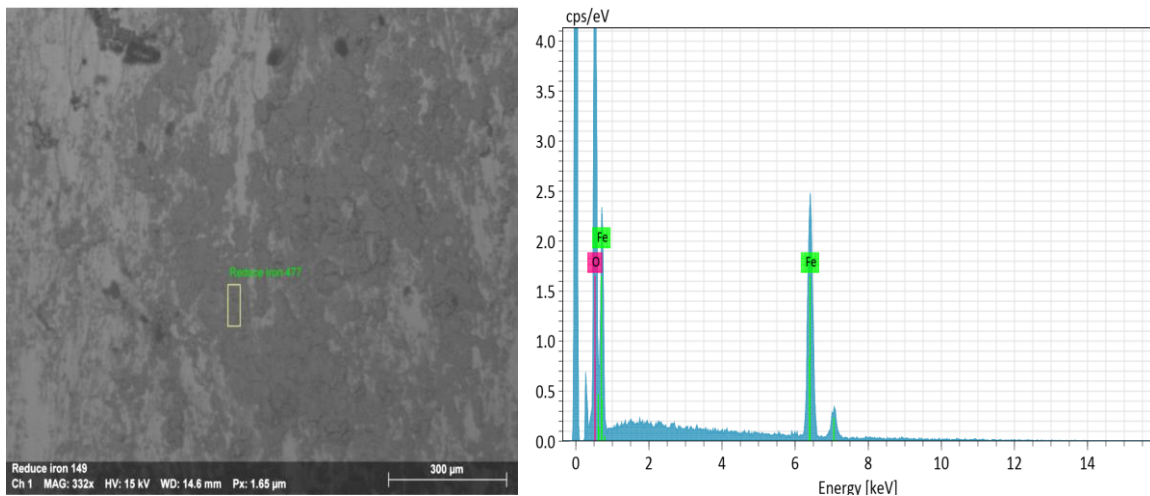


**Figure 5.10 SEM-EDS Analysis of Palm Kernel Cake Buried Rod at Region 4**

**Table 5.10 SEM-EDS Analysis of Palm Kernel Cake Buried Rod at Region 4**

Element	Mass %	Atom %
Carbon	7.29	16.18
Oxygen	33.36	55.56
Iron	59.11	28.20
Rhodium	0.24	0.06
<b>Total</b>	<b>100.00</b>	<b>100.00</b>

## Tyre ash

The two tyre ash samples that were analysed brought out metals such as carbon, iron, aluminium, rubidium, nitrogen, oxygen, and dysprosium. Once again, the presence of oxygen depicted the presence of corrosion as shown in Figure 5.11.

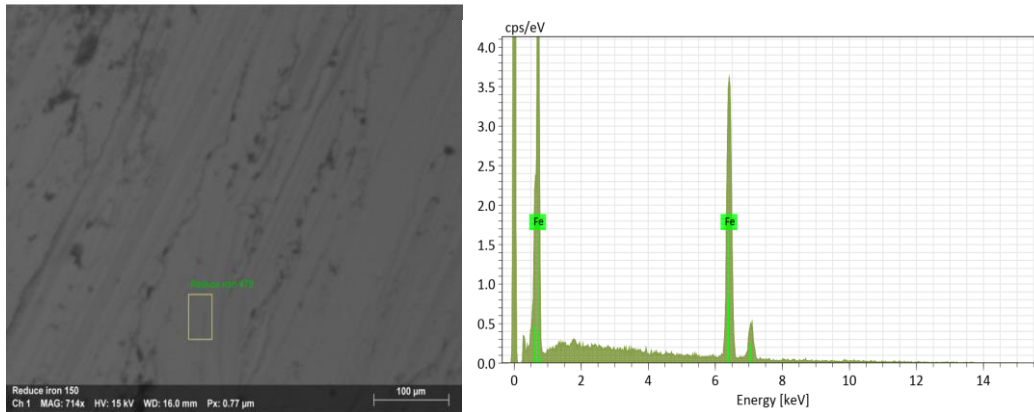


**Figure 5.11 SEM-EDS Analysis of Tyre Ash Rod at Region 1**

**Table 5.11 SEM-EDS Analysis of Tyre Ash Rod at Region 1**

Element	Mass %	Atom %
Carbon	5.42	21.02
Aluminium	0.33	0.57
Iron	93.60	78.06
Rubidium	0.65	0.35
<b>Total</b>	<b>100.00</b>	<b>100.00</b>

Here, the captured area was that of the light side, which formed about 95% of the whole SEM-EDS and the 5% made up of the dark side as seen in Figure 5.11. The absence of oxygen showed that corrosion did not take place in the scanned area. Iron recorded a percentage of 93.60 as proof that the rod did not lose its iron content as seen in Table 5.11. The aluminium and rubidium formed part of the metal as a result of its interaction with the soil.

For the second captured analysis in Figure 5.12, it also had the light side forming about 95% of this SEM-EDS and the rest forming the dark area. The area that was scanned was that of the dark side. Tyre ash recorded the highest value of carbon, and this was as a result of the carbon content in the backfill material. Metals in the soil and in the backfill material attached themselves to the rod after corrosion had taken place thereby, increasing the number of

metals in this selected region. Examples of these metals included aluminium, sodium, potassium, nitrogen, iron, dysprosium and chlorine. The presence of oxygen was recorded as 29.73% showing massive corrosion took place as shown in Table 5.12.

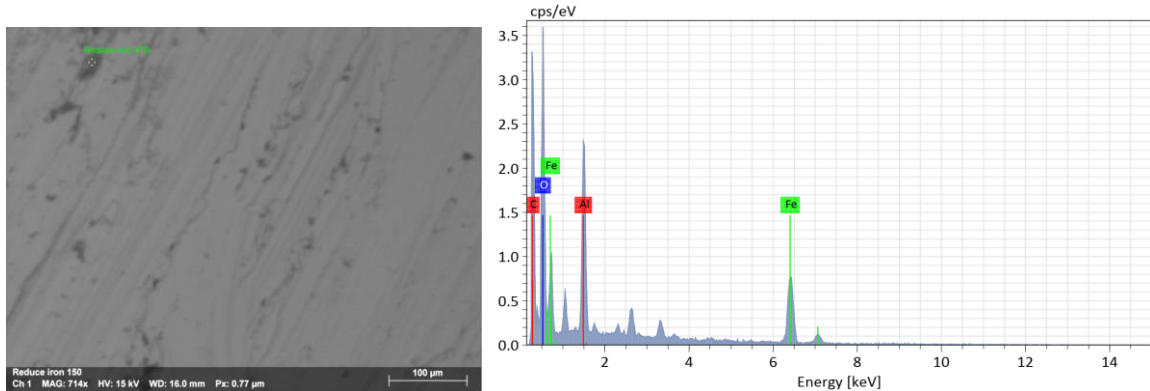


**Figure 5.12 SEM-EDS Analysis of Tyre Ash Rod at Region 2**

**Table 5.12 SEM-EDS Analysis of Tyre Ash Rod at Region 2**

Element	Mass %	Atom %
Carbon	32.84	47.11
Nitrogen	7.86	9.67
Oxygen	29.73	32.03
Sodium	1.67	1.25
Aluminium	6.13	3.91
Chlorine	0.95	0.46
Potassium	0.71	0.31
Iron	15.40	4.72
Dysprosium	4.72	0.50
Tantalum	0.00	0.00
<b>Total</b>	<b>100.00</b>	<b>100.00</b>

*Charred coconut husk*

Charred coconut husk had four different SEM-EDS to show the effects of the material on the rods. In all the pictures from Figures 5.13, 5.14, 5.15 and 5.16, iron recorded the highest values, which ranged from 66.80 - 89.46%. The metals or elements that were common in all four images included iron, carbon, oxygen and aluminium.

The image, as seen from Figure 5.13, was made up of the light, grey side and darker area. The first of the four SEM-EDS captured a dark area found at the right side of the image. The presence of oxygen depicted that corrosion took place. The percentage (3.21%) of oxygen from Table 5.13 showed the extent of the corrosion. Aluminium and silicon were present as a result of the interaction of the rod with the soil and the backfill material.

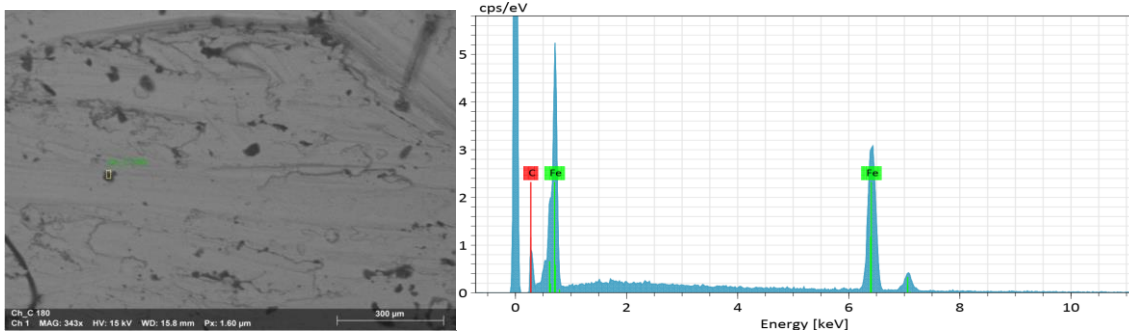


**Figure 5.13 SEM-EDS Analysis of Charred Coconut Husk at Region 1**

**Table 5.13 SEM-EDS Analysis of Charred Coconut Husk at Region 1**

Element	Mass %	Atom %
Carbon	5.65	20.17
Oxygen	3.21	8.61
Aluminium	0.53	0.84
Silicon	1.14	1.74
Iron	89.46	68.64
<b>Total</b>	<b>100.00</b>	<b>100.00</b>

The second image captured in Figure 5.14, is also made up of dark, light and grey areas. The area captured is that of the grey area, however, only two metals were captured. These metals included carbon (15.94%) and iron (84.06%) as seen in Table 5.14. There was no presence of oxygen, which indicated that corrosion did not take place.

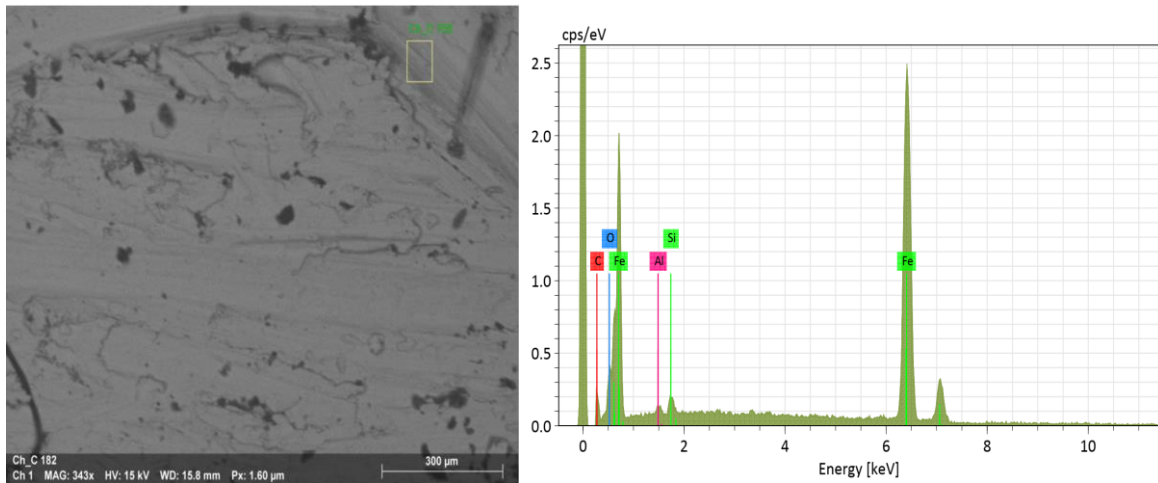


**Figure 5.14 SEM-EDS Analysis of Charred Coconut Husk at Region 2**

**Table 5.14 SEM-EDS Analysis of Charred Coconut Husk at Region 2**

Element	Mass %	Atom %
Carbon	15.94	46.85
Iron	84.06	53.15
<b>Total</b>	<b>100.00</b>	<b>100.00</b>

Images with dark EDS scattered in light, grey and dark areas meant there were corroded points in the rod and that is typical of pitting corrosion as seen in Figure 5.15. The metals that were seen in Table 5.15 included carbon (5.75%), oxygen (5.31%) and carbon (88.94%). The presence of oxygen, as said earlier, depicted the presence of corrosion. The percentage of oxygen recorded showed that the corrosion that took place was not very severe.

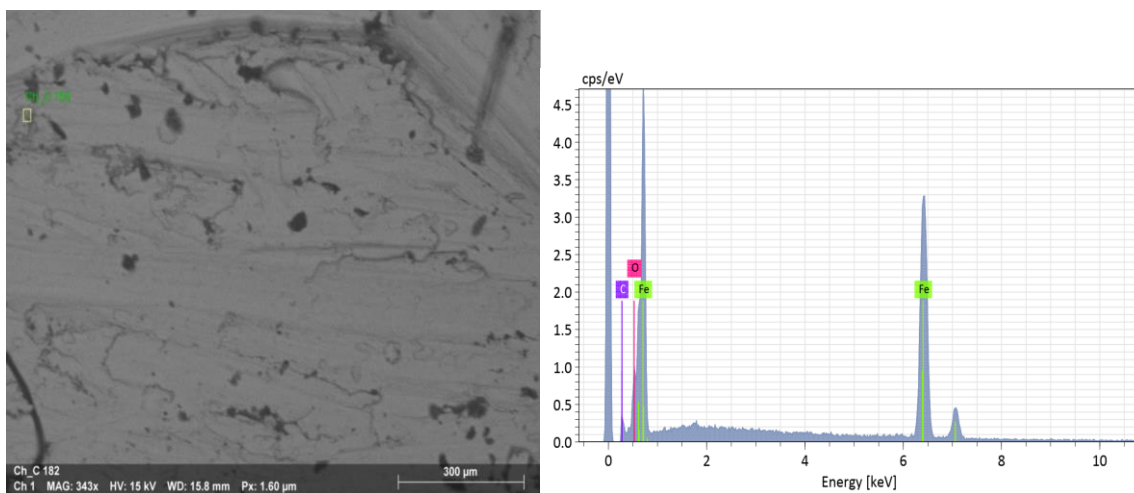


**Figure 5.15 SEM-EDS Analysis of Charred Coconut Husk at Region 3**

**Table 5.15 SEM-EDS Analysis of Charred Coconut Husk at Region 3**

Element	Mass %	Atom %
Carbon	5.75	19.93
Oxygen	5.31	13.81
Iron	88.94	66.26
<b>Total</b>	<b>100.00</b>	<b>100.00</b>

The last part captured under charred coconut husk can be seen in Figure 5.16. Here, the EDS scan showed the dark, light and grey parts. The type of area captured was that of the dark side showing evidence of corrosion. This led to the existence of many metals as seen in Table 5.16. Iron recorded a value of 66.80, followed by carbon, 15.10, oxygen, 11.45, silicon, 2.87, aluminium, 2.77 and calcium 1.03 as mass percentages. The presence of the last three (3) metals was a result of the interaction of the soil and the backfill material on the rod. The percentage of oxygen showed that corrosion took place.

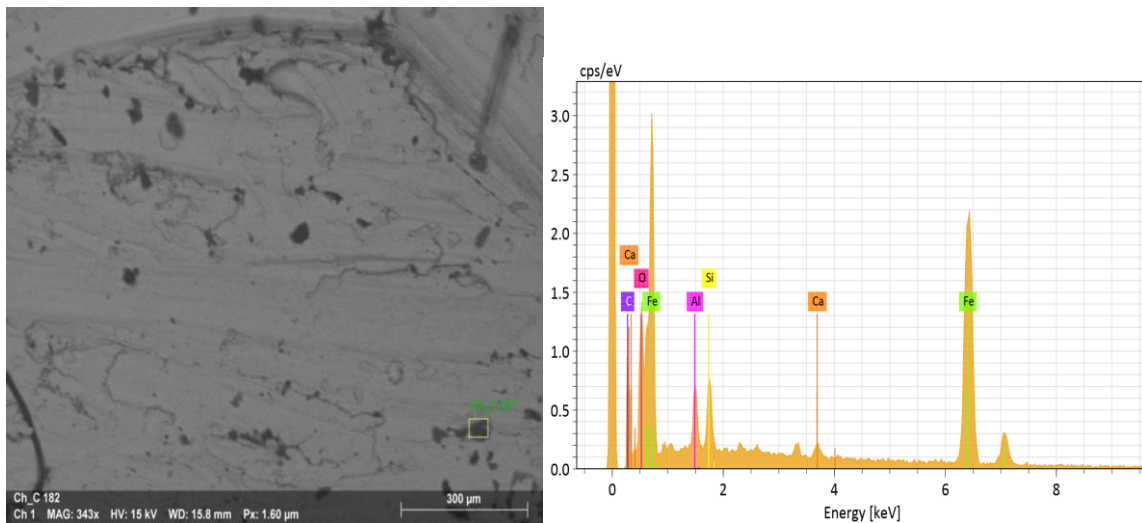


**Figure 5.16 SEM-EDS Analysis of Charred Coconut Husk at Region 4**



**Table 5.16 SEM-EDS Analysis of Charred Coconut Husk at Region 4**

Element	Mass %	Atom %
Carbon	15.10	36.98
Oxygen	11.45	21.05
Aluminium	2.77	3.02
Silicon	2.87	3.00
Calcium	1.03	0.75
Iron	66.80	35.19
<b>Total</b>	<b>100.00</b>	<b>100.00</b>

*Coconut coir*

Coconut coir scanned three EDS images for analysis after burial for twenty-two months. The metals that were common in all three scans included iron, with the highest mass percentage values, and carbon. Two oxygen mass percentages of values (1.93 and 10.39) were recorded from Tables 5.17 and 5.18, meaning corrosion took place in these two scenarios. The last scan without the presence of oxygen, also indicated the absence of corrosion.

The first scan recorded showed the three areas, light, dark and grey areas. The rectangle captured an area made up of a light area with grey spots. The metals that were seen from Table 5.19 included iron of mass percentage 93.47, carbon with 4.60 and oxygen of 1.93 showing corrosion took place but not severe as seen from the percentage and the captured area.

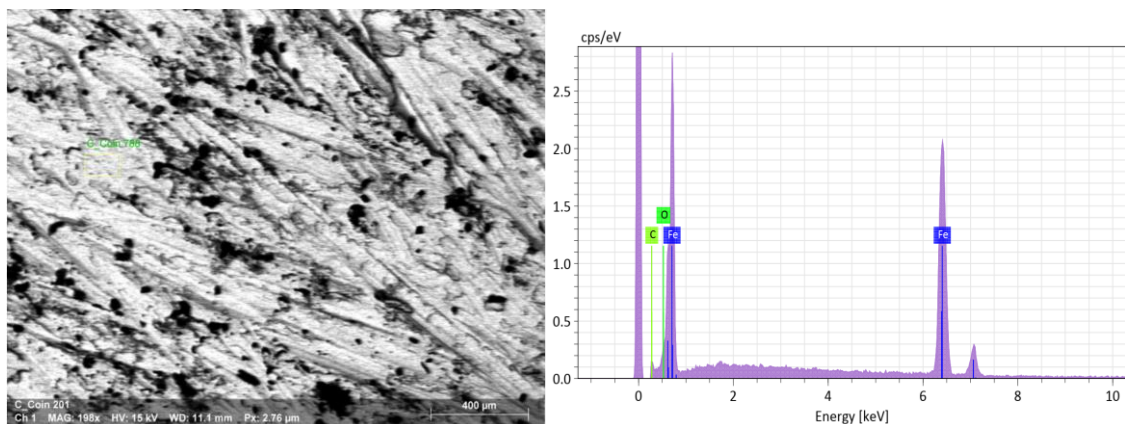


**Figure 5.17 SEM-EDS Analysis of Coconut Coir at Region 1**

**Table 5.17 SEM-EDS Analysis of Coconut Coir at Region 1**

Element	Mass %	Atom %
Carbon	4.60	17.57
Oxygen	1.93	5.55
Iron	93.47	76.88
<b>Total</b>	<b>100.00</b>	<b>100.00</b>

The second area, as seen from Figure 5.18, showed a mixture of the light, dark and grey areas. The captured area was made up of about 90% of dark area and some few dots of light areas. The scanned area alone indicated that corrosion has taken place in addition to the presence of oxygen in Table 5.18 with a mass percentage of 10.39. The rest of the metals found were iron with 74.82%, carbon, 13.97% and silicon with the least value of 0.82%.

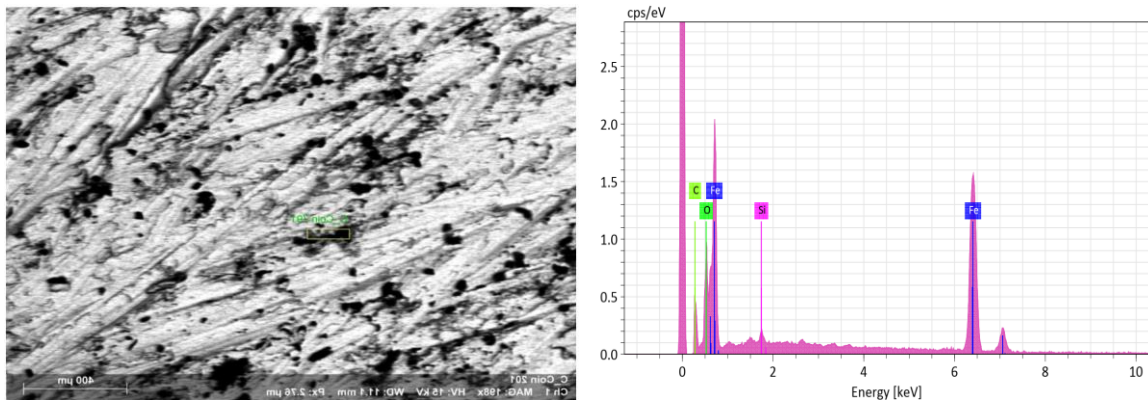


**Figure 5.18 SEM-EDS Analysis of Coconut Coir at Region 2**

**Table 5.18 SEM-EDS Analysis of Coconut Coir at Region 2**

Element	Mass %	Atom %
Carbon	13.97	36.55
Oxygen	10.39	20.42
Silicon	0.82	0.92
Iron	74.82	42.11
<b>Total</b>	<b>100.00</b>	<b>100.00</b>

This third scan was made up of dark, light and grey parts. The whole area is made up of a light area with little shades of dark and grey as seen from Figure 5.19. The metals seen here

in Table 5.19 included iron of 94.83%, carbon 4.64% and silicon of 0.52%. There was no record of oxygen, indicating the absence of corrosion.

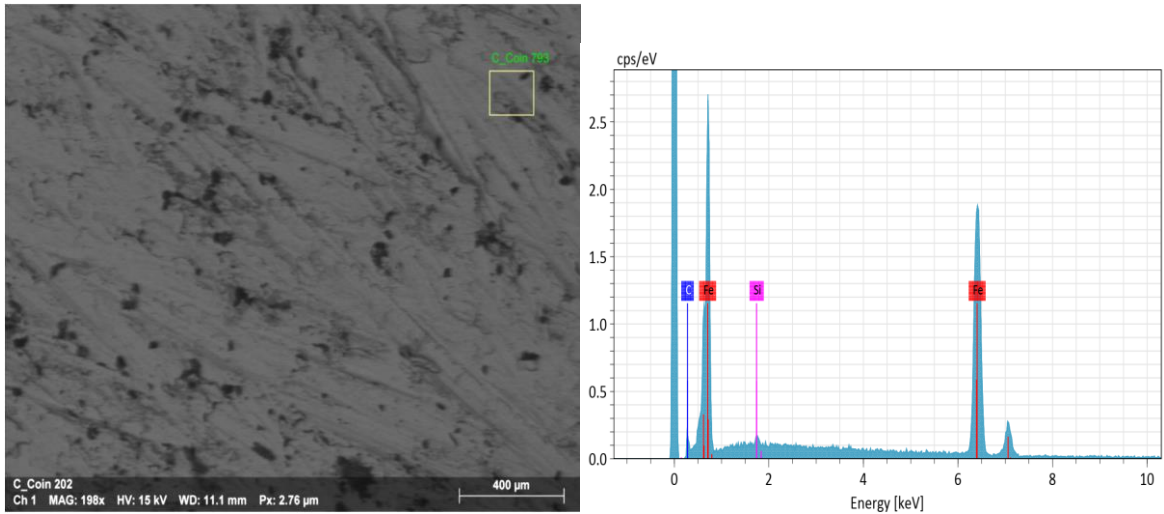


**Figure. 5.19 SEM-EDS Analysis of Coconut Coir at Region 3**

**Table 5.19 SEM-EDS Analysis of Coconut Coir at Region 3**

Element	Mass %	Atom %
Carbon	4.64	18.38
Silicon	0.52	0.89
Iron	94.83	80.73
<b>Total</b>	<b>100.00</b>	<b>100.00</b>

### *Reference*

The reference refers to the rod that was buried without any backfill material. Two scans were taken of this rod. Iron recorded the highest mass percentage of 100 from Tables 5.20 and 5.21. Oxygen and carbon were seen in only Table 5.20.

The EDS, as seen from Figure 5.20, is made up of mainly light parts with spots of dark parts and some trends of grey, however, the captured area for analysis was seen to be made up of only the dark parts. This resulted in the presence of oxygen although not in a high percentage of 6.55. Iron and carbon were the other two metals that were captured with their percentage masses as seen in Table 5.20. Corrosion took place in this area.

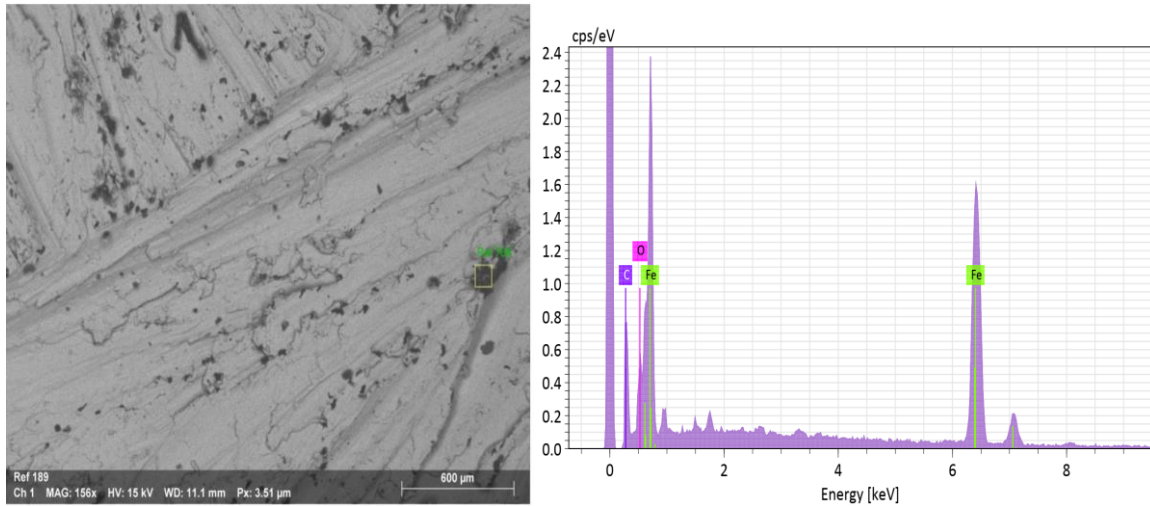


**Figure 5.20 SEM-EDS Analysis of Reference at Region 1**

**Table 5.20 SEM-EDS Analysis of Reference at Region 1**

Element	Mass %	Atom %
Carbon	21.58	51.44
Oxygen	6.55	11.71
Iron	71.87	36.85
<b>Total</b>	<b>100.00</b>	<b>100.00</b>

The EDS captured is no different from Figure 5.20. The captured part differed with the presence of only light and grey parts without any record of the dark part as seen from Figure 5.21. This particular spectrum represented results from the unburied rod showing only the three major elements. Table 5.21 recorded only iron of mass percentage of 100. There was no mention of carbon, which mostly accompanied iron and also oxygen which indicated corrosion had taken place.

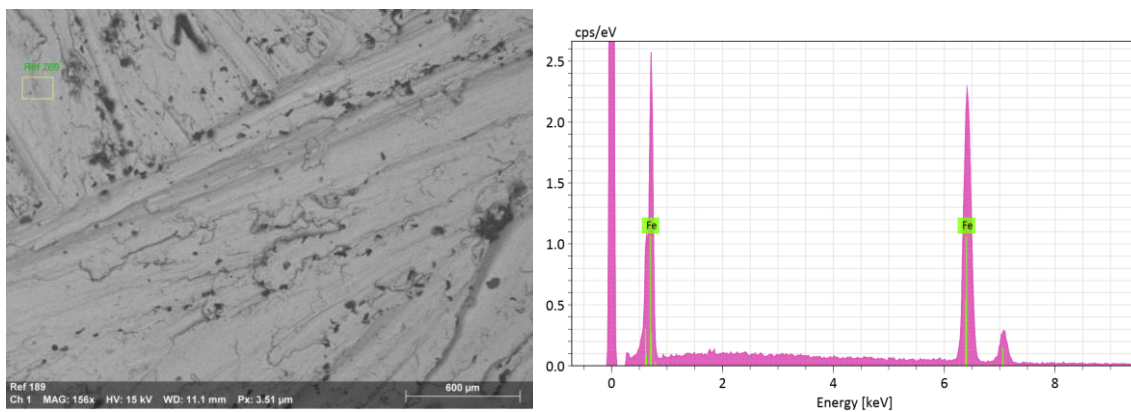


**Figure 5.21 SEM-EDS Analysis of Reference at Region 2**

**Table 5.21 SEM-EDS Analysis of Reference at Region 2**

<b>Element</b>	<b>Mass %</b>	<b>Atom %</b>
Iron	100.00	100.00
<b>Total</b>	100.00	100.00

## **5.5 Computer Simulation Results**

The simulation results from the use of fuzzy logic system and neural network were discussed in this section. These are the results from the prediction that was conducted by the two AI techniques used.

### **5.5.1 Fuzzy Logic System**

Once these rules have been established in the FIS, the rule viewer is activated. Figure 5.22 shows some of the rules displayed by the rule viewer. The various variables are varied to see their effects on the output variable, that is, the corrosion rate.

Any two input variables with corrosion rate can be observed using three-dimensional (3-D) plots of each variable in the dataset. Different colour patterns were used to portray the various relationships that exist between the input and output variables. One such plot is shown in Figure 5.23.

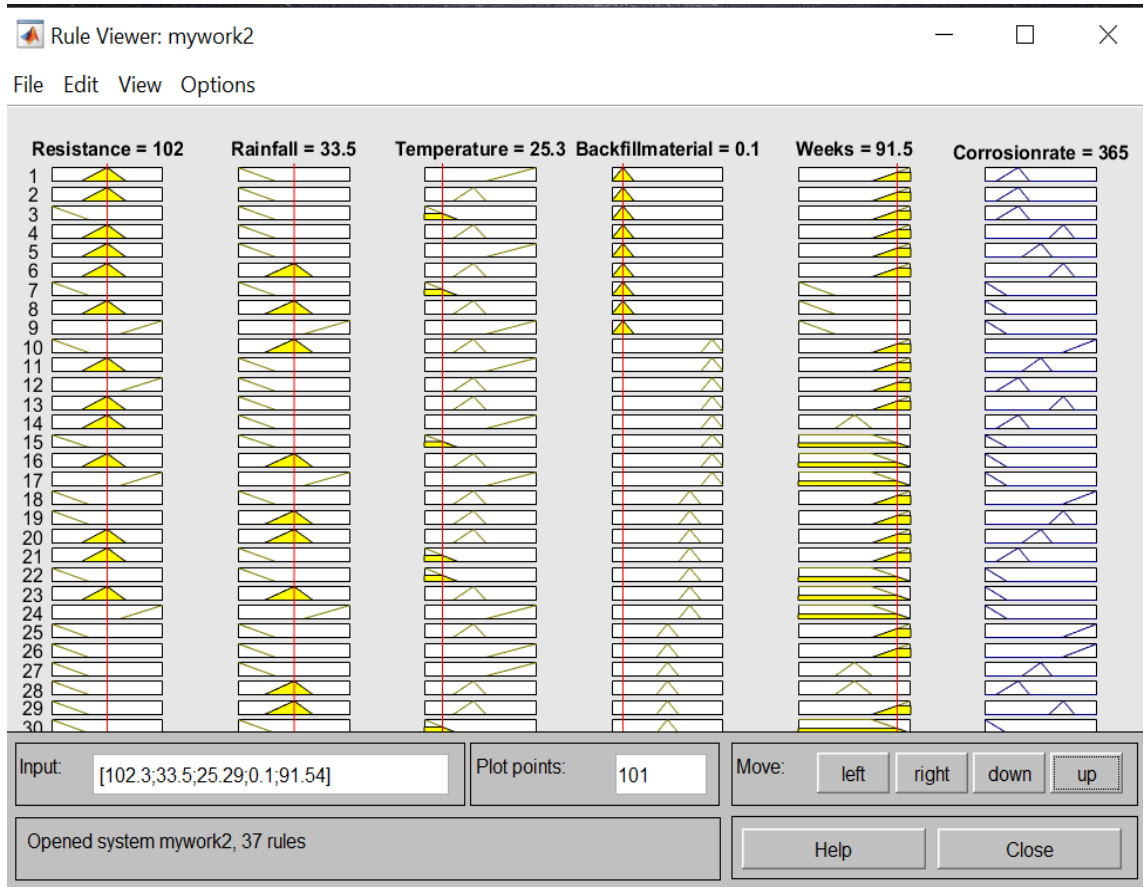


**Figure 5.22 Rule Viewer for Some Membership Functions**

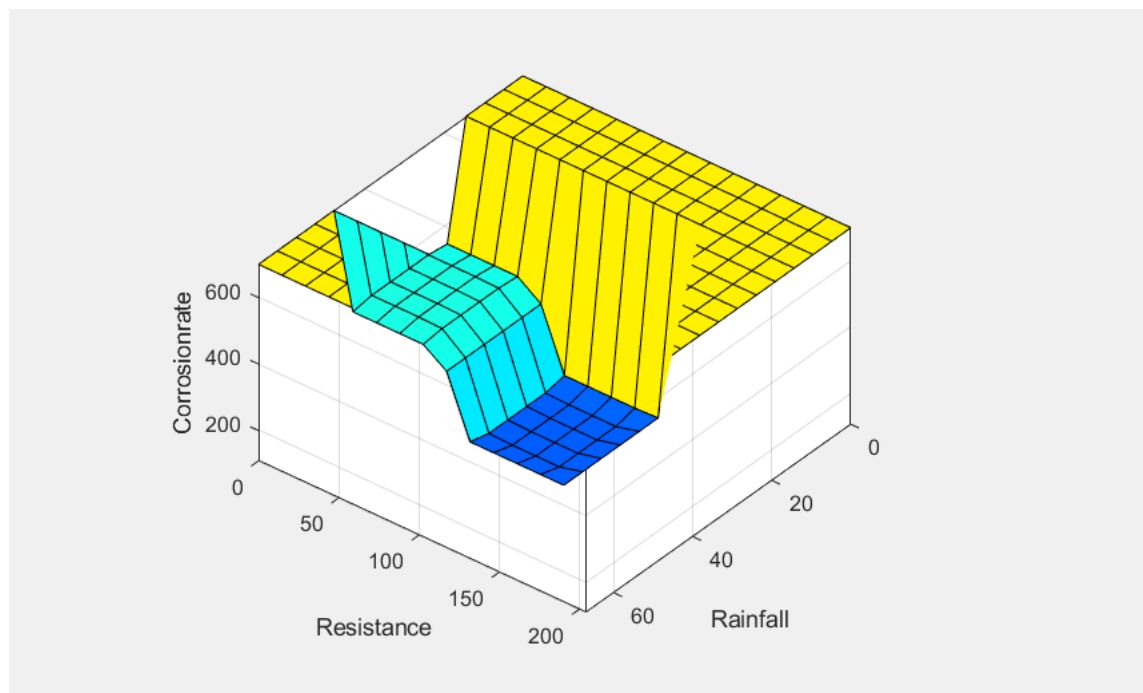


**Figure 5.23 Three-dimensional Plot of Corrosion Rate Against Resistance and Rainfall**

The 3-D plot in Figure 5.23 shows a valley-like shape for the variation of corrosion rate with resistance and rainfall. There is a rapid reduction in the corrosion rate with growing rainfall and resistance. The deep blue pattern denotes a low corrosion rate reflecting on the highest values of resistance and rainfall. The light blue pattern showed a periodical increase in corrosion rate with a decrease in the two parameters. The yellow pattern increased drastically for the corrosion rate with the least values of rainfall and resistance.

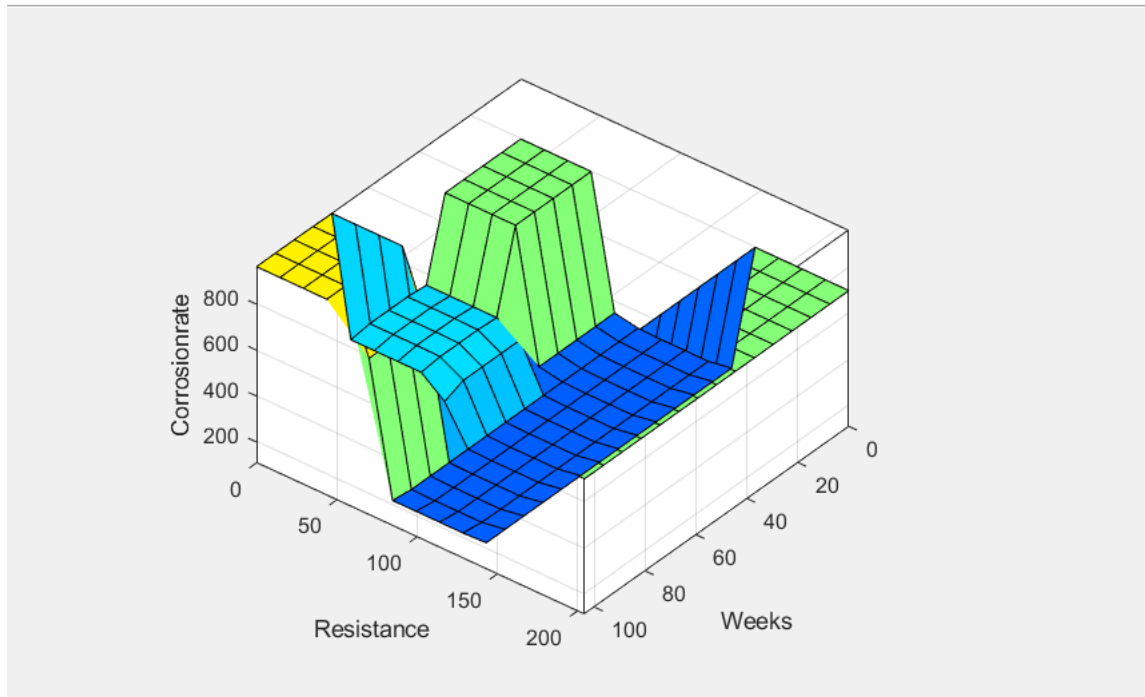


**Figure 5.24 Three-dimensional Plot of Corrosion Rate Against Resistance and Time (Weeks)**

The relationship that exists between resistance and time (weeks) is quite unpredictable. This is because other factors play a major role in making this decision but for the sake of this research, these two factors would be elaborated on. Four different colour patterns, namely, yellow, deep blue, light blue and green were portrayed in the Figure 5.24 to establish the relationship between the parameters. Corrosion rate rises with an increase in time as a result of the reaction that took place in the soil from chapter 3. Resistance values within 100  $\Omega$  and 150  $\Omega$  along the minimum weeks recorded corrosion rates less than 200  $\text{Am}^{-2}\text{s}^{-1}$ . Corrosion rate increased to its maximum value, whereas resistance values decreased to almost 0  $\Omega$  with an increase in time (weeks). Figure 5.24 shows the relationship between the two parameters and corrosion rate.

Another relationship exists between resistance and corrosion rate. Resistance is indirectly proportional to the corrosion rate as can be seen from Figure 5.25. An increase in resistance instantly led to a decrease in corrosion rate and vice versa.

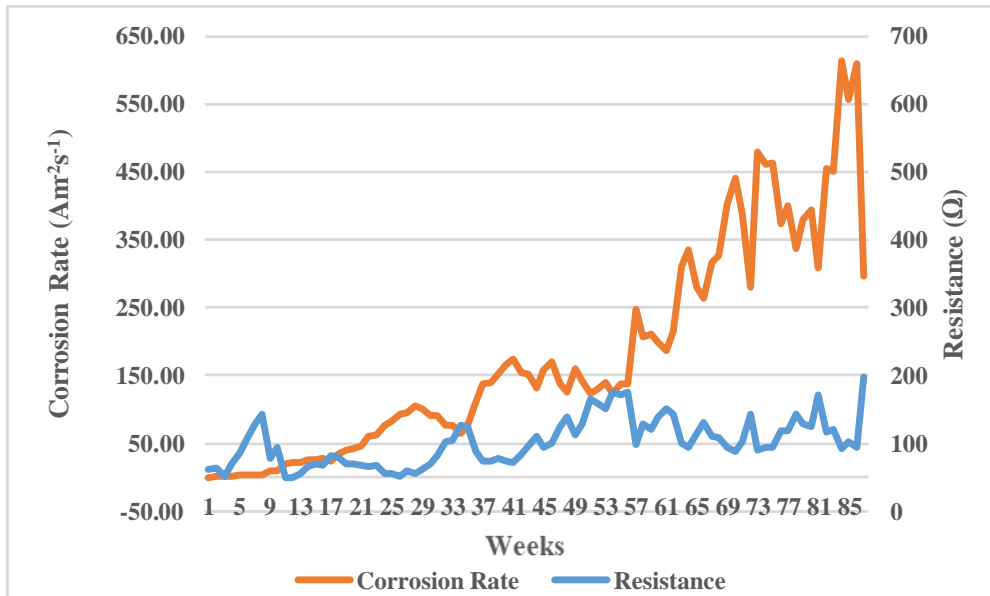


**Figure 5.25 Graph of Relationship Between Corrosion Rate and Resistance**

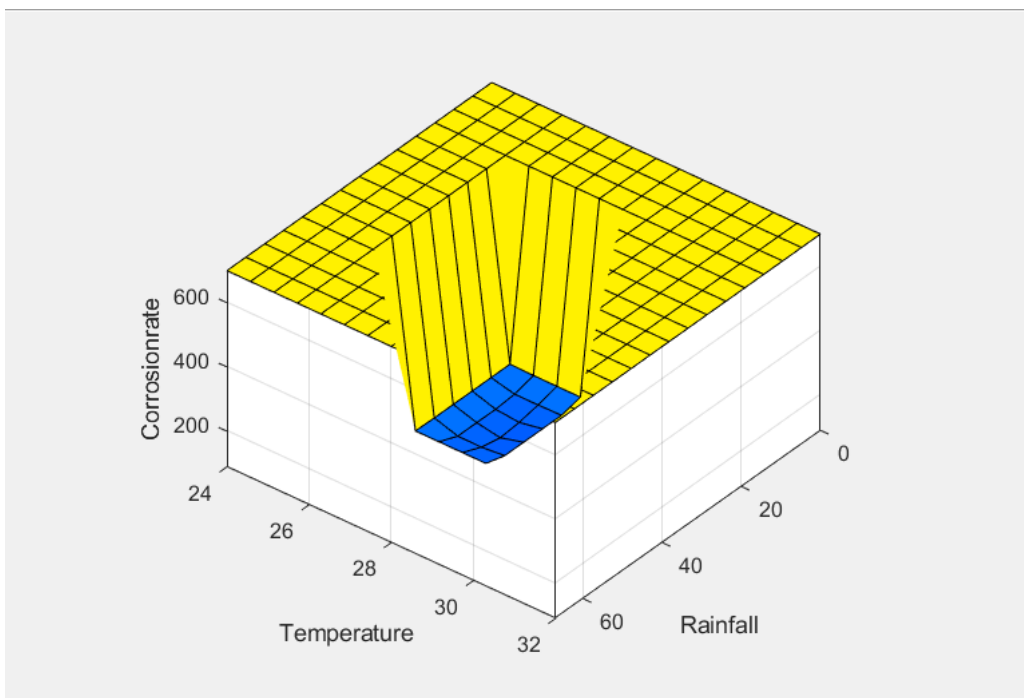


**Figure 5.26 Three-dimensional Plot of Corrosion Rate Against Temperature and Rainfall**



Temperature and rainfall share the same relationship to the corrosion rate. They all increase with an rise in the corrosion rate. From the figure, the blue pattern showed the peak of all the three parameters together because of their similarities.

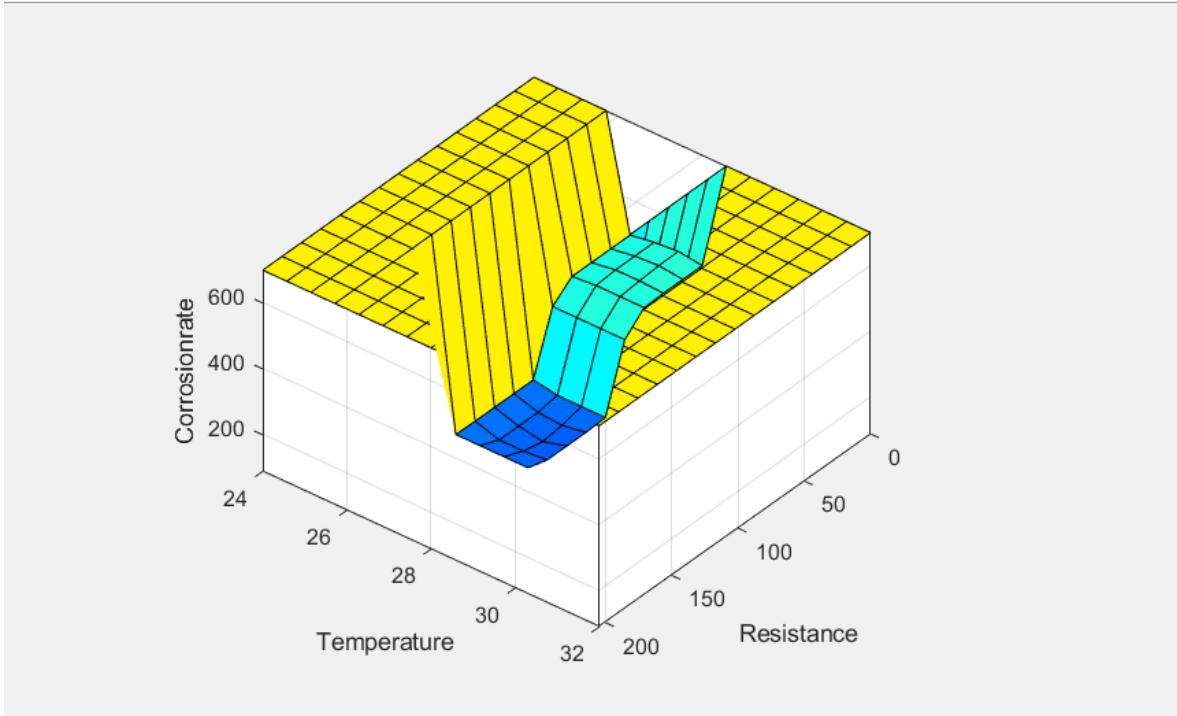


**Figure 5.27 Three-dimensional Plot of Corrosion Rate Against Resistance and Temperature**

Temperature increases with an increase in corrosion rate whereas resistance is indirectly proportional to corrosion rate meaning corrosion increases with a decrease in resistance. The combination of these two parameters resulted in an increased corrosion rate to the highest peak as seen in Figure 5.27.

Backfill materials throughout this research depicted their importance in corrosion rate analysis. Each point in Figure 5.28 denotes a particular backfill material and its effects on resistance and corrosion. The deep blue pattern within the range of 50  $\Omega$  and 150  $\Omega$  for resistance and that for backfill materials (0.4 – 1) have a gradual increase in corrosion rate. The light blue pattern showed a sharp increase in corrosion rate as resistance values decreased to values of less than 50  $\Omega$ .

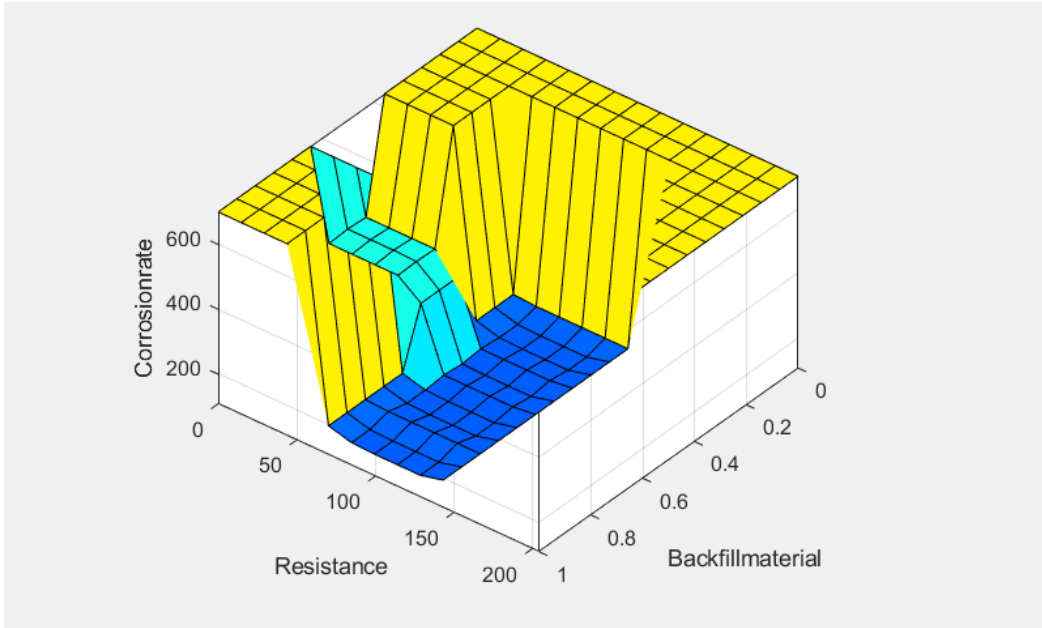


**Figure 5.28 Three-dimensional Plot of Corrosion Rate Against Resistance and Rainfall**

The relationship between rainfall and corrosion rate is the same as that of resistance. Corrosion increases with an increase in rainfall. This occurs when moisture-saturated air combines with oxygen and electrons on the metal's surface. In general, the longer metal components are exposed to humid air, the faster they corrode. Figure 5.29 shows the graph for this relationship.

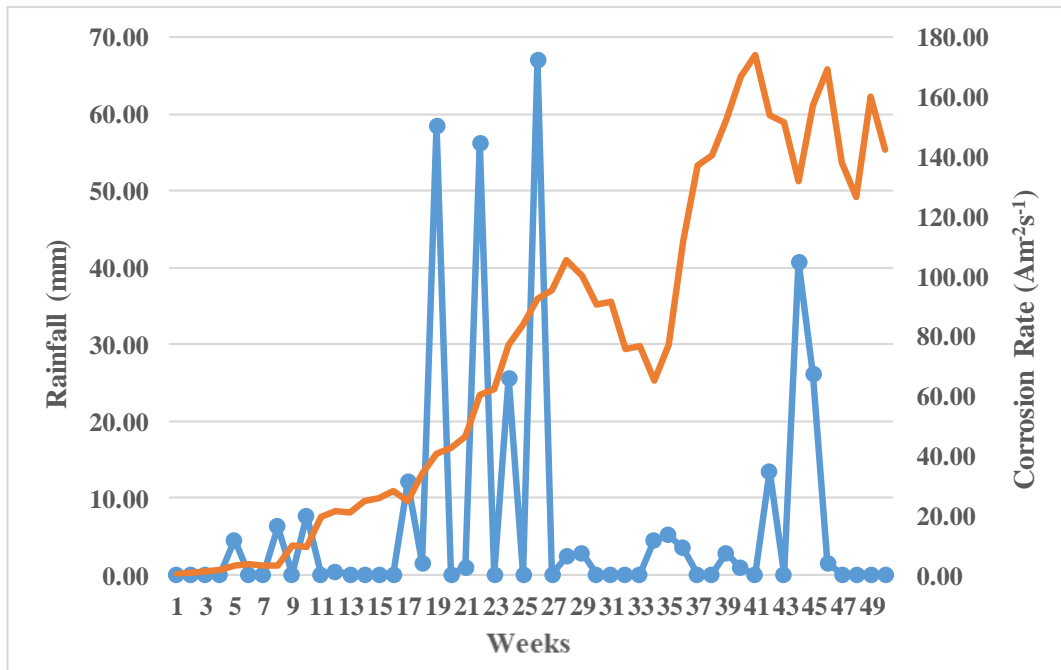


**Figure 5.29 Graph of Relationship Between Corrosion Rate and Rainfall**

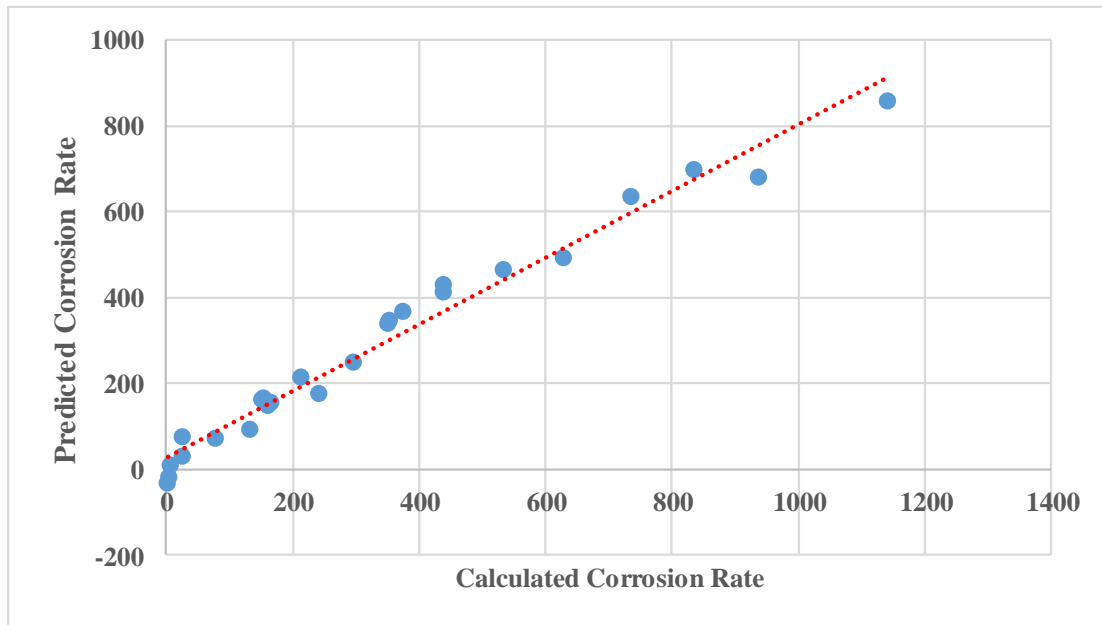


**Figure 5.30 Graph of Predicted and Calculated Corrosion Rates for Fuzzy Logic System**

A graph showed the relationship that existed between the calculated and predicted corrosion rate values. Table 5.22 showed the error and relative error that was calculated to establish the relationship that exist between the predicted and calculated corrosion rate values. The weeks were randomly picked for this analysis. Figure 5.30 also gives a diagram of the predicted and calculate corrosion rates.

**Table 5.22 The Computed Errors for Fuzzy Logic System**

Backfill Material	Weeks	Calculated Corrosion Rate ( $\text{Am}^{-2}\text{s}^{-1}$ )	Predicted Corrosion Rate ( $\text{Am}^{-2}\text{s}^{-1}$ )	Error ( $\text{Am}^{-2}\text{s}^{-1}$ )	Relative Error (%)
Palm Kernel Cake	76.00	373.93	354.78	19.16	5.12
Reference	30.00	132.15	128.06	4.11	3.10
Coconut Coir	40.00	160.82	114.57	46.25	28.76
Tyre Ash	84.00	353.66	360.74	-7.09	-2.00
Charred Coconut Coir	91.00	1141.74	1185.29	-43.55	-3.81

## 5.5.2 Neural Network System

The results from the use of neural network were made up of mainly graphs. Figure 5.31 below is the results of the training network. Here, the training algorithm that was used can be perceived on the upper left side of the picture. Opposite the choice of the algorithm are results for the MSE and R that was generated from the training and they were close to “0” and “1” respectively giving good results.

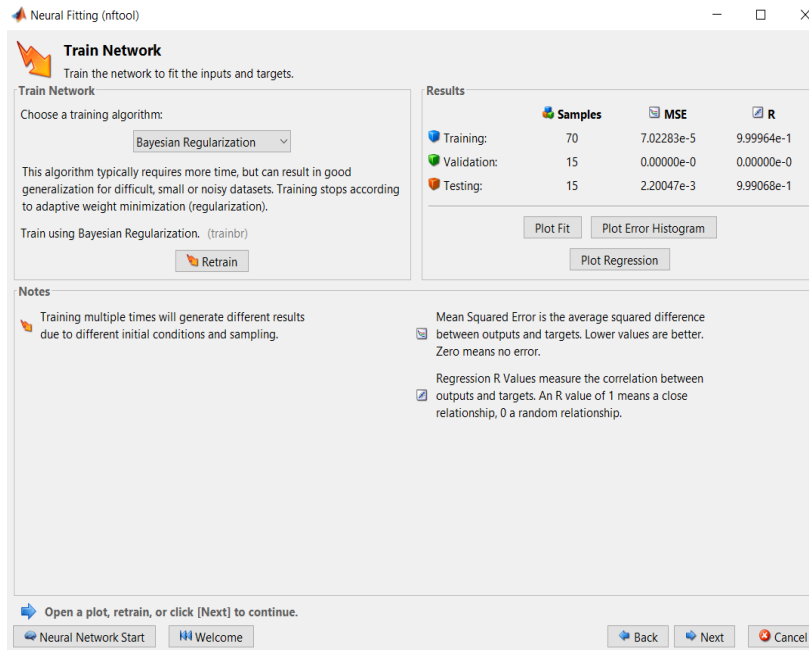


**Figure 5.31 Results from Network Training**

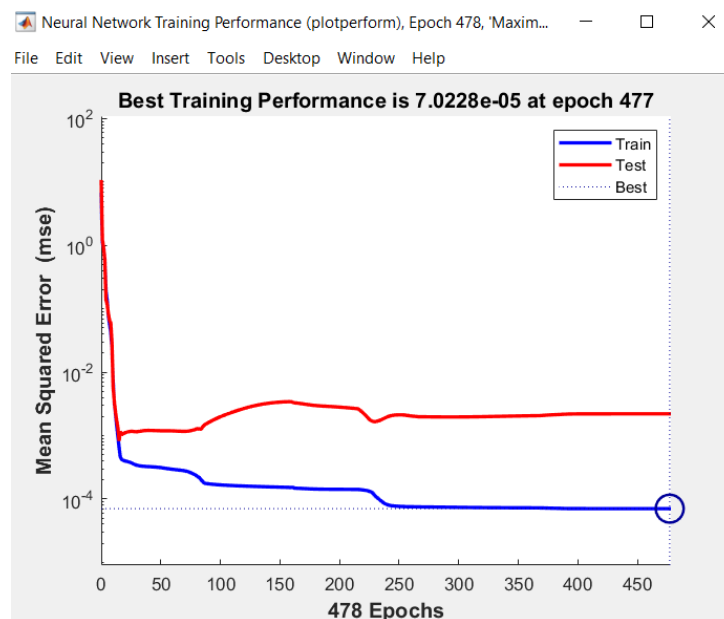


**Figure 5.32 Neural Network Performance at Epoch 478**

At epoch 477, the best validation turbulence is at  $7.0228e-05$  and it took place at the 250<sup>th</sup> iteration. There was linearity throughout the 477<sup>th</sup> epoch as seen from Figure 5.32.

The neural network training regression featured training, test and All. The closer the R-value is to 1, the more accurate the training is. In this case of Figure 5.33, the R-value for the training is 0.9994, that of the test is 0.99726 and that for All is 0.99956, which are closer to 1 by 0.00006, 0.00274 and 0.00044 respectively. Figure 5.33 shows the regression values for training, test and all.

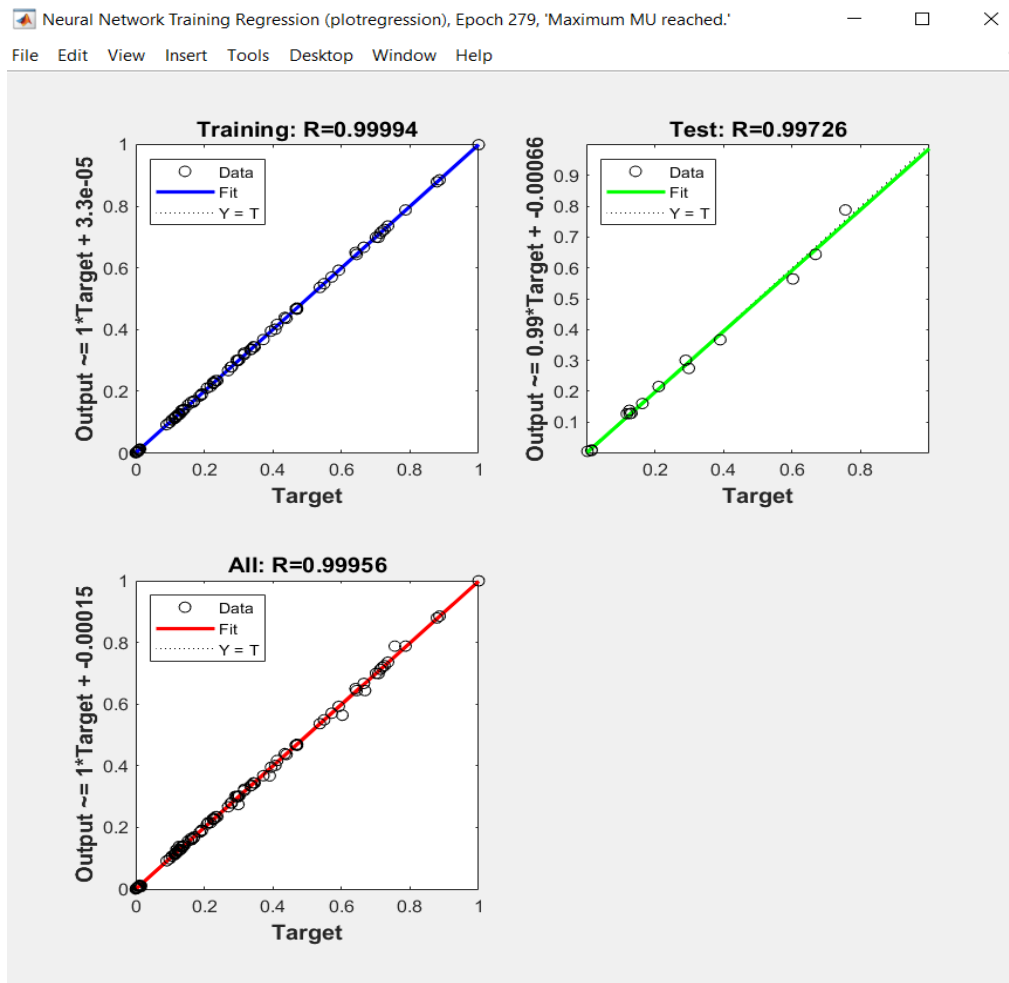
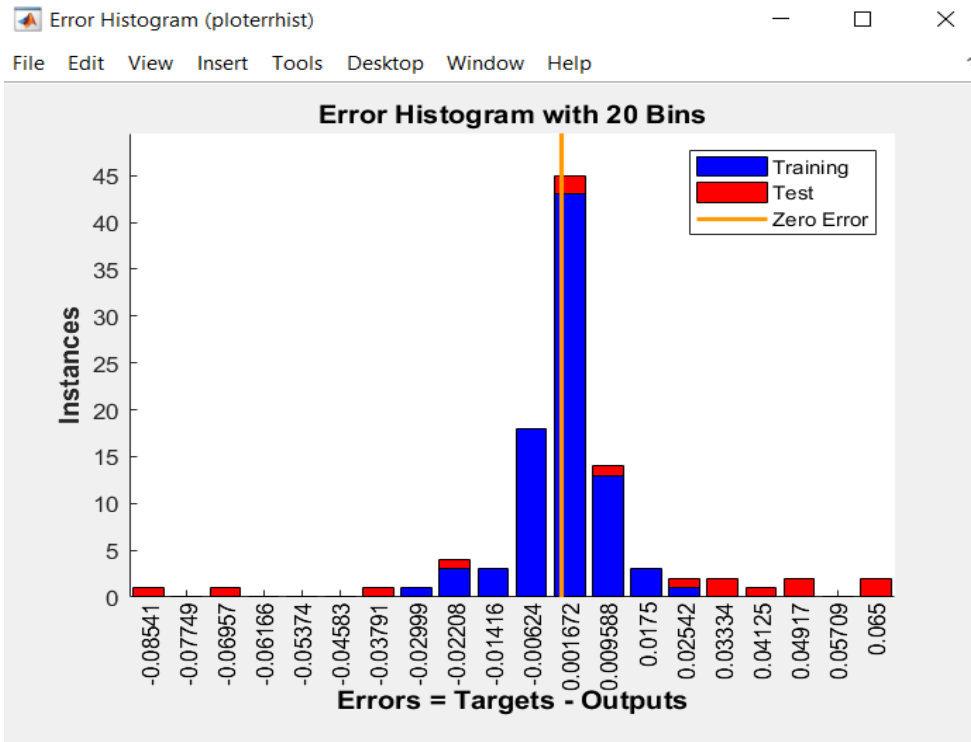
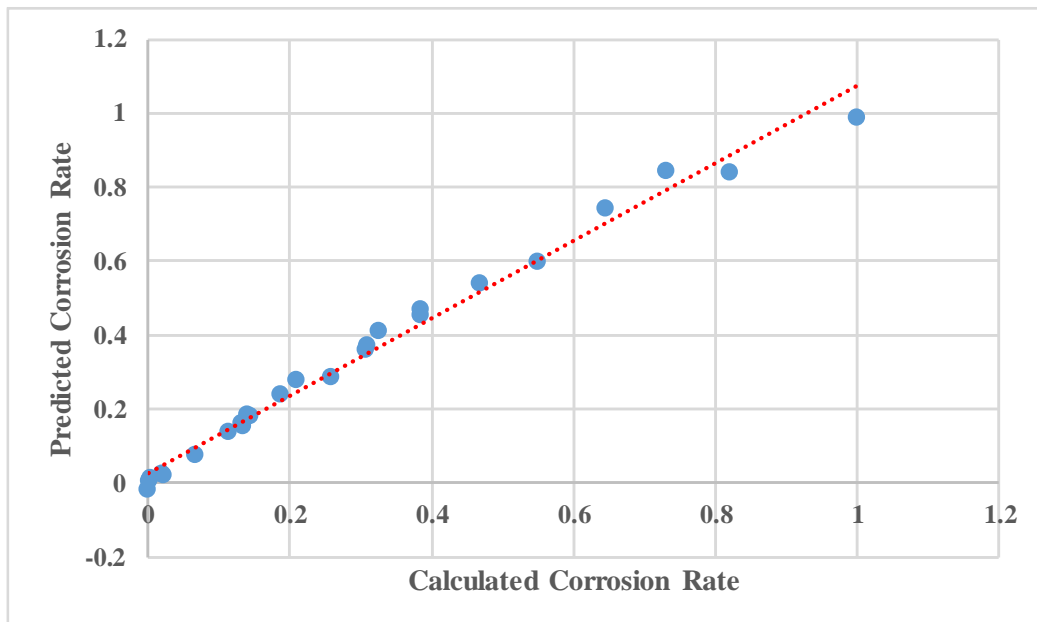


Figure 5.33 Neural Network Performance for Regression



**Figure 5.34 Error Histogram**

A histogram showing how many instances a particular error (calculated – predicted value) is spread out through the data set that was used to train the ANN. The zero error captured the instance where a zero error was recorded. Figure 5.34 gave a representation of the error.



**Figure 5.35 Graph of Predicted and Calculated Corrosion Rates**

Figure 5.35 is the scatter diagram for the comparison predicted and calculated corrosion rates of the training samples. The 0 - 45° diagonal line in this figure is made up of many dots representing the conformity of the predicted and calculated values. The closer the dots are to the dotted line, the more accurate are the predicted values. The figure also gave a different graph showing the relationship between the predicted and calculated values for the corrosion rate. Statistically, the ANN model needed to be evaluated to know the errors that came up from the prediction which the scatter diagram refused to show. Table 5.23 shows the error and relative error that was calculated to establish that relationship.

**Table 5.23 The Computed Errors for Neural Network**

<b>Backfill Material</b>	<b>Weeks</b>	<b>Calculated Corrosion Rate (Am<sup>-2</sup>s<sup>-1</sup>)</b>	<b>Predicted Corrosion Rate (Am<sup>-2</sup>s<sup>-1</sup>)</b>	<b>Error (Am<sup>-2</sup>s<sup>-1</sup>)</b>	<b>Relative Error (%)</b>
Palm Kernel Cake	76	373.93	366.68	7.25	1.94
Reference	30	132.15	94.38	37.78	28.58
Coconut Coir	40	160.82	148.04	12.79	7.95
Tyre Ash	84	353.66	348.16	5.49	1.55
Charred Coconut Coir	91	1141.74	856.84	284.89	24.95

## 5.6 Summary of Findings

The results gathered from this chapter made it evident that corrosion took place when the rods were buried in the soil for twenty-two months when four methods namely: visual inspection, change in thickness and use of XRF and SEM/EDS were used. Fuzzy Logic System and Neural Network were the AI techniques that were used for the prediction of corrosion rate.

The findings of this research are summarised as follow:

- i. The presence of heavy metals in the soil and the backfill materials played a role in the corrosion of the rods;
- ii. All the resistance values that were recorded for the rods that were backfilled were less than that of the reference that was not backfilled irrespective of the rainfall pattern;

- iii. Resistance values decreased in the wet season and increased in the dry season;
- iv. The colour change from reddish-brown to grey and increase in thickness and weight indicated that corrosion had taken place;
- v. The increase in the amount of iron and decrease in the amount of the rest of the other elements under the XRF and SEM-EDS analysis also proved that corrosion took place; and
- vi. The error margin from the use of the Fuzzy Logic System and Neural Network System proved that the corrosion rate prediction was accurate.

### **5.7 Research Contribution to Knowledge**

Contributions that were made to support general knowledge in literature from the research deductions are as follow:

A lot of work has been done on the use of locally acquired backfill materials for improvement in resistance values of earthing systems. Palm kernel cake for instance has been nationally recognised by ECG to be a very good conductive material for this purpose. The introduction of coconut was from its ability to retain moisture or water which is a prerequisite for resistance improvement. The thought of charring the coconut husk was to test its organic carbon content and its effects on the rod. The main focus of these research studies was on the generation and transmission stations of electrical power, but this work focused on the consumers' side, that is, the individual's responsibility to protect their gadgets.

The data for this research was generated from weekly resistance readings that were taken for twenty-two months with a megger. Temperature and rainfall data were taken from the Meteorological Office of UMaT. Parameters such as current, area, current density, volume and voltage were computed with their formulae in Microsoft Excel to aid in the corrosion prediction. Other research studies simulated the study area in the laboratory to represent what would have taken place in the field.

Most researchers ended here with the assumption that the performance of these materials was enough once they recorded lower resistance values without analysing the effects of the backfill materials on the rods in a corrosion sense but this research went on to analyse the rod samples using XRF and SEM-EDS.



Finally, this research now compared the results of two AI techniques that were used namely: Fuzzy Logic System and Neural Network to predict the corrosion rates.

## CHAPTER 6

### CONCLUSION AND RECOMMENDATIONS

#### 6.1 Conclusion

Palm kernel cake, tyre ash, coconut coir and charred coconut husk were the backfill materials that were acquired locally to improve the earth resistance. These materials were prepared and buried with the copper coated iron rods for twenty-two months. The Wenner point method was used to take weekly resistance values with the aid of Megger Det 32. Some of the rods that were backfilled recorded higher resistance values than that of the reference. This situation changed during the wet season. From then, all the rods buried with the backfill materials recorded lower resistance values as compared to that of the reference (buried without backfill material) rod. The inevitability of corrosion was clearly seen as all the buried rods showed evidence of corrosion activities, however, palm kernel cake and charred coconut husk recorded the least corrosion rate values with tyre ash recording the highest rate of corrosion.

Four methods, namely, visual inspection, change in thickness, analysis by XRF and SEM-EDS and use of Fuzzy Logic System and Artificial Neural Network were conducted to determine the extent of corrosion of these rods. Visual inspection revealed a colour change of the rod, from reddish-brown to grey, indicating that corrosion might have taken place. Measurement of thickness by Vernier calliper showed an increase in thickness from 1.2 mm to a maximum of about 1.9 mm, suggesting corrosion activity. The XRF analysis recorded an increase in the percentage values of the iron content for all buried rods with charred coconut husk recording the highest value of 99.42% and 88.58% as least for the unburied rod. SEM-EDS results showed content at several points of the micrographs for the buried rods. The rod buried in tyre ash backfill recorded 29.73% for the highest oxygen value with no oxygen value for the reference. These were proof of corrosion activity for the two analyses that were conducted.

FLS and ANN are the two AI techniques that were used for the prediction of the corrosion rates of the rods that were buried with backfill materials. 70% of the data was used for training whereas the 30% was for testing. The Mamdani Fuzzy Inference System and Bayesian Algorithm Feedforward Propagation was utilised for the prediction of corrosion rate for the FLS and ANN, respectively. The independent variables for the prediction of the

dependent variable (corrosion rate) were resistance, temperature, rainfall, time, backfill material. The ANN recorded a lower MSE of 0.0865 as compared to that of the Mamdani Fuzzy Logic Model, which recorded 0.3583. The publications that came out of this research are in Appendix E.

### **6.3 Recommendations**

Based on the findings of this investigation, the following recommendations were made:

- a. More rods (copper) should be buried each with new locally acquired backfill material in different types of soils for a minimum of five years and removed periodically at (six months) interval to track and observe the pattern of corrosion that will take place.
- b. The Energy Commission of Ghana should ensure that the standard of metal for earthing is used by all electricians.
- c. The Electricity Company of Ghana should adopt the use of charred coconut husk as backfill material for earthing systems at the consumers' end.

### **6.4 Future Research Directions**

The following research directions can be considered as future works:

- a. Burial of new set of rods at a suitable site with an application of current to present a real-time study.
- b. The need to combine the fuzzy logic system and neural network techniques with a larger (3 - 6) years of weekly data collection would go a long way to give more data points and accurate prediction of corrosion of these buried earth rods;

## REFERENCES

- Abbas, M. H. (2016), "Modelling CO<sub>2</sub> Corrosion of Pipeline Steels" *Doctoral Dissertation*, Newcastle University, 339 pp.
- Abdullah, A., Mazelan, N., Tadza, M. Y. M. and Abd Rahman, R. (2021), "The Use of Gypsum and Waste Gypsum for Electrical Grounding Backfill", In *Proceedings of the 11th National Technical Seminar on Unmanned System Technology 2019*, Springer, Singapore, pp. 1213 - 1226.
- Adada, A. A., de Matos, T. S., de Lacerda, L. A. and de Almeida, L. M. (2020), "Corrosion Grade on Anchor Rods of Guyed Transmission Towers Applying Machine Committee", *Brazilian Journal of Development*, Vol. 6, No. 10, pp. 82988 - 83002.
- Adkins, S., Foale, M. and Hugh, H. (2011), "Growth and Crop Production", *Soils, Plant Growth and Crop Production*, Vol. 7, pp. 1 - 7.
- Agyenim-Boateng, A., Tikwa, A., Awuvey, D., Amoakohene, E., Kwaasi, E. and Dagadu, C. (2014), "Determination of Corrosion Rate and Remaining Life of Pressure Vessel Using Ultrasonic Thickness Testing Technique", *Global Journal of Engineering, Design and Technology*, Vol. 3, No. 2, pp. 43 - 50.
- Aharinnejad, S. H. and Lametschwandtner, A. (1992), "Fundamentals of Scanning Electron Microscopy", *Microvascular Corrosion Casting in Scanning Electron Microscopy*, Springer, Vienna, pp. 44 - 51.
- Ahmed, I., Islam, A. and Ali, N. (2017), "Determination of Corrosion Rate of Mild Steel in Different Medium Measuring Current Density", *International Conference on Mechanical Engineering and Renewable Energy*, Chittagong, Bangladesh, pp. 18 - 20.
- Aibangbee, O. J. and Ikehelo, O. S. (2018), "Evaluation of High Voltage Transmission Line Towers Footing Earth Resistance under High Impulse Currents", *The International Journal of Innovation Research and Development*, Vol. 7, No. 8, pp. 1 - 9.
- Akoto, J. (2014), "Assessment of the Zone of Influence of Tyre Ash as a Conductive Backfill of Ground Electrodes", *Unpublished MPhil Thesis Report*, University of Mines and Technology, Tarkwa, 27 pp.

- Akwukwaegbu, I. O. and Okwe, G. I. (2017), “Soil Resistivity Measurement and Evaluation for Power System Earthing: A Case Study of Radio Nigeria Pacesetter FM Umuahia, Nigeria”, *US Open Science and Technology Journal*, Vol. 1, No. 1, pp. 1 - 9.
- Allahkaram, S. R., Isakhani-Zakaria, M., Derakhshani, M., Samadian, M., Sharifi-Rasaey, H. and Razmjoo, A. (2015), “Investigation on Corrosion Rate and a Novel Corrosion Criterion for Gas Pipelines Affected by Dynamic Stray Current”, *Journal of Natural Gas Science and Engineering*, Vol. 26, pp. 453 - 460.
- Alcántara, J., Chico, B., Simancas, J., Díaz, I. and Morcillo, M. (2017), “Marine Atmospheric Corrosion of Carbon Steel: A review”, *Materials*, Vol. 10, No. 4, 406 pp.
- Alsultani, K. F. and Mutasher, Z. Q. (2021), “Corrosion Behavior in External Surface of API 5L X52 Underground Pipelines in Buzurgan Region/Missan province”, *Journal of Petroleum Research and Studies*, Vol. 11, No. 1, pp. 36 - 52.
- Amfo-Otu, R., Agyenim, J. B. and Adzraku, S. (2014), “Meat Contamination Through Singeing with Scrap Tyres in Akropong-Akuapem Abattoir, Ghana”, *Applied Research Journal*, Vol. 1, No. 1, pp. 12 -19.
- Androvitsaneas, V. P., Gonos, I. F. and Stathopoulos, I. A. (2012), “Performance of Ground Enhancing Compounds During the Year”, *2012 International Conference on Lightning Protection (ICLP)*, Vienna, Austria, pp. 1 - 5.
- Androvitsaneas, V. P., Asimakopoulou, F. E., Gonos, I. F. and Stathopoulos, I. A. (2012), “Estimation of Ground Enhancing Compound Performance Using Artificial Neural Network”, In *2012 International Conference on High Voltage Engineering and Application*, Shanghai, China, IEEE, pp. 145 - 149.
- Anon. (2018), “Assessment of the Global Cost of Corrosion”, <http://impact.nace.org/economic-impact.aspx>, Accessed: June 4, 2021.
- Anon. (2019), “Low Resistance Earthing Compounds”, [www.matrixincorporation.com](http://www.matrixincorporation.com), Accessed: February 4, 2020.
- Anon., (2020), “Ground Enhancement Material”, <https://www.erico.com/catalog/literature/E978B-WWEN.pdf>, Accessed: February 4, 2020.

- Arbabi, H. (2018), “Corrosive Soils, Causes, Effects and Mitigation”, <http://www.testing-engineers.com/case1.html>, Accessed: November 16, 2018.
- Arnoux, C. (2012), “Earth or Ground Resistance and Soil Resistivity Testers, Earth or Ground Measurement Guide”, 1<sup>st</sup> edition, pp. 1-31.
- Arriba-Rodriguez, L., Villanueva-Balsera I. D, J., Ortega-Fernandez, F and Rodriguez-Perez, F. (2018), “Methods to Evaluate Corrosion in Buried Steel Structure: A Review”, *Metal*, Vol. 8, No. 5, pp. 1 - 21.
- Azmi, A., Ahmad, N. A., Yiew, L. K. and Abdul-Malek, Z. (2019), “The Use of Enhancement Material in Grounding System: A Review”, *Indonesian Journal of Electrical Engineering and Computer Science*, Vol. 13, No. 2, pp. 453 - 460.
- Baboian, R. (2005), “Corrosion Tests and Standards: Application and Interpretation”, *ASTM International*, Pennsylvania, Vol. 20, 120 pp.
- Badea, G. E., Caraban, A., Sebesan, M., Dzitac, S., Cret, P. and Setel, A. (2010), “Polarisation Measurements Used for Corrosion Rates Determination”, *Journal of Sustainable Energy*, Vol. 1, No. 1, 1 pp.
- Baljlit, S. T., Hardik, R., Parth, P., Akshat, P. and Dhruv, P. (2020), “Digital Earth Resistance Measurement System, <https://www.electricalindia.in>, Accessed: February 10, 2020.
- Barbrauskas, V. (2010), “Fire Damage, or Equipment Break Down”, *International Conference on Fire Investigation Science and Technology*, At College Park, MD, USA, pp. 119 - 130.
- Bastian, B. T., Jaspreeth, N., Ranjith, S. K. and Jiji, C. V. (2019), “Visual Inspection and Characterisation of External Corrosion in Pipelines Using Deep Neural Network”, *NDT & E International*, Vol. 107, pp. 1 -11.
- Bataineh, M. H. (2012), *Artificial Neural Network for Studying Human Performance*, The University of Iowa, USA.
- Belavkin, R. V. (2014), Lecture 4: Feed–Forward Neural Networks
- Bell, T. (2017), “What is Corrosion”, <https://www.thebalance.com>, Accessed: March 29, 2018.

- Bensaada, S., Bouziane, M. T., Mohammed, F. and Achour, B. (2013), "Phenomenon of Corrosion and the Industrial Safety", *Larhyss Journal*, No. 15, pp. 7 -19.
- Bell, T. (2018), "Corrosion Prevention for Metals", <https://www.thebalance.com>, Accessed: May 16, 2020.
- Biezma, M. V., Agudo, D. and Barron, G. (2018), "A Fuzzy Logic Method: Predicting Pipeline External Corrosion Rate", *International Journal of Pressure Vessels and Piping*, Vol. 163, pp. 55 - 62.
- Bony, S. (2013), "Differences between Wet and Dry Corrosion", [acedguardians.blogspot.com](http://acedguardians.blogspot.com), Accessed: April 9, 2019.
- Boukerche, S., Himour, A., Bououdina, M., Bensouici, F. and Ouchenane, S. (2019), "Multilayered ZnO/TiO<sub>2</sub> Nanostructures as Efficient Corrosion Protection for Stainless Steel 304", *Materials Research Express*, Vol. 6, No.5, pp. 540 - 552.
- Bullard, S. J., Covino, B. S., Russell, J. H., Holcomb, G. R., Cramer, S. D., Ziomek-Moroz, M. E. D. (2003), *Laboratory Evaluation of an Electrochemical Noise System for Detection of Localised and General Corrosion of Natural Gas Transmission Pipelines*, NACE International: Houston, TX, USA, pp. 1 - 8.
- Brycki, B. E., Kowalczyk, I. H., Szulc, A., Karczewska, O., Pakiet, M. and Aliofkhazraei, M. (2017), *Organic Corrosion inhibitors, InTech Open, Corrosion Inhibitors, Principles and Recent Applications*, No. 1, 420 pp.
- Castillo, O., Melin, P., Kacprzyk, J. and Pedrycz, W. (2007), "Type-2 Fuzzy Logic: Theory and Applications." In *2007 IEEE International Conference on Granular Computing (GRC 2007)*, San Jose, California, pp. 145 - 145.
- Chandima, G., Chamath, L and Chamalee, P. (2010), "Improvement of Earthing Systems with Backfill Materials", *30<sup>th</sup> International Conference on Lightning Protection*, Cagliari, Italy, pp. 1- 9.
- Chao, L. C. and Skibniewski, M. J. (1998), "Fuzzy Logic for Evaluating Alternative Construction Technology", *Journal of Construction Engineering and Management*, Vol. 124, No. 4, pp. 297 - 304.
- Chen, X. X. and Zhao, Y. (2017) "Research on Corrosion Protection of Buried Steel Pipeline". *Engineering*, Vol. 9, pp. 504 - 509.

- Churchill, S. E. and Prakash, S. (2019), "Study of Galvanic Corrosion Effect between Metallic and Non-metallic Constituent Materials of Hybrid Composites", In *International Conference on Emerging Current Trends in Computing and Expert Technology*, Springer, Cham, pp. 387 - 397.
- Cole, I. S. and Marney, D. (2012), "The Science of Pipe Corrosion: A Review of the Literature on the Corrosion of Ferrous Metal in Soils", *Corrosion Science*, Vol. 56, pp. 5 -16.
- Cottis, R. A. (2010), *Shreir's Corrosion*, Elsevier, 2463 pp.
- Csanyi, E. (2016), "A Practical Guide to Earth Resistance Testing by Megger", <http://electrical-engineering-portal.com/improve-earth-electrode-resistance>, Accessed: April 12, 2018.
- Csanyi, E. (2018), "Measurements and Calculations of Earth Electrode System", <http://electrical-engineering-portal.com>. Accessed: May16, 2018.
- Czichos, H., Saito, T. and Smith, L. E. (2011), *Springer Handbook of Metrology and Testing*, Springer Science & Business Media, pp. 667 - 741.
- Dărab, P. C., Turcu, A., Constantin, P. I. C. Ȃ., Pavel, S. G. and Beleiu, H. (2018), "Reducing Earth Grounding Electrical Resistance by Using Metallurgy Industrial Waste as Backfill Materials", *Acta Technica Napocensis-Series: Applied Mathematics, Mechanics, and Engineering*, Vol. 6, No.1, pp. 1 - 4.
- De Aquino Lima, F., De Moura Santos, A. P. N. and Da Silveira, D. M. (2020), "Corrosion of AISI 316L Stainless Steel Pipe in a Complex Ammoniacal Medium", In *Brazilian Technology Symposium Springer*, Cham, pp. 617 - 626.
- De Masi, G., Gentile, M., Vichi, R., Bruschi, R. and Gabetta, G. (2015), "Machine Learning Approach to Corrosion Assessment in Subsea Pipelines", In *OCEANS 2015-Genova*, IEEE, pp. 1 - 6.
- Detyniecki, M., Moubeche, B., and Bouchon-Meunier, B. (2012), "On the Paradoxical Success of Mamdani's Minimum-based Inference, Studies in Fuzziness and Soft Computing, Combining Experimentation and Theory", *Scientific Publishing Services, Springer*, Chennai, India, Vol. 271, pp. 259 - 270.



- Devaraju, S. and Ramakrishnan, S. (2014), "Performance Comparison for Intrusion Detection System Using Neural Network with Kdd Dataset", *Intact Journal on Soft Computing*, Vol. 4, No.3, pp. 743 - 752.
- Dilmegani, C. (2017), "Dark Side of Neural Networks Explained", <https://research.aimultiple.com/how-neural-networks-work/>, Accessed: February 12, 2021.
- Djokoto, A. A. (2013), "Exploring Coconut Tree as an Alternative Wood Carving Material", *Unpublished MA Thesis Report*, Kwame Nkrumah University of Science and Technology, Kumasi, 103 pp.
- Du, J., Yan, L., Wang, H. and Huang, Q. (2018), "Research on Grounding Grid Corrosion Classification Method Based on Convolutional Neural Network", *In MATEC Web of Conferences EDP Sciences*, Vol. 160, pp. 1 - 5.
- Ebnesajjad, S. and Ebnesajjad, C. (2014), *Surface Treatment of Materials for Adhesive Bonding*, William Andrew, Oxford, 2<sup>nd</sup> edition, 337 pp.
- Eckert, M. (2012), "Max Von Laue and the Discovery of X-ray Diffraction in 1912", *Ann. Phys.* pp. 83 - 85.
- Eduful, G. and Cole, J. E. (2009), "Electricity Palm Kernel Oil Cake as an Alternative to Earth Resistance-Reducing Agent", *Centre for Scientific and Industrial Research*, pp. 1 - 2.
- Eduful, G., Cole J. E. and Okyere P. Y. (2013), "Optimum Mix of Ground Electrode and Conductive Backfills to Achieve a Low Ground Resistance", *2<sup>nd</sup> International Conference on Adaptive Science and Technology*, Accra, Ghana, pp. 140 -145.
- El-Tous, Y. and Alkhaldeh, S. A. (2014), "An Efficient Method for Earth Resistance Reduction Using the Dead Sea Water", *Energy and Power Engineering*, Vol. 6, No. 4, pp. 47 - 53.
- Emran, K. M., Ali, S. M. and Lehaibi, H. A. A. (2018), "Green Methods for Corrosion Control", *Corrosion Inhibitors, Principles and Recent Applications. In Tech*, London, pp. 61 - 77.
- Farid, S. S. N. (2012), "Corrosion Detection and Prediction Studies", *Published Postgraduate Thesis in Safety Engineering*, Texas A & M University, 96 pp.

- Fayomi, O. S. I. and Popoola, A. P. I. (2019), “Surface Protection Progresses: A Paradigm Shift on Composite Deposition and Matrixe”, In *Journal of Physics: Conference Series*, Vol. 1378, No. 2, pp. 227.
- Febrero, L., Granada, E., Patiño, D., Eguía, P. and Regueiro, A. (2015), “A Comparative Study of Fouling and Bottom Ash from Woody Biomass Combustion in a Fixed-bed Small-scale Boiler and Evaluation of the Analytical Techniques Used”, *Sustainability*, Vol. 7, No. 5, pp. 5819 - 5837
- Feldman, F. (2019), “What is Electric Shock: Causes, Symptoms, Treatments and Safety”, <https://www.electrocuted.com>, Accessed: February 10, 2020.
- Folorunso, D. O., Olubambi, P. and Borode, J. O. (2014), “Characterisation and Qualitative Analysis of Some Nigerian Clay Deposits for Refractory Applications”, *IOSR Journal*
- Gautam, A. (2019), *Nerve Cells*, Springer International Publishing, 3 pp.
- Gerrit, B. (2014), “Principles and Testing Methods of Earth Ground Resistance”, *EE Publishers Limited*, Gauteng, South Africa, 10 pp.
- Gerrit, B. (2014), “Principles and Testing Methods of Earth Ground Resistance”, <https://www.ee.co.za/article>, Accessed: February 4, 2020.
- Ghavamian, A., Maghami, M. R., Dehghan, S. and Gomes, C. (2015), “Concerns of Corrosive Effects with Respect to Lightning Protection Systems”, *Engineering Failure Analysis*, Vol. 57, pp. 434 - 443.
- Gillaspy, R. (2019), “Definition, Structure and Types of Soil” <https://study.com/academy/lesson/what-is-soil-definition-structure-types.html>, Accessed: February 24, 2019.
- Godil, S. S., Shamim, M. S., Enam, S. A. and Qidwai, U. (2011), “Fuzzy Logic: A “Simple” Solution for Complexities in Neurosciences”, *Surgical Neurology International*, Vol. 2, 10 pp.
- Gomes, C. Lim, S. C. and Ab Kadir, M. Z. A. (2013), “Electrical Earthing in Troubled Environment”, *International Journal of Electrical Power & Energy Systems*, Vol. 47 pp. 117 - 128.

- Gomez, I. (2021), “Neural Networks, What They are and Why They Matter”, [https://www.sas.com/en\\_us/insights/analytics/neural-Networks.html](https://www.sas.com/en_us/insights/analytics/neural-Networks.html), Accessed: February 12, 2021
- Groysman, A. (2010), *Corrosion for Everybody*, Springer, Karmiel, Israel, 365 pp.
- Hamarsheh, Q. (2018), “Neural Networks and Fuzzy Logic (630514) Lecture 18” [www.philadelphia.edu.jo/academics/qhamarsheh/uploads/Lecture%2018 Different %20Types%20of%20Membership%20Functions%201.pdf](http://www.philadelphia.edu.jo/academics/qhamarsheh/uploads/Lecture%2018%20Different%20Types%20of%20Membership%20Functions%201.pdf), Accessed: February 8, 2020.
- Hameed, K.W., Yaro, A. S. and Khadom, A. A. (2016), “Mathematical Model for Cathodic Protection in a Steel-saline Water System”, *Journal of Taibah University for Science*, Vol. 10, No. 1, pp. 64 - 69.
- Hammuda1, A., Nouri, H. and Al-Ayoubi, M. (2011), “An Investigation into Substation Grounding and its Implementation on Gaza Substation”, *Energy and Power Engineering*, Vol. 3, pp. 593 - 599.
- Han, J. and Du, J. (2017), “A Method for Grounding Grid Corrosion Rate Prediction”, In *IOP Conference Series: Earth and Environmental Science*, Vol. 69, No. 1, 8 pp.
- Haynes, G. S. (1985), “Laboratory Corrosion Tests and Standards”, *ASTM International*, West Conshohocken, PA, USA, 543 pp.
- Heißing, B. and Ersoy, M. (2011), *Chassis Handbook: Fundamentals, Driving Dynamics, Components, Mechatronics, Perspectives*, Springer Science & Business Media, 1st edition, pp. 591.
- Herhold, L. A. (2021), “Neural Networks, What They are and Why They Matter”, [https://www.sas.com/en\\_us/insights/analytics/neural-Networks.html](https://www.sas.com/en_us/insights/analytics/neural-Networks.html), Accessed: February 12, 2021.
- Howard, B. D., Gibbs, K. and Elder III, J. B. (2004), “Corrosion Detection Devices”, *Army Corrosion Summit*, Oklahoma, USA, pp. 1 - 8.
- Hu, H., Nie, X. and Ma, Y. (2014), “Corrosion and Surface Treatment of Magnesium Alloys”, *Magnesium Alloys-Properties in Solid and Liquid States*; Czerwinski, F., (ed), pp. 67-108.

- Huang, H., Liu, Y. C., Xing, Y., Wu, J. R., Mao, X. Y., Ma, X. H. and Sun, H. B. (2019), “Method and Development Trend of Corrosion State Prediction of Grounding Grid”, *In IOP Conference Series: Earth and Environmental Science*, Vol. 342, No. 1, pp. 1 - 5.
- Hunt, N. and Gilkes, R. (1992), *Farm Monitoring Handbook*, University of Western Australia, Australia, 50 pp.
- Idoniboyeobu, D. C., Bala, T. K. and Okekem, E. (2018), “Assessment and Evaluation of Soil Effect on Electrical Earth Resistance: A Case Study of Woji Area, Port-Harcourt, Nigeria”, *International Journal of Engineering and Technical Research*, Vol. 8, No. 6, pp. 84 - 94.
- Ikechukwu, A. S., Ugochukwu, N. H., Ejimofor, R. A. and Obioma, E. (2014), “Correlation between Soil Properties and External Corrosion Growth Rate of Carbon Steel”, *International Journal of Engineering and Science*, Vol. 3, No. 10, pp. 38 - 47.
- Ismail, M., Noor, N. M., Yahaya, N., Abdullah, A., Rasol, R. M. and Rashid, A. S. A. (2014), “The Effect of pH and Temperature on Corrosion of Steel Subject to Sulphate-reducing Bacteria”, *J. Environ. Sci. Technol*, Vol. 7, pp. 209 - 217.
- Iyer, S. (2018), “What is Plate Earthing”, <https://www.quora.com/What-is-plate-earthing>, Accessed: September 9, 2019.
- Jana, D. K., Bej, B., Abd Wahab, M. H. and Mukherjee, A. (2017), “Novel Type-2 Fuzzy Logic Approach for Inference of Corrosion Failure Likelihood of Oil and Gas Pipeline Industry”, *Engineering Failure Analysis*, Vol. 80, pp. 299 - 311.
- Jančíková, Z., Zimný, O. and Košťial, P. (2013), “Prediction of Metal Corrosion by Neural Networks”, *Metalurgija*, Vol. 52, No.3, pp. 379 - 381.
- Jasni, J. L., Siow, K., Kadir, M. Z. A. and Ahmad, W. F. W. (2010), “Natural Materials as Grounding Filler for Lightning Protection System”, *30th International Conference on Lightning Protection - ICLP 2010*, Cagliari, Italy, pp. 22 - 24.
- Jithin, K. M. (2016), “Electrical Earthing System”, <https://www.mepits.com>, Accessed: February 10, 2020.
- Kamnitsas, K., Ledig, C., Newcombe, V. F., Simpson, J. P., Kane, A. D., Menon, D. K., Rueckert, D. and Glocker, B. (2017), “Efficient Multi-scale 3D CNN with Fully

Connected CRF for Accurate Brain Lesion Segmentation”, *Medical Image Analysis*, Vol. 36, pp. 61 - 78.

Katsifas, C. S. and Zachariadis, A. G. (2019), “EDXRF Spectrometry and Complementary Non-destructive Analytical Techniques in the Archaeometric Study of Copper Artefacts”, *Current Analytical Chemistry*, Vol. 15, No. 7, pp.776 - 787.

Kechit, G. (2020), “Fuzzy Logic in Artificial Intelligence: Architecture, Applications, Advantages & Disadvantages”, <https://www.upgrad.com/blog/fuzzy-logic-in-artificial-intelligence/>, Accessed: December 9, 2020.

Khan, M. M., Mokhtar, A. A. and Hussin, H. (2016), “A Fuzzy-based Model to Determine CUI Corrosion Rate for Carbon Steel Piping Systems,” *ARPJ. Eng. Appl. Sci*, Vol. 11, pp. 13325 - 13330.

Khan, M.M., Mokhtar, A.A., Hussin, H. and Muhammad, M. (2018), “Prediction for CUI in Piping Systems using Fuzzy Logic with Sensitivity Analysis of Corrosion Producing Factor”, In *MATEC Web of Conferences EDP Sciences*, Vol. 225, 8 pp.

Khatak, H. S. and Baldev, R. (2010), *Corrosion of Austenitic Stainless Steels: Mechanism, Mitigation and Monitoring*, Woodhead Publishing Limited, Cambridge England, pp. 377 pp.

Kim, S. J. and Choe, B. H. (2017), “A Model-based Approach to Reliability Assessment of Corroded Pipelines”, *Proceedings of the International Conference on Industrial Engineering and Operations Management Rabat*, Morocco, pp. 1807 - 1814.

Kouchaki, B. M. (2017), “Laboratory Resistivity Measurements for Soil Characterisation”, *Published MSc Thesis Report*, University of Arkansas, Fayetteville, 61 pp.

Krishnamurthy, N., Vallinayagam, P. and Madhavan, D. (2019), *Engineering chemistry*. PHI Learning Pvt. Ltd, 465 pp.

Křivý, V., Urban, V. and Kubzová, M. (2016), “Thickness of Corrosion Layers on Typical Surfaces of Weathering Steel Bridges”, *Procedia Engineering*, Vol. 142, pp. 56 - 62.

Kulor, F., Dzah, C., Markus, D. E., Apprey, W. M. and Kagbetor, P. (2021) "Comparative Study of Tyre Ash and Palm Kernel Oil Cake as Back-filling Agents for Effective Grounding." *In IOP Conference Series: Materials Science and Engineering*, Vol. 1088, No. 1, pp. 1 - 7.

- Kumar, K. (2019), “What is Neural Network: Overview, Applications, and Advantages”, <https://www.simplilearn.com/tutorials/deep-learning-tutorial/what-is-neural-network>, Accessed: February 12, 2021.
- Kuppan, T. (2017), *Earthing and Surge Protection Devices for Signal and Telecommunication Installations*, Indian Railways Centre for Advanced Maintenance Technology, Maharajpur, Gwalior, 56 pp.
- Lamay, M. (2017), “What is Rod Earthing?”, <https://www.quora.com>, Accessed: February 10, 2020.
- LaCroix, R., Weindorf, D. and Fisk, S. V. (2020), “Soil Basics”, <https://www.soils.org/about-soils/basics>, Accessed: February 24, 2020.
- Lateef, Z. (2020), “Types of Artificial Intelligence you Should Know”, [www.edureka.co/blog/types-of-artificial-intelligence/](http://www.edureka.co/blog/types-of-artificial-intelligence/), Accessed: February 8, 2020.
- Liengen, T., Basseguy, R., Damien F., Beech, I. and Birrien, I. (2014), *Understanding Biocorrosion: Fundamentals and Applications*, Elsevier, 1223 pp.
- Lin, H. T., Lo, C. M. and Lin, M. D. (2017), “Application of Artificial Neural Networks on Predicting Corrosion Rates of Carbon Steel in Taiwan Industrial Zones, Advances in Intelligent Systems Research, Vol. 3, pp. 278 - 282.
- Liu, J. (2013), “Research on Soil Corrosion of 20 Steel Buried Gas Pipelines in Chongqing”, *Thesis*, Chongqing University, Chongqing, No. 1, pp. 51 - 53.
- Loboda, M., and Marciniak, R. (2006), “Laboratory and Field Corrosion Tests for LPS (Lightning Protection System)”, In *Proceedings of the 28th International Conference on Lightning Protection*, Uppsala, Sweden, pp. 644 - 648.
- López, F. A., García-Díaz, I., Rodríguez Largo, O., Polonio, F. G. and Llorens, T. (2018), “Recovery and Purification of Tin from Tailings from the Penouta Sn–Ta–Nb Deposit”, *Minerals*, Vol. 8, No.1, pp. 1 - 13.
- Loubser, M. and Verryin, S. (2008), “Combining XRF and XRD Analyses and Sample Preparation to Solve Mineralogical Problems”, *South African Journal of Geology*, Vol. 111, No. 23, pp. 229 - 238.

- Mabbutt, S., Picton, P., Shaw, P. and Black, S. (2012), "Review of Artificial Neural Networks (ANN) Applied to Corrosion Monitoring", In *Journal of Physics: Conference Series* IOP Publishing, Vol. 364, No. 1, 9 pp.
- Mamdani, E.H. and S. Assilian. (1975), "An Experiment in Linguistic Synthesis with a Fuzzy Logic Controller", *International Journal of Man-Machine Studies*, Vol. 7, No. 1, pp. 1-13.
- Manas, T. (2016), "Corrosion of Earthing and Lightning Protection Systems", *Bulletin of Electrical Protection + Safety*, pp. 1 - 3.
- Manso, M., Carvalho, M.L., Queralt, I., Vicini, S. and Princi, E. (2011), "Investigation of the Composition of Historical and Modern Italian Papers by Energy Dispersive X-ray Fluorescence (EDXRF), X-ray Diffraction (XRD), and Scanning Electron Microscopy Energy Dispersive Spectrometry (SEM-EDS)", *Applied Spectroscopy*, Vol. 65, No.1, pp. 52 - 59.
- Mathias, J. (2015), "Scanning Electron Microscopy: a Tool for Science and Business", <https://www.innovatechlabs.com/newsroom/742/scanning-electron-microscopy/>, Accessed: June 24, 2021.
- Mhatre, M.S., Siddiqui, F., Dongre, M. and Thakur, P. (2017), "A Review Paper on Artificial Neural Network: A Prediction Technique", *International Journal of Scientific and Engineering Research (IJSER)*, Vol. 8, pp. 2229 - 5518.
- Michaud, D. (2017), "Differences between XRF and XRD", <https://www.911metallurgist.com/equipment/xrf/>, Accessed: January 14, 2020.
- Mohan, K. J. (2016), "Electrical Earthing System", <https://www.mepits.com/tutorial/497/electrical/electrical-earthing-grounding>, Accessed: May 22, 2018
- Mohsin, K. M., Mokhtar, A. A. and Peter, W. T. (2019), "A Fuzzy Logic Method: Predicting Corrosion under Insulation of Piping Systems with Modelling of CUI 3D Surfaces", *International Journal of Pressure Vessels and Piping*, Vol. 175, pp. 1 - 34.
- Moudgil, H. K. (2015), *Textbook of Physical Chemistry*, PHI Learning Private Limited, Delhi, pp. 565 - 570.

- Murad, O. F. (2012), "Obtaining Chemical Properties Through Soil Electrical Resistivity", *Journal of Civil Engineering Research*, Vol, 2, No. 6, pp. 120 - 128.
- Myers, R. J. and Cohen, A. (1984), "Conditions for Contributing to Underground Copper Corrosion", *American Waters Works Association Journal*, Vol 76, No. 8, pp. 68 -71.
- Ng, F. (2015), "SEM Analysis/ESM-EDS Analysis", <https://www.polymersolutions.com>, Accessed: January 16, 2020.
- Naxakis, I., Mihos, G. Pastromas, S. and Pyrgioti, E. (2018), "Examining the Operation of the Grounding System of a PV Installation", *In 2018 IEEE International Conference on High Voltage Engineering and Application (ICHVE)*, Wuhan, China, pp. 1- 4.
- Nyuykonge, P. L., Djongyang, N., Venasius, W. L. and Fagbenro John Adeneyi, J. F. (2015), "An Efficient Method for Electrical Earth Resistance Reduction Using Biochar", *International Journal of Energy and Power Engineering*, Vol. 4, No. 2, pp. 65 - 70.
- Okolo, O. S. (2017) "An Improved Fault Detection and Protection Scheme for a 200 MVA Transformer Using Fuzzy Logic", *Published PhD Thesis Report*, University of Nigeria, Nsukka, 88 pp.
- Olise, F. S., Owoade, O. K., Adekola, S. A., Olaniyi, B. H., Mtshali, B. C., Przybylowicz, J. W., Pineda-Vargas C. A. and Maaza, M. (2017), "A Combination of  $\mu$ -PIXE, XRF, SEM-EDS and XRD Techniques in the Analyses of Sn-Mine Tailings", *Journal of Radiation and Nuclear Applications*, Vol. 2, No. 3, pp. 95 - 102.
- Oloche, O. B., Yaro, S. A. and Okafor, E. G. (2009), "Analytical Correlation Between Varying Corrosion Parameters and Corrosion Rate of Al-4.5Cu/10%ZrSiO<sub>4</sub> Composite in Hydrochloric Acid by Rare Earth Chloride", *Journal of Alloys and Compounds*, Volume 472, No. 1 - 2, pp. 178 - 185.
- Owoyele, B. V. and Owolabi, G. O. (2014), "Traditional Oil Palm (*Elaeis Guineensis* Jacq.), and its Medicinal Uses: A Review", *TANG*, Vol. 4, No. 3, pp. 15 - 22.
- Oyedotun, T. D. T. (2018), "X-ray fluorescence (XRF) in the Investigation of the Composition of Earth Materials: A Review and an Overview", *Geology, Ecology, and Landscapes*, Vol. 2, No. 2, pp.148 - 154.



- Oyubu, A. O. (2015), "Soil Resistivity and Soil pH Profile Investigation: A Case Study of Delta State University Faculty of Engineering Complex", *International Journal of Scientific & Engineering Research*, Vol, 6, No.10, pp. 583 - 589.
- Palanisamy, G. (2019), "Corrosion Inhibitors", In *Corrosion Inhibitors*. IntechOpen, 255 pp.
- Palou, R. M., Olivares-Xomelt, O. and Likhanova, N. V. (2014), "Environmentally Friendly Corrosion Inhibitors", *Developments in Corrosion Protection*, pp. 431 - 465.
- Popov, B. N. (2015), "*Corrosion Engineering: Principles and Solved Problems*, Elsevier, pp. 768.
- Parczewski, K. and Wnęk, H. (2015), "The Tyre Characteristics of the Physical Model Used to Investigate the Lateral Stability of a Vehicle", *Proceedings of the Institution of Mechanical Engineers, Part D: Journal of Automobile Engineering*, Vol. 229, No. 10, pp. 1419 - 1426.
- Paritosh, K. (2016), "Types of Corrosion", <https://www.slideshare.net>, Accessed: May 7, 2019.
- Perera, L. P., Carvalho, J. P. and Soares, C. G. (2013), "Solutions to the Failures and Limitations of Mamdani Fuzzy Inference in Ship Navigation", *IEEE Transactions on Vehicular Technology*, Vol. 63, No. 4, pp. 1539 - 1554.
- Pole, M. K. and Sharma, A. K. (2013), "Analysis on the Factors Affecting Resistance of the Earth Electrode", *International Journal of Engineering Research & Technology (IJERT)*, Vol. 2, pp. 1304 - 1307.
- Prabhakar, S. and Goswami, G. (2019), "Design, Management and Key Success Factors of an Offshore Cathodic Protection System for Corrosion Control", *International Journal of Engineering and Management Research (IJEMR)*, Vol. 9, No.2, pp. 171 - 177.
- Prithwiraj, P., Budhaditya, B., Santanu, D. and Chiranjib, K. (2013), *Electrical and Electronics Measurements and Instrumentation*, McGraw Hill Education (India) Private Limited, New Delhi, 652 pp.

- Krishna, T. Y. and Biswal, K. (2015), “Speed Control of Separately Excited DC Motor using Fuzzy Logic Controller” *Published PhD Thesis Report*, National Institute of Technology, Rourkela, 35 pp.
- Reeve, W. D. (2008), *Principles and Practice of Earth Electrode Measurements*, EE Publishers (Pty) Limited, Muldersdrift, South Africa, 38 pp.
- Revie, R. W. and Uhlig, H. H. (2008), “Corrosion and Corrosion Control: An Introduction to Corrosion Science and Engineering”. *John Wiley & Sons*, New Jersey, 4<sup>th</sup> edition, 513 pp.
- Ricker, R. E. (2010), “Analysis of Pipeline Steel Corrosion Data from NBS (NIST) Studies Conducted between 1922–1940 and Relevance to Pipeline Management”, *Journal of Research of the National Institute of Standards and Technology*, Vol. 115, No. 5, pp. 373 - 392.
- Roberge, P. R. (2016), *Handbook of Corrosion Engineering*, McGraw-Hill, Columbus, OH, USA, 1130 pp.
- Robotti, S., Rizzi, P., Soffritti, C., Garagnani, G. L., Greco, C., Facchetti, F., Borla, M., Operti, L. and Agostino, A. (2018), “Reliability of Portable X-ray Fluorescence for the Chemical Characterisation of Ancient Corroded Copper-tin Alloys”, *Spectrochimica Acta Part B: Atomic Spectroscopy*, Vol. 146, pp. 41 - 49.
- Rocabruno-Valdés, C. I., González-Rodríguez, J. G., Díaz-Blanco, Y., Juantorena, A. U., Muñoz-Ledo, J. A., El-Hamzaoui, Y. and Hernández, J. A. (2019), “Corrosion Rate Prediction for Metals in Biodiesel Using Artificial Neural Networks”, *Renewable Energy*, Vol. 140, pp. 592 - 601.
- Rothwell, G. P. (2014), Corrosion Phenomenon – An Introduction, [www.iims.org.uk](http://www.iims.org.uk), Accessed: September 10, 2019.
- Rotvold, B. (2011), “External Grounding” [www.google.com](http://www.google.com). Accessed: November 17, 2017.
- Sadollah, A. (2018), “Introductory Chapter: Which Membership Function is Appropriate in Fuzzy System”, In *Fuzzy Logic Based in Optimisation Methods and Control Systems and its Applications*. IntechOpen, 5 pp.

- Salam, A., Rahman, Q. M., Ang, S. P. and Wen, F. (2017), "Soil Resistance for Dry and Wet Soil", *Journal of Modern Power and Clean Energy*, Vol. 5, No. 2, pp. 290 - 297.
- Sahoo, P., Das, S. K. and Davim, J. P. (2017), "Surface Finish Coatings", *Elsevier*, 5 pp.
- Schindelholz, E. and Robert, G. K. (2012). "Wetting Phenomena and Time of Wetness in Atmospheric Corrosion: A Review", *De Gruyter*, pp. 135 - 170.
- Schmitt, G. (2009), "Global Needs for Knowledge Dissemination, Research, and Development in Materials Deterioration and Corrosion Control", *World Corrosion Organisation*, Vol. 38, 14 pp.
- Senin, M. S., Shahidan, S., Leman, A. S. and Hannan, N. I. R. R. (2016), "Analysis of Physical Properties and Mineralogical of Pyrolysis Tires Rubber Ash Compared Natural Sand in Concrete Material", In *IOP Conference Series: Materials Science and Engineering*, Bahru, Malaysia, Vol. 160, No. 1, pp. 2 - 11.
- Senouci, A., El-Abbasy, M. S. and Zayed, T. (2014), "Fuzzy-based Model for Predicting Failure of Oil Pipelines", *Journal of Infrastructure Systems*, Vol. 20, No. 4, pp. 401 - 408.
- Shabalin, A. (2016), "Coherent X-ray Diffraction Studies of Mesoscopic Materials", *Unpublished Thesis Report*, University of Hamburg, Hamburg, 130 pp.
- Shankland, R. (2017), "What is Rod Earthing?" <https://www.quora.com>, Accessed: February 10, 2020.
- Shreir, L. L. (2010), "Basic Concept of Corrosion", Elsevier, Vol. 1, pp. 89 - 100.
- Shukla, P. and Singh, R. C. (2018) "A Review on the Effect of Bagasse Ash and Rubber Tyre Waste in Strength of Concrete", *International Research Journal of Engineering and Technology*, Vol. 4, No. 12, pp. 442 - 445.
- Shukla, R., Sumit G., Sajal S., Dwivedi, P. K. and Mishra, A. (2012), "Medicinal Importance of Bamboo", *International Journal of Biopharm and Phytochemical Research*, Vol. 1, No. 1, pp. 9 - 15.
- Sibiya, M. and Sumbwanyambe, M. (2021), "Automatic Fuzzy Logic-Based Maize Common Rust Disease Severity Predictions with Thresholding and Deep Learning", *Pathogens*, Vol. 10, No. 2, 131 pp.

- Siow, C. L., Chandima, G. and Mohd, Z. A. A. (2013), “Characterising of Bentonite with Chemical, Physical and Electrical Perspectives for Improvement of Electrical Grounding Systems”, *International Journal of Electrochemical Science*, Vol. 8, pp. 11429 - 11447.
- Smith, R. W. and Barrett, Z. (2006), “Direct Assessment (Da) White Paper”, *2006 International Pipeline Conference, American Society of Mechanical Engineers*, pp. 1 - 4.
- Smith, A. (2010), “X-Ray Diffraction (XRD) and X-Ray Fluorescence (XRF)”, *Engineering Material Culture ARCH 1860 XRD/XRF and SEM-EDS Exercises*, 1 pp.
- Srivaro, S., Matan, N. and Lam, F. (2018), “Property Gradients in Oil Palm Trunk (*Elaeis guineensis*)”, *Journal of Wood Science*, Vol. 64, pp. 709 - 719.
- Stratful, R. F. (1961), “A New Test for Estimating Soil Corrosivity Based on Investigation of Metal Highway Culverts”, *Corrosion*, Vol. 17, No. 10, 493 - 496.
- Stott, J. F. D. and John, G. (2010), “Corrosion in Soils”, *Intertek – CAPCIS Ltd*, Bainbridge House, 86 – 90 London Road, Manchester M1 2PW, UK, pp. 1166 - 1170.
- Sugeno, M. (1985), “*Industrial Applications of Fuzzy Control*”, *Elsevier Science Pub.Inc.*
- Sully, J. R. and Taylor, D. W. (1987), *Electrochemical Methods of Corrosion Testing*, Metals Hand Book, Vol. 13, 1099 pp.
- Sundaravaradan, N. A. and Reddy, M. J. B. (2018), “How is Earthing Done?”, *IEEE Potentials*, Vol. 37, No. 2, pp. 42 - 46.
- Sunil, B. R. (2020), *Corrosion of Metallic Biomaterials: Testing, Analysis and Controlling*, CRC Press, 777 pp.
- Swapp, S. (2017), “Scanning Electron Microscopy (SEM)”, [https://serc.carleton.edu/research\\_education/geochemsheets/techniques/SEM.html](https://serc.carleton.edu/research_education/geochemsheets/techniques/SEM.html). Accessed: January 16, 2020.
- Tait, W. S. (2018), “Controlling Corrosion of Chemical Processing Equipment”, In *Handbook of Environmental Degradation of Materials*, William Andrew Publishing, pp. 583 - 600.

- Tong, X., Zheng, Z., Tan, B., LU, L. and Wen, X. (2018), “Corrosion Rate Simulation and Influence Factors of a Vertical DC Grounding Electrode”, *IEEE Access*, Vol. 6, pp. 57230 - 57238.
- Trifunovic, J. and Kostic, M. (2014), “Analysis of Influence of Imperfect Contact Between Grounding Electrodes and Surrounding Soil on Electrical Properties of Grounding Loops” *Electrical Engineering*, Vol. 96, No. 3, pp.255 - 265.
- Ul-Hamid, A., Al-Hems, L. M., Quddus, A., Muhammed, A.I. and Saricimen, H. (2017), “Corrosion Performance of Aluminium in Atmospheric, Underground and Seawater Splatter Zone in the North Eastern Coast of Arabian Peninsula”, *Anti-Corrosion Methods and Materials*, Vol. 64, No. 3, pp. 326 – 334.
- Umoren, S.A., Eduok, U.M., Isreal, A. U., Obot, I. B. and Solomon, M. M. (2012), “Coconut Coir Dust Extract: A Novel Eco-friendly Corrosion Inhibitor for Al in HCl Solutions”, *Green Chemistry Letters and Reviews*, Vol. 5, No. 3, pp. 303 - 313.
- Veneranda, M., Costantini, I., de Vallejuelo, S. F. O., Garcia, L., García, I., Castro, K., Azkarate, A. and Madariaga, J. M. (2016), “Study of Corrosion in Archaeological Gilded Irons by Raman Imaging and a Coupled Scanning Electron Microscope–Raman System”, *Philosophical Transactions of the Royal Society A: Mathematical, Physical and Engineering Sciences*, Vol. 374, No. 20, pp. 1 - 13.
- Vilda III, W. S. (2009), *Corrosion in the Soil Environment: Soil Resistivity and pH Measurement*, Corrpro Companies, Inc., 200 pp.
- Wang, H., Yu, C., Wang, S. and Gao, J. (2014), “Electrochemical Corrosion Behaviour and Prediction of Corrosion Rate for Low Alloy Steel after Tempering Treatment”, *International Journal of Electrochemical Science*, Vol. 10, pp. 1169 - 1185.
- Wang, H., Yu, C., Wang, S. and Gao, J. (2015), “Electrochemical Corrosion Behavior and Prediction of Corrosion Rate for Low Alloy Steel after Tempering Treatment”, *International Journal of Electrochemical Science*, Vol. 10, No. 2, pp.1169 - 1185.
- Wang, H., Yajima, A., Liang, R.Y. and Castaneda, H. (2015), “A Clustering Approach for Assessing External Corrosion in a Buried Pipeline Based on Hidden Markov Random Field Model”, *Elsevier Science*, Vol. 56, 18 - 29.

- Ward, R. (2015), “Corrosion Monitoring, Detection, and Measurement. Inspection Trends”, [www.aws.org/ad.index](http://www.aws.org/ad.index). Accessed: June 13, 2019.
- Wasim, M., Shoaib, S., Mubarak, N. M. and Asiri, A. M. (2018), “Factors Influencing Corrosion of Metal Pipes in Soils”, *Environmental Chemistry Letters*, Vol. 16, No. 3, pp. 861 - 879.
- Wasim, M. (2018), “External Corrosion and Its Effects on Mechanical Properties of Buried Metal Pipes”, *Unpublished BE Project Report, Ned University of Engineering and Technology*, Karachi, 314 pp.
- Weltje, G. J. and Tjallingii, R. (2008), “Calibration of XRF Core Scanners for Quantitative Geochemical Logging of Sediment Cores: Theory and Application”, *Earth Planet Science Letters*, Vol. 274, No. 3, pp. 423 - 438.
- Wenner, D., Rodrigo, Dos, S. H. S., De, A. Costa, E. G., Carrer, J. A. M. and Lacerda, L. A., (2010), "Two (2)-dimensional Simulation of the Wenner Method with the Boundary Element Method - Influence of the Layering Discretisation". *Mecánica Computacional*, Vol. 29, pp. 2255 - 2266.
- West, M., Ellis, A. T., Potts, P. J., Strelci, C., Vanhoof, C. and Wobrauschek, P. (2014), “Atomic Spectrometry Update—a Review of Advances in X-ray Fluorescence Spectrometry”, *Journal of Analytical Atomic Spectrometry*, Vol. 29, No. 9, pp. 1516 - 1563.
- Wirh, K. (2019), X-Ray Fluorescence (XRF)  
[https://serc.carleton.edu/research\\_education/geochemsheets/techniques/XRF.html](https://serc.carleton.edu/research_education/geochemsheets/techniques/XRF.html),  
Accessed: January 14, 2020.
- Wolf, D. R. (2012), “Implementation, Analytical Characterisation and Application of a Novel Portable XRF/XRD Instrument”, *Unpublished MSc Thesis Report*, Ghent University, Ghent, 90 pp
- Yadav, D. K. M., (2017), *Handbook on Earthing and Surge Protection Devices for SAND Installations*, Maharajpur, Gwalior (M.P.), 56 pp.
- Yajima, A. (2019), “Assessment of Soil Corrosion in Underground Pipelines via Statistical Inference”, *Unpublished PhD Thesis Report*, University of Akron, Ohio, 150 pp.

- Yilmaz, E., Belem, T., Bussiere, B. and Benzaazoua, M. (2011), "Relationships between Microstructural Properties and Compressive Strength of Consolidated and Unconsolidated Cement Paste Backfills", *Cement and Concrete Composites*, Name of journal Vol. 33, No. 6, pp. 702 - 715.
- Yu, C. W. (2018), "The Need for Earthing", <http://city.edu.hk/fmol>, Accessed: May 18, 2018.
- Zadeh, L. A. (1965), "Fuzzy Sets", *Information and Control*, No. 8, No. 3, pp. 338 - 353.
- Zadeh, L. A. (1973), "Outline of a New Approach to the Analysis of Complex Systems and Decision Processes", *IEEE Transactions on Systems, Man, and Cybernetics*, Vol. 1, pp. 28 - 44.
- Zai, A., Mathur, V., Narang, R. and Joshi, G. K. (2018), "A Review on Earthing", *International Journal of Research and Analytical Reviews*, Vol. 5, No. 3, pp. 218 - 222.
- Zaranezhad, A., Mahabadi, H. A. and Dehghani, M. R. (2019), "Development of Prediction Models for Repair and Maintenance-related Accidents at Oil Refineries Using Artificial Neural Network, Fuzzy System, Genetic Algorithm, and Ant Colony Optimisation Algorithm", *Process Safety and Environmental Protection*, Vol. 131, pp. 331 - 348.
- Zarras, P. and Stenger-Smith, J. D. (2015), "Smart Inorganic and Organic Pretreatment Coatings for the Inhibition of Corrosion on Metals/Alloys", In *Intelligent Coatings for Corrosion Control*, pp. 59 - 91.
- Zhang, Z., Gao, P., Dan, Y., Liu, G., Xiang, R. and Zou, J. (2018), "A Simulation Study of the Direct Current Corrosion Characteristics of Carbon Steel Grounding Electrode with Ground Lead", *International Journal of Electrochemical Science*, Vol. 13, pp. 11974 - 11985.
- Zhang, Z., Ye, H., Dan, Y., Duanmu, Z., Li, Y. and Deng, J. (2020), "Novel Method for Comprehensive Corrosion Evaluation of Grounding Device", *IEEE Access*, 8 pp.
- Zhao, Y., Wang, G., Zhang, H. and Li, L. (2018), "Material Corrosion Classification Based on Deep Learning", *Chemical Engineering Transactions*, Vol. 71, pp. 775 - 780.

Zhao, C., Zhang, Y., Wang, C. C., Hou, M. and Li, A. (2019), “Recent Progress in Instrumental Techniques for Architectural Heritage Materials”, *Heritage Science*, Vol. 7, No. 1, 36 pp.

Zheng, Z. H., Cai, H. S., Hu, S. M., Jing, M. H. Liu, G., Ja, L. LU, H. L. and Wen, S. (2018), “Electrochemical Test and Simulation of Corrosion Rate of Five Common Ground Electrode Materials” *2018 IEEE International Conference on High Voltage Engineering and Application, (ICHVE)*, Wuhan, China, pp. 1- 4.

Ziyad, S. (2019), “Artificial Intelligence Definition, Ethics and Standards, Electronics and Communications”, *Law, Standards and Practice 18ELEC071*, 10 pp.



## APPENDICES

### APPENDIX A

#### FIELD RAW DATA OF RESISTANCE READINGS FOR THE YEAR 2018

**Table A1 Field Raw Data of Resistance Readings for the Year 2018**

Month	Date	Resistance Readings for the Year 2018 in Ohms				
		Palm Kernel Cake	Coconut Coir	Tyre Ash	Charred Coconut Husk	Reference
Jan	6th	61.1	75.1	59.9	150.4	96.3
	13th	62.7	61.8	69.5	138.0	107.3
	20th	50.5	52.3	56.3	38.5	124.2
	27th	68.8	75.8	59.1	47.7	141.0
Feb	3rd	86.6	92.9	63.9	71.5	134.2
	10th	105.5	103.5	70.5	90.0	174.9
	17th	128.7	121.9	82.7	92.4	198.8
	24th	143.7	122.0	84.1	84.3	204.5
Mar	3rd	77.1	103.9	48.6	68.1	172.1
	10th	94.0	121.7	58.8	80.5	180.7
	17th	49.2	96.7	63.2	66.2	116.7
	24th	48.5	103.1	28.7	84.4	139.8
	30th	49.7	107.8	35.8	87.8	115.15
Apr	7th	66.0	130.1	24.8	89.2	139.1
	14th	69.3	125.8	37.3	90.0	139.7
	22nd	67.7	121.2	32.5	69.9	154.4
	28th	82.0	116.5	35.3	78.8	148.1
May	5th	79.2	126.8	34.8	84.9	148.5
	12th	69.7	99.1	26.1	63.5	121.7
	19th	70.5	108.0	26.2	58.1	113.1
	26th	68.1	87.2	25.4	54.0	105.9
Jun	2nd	65.5	66.0	27.9	54.0	104.4
	9th	66.9	63.3	26.1	53.4	100.7
	16th	56.2	65	26.5	52.7	91.5

**Table A1 Cont'd**

Month	Date	Resistance Readings for the Year 2018 in Ohms				
		Palm Kernel Cake	Coconut Coir	Tyre Ash	Charred Coconut Husk	Reference
Jun	23rd	56.3	49.6	25.5	92.2	98.5
	30th	51.0	38.0	21.8	50.1	88.9
Jul	7th	60.0	47.2	22.3	49.4	91.0
	14th	56.2	50.3	21.9	46.6	87.1
	21st	61.4	50.1	28.6	48.2	85.9
	28th	70.2	61.3	31.0	48.6	89.5
Aug	4th	82.1	65.4	30.6	50.4	106.2
	11th	102.6	91.7	32.6	69.6	115.7
	17th	104.8	101.0	33.8	79.4	150.9
	25th	127.4	102.4	53.3	78.2	153.8
Sep	1st	124.6	131.5	40.0	92.2	161.2
	8th	88.3	83.5	31.9	85.9	110.6
	22nd	73.9	81.0	32.2	70.3	106.4
	29th	74.2	77.2	32.2	72.3	99.7
Oct	6th	78.1	77.6	33.2	74.3	103.4
	13th	73.1	76.0	32.5	60.9	102.8
	20th	71.9	77.2	33.3	57.5	87.7
	27th	83.5	77.7	34.6	56.3	98.6
Nov	10th	95.4	80.7	37.6	53.5	103.9
	17th	109.8	86.3	37.4	54.3	105.6
	24th	94.1	88.1	38.0	55.1	104.2
Dec	1st	99.7	110.4	33.9	56.6	118.7
	8th	125.1	101.0	41.3	64.9	121.0
	15th	139.6	116.6	44.7	94.5	137.6
	22nd	112.6	150.5	43.2	141.0	148.5
	28th	129.1	134.9	50.2	119.8	156.6

## APPENDIX B

### FIELD RAW DATA OF RESISTANCE READINGS FOR THE YEAR 2019

**Table B1 Field Raw Data of Resistance Readings for the Year 2019**

Month	Date	Resistance Readings for the Year 2018 in Ohms				
		Palm Kernel Cake	Coconut Coir	Tyre Ash	Charred Coconut Husk	Reference
Jan	5th	155.9	152.8	52.4	132.9	160.0
	12th	166.0	161.1	55.7	146.0	162.2
	19th	166.0	168.3	55.9	95.3	144.9
	26th	159.2	112.4	55.2	133.7	123.6
Feb	2nd	151.8	119.3	53.1	84.5	115.2
	9th	175.2	127.4	55.2	120.5	131.2
	15th	171.3	143.8	60.8	155.5	143.2
	23rd	174.4	159.1	57.2	144.6	150.4
Mar	2nd	99.0	100.3	44.8	90.9	102.1
	9th	128.7	120.0	62.4	109.9	121.4
	16th	121.1	108.2	46.9	104.6	119.5
	23rd	139.6	130.8	50.5	131.5	136.0
	30th	150.4	140.0	64.5	142.4	149.8
April	6th	142.6	138.1	53.3	99.5	145.2
	13th	100.1	97.2	47.8	101.0	114.4
	20th	94.1	93.3	47.4	108.0	175.9
	27th	114.6	109.9	51.3	116.9	131.5
May	11th	130.8	108.8	54.5	122.1	138.3
	18th	110.9	109.2	52.7	118.2	127.1
	25th	108.9	98.4	33.3	118.1	121.4
Jun	1st	95.0	80.2	48.5	87.4	109.7
	8th	88.3	72.4	48.0	80.0	108.1
	15th	101.6	73.5	50.5	74.3	105.0
	22nd	143.1	72.2	47.1	74.4	104.9
	29th	89.4	63.3	46.6	71.6	98.0

**Table B1 Cont'd**

<b>Month</b>	<b>Date</b>	<b>Resistance Readings for the Year 2018 in Ohms</b>				
		<b>Palm Kernel Cake</b>	<b>Coconut Coir</b>	<b>Tyre Ash</b>	<b>Charred Coconut Husk</b>	<b>Reference</b>
Jul	6th	94.1	65.1	53.4	70.9	97.0
	13th	94.8	64.6	48.3	73.7	99.2
	20th	119.1	80.3	51.9	84.5	111.4
	27th	118.7	100.4	56.8	96.9	116.1
Aug	3rd	143.2	123.8	56.4	126.4	128.4
	10th	128.7	111.0	53.0	101.0	114.1
	17th	125.2	96.6	43.2	99.7	110.6
	31st	170.5	127.9	59.2	177.1	135.4
Sept	14th	116.8	88.1	53.5	88.3	120.8
	21st	119.5	77.6	50.5	76.5	115.0
	28th	92.9	68.7	63.1	75.3	162.4
Oct	5th	102.5	67.0	50.2	74.9	257.0
	19th	94.9	102.8	42.4	68.7	92.7.0

## APPENDIX C

### FUZZY LOGIC MATLAB SCRIPT

[System]

Name='mywork2'

Type='mamdani'

Version=2.0

NumInputs=5

NumOutputs=1

NumRules=56

AndMethod='min'

OrMethod='max'

ImpMethod='min'

AggMethod='max'

DefuzzMethod='centroid'

[Input1]

Name='Resistance'

Range=[0 204.5]

NumMFs=3

MF1='low': 'trimf', [-85.21 0 68.17]

MF2='medium': 'trimf', [55 102.3 136.3]

MF3='high': 'trimf', [125 204.5 289.7]

[Input2]

Name='Rainfall'

Range=[0 67]

NumMFs=3

MF1='low': 'trimf', [-27.92 0 22.33]

MF2='medium': 'trimf', [15.83 33.5 44.67]

MF3='high': 'trimf', [39.08 67 94.92]

[Input3]

Name='Temperature'

Range=[24 32]  
NumMFs=3  
MF1='low':'trimf',[20.67 24 26.36]  
MF2='medium':'trimf',[26.05 27.5 28.38]  
MF3='high':'trimf',[28.39 32 35.33]

[Input4]

Name='Backfillmaterial'

Range=[0 1]

NumMFs=5

MF1='Ref':'trimf',[0 0.1 0.2]

MF2='PKC':'trimf',[0.2 0.3 0.4]

MF3='TA':'trimf',[0.4 0.5 0.6]

MF4='CC':'trimf',[0.6 0.7 0.8]

MF5='CCH':'trimf',[0.8 0.9 1]

[Input5]

Name='Weeks'

Range=[0 104]

NumMFs=3

MF1='low':'trimf',[-43.1 0.22 34]

MF2='medium':'trimf',[34 52 68]

MF3='high':'trimf',[68 104 147]

[Output1]

Name='Corrosionrate'

Range=[0 1400]

NumMFs=5

MF1='low':'trimf',[140.7 420.5 560]

MF2='high':'trimf',[799.7 980.5 1120]

MF3='very\_low':'trimf',[-10 0 280]

MF4='medium':'trimf',[466.6 700.5 840]

MF5='veryhigh':'trimf',[963.4 1400 1800]

[Rules]

2 1 3 1 3, 1 (1) : 1

2 1 2 1 3, 1 (1) : 1

1 1 1 1 3, 1 (1) : 1

2 1 2 1 3, 2 (1) : 1

2 1 3 1 3, 4 (1) : 1

2 2 2 1 3, 2 (1) : 1

1 1 1 1 1, 3 (1) : 1

2 2 2 1 1, 3 (1) : 1

3 3 3 1 1, 3 (1) : 1

1 2 2 5 3, 5 (1) : 1

2 1 3 5 3, 4 (1) : 1

3 1 2 5 3, 1 (1) : 1

2 1 2 5 3, 2 (1) : 1

2 1 3 5 2, 1 (1) : 1

1 1 1 5 -3, 3 (1) : 1

2 2 2 5 -3, 3 (1) : 1

3 3 3 5 -3, 3 (1) : 1

1 1 2 4 3, 5 (1) : 1

1 2 2 4 3, 2 (1) : 1

2 2 2 4 3, 4 (1) : 1

2 1 1 4 3, 1 (1) : 1

1 1 1 4 -3, 3 (1) : 1

2 2 2 4 -3, 3 (1) : 1

3 3 3 4 -3, 3 (1) : 1

1 1 2 3 3, 5 (1) : 1

1 1 3 3 3, 5 (1) : 1

1 1 3 3 2, 4 (1) : 1

1 2 2 3 2, 1 (1) : 1

1 2 2 3 3, 2 (1) : 1

1 1 1 3 -3, 3 (1) : 1

2 2 2 3 -3, 3 (1) : 1

2 1 2 2 3, 1 (1) : 1

1 1 1 2 -3, 3 (1) : 1

2 2 2 2 -3, 3 (1) : 1  
3 3 3 2 -3, 3 (1) : 1  
3 2 1 1 3, 1 (1) : 1  
2 2 1 1 3, 1 (1) : 1  
2 3 3 4 3, 4 (1) : 1  
3 1 3 1 1, 3 (1) : 1  
2 1 1 1 1, 3 (1) : 1  
3 1 1 3 1, 3 (1) : 1  
2 1 3 4 1, 3 (1) : 1  
2 1 2 4 2, 3 (1) : 1  
2 1 3 4 2, 3 (1) : 1  
2 1 2 4 3, 1 (1) : 1  
2 1 3 4 3, 4 (1) : 1  
1 1 2 2 1, 3 (1) : 1  
2 1 2 2 2, 3 (1) : 1  
3 1 3 2 2, 3 (1) : 1  
3 1 2 2 3, 1 (1) : 1  
2 1 3 3 1, 3 (1) : 1  
1 1 3 3 1, 3 (1) : 1  
3 1 2 1 3, 1 (1) : 1  
2 1 3 1 2, 1 (1) : 1  
1 1 2 5 1, 3 (1) : 1  
2 1 3 5 1, 3 (1) : 1

Prediction code

clc

%% ReadMe

% Data Input Structure: [Resistance Rainfall Temperature BackfillMaterial Weeks]

% Backfill Material Ranges:

% Reference (Ref) = 0.0-0.2



```
% Palm Kernel Cake (PKC) = 0.2-0.4
% Tyre Ash (TA) = 0.4-0.6
% Coconut Coir (CC) = 0.6-0.8
% Charred Coconut Husk (CCH)= 0.8-1
%%
%A = [10 0 24.21 0.9 30]
% 10 3 24.21 0.1 30];% Insert input data
% Loading testing data
load testdata.mat;
A = testdata;
shipfis = readfis('mywork2.fis'); % Read/Import FIS

% Evaluate FIS
result = evalfis(shipfis,A);
```

## APPENDIX D

### ARTIFICIAL NEURAL NETWORK MATLAB SCRIPT

```
function [Y,Xf,Af] = mycorrosion(X,~,~)
%MYNEURALNETWORKFUNCTION neural Network simulation function.
%
% Auto-generated by MATLAB, 15-Dec-2020 17:29:56.
%
% [Y] = myNeuralNetworkFunction(X,~,~) takes these arguments:
%
% X = 1xTS cell, 1 inputs over TS timesteps
% Each X{1,ts} = Qx5 matrix, input #1 at timestep ts.
%
% and returns:
%
% Y = 1xTS cell of 1 outputs over TS timesteps.
% Each Y{1,ts} = Qx1 matrix, output #1 at timestep ts.
%
% where Q is number of samples (or series) and TS is the number of timesteps.

%#ok<*RPMTO>

% ===== NEURAL NETWORK CONSTANTS =====

% Input 1
x1_step1.xoffset = [0;0;0;0;0];
x1_step1.gain = [2;2;2;2;2];
x1_step1.ymin = -1;

% Layer 1
b1 = [-0.19081884931071541045;-
0.41494957207590316139;0.089187096572624927071;-
0.36899547259599951854;0.25326513392023297655;0.55784174355948346058;-
2.2371054117919189075;-0.38966121114062735042;-
0.71033513498541644982;0.38066998597572976326];
```

```

IW1_1 = [0.84586079324616736397 0.05772906097897122224
0.3331648013788229834 -0.041609936250422058235 -0.0033552240129435598193;-
0.33688585661601860854 0.06245729104240202445 0.33849625727357790517 -
0.30558552350752399285 0.32734739764436726617;0.021099514141419917213 -
0.096871289285654416101 0.50587983499264654874 0.63894722918454815996
0.42263874659069633477;-0.47956329464002289686 -0.31844598060983675403 -
0.88755910778014812657 -0.055574655336286415963 -
0.32866090454150825861;0.58421593805606997218 -0.21856993659220277926
0.25209152054965749956 -0.28144911254861970651 -0.5328016367578437551;-
0.004834882667531639755 -0.12904608830629979432 0.34230004909239625244
0.2458824131017923742 -0.15097023017649793819;-1.5991047447901649559 -
0.060609184006717074789 0.031778891830060752854 -0.05950013554576582403
0.77766856029157094277;-0.40853274852555365726 0.11967236847403109334
0.025682162745874644733 -0.019892063172779823194 -0.87881063211021048787;-
0.41099551441769693882 -0.0037818329203393847258 -0.59320765942170472496
0.055104789317821104011 0.81636036163147018829;0.12369040829190830477 -
0.20477651696198492792 -0.49379757211037506037 0.22574106520305972645 -
0.9988780849660356953];

```

```
% Layer 2
```

```

b2 = 0.30711998129844408911;
LW2_1 = [-0.6176432489172124507 -0.78300455601751439705 -
0.35467841478407963196 -0.45253804811161763011 0.39564434552307958803
0.66437970918997535374 1.5617085697852728376 -0.27355866324610284002
0.63712325084406862263 -0.49022336910477937177];

```

```
% Output 1
```

```

y1_step1.ymin = -1;
y1_step1.gain = 2;
y1_step1.xoffset = 0;

```

```
% ===== SIMULATION =====
```

```
% Format Input Arguments
```

```

isCellX = iscell(X);
if ~isCellX
    X = {X};
end

% Dimensions
TS = size(X,2); % timesteps
if ~isempty(X)
    Q = size(X{1},1); % samples/series
else
    Q = 0;
end

% Allocate Outputs
Y = cell(1,TS);

% Time loop
for ts=1:TS

    % Input 1
    X{1,ts} = X{1,ts}';
    Xp1 = mapminmax_apply(X{1,ts},x1_step1);

    % Layer 1
    a1 = tansig_apply(repmat(b1,1,Q) + IW1_1*Xp1);

    % Layer 2
    a2 = repmat(b2,1,Q) + LW2_1*a1;

    % Output 1
    Y{1,ts} = mapminmax_reverse(a2,y1_step1);
    Y{1,ts} = Y{1,ts}';
end

```

```
% Final Delay States
```

```
Xf = cell(1,0);
```

```
Af = cell(2,0);
```

```
% Format Output Arguments
```

```
if ~isCellX
```

```
    Y = cell2mat(Y);
```

```
end
```

```
end
```

```
% ===== MODULE FUNCTIONS =====
```

```
% Map Minimum and Maximum Input Processing Function
```

```
function y = mapminmax_apply(x,settings)
```

```
y = bsxfun(@minus,x,settings.xoffset);
```

```
y = bsxfun(@times,y,settings.gain);
```

```
y = bsxfun(@plus,y,settings.ymin);
```

```
end
```

```
% Sigmoid Symmetric Transfer Function
```

```
function a = tansig_apply(n,~)
```

```
a = 2 ./ (1 + exp(-2*n)) - 1;
```

```
end
```

```
% Map Minimum and Maximum Output Reverse-Processing Function
```

```
function x = mapminmax_reverse(y,settings)
```

```
x = bsxfun(@minus,y,settings.ymin);
```

```
x = bsxfun(@rdivide,x,settings.gain);
```

```
x = bsxfun(@plus,x,settings.xoffset);
```

```
end
```

## **APPENDIX E**

### **LIST OF PUBLICATIONS**

**Ohene Adu, S.**, Nunoo, S. and Dankwah, J. R. (2020), “Evaluation of Local Backfill Materials on Earthing Systems”, Proceedings of 6th UMaT Biennial International Mining and Mineral Conference, Tarkwa, Ghana, pp. 51 - 57.

**Ohene Adu, S.**, Nunoo, S. and Dankwah, J. R. (2021), “Evaluation of Underground Corrosion on Backfilled Earthing Systems”, Ghana Journal of Technology, Vol. 6, No. 1, pp. 47 - 56.